DEVELOPMENT OF A HYBRID BRIDGE EVALUATION SYSTEM

by

ANDREAS JOHANN FELBER

B.A.Sc., The University of British Columbia, 1988
M.A.Sc., The University of Toronto, 1990

A THESIS IN PARTIAL FULFILLMENT OF

THE REQUIREMENTS FOR THE DEGREE OF

DOCTOR OF PHILOSOPHY

in

THE FACULTY OF GRADUATE STUDIES

Department of Civil Engineering

We accept this thesis as conforming
to the required standard

THE UNIVERSITY OF BRITISH COLUMBIA

December 1993

In presenting this thesis in partial fulfilment of the requirements for an advanced degree at the University of British Columbia, I agree that the Library shall make it freely available for reference and study. I further agree that permission for extensive copying of this thesis for scholarly purposes may be granted by the head of my department or by his or her representatives. It is understood that copying or publication of this thesis for financial gain shall not be allowed without my written permission.

(Signature)

Department of CIVIL ENGINEERING

The University of British Columbia
Vancouver, Canada

Date 9 Dec 1993

DE-6 (2/88)

Abstract

There is an increasing need to verify analytical dynamic models used for the seismic evaluation of existing bridges. During a retrofit evaluation, analytical models are created to predict the bridge response and damage levels due to seismic loading. These models should be verified so damage levels can be determined more confidently. Currently experimental studies are only occasionally performed on existing structures to verify analytical models because existing testing methods are too costly, require traffic shutdowns, and do not deliver results quickly enough for routine use.

To overcome these limitations, the hybrid bridge evaluation system (HBES) was developed using ambient vibration techniques to inexpensively and quickly determine the dynamic characteristics of a large variety of structures. The HBES combines state of the art vibration measurement hardware with a series of custom developed programs to expedite ambient vibration studies. In particular, two new functions were developed and implemented as part of the HBES software to interpret the data quickly. These functions made it possible to analyse the data obtained from ambient vibration measurements in the field. This is a considerable advancement over traditional systems which require several weeks of data analysis after the field work is completed. Since partial experimental results can be obtained with the HBES while some of the tests are still in progress, the quality of the collected information can be assessed before leaving the site. After returning from the site, the experimental results can be used to verify and tune analytical models.

A number of tests were conducted as part of this thesis which demonstrate the HBES' performance. The study of the Shipshaw Bridge data, which was analyzed in one day, demonstrated the unique

speed of the system. The study of the Squamish Wharf demonstrated the system's capability to determine the dynamic characteristics of structures with very small ambient vibrations levels (+/- 0.02 mg). The complete study of the Colquitz River Bridge was used to evaluate the HBES' components and their integration. This study confirmed the suitability of the hardware and demonstrated that the integrated programs were capable of expeditiously acquiring, analyzing, and interpreting large amounts of data. The experimentally obtained characteristics of the structure were used to refine the structure's analytical models. The HBES system can now be used as an effective tool in the seismic evaluation of bridges.

Table of Contents

List of Tables

List of Figures

Nomenclature

An index of terms and abbreviations used in this document is given in Appendix G and the symbols used for the main body of this document are listed below.

c	damping constant
C_c	coherence cut off value
C_{xy}	real component of one side cross spectral density
f	frequency in Hz
f_c	Nyquist frequency in Hz
g	acceleration due to gravity ($9.81 m/\sec^2$)
f_d	damped natural frequency in Hz
f_n	natural frequency in Hz
$G_{jj}(\omega)$	auto spectral density, power spectral density (PSD)
$G_{ij}(\omega)$	cross spectral density
$h(t)$	impulse response function
$H(\omega)$	frequency response function
i, j, k, l	integer indexes
n	number of channels, vector length
N	number of points per segment
m	nodal mass

$p(t)$	forcing function
$P(\omega)$	Fourier Transform of forcing function
Q_{xy}	imaginary component of one side cross spectral density
T	length of a segment
t	time index
x, y	time series of nodal displacements
$\dot{x}, \dot{y}$	nodal velocity
$\ddot{x}, \ddot{y}$	nodal acceleration
X, Y	Fourier Transform of time series
X^*, Y^*	complex conjugate of Fast Fourier Transform of time series
x_o	initial nodal displacement
β	frequency ratio
$\gamma_{ij}^2(\omega)$	coherence
ν	mean value of time series
ϕ_{ij}	phase angle in degrees
ϕ_c	Modal-Cut-Off angle
ω	frequency in radians/sec
ω_d	damped natural frequency in radians/sec
ω_n	natural frequency in radians/sec
ξ	critical damping ratio

Acknowledgements

First I would like to thank my parents Andreas and Inge Felber, my fiance Elizabeth Kao and my personal friends who were very understanding and supportive throughout my graduate studies.

I gratefully acknowledge the continued support of my supervisor, Professor Stiemer, throughout the project. Furthermore I would like to thank the members of my Ph. D. committee; professors D. L. Anderson, R. O. Foschi, H. G. L. Prion, R. G. Sexsmith, C. E. Ventura of the Department of Civil Engineering and Dr. D. P. Romilly of the Department of Mechanical Engineering for their involvement in this thesis. I am indebted Dr. W. D. L. Finn and particularly to Dr. Ventura for their many suggestions throughout the project.

The research project was made possible by financial support of the Ministry of Transportation and Highways of British Columbia. In particular, I would like to thank the following individuals (alphabetically listed): Peter Brett, Kang Ho, Earl Lund, Ron Mathieson, Fabiola Owen, Brock Radloff and Dewis Rozell of the Ministry for their involvement in this project. Additional funding for testing equipment was provided by a Natural Science and Engineering Research Council (NSERC) of Canada equipment grant to Dr. Ventura. The funding received from a NSERC postgraduate scholarship and a UBC graduate fellowship is gratefully acknowledged.

I am grateful to Dr. P. R. Taylor, of Buckland and Taylor Ltd. of North Vancouver, for providing me with the opportunity to perform tests on the Second Narrows Bridge and for sharing some of his experience and making valuable suggestions to the project.

The author would like to thank Professors A. Filiatrault and R. Tinawi of Ecole Polytechnique as well as the Quebec Ministry of Transportation for sharing the Shipshaw bridge data.

Carol Shoji's considerable efforts in editing this manuscript are acknowledged.

I am obliged to Mr. Howard Nichol, the technician of the UBC Earthquake Engineering Laboratory, for his valuable assistance in preliminary testing and preparatory work. My colleague Steven Yee helped with the field work and together with Norman Schuster reviewed drafts of this thesis.

Bruce Lussin of Upland Excavation, in Campbell River B.C., provided many technical suggestions for the development of the Quick Release Mechanism and the field testing.

Finally, as part of this study the author spent some time with the finite element research group of Dr. E. Ramm in Stuttgart, Germany. I would like to thank Dr. Ramm and his group for their hospitality. During my stay I met Dr. E. Luz to whom I am grateful for introducing me to the fundamentals of ambient vibration testing.

To John Galt

Chapter 1

Introduction

The research in this thesis was aimed at developing a system that can be used to determine the dynamic characteristics of bridges quickly and inexpensively. This was accomplished by developing special algorithms and functions to facilitate the automatic and speedy analysis of ambient vibration data.

The increasing traffic demands placed on the aging transportation infrastructure and increased awareness for seismic hazard retrofits has increased the need to evaluate bridges. This increased demand for bridge evaluation, coupled with tightening government budgets have warranted the need for this research.

1.1 General Problem

During the last decade, the focus of structural engineering has shifted from building new structures, to maintaining and upgrading existing structures. Provincial and state operating and construction budgets are tightening and, therefore, existing structures can not always be replaced. Structures must be retrofitted to improve their capability or increase their service life.

In 1989 an elevated portion of the I-880 Highway in Oakland, California collapsed during the Loma Prieta earthquake. This earthquake had its epicenter near Santa Cruz, California and registered 7.0 on the Richter Scale. During this event the Embarcadero Freeway in San Francisco was extensively damaged and needed to be retrofitted. This event demonstrated the

vulnerability of the aging transportation infrastructure to seismic loading. As a consequence, California, British Columbia, and many other jurisdictions have undertaken major programs to evaluate and retrofit bridges.

As part of these evaluations, structures are analyzed to determine their vulnerability using dynamic models. Analytical models are created to determine the dynamic characteristics of the bridges. These models are then used to estimate the amount of damage expected from various design level earthquakes. Retrofitting schemes are developed and implemented based on these damage estimates. For this reason, it is important to have analytical models that can accurately predict the behavior of the structure.

Generally, analytical models are based on geometric properties taken from old drawings and material properties obtained from small specimens obtained from the bridge. A series of assumptions are also made to account for the soil structure interaction and the composite behavior of structural elements of the bridge.

The effectiveness of the analytical model can be verified by dynamic testing. After a model has been verified, the predicted damage levels can be estimated with greater confidence.

In the past dynamic tests were not conducted routinely because of the large costs associated with them. In addition, detailed experimental results were generally not available until several weeks or even months after the testing was complete. A system needed to be developed that could be used to determine the dynamic properties of bridges quickly and economically so that the dynamic models used in the retrofit studies of bridges could be routinely verified.

In the field of mechanical engineering, where the verification of dynamic models through testing is widespread, there are a number of integrated systems which can handle the experimental

testing, system identification, and model refinement. These integrated systems are very sophisticated as they combine the results of several decades of research in the field. All of these systems are based on forced vibration tests which range from simple impact tests to complex test setups involving several uncorrelated random input exciters. Due to their relatively small size, most mechanical specimens can be tested in laboratories under controlled conditions.

The integrated system developed for mechanical engineering applications can not be applied economically to large civil engineering structures such as bridges. Bridges form vital links in transportation networks and, therefore, traffic shutdowns associated with forced vibration testing would be costly. Therefore routine dynamic tests of bridges must be based on ambient methods which do not interfere with the bridge's operation.

The research in this thesis is aimed at developing an ambient vibration based system to verify models quickly and inexpensively, similar to the forced vibration based systems used by mechanical engineers.

1.2 Current Research

Both forced vibration and ambient methods have been used in the past and are capable for determining the dynamic characteristics of structures.

Pull-back or quick-release tests have been used to test a variety of bridges (Douglas & Reid, 1982), (Werner, Beck & Nisar, 1992), and (Douglas, Margakis, & Nath, 1990).

Shakers have also been used to test bridges (Cantieni & Pietzko, 1993), (Yamada, Yamamoto, & Akiyama, 1988), (Bollo, Mahin, Moehle, Stephen, & Qi, 1990), (Cantieni & Pietrzko, 1993),

(Flesch & Kernbichler, 1990), and (Panzeri & Pezolli, 1989), and buildings (developed by Hudson, 1964) and used by (Jennings, Matthiesen, & Hoerner, 1972), (Nielson, 1964), and (Mathesion, Benya, & Shanman, 1970).

Impact tests have been used to measure the dynamic response of small bridges by a variety of researchers (Green & Cebon, 1993), (Agardh, 1991), and (Biswas, Pandey & Samman, 1990).

All these systems use forced vibration methods to determine the dynamic characteristics of structures. Forced vibration methods require traffic shutdowns, which are costly and disruptive. Large bridges are difficult to excite significantly with forced vibration methods.

Ambient tests have been used to test bridges (Abdel-Ghaffar, & Scanlan, 1985), (Muria-Vila, Gomez & King, 1991), nuclear power plants (Luz, Gurr-Beyer, & Stoecklin, 1984), offshore platforms (Rubin 1980), and buildings (Aktan 1992) and (Trifunac 1972). While ambient tests do not require traffic shut downs, it can take several weeks to analyse the data thoroughly. This is because an integrated approach has not been used to analyse the data.

1.3 Objectives and Outline of this Thesis

Current methods for verifying analytical models of bridges are too time consuming and costly for routine use on a variety of structures. It is evident, from the discussions above, a system needs to be developed that can determine the dynamic characteristics of bridges quickly and inexpensively.

The research described in this thesis was aimed at developing a system which would meet the following criteria.

1. The test results should be useful for optimizing analytical models of bridges.

2. The system should perform well on a large variety of bridges.

3. Preliminary results should be available shortly after the testing.

4. The testing should be relatively inexpensive.

5. The testing must be conducted without interruption to the normal operation of the bridge.

In this thesis I will describe how I developed an integrated system that uses ambient testing techniques to meet these objectives.

In Chapter 2, I will review the basic concepts of dynamic testing, analysis and model refinement. This chapter will help give you the background needed to appreciate the new concepts of ambient testing developed for this thesis. In Chapter 3, I will describe the hardware and software components of the hybrid bridge evaluation system and how the components work together. In Chapter 4, you will see how the individual custom programs were tested before they were implemented into the HBES and how the HBES was successfully used for studies on the Shipshaw Bridge, Colquitz River Bridge and the Squamish Wharf. In Chapter 5, I will summarize the main features of the HBES.

For detailed information, a number of Appendices have been included at the end of this thesis. User manuals for each of the custom programs of the HBES and a detailed description of the test data format and setups are included.

1.4 Future Applications

While the HBES will be used to measure structures and verify their analytical models, as was intended for this research, it could also be used to:

- o systematically take dynamic signatures of new bridges,
- o compare the dynamic characteristics of a bridge before and after a retrofit, or an earthquake
- o measure displacements directly.

A bridge's dynamic properties, such as natural frequencies and mode shapes, could be obtained before a new bridge is open to traffic. This information could then be stored on file and used later to see how the bridge's characteristics have changed over time. When trouble exists, you could compare the damaged bridge's characteristics to its characteristics when it was new. These methods are being used in Europe but are not currently practiced in Canada.

The system could also be used to investigate the changes in the dynamic characteristics of a structure before and after a retrofit. If the structure's dynamic characteristics are determined before and after a retrofit, you could verify the retrofit achieved the desired change in the bridge's behavior. In addition, if a structure's dynamic characteristics were determined prior to an earthquake, changes in dynamic characteristics due to seismic loading could be assessed afterwards.

A series of optically based sensors could be added to the HBES that would allow the direct measurement of displacements. Currently the system uses accelerometers to measure the ambient vibrations of the structure, however, at very low frequencies, (below 0.5 Hz), ambient acceleration records are sometimes very small and better results could be obtained by measuring the displacement time histories. Currently accurate optic based sensors are expensive but in five to ten years their use may become economical.

Chapter 2

Review of Structural Dynamic Testing Concepts

Dynamic testing is used to measure the dynamic characteristics of single and multi-degree of freedom systems. These characteristics can include: natural frequencies, mode shapes, and damping. A variety of dynamic testing methods can be used to obtain these characteristics. These methods can be separated into two categories: forced and ambient.

This chapter will help review basic concepts of structural dynamics. I will review: how to determine the dynamic characteristics of single and multi-degree of freedom systems; describe the three most popular methods of forced vibration testing: shakers, impact, and pullback tests; and show how to analyse data from ambient vibration tests. These concepts will provide the basic understanding needed to appreciate the new developments created for this thesis.

2.1 Theoretical Background on Structural Dynamics

In this section, I will review the basic concepts of single and multi-degree of freedom systems. This information will be required to understand the basic dynamic testing methods described later in this chapter.

2.1.1 Background on the Dynamics of Single Degree of Freedom Systems

The idealized single degree of freedom system (SDOF), shown in Fig. 2.1, consists of a mass m, a spring with a stiffness k, and a viscous damper c. The equilibrium equation for this

system, subject to the force $P(t)$ is:

$$m\ddot{x} + c\dot{x} + kx = P(t) \tag{2-1}$$

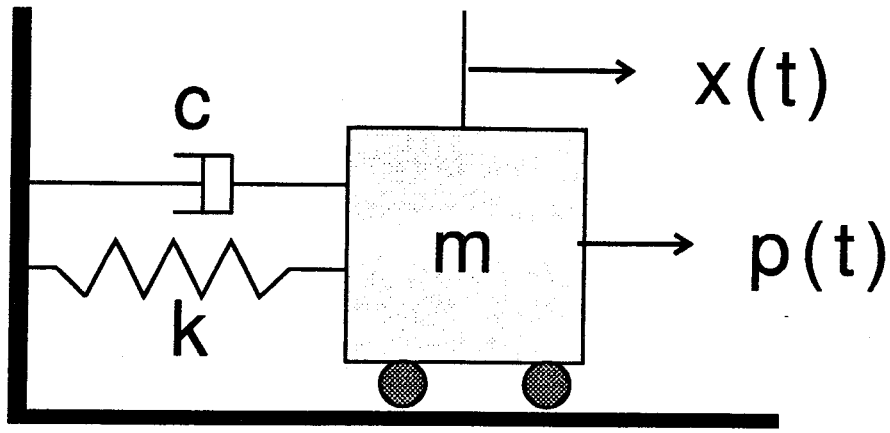

Fig. 2.1: Idealized Single Degree of Freedom Model

The displacement x(t) of this system can be calculated using the Duhamel integral shown in Eqn. (2-2).

$$x(t) = \int_o^t \frac{h(t-\tau)}{m} P(t)dt \tag{2-2}$$

where $h(t)$ is the impulse response function of the SDOF and is expressed as

$$h(t) = \frac{1}{\omega_d} e^{-\xi\omega_n t} \sin(\omega_d t) \tag{2-3}$$

in which

$$\omega_d = \sqrt{\frac{k}{m} - \left(\frac{c}{2m}\right)^2} = \sqrt{\omega_n^2 - \xi^2} \tag{2-4}$$

and

$$\xi = \frac{c}{2m\omega_n} \qquad \omega_n = \sqrt{\frac{k}{m}} \tag{2-5}$$

ξ is known as the critical damping ratio and ω_n is the undamped natural frequency of the system.

Eqn. (2-2) represents the convolution of the forcing function $P(t)$ and the impulse response function $h(t)$ divided by the mass m. Eqn. (2-2) is transformed into the frequency domain using fast Fourier transforms to avoid dealing with the convolution in the time domain. Since convolution in the time domain is equivalent to multiplication in frequency domain, the following equation can be obtained:

$$X(\omega) = H(\omega)P(\omega) \tag{2-6}$$

ω is the circular frequency in radians per second. $X(\omega)$ is the Fourier transform of the displacement $x(t)$. $P(\omega)$ is the Fourier transform of the excitation force $p(t)$. The frequency response function (FRF), $H(\omega)$, is the Fourier transform of the impulse response function $h(t)$, divided by the mass m.

For small structures, it is sometimes possible to measure the excitation force $p(t)$ and the resulting displacements $x(t)$ directly.

The FRF $H(\omega)$ can be obtained from

$$H(\omega) = \frac{X(\omega)}{P(\omega)} \tag{2-7}$$

If k, m, and c are known, $H(\omega)$ can be evaluated analytically to give:

$$H(\omega) = \frac{1}{k - \omega^2 m + i\omega c} \tag{2-8}$$

Using the frequency ratio $\beta = \omega/\omega_n$, Eqn. (2-8) can be rewritten to yield the dimensionless FRF, $H_o(\beta)$.

$$H(\beta) = \frac{1}{k} H_o(\beta) \quad \text{with} \quad H_o(\beta) = \frac{1}{1 - \beta^2 + i2\beta\xi} \tag{2-9}$$

The dimensionless FRF, $H_o(\beta)$, is complex valued and is more commonly expressed in terms of its magnitude $|H_o(\beta)|$ and phase angle $\phi(\beta)$:

$$|H_o(\beta)| = \frac{1}{k} \frac{1}{\sqrt{(1-\beta^2)^2 + (2\beta\xi)^2}} \tag{2-10}$$

$$\phi(\beta) = arctan\left(\frac{2\beta\xi}{1-\beta^2}\right) \tag{2-11}$$

Fig. 2.2 shows the magnitude and phase information of the dimensionless FRF, $H_o(\beta)$, for a variety of damping values. This figure shows that both the magnitude and phase of the FRF are very sensitive to the amount of damping. When excited near the natural frequencies ($\beta = 1$), lightly damped structures experience resonance. At resonance, the phase angle between the excitation and the response is 90°. At the low frequencies ($\beta \rightarrow 0$), all the dimensionless FRFs approach unity ($H_o(0) = 1$).

You can use the FRF, $H(\omega)$, obtained from measurements to identify the system's stiffness, mass, and damping.

Estimate the stiffness by rewriting Eqn. (2-9) to yield:

$$k = \frac{H_o(\omega)}{H(\omega)} \tag{2-12}$$

Knowing that $H_o(0) = 1$, the stiffness estimate, $\hat{k}$, can be determined as

$$\hat{k} = \frac{1}{H(0)} \tag{2-13}$$

For a structure with small damping ($\xi < 0.05$), the damped frequency ω_d and the natural frequency ω_n are approximately equal and correspond to the peak of the FRF. You can estimate the mass $\hat{m}$ of the system by rewriting the experimentally obtained natural frequency estimate $\hat{\omega}_n$, in Eqn. (2-5), from

$$\hat{m} = \frac{\hat{k}}{\omega_n^2} \tag{2-14}$$

You can estimate damping using the magnitude of the FRF at resonance $H(\hat{\omega}_n)$. Using the fact that $\beta = 1$ at resonance, you can rewrite Eqn. (2-9) to estimate damping.

$$\hat{\xi} = 2 * \hat{k} * H(\hat{\omega}_n) \tag{2-15}$$

The techniques presented above are very basic. Many sophisticated methods have been developed to identify dynamic characteristics of structures, but are beyond the scope of this discussion. For information on these methods, refer to Maia (1990) and Allemang (1983).

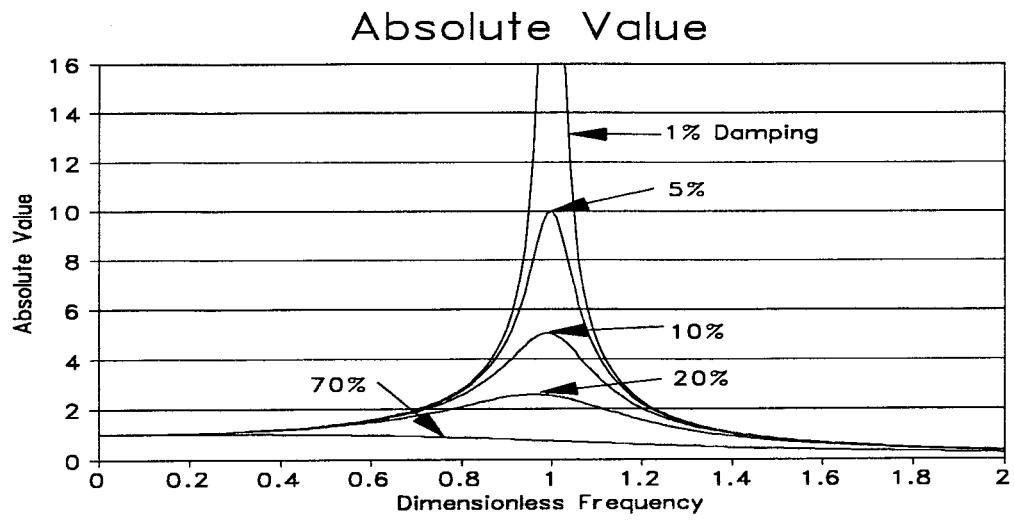

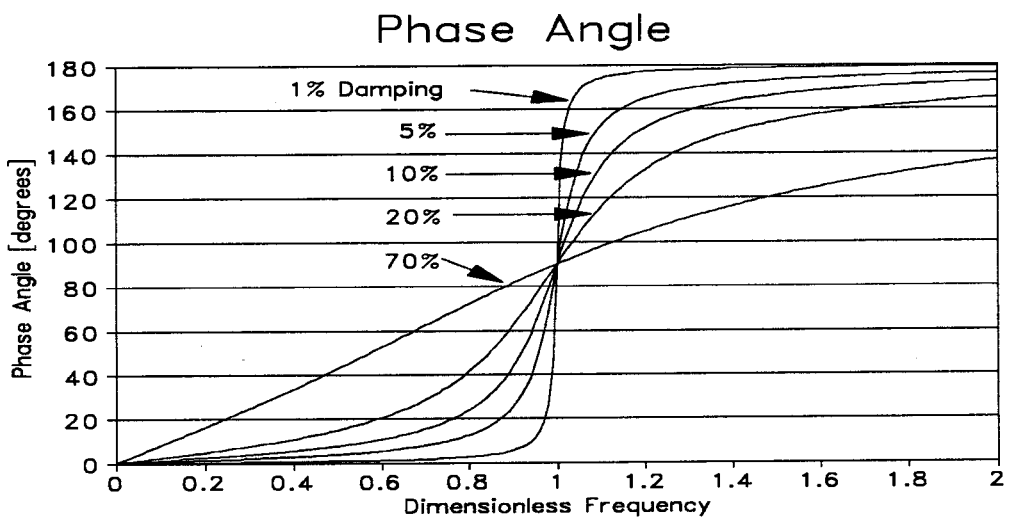

Fig. 2.2 : Absolute Value and Phase Angle of the Dimensionless Frequency Response Function

2.1.2 Background on the Dynamics of Multi Degree of Freedom Systems

The concepts introduced for single degree of freedom systems can be expanded to multi-degree of freedom (MDOF) systems. I will use the three degree of freedom model shown in Fig. 2.3 to illustrate multi-degree of freedom concepts.

The MDOF system in Fig. 2.3 represents a three story structure with masses m concentrated at each story level. The stories are interconnected by columns with a stiffness k and dampers with a viscous damping constant c. This three degree of freedom system has three natural frequencies and three corresponding modes of vibration. These frequencies and mode shapes are characteristics of the system which can be used to describe the system's response to arbitrary dynamic loading. Therefore, it is important to compute these frequencies and mode shapes analytically and to verify them by experimental means.

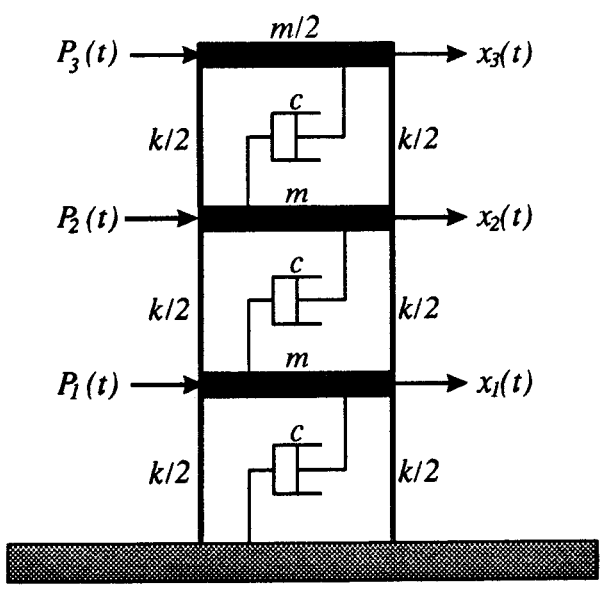

Fig. 2.3: Three Degree of Freedom Example

The equation of motion for the three degree of freedom example, above, in matrix form is:

$$\begin{bmatrix} 2k & -k & 0 \\ -k & 2k & -k \\ 0 & -k & k \end{bmatrix}\begin{Bmatrix} x_1 \\ x_2 \\ x_3 \end{Bmatrix}+\begin{bmatrix} 2c & -c & 0 \\ -c & 2c & -c \\ 0 & -c & c \end{bmatrix}\begin{Bmatrix} \dot{x}_1 \\ \dot{x}_2 \\ \dot{x}_3 \end{Bmatrix}+\begin{bmatrix} m & 0 & 0 \\ 0 & m & 0 \\ 0 & 0 & 0.5m \end{bmatrix}\begin{Bmatrix} \ddot{x}_1 \\ \ddot{x}_2 \\ \ddot{x}_3 \end{Bmatrix}=\begin{Bmatrix} p_1 \\ p_2 \\ p_3 \end{Bmatrix} \tag{2-16}$$

Defining the symbols $[K]$, $[C]$, and $[M]$ as the stiffness, damping, and mass matrices, Eqn. 2-16 can be written in more compact notation:

$$[K]\{x_i(t)\}+[C]\{\dot{x}_i(t)\}+[M]\{\ddot{x}_i(t)\}=\{p(t)\} \tag{2-17}$$

Eqn. 2-17 represents a coupled second order system of equations which can be uncoupled using eigenvectors φ_j and eigenvalues λ_j. If the system of equations satisfies the identity in Eqn. 2-18, given by Caughey and Kelly (1965), the eigenvectors will be identical to those of the undamped system. This solution procedure is well established and is described in detail by Clough & Penzien (1975) and Weaver, Timoshenko, & Young (1990).

$$[C][M]^{-1}[K]=[K][M]^{-1}[C] \tag{2-18}$$

The real parts of the eigenvalues λ_j correspond to the square of the natural frequencies ω_j. The eigenvectors used to uncouple the system of equations represents the mode shapes associated with the free vibration of the system at each natural frequency ω_j. If you assume the three degree of freedom example, above, has a stiffness $k = 1MN/m$, mass $m = 1000Kg$, and damping $c = 300N\sec/m$, you can compute the following natural frequencies and mode shapes:

$$\omega_j=\begin{Bmatrix} \sqrt{2-\sqrt{3}} \\ \sqrt{2} \\ \sqrt{2+\sqrt{3}} \end{Bmatrix}*\sqrt{\frac{k}{m}} \qquad \varphi_1=\begin{Bmatrix} 1 \\ \sqrt{3} \\ 2 \end{Bmatrix} \qquad \varphi_2=\begin{Bmatrix} 1 \\ 0 \\ -1 \end{Bmatrix} \qquad \varphi_3=\begin{Bmatrix} 1 \\ -\sqrt{3} \\ 2 \end{Bmatrix}$$

$$f_j=\begin{Bmatrix} 2.605 & Hz \\ 7.118 & Hz \\ 9.723 & Hz \end{Bmatrix}$$

where $f = \omega/2\pi$ is the frequency in cycles per second (Hz). The mode shapes are illustrated in Fig. 2.4.

The mode shape vectors of a MDOF have the following orthogonality characteristics:

$$\{\varphi_j\}^T [M] \{\varphi_j\} = M_j \tag{2-19}$$

$$\{\varphi_j\}^T [M] \{\varphi_i\} = 0$$

$$\{\varphi_j\}^T [K] \{\varphi_j\} = K_j$$

$$\{\varphi_j\}^T [K] \{\varphi_i\} = 0$$

Where M_j is the modal mass and K_j is the modal stiffness associated with mode j.

You can determine the displacements of the n degree of freedom system using:

$$\{x(t)\} = \sum_{j=1}^{j=n} \{\varphi_j\} y_j(t) \tag{2-20}$$

You can obtain the normalized coordinates $y_j(t)$ by solving the uncoupled single degree of freedom systems shown in Eqn. 2-21.

$$M_j \ddot{y}_j(t) + C_j \dot{y}_j(t) + K_j y_j(t) = P_j(t) \tag{2-21}$$

where $P_j(t)$ is the nodal excitation given by:

$$P_j = \{\varphi_j\}^T \{p(t)\} \tag{2-22}$$

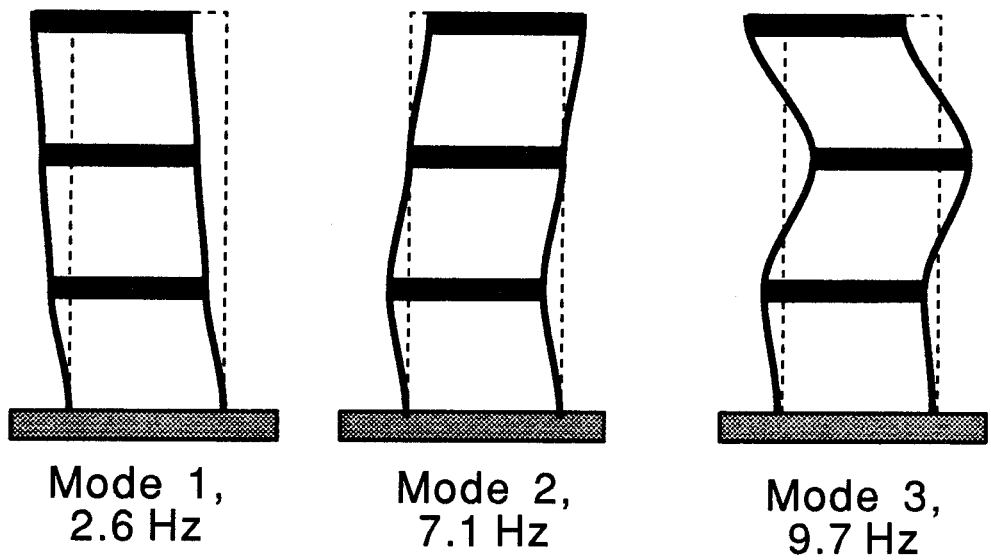

Fig. 2.4: Mode Shapes and Natural Frequencies of the Three Degree of Freedom Example

As you can see from the equations above, the behaviour of a MDOF system is described by a series of SDOF systems with associated time invariant mode shapes. Each of these SDOF systems has associated mass M_j, damping C_j and stiffness K_j as well as natural frequencies ω_j and mode shapes $\{\varphi_j\}$.

2.2 Forced Vibration Testing Methods

Forced vibration tests are performed to determine the dynamic characteristics of single and multi-degree of freedom systems. In these tests, controlled forces are applied to a structure to induce vibrations. By measuring the structure's response to these known forces, you can determine the structure's dynamic properties.

You can apply controlled excitation forces to a structure using several different methods. The three most popular methods are shaker, impact, and pullback tests. These methods are briefly described in the following sections.

2.2.1 Shaker Tests

Shakers are used to apply forces to structures in a controlled manner to excite them dynamically.

A shaker must produce sufficiently large forces to effectively excite a bridge in the frequency range of interest. For large bridges, the frequencies of interest are commonly less than 1Hz. At such low frequencies shakers can not provide very large forces. This is illustrated in Eqn. 2-23 which gives the sinusoidal forcing function for shakers with counter rotating eccentric masses.

$$F(t) = m_e r \omega_e^2 \sin(\omega_e t) \tag{2-23}$$

where m_e is the eccentric mass, r is the eccentricity and ω_e is the excitation frequency.

Eqn. 2-23 shows the force amplitude is proportional to the frequency squared. While you can produce considerable forces with relatively small shakers at high frequencies, it is difficult to produce forces large enough to excite a structure at low frequencies. Eqn. 2-24 shows that to produce a sinusoidal forcing function $F(t)$ with an amplitude of 10kN at 0.2Hz using a shaker with an eccentricity of 1 m, you would require an eccentric mass of more than 6 tonnes.

$$m_e = \frac{F_{\max}}{r\omega_e^2} = \frac{F_{\max}}{r4\pi^2 f^2} = \frac{10000}{1*4\pi^2 0.2^2} Kg = 6332 Kg \tag{2-24}$$

While it is possible to construct shakers this size (Yamada et. al. 1988), such massive low frequency shakers are expensive to construct, transport, and mount. Because one of the objectives of this thesis was to develop a testing system for large bridges that is economical to acquire and use, shakers were not implemented in the HBES.

2.2.2 Impact Tests

Impact testing is another method of forced vibration testing. Mechanical engineers commonly use impact tests to identify the dynamic characteristics of machine components and small assemblies.

The test object is instrumented with accelerometers and is struck with a hammer that is instrumented with a force transducer. The impact force and acceleration response time histories are then used to compute frequency response functions (FRFs). As reviewed earlier in section 2.1, you can determine the natural frequencies, mode shapes, and damping values of the structure from these FRFs.

While impact testing has been used by a variety of researchers to evaluate small bridges (Agardh 1991), (Green & Cebon 1993), a number of problems occur when this method is used to test larger bridges. To excite lower modes of large bridges sufficiently, the impact hammer needs to be very large. Not only is it difficult to instrument large impact hammers with force transducers, large hammers could also cause considerable local damage to the bridge.
Impact testing was not implemented in the HBES because one of the objectives of this thesis is to develop a testing system which can be used effectively on large bridges.

2.2.3 Pullback Tests

Pullback testing is another method used for forced vibration testing. This method generally involves displacing a structure and quickly releasing it, causing the structure to vibrate freely. Hydraulic rams, cables, bulldozers, tug boats, or chain blocks can be used to apply loads that produce a static displacement of the structure. When the load is released, the free vibrations of the structure are recorded as the structure tries to return to its position of static equilibrium. The results from quick release tests can be used to determine natural frequencies, mode shapes, and damping values for the structure's principal modes.

Eqn. 2-25 characterizes the free vibration displacement response of a SDOF system.

$$x(t) = x_o e^{-\xi\omega t}\left(\frac{\xi}{\sqrt{1-\xi^2}}\sin\omega_D t + \cos\omega_D t\right) \tag{2-25}$$

You can calculate the acceleration of the system by differentiating Eqn. 2-25 twice.

$$\ddot{x}(t) = \omega^2 x_o e^{-\xi\omega t}\left(\frac{\xi}{\sqrt{1-\xi^2}}\sin\omega_D t - \cos\omega_D t\right) \tag{2-26}$$

From these expressions you can see that the level of acceleration for a given initial displacement depends on the natural frequency of the system. You can compute the acceleration from a pullback test for any system if you know the initial displacement x_o. Fig. 2.5 shows anticipated acceleration levels for initial displacements of 1 mm, 10 mm, 0.1 m and 1 m. You can use Fig. 2.5 to predict the response of dynamic systems to pullback tests. If a SDOF system with a natural frequency of 1Hz is pulled back 10mm, the anticipated free vibration acceleration is 0.04 g. If the same displacement is applied to a SDOF system with a natural frequency of 5 Hz, the acceleration is 1.0 g.

The same concepts can be used to determine the response of a MDOF system. If the initial deformation of a structure at a particular location is made up of 10 mm associated with the first mode ($\omega_1 = 1Hz$) and 1 mm associated with the second mode ($\omega_2 = 5Hz$), the recorded acceleration at this location will be a combination of two responses. The first response will be associated with the first natural frequency and will have a maximum amplitude of approximately 0.04 g, while the response associated with the second mode will have a maximum amplitude of approximately 0.1 g. This example illustrates how the acceleration time histories obtained from a pullback test on a MDOF system have significant accelerations associated with higher modes.

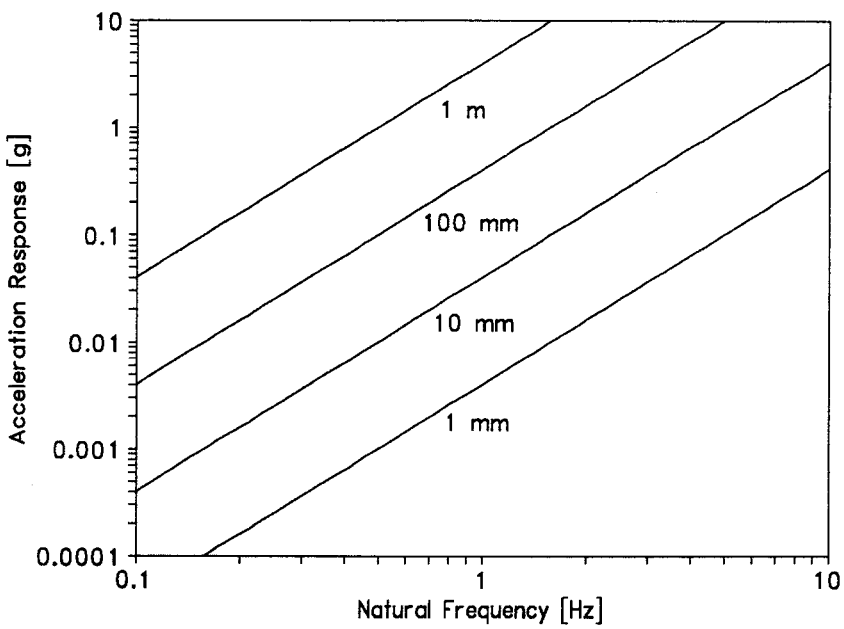

Fig. 2.5: Acceleration Response of a Undamped SDOF Systems to Initial Displacements.

The analysis of pullback test data obtained from the Colquitz River Bridge described in section 4.3.5.2 illustrates some of these concepts in more detail.

Before conducting a pullback test, you must consider how you are going to initially displace the structure. Access, jacking locations, budgets, and jurisdictions vary from one structure and pullback test to another. To completely control the forces applied to the bridge, traffic can not be allowed on the structure during forced vibration tests. Because one of the objectives of this thesis was to develop a system for the dynamic identification of a variety of bridges, the pull back method was not selected as the primary means for determining dynamic characteristics of bridges.

To avoid the costly traffic shut downs of forced vibration methods and to analyse data quickly, an integrated system based on ambient vibration techniques was developed for this thesis.

For more information on the various dynamic testing methods for full scale structures, refer to Hudson (1977). For algorithms used to determine the dynamic characteristics of structures using forced vibration methods, refer to Ewins (1984).

2.3 Ambient Vibration Testing Method

When ambient vibration testing, a structure is excited by wind, micro tremors, machinery, and traffic. Unlike forced vibration testing, you do not control the force that is applied to vibrate the structure. Natural frequencies and mode shapes are obtained by measuring the vibrations of the structure simultaneously at several locations on the structure. The basic concepts of ambient vibration testing are presented in the following sections. For additional information on the theoretical derivation, refer to Diehl (1991) and Luz (1986,1987).

2.3.1 Theoretical Background on Ambient Vibration Testing

You can obtain reliable estimates of modal frequencies and shapes when you analyse ambient vibration data, provided the following conditions are met:

1. **Linearity:**

   The structure behaves as a linear system. This means that a linear combination of individual force inputs will result in the same linear combination of the corresponding individual responses.

2. **Excitation**:

   It is assumed that the structural modes of interest are significantly excited. This means that the power spectrum of the excitation should be continuous for the frequency range of interest.

3. **Modes Well Separated and Lightly Damped**

   It is assumed that the modes of interest are well separated and lightly damped (less than 5% of critical damping). Thus the response at a natural frequency is dominated by the corresponding mode shape and the peaks in the power spectrum can be used to identify natural frequencies.

4. **Classical Damping:**

   If the structure is classically damped (i.e. satisfying Eqn. 2-18) and, therefore, only has real valued modes, then at resonance the signals from two degrees of freedom are either perfectly in phase or out of phase. Should this condition not be satisfied the data can still be used to identify mode shapes. However, the discussion of complex modes is beyond the scope of this thesis, since most numerical analysis of bridge for retrofit studies currently only address real modes.

The ambient vibrations at any location of a structure can be measured as displacement $x(t)$, velocity $\dot{x}(t)$, or acceleration $\ddot{x}(t)$. As was shown in Eqn. 2-20 in section 2.1.2, the displacements of the structure can be expressed as a linear combination of the mode shapes. In expanded form this equation looks like:

$$\{x(t)\} = \{\varphi_1\}y_1(t) + \{\varphi_2\}y_2(t) + \ldots + \{\varphi_n\}y_n(t) \tag{2-27}$$

For convenient manipulation, you can transfer this equation into the frequency domain to yield:

$$\{X(\omega)\} = \{\varphi_1\}Y_1(\omega) + \{\varphi_2\}Y_2(\omega) + \ldots + \{\varphi_n\}Y_n(\omega) \tag{2-28}$$

Where the normalized coordinates $Y_j(\omega)$ are defined as:

$$Y_j(\omega) = H_j(\omega)P_j(\omega) \tag{2-29}$$

and the frequency response function of the jth mode $H_j(\omega)$ is given by

$$H_j(\omega) = \frac{1}{K_j - \omega^2 M_j + i\omega C_j} \tag{2-30}$$

Using equations 2-26 and 2-28, and the fact $\ddot{X}(\omega) = \omega^2 X(\omega)$, you can express the accelerations of the structure in the frequency domain as:

$$\{\ddot{X}(\omega)\} = \omega^2[\{\varphi_1\}H_1(\omega)P_1(\omega) + \{\varphi_2\}H_2(\omega)P_2(\omega) + \ldots + \{\varphi_n\}H_n(\omega)P_n(\omega)] \tag{2-31}$$

An individual complex valued acceleration response $\ddot{X}_i(\omega)$ can be expressed as:

$$\ddot{X}_i(\omega) = \omega^2[A_{1i}H_1(\omega) + A_{2i}H_2(\omega) + \ldots + A_{ni}H_n(\omega)] \tag{2-32}$$

where $A_{ji} = \varphi_{ji}P_j(\omega)$

Using the three degree of freedom system introduced in section 2.1.2, as an example, and setting $A_{ji} = 1$ for all js, you can compute the magnitude of the individual acceleration response functions $\omega^2 |H_j(\omega)|$ and their combination $|\ddot{X}_i(\omega)|$. By plotting the combined response

$|\ddot{X}_i(\omega)|$ and the first two individual acceleration response functions, $|\omega^2 H_1(\omega)|$ and $|\omega^2 H_2(\omega)|$, (see Fig. 2.6), you can clearly see three peaks corresponding to the damped frequencies of the system. This indicates the natural frequencies of a structure can be estimated using the Fourier transforms of ambient vibration acceleration records.

Fig. 2.6 also shows that at the natural frequencies ω_j, the acceleration response $|\ddot{X}_i(\omega_j)|$ is dominated by the $|\omega_j^2 H_j(\omega_j)|$ term. This means you can estimate the acceleration response at the natural frequencies using:

$$\ddot{X}_i(\omega_j) \cong \varphi_{ji}\omega_j^2 H_j(\omega_j) P_j(\omega_j) \tag{2-33}$$

If two acceleration records obtained simultaneously at location a and b are used, you can estimate the modal amplitude ratio of the jth mode for the two locations using:

$$\frac{\ddot{X}_a(\omega_j)}{\ddot{X}_b(\omega_j)} \cong \frac{\varphi_{ja}\omega_j^2 H_j(\omega_j) P_j(\omega_j)}{\varphi_{jb}\omega_j^2 H_j(\omega_j) P_j(\omega_j)} = \frac{\varphi_{ja}}{\varphi_{jb}} \tag{2-34}$$

You can then determine the mode shapes experimentally using the ratios of the Fourier amplitudes at natural frequencies. However, it is important to keep in mind that this estimate can only be made if the natural frequencies are well separated and lightly damped such that the response at a natural frequency is indeed dominated by the corresponding mode shape.

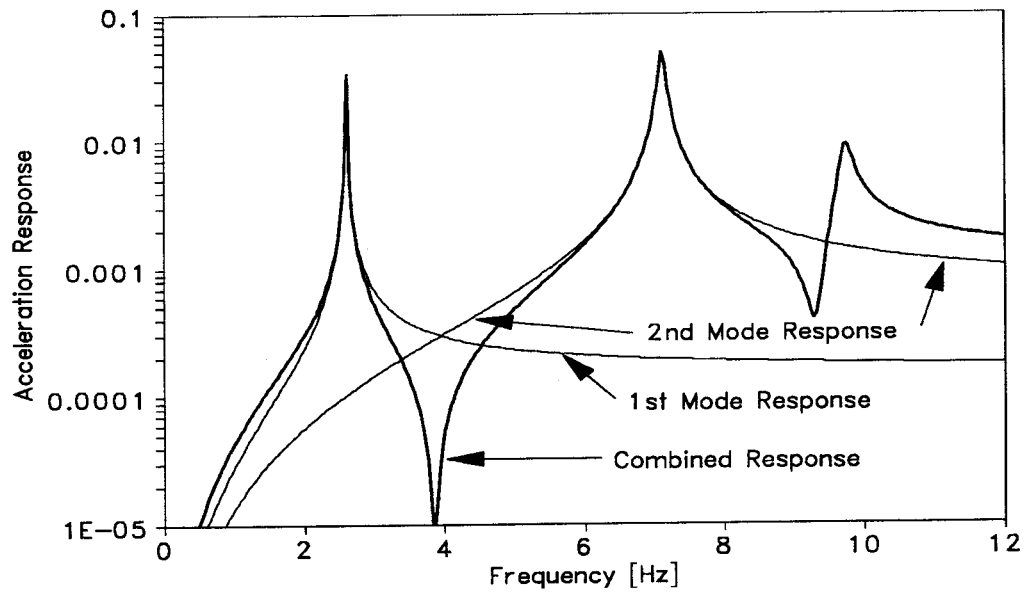

Fig. 2.6: Roof Acceleration Response of a Three Degree of Freedom System Subject to White Noise Excitation

2.3.2 Analyzing Ambient Vibration Data

This section briefly describes how natural frequencies, mode shapes and damping were traditionally estimated, using ambient vibration measurements. In chapter 3 you will see how these techniques were refined and incorporated into the hybrid bridge evaluation system that was developed for this thesis.

2.3.2.1 Estimating Natural Frequencies

Natural frequencies ω_j of structures are determined from the peaks of the auto spectra or power spectral density (PSD) of an ambient vibration acceleration record. This PSD is defined as

$$G_{\ddot{i}\ddot{i}}(\omega) = \ddot{X}_i(\omega)\ddot{X}_i^*(\omega) \tag{2-35}$$

$G_{\ddot{i}\ddot{i}}(\omega)$ corresponds to the square of the magnitude of the complex valued acceleration response in Eqn. (2-32) and $\ddot{X}_i^*(\omega)$ is the complex conjugate of $\ddot{X}_i(\omega)$. Fig. 2.7 shows the PSD of the top mass for the three degree of freedom system discussed in section 2.3.1. In this figure the PSD has local peaks where $\omega = \omega_d$ and, for small damping values, $\omega_d \cong \omega_n$. This indicates you can estimate the natural frequencies, $\hat{\omega}_n$, from PSD plots. To estimate natural frequencies more accurately, you can use the averages of PSDs for a number of time histories.

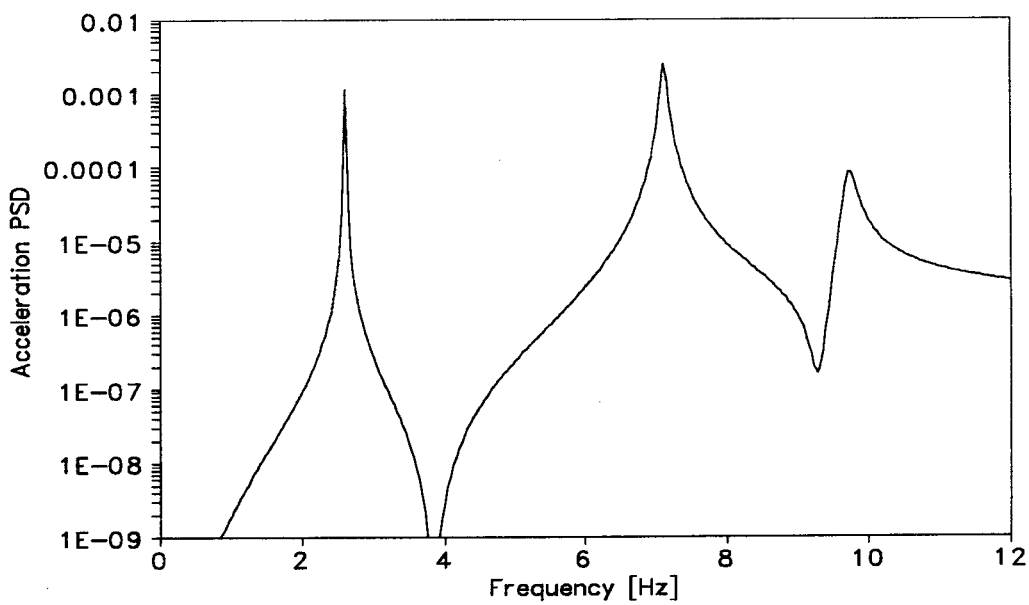

Fig. 2.7: Acceleration PSD of the Top Mass of the Three DOF System Subject to White Noise Excitation

2.3.2.2 Estimating Mode Shapes

The mode shapes estimates $\hat{\varphi}_j$ associated with the natural frequency estimates $\hat{\omega}_j$ are determined using a series of simultaneously recorded ambient vibration time histories $x_j(t)$. You can compute the transfer functions $T_{il}(\omega)$ between the Fourier transform of individual signals using:

$$T_{il}(\omega) = \frac{\ddot{X}_l(\omega)}{\ddot{X}_i(\omega)} = \frac{\ddot{X}_l(\omega)\ddot{X}_i^*(\omega)}{\ddot{X}_i(\omega)\ddot{X}_i^*(\omega)} \tag{2-36}$$

This complex valued transfer function can also be expressed in terms of its magnitude $|T_{il}(\omega)|$ and phase angle $\phi_{il}(\omega)$. Using the approximation given in Eqn. 2-33, you can estimate the absolute value of the ratio $|r_{j_{il}}| = |\varphi_{jl}/\varphi_{ji}|$ of the jth modal amplitudes between coordinates i and l using:

$$|r_{j_{il}}| \cong |T_{il}(\omega_j)| \tag{2-37}$$

The sign of the modal ratio, $r_{j_{il}}$, is determined from the phase angle $\phi_{il}(\omega_j)$. When the phase angle is near 0°, movements of the degrees of freedom i and l are in phase and the modal ratio is positive. On the other hand, when $\phi_{il}(\omega_j)$ is near 180°, the two motions of the coordinates are perfectly out of phase and the modal ratio is negative.

Better estimates of the modal ratio are obtained if transfer functions averaged over several data segments $\overline{T_{il}(\omega)}$ are used. In addition to the transfer functions, average cross spectra $\overline{G_{il}(\omega)}$ and coherence functions γ^2 are used to interpret ambient vibration data. The cross spectrum $G_{il}(\omega)$ of two signals is used to compute the coherence function. The cross spectrum is defined as:

$$G_{il}(\omega) = \ddot{X}_i^*(\omega)\ddot{X}_l(\omega) \tag{2-38}$$

Because the cross spectra is a measurement of the amount of energy in both signals, peaks in the cross spectra correspond to natural frequencies of the structure.

The coherence function, $\gamma_{il}^2(\omega)$, is a measure of the likeness of two signals. It can be used to evaluate the amount of noise in the data. The coherence function, between signals i and l is computed in the frequency domain as:

$$\gamma_{il}^2(\omega) = \frac{\overline{G_{il}(\omega)}^2}{\overline{G_{ii}(\omega)}\ \overline{G_{ll}(\omega)}} \tag{2-39}$$

A maximum coherence value of 1 indicates that there is no noise in the data. Small coherence values indicate that the two signals are uncorrelated and/or the data is contaminated with noise. If the noise in the data is assumed to have white noise characteristics at natural frequencies, where the signal is strong, the signal to noise ratio is low and the coherence value is high. This means the coherence should be close to 1 at natural frequencies.

Traditionally the magnitude and phase of the transfer functions, cross spectral density functions, and coherence functions of all pairs of ambient vibration records were computed. These functions were then interpreted manually and the natural frequencies and mode shapes were determined. Because of the large number of functions involved, the manual data interpretation process was very time consuming. Refinements to this procedure needed to be developed and implemented so ambient vibration data could be analyzed on site. These refinements were developed for this thesis and are described in section 3.3.2.1.

2.3.2.3 Estimating Damping

As was demonstrated in section 2.3.1, the peaks of the Fourier transform of an acceleration record can be approximated near resonance by the SDOF response. You can then use this approximation to estimate modal damping. You can estimate modal damping using a half power band width approach (Clough and Penzien 1975) or peak fitting routines (Brownjohn

1988).

In 1988 Brownjohn presented a detailed study of factors contributing to the error of damping estimates. This study shows that damping estimates based on records from the same ambient vibration study can vary by more than 100% depending on the analysis technique used.

In 1992 Okauchi, Miyata, Tatsumi & Kiyota presented results from tests on three suspension bridges in Japan. These test were designed specifically to identify the damping values of the lower modes of the bridges. The results of this study show that damping values depend on the amplitude of the excitation as well as the temperature of the structure. In particular, the damping values doubled for some of the modes when the excitation amplitude was doubled. At larger amplitudes (up to 300 mm) the damping values approached approximately constant values. At the small amplitudes associated with ambient vibration testing, all of the damping estimates showed significant amplitude dependence. Also, for one of the modes of the Ohshima bridge, Okauchi et al. reported a 50% reduction in the damping value due to a temperature increase of approximately $20°C$.

As the results by Okauchi et al. have pointed out, damping is not constant at small vibration levels which are representative of ambient vibrations. Because ambient vibration theory assumes that the structure is linear, i.e. mass, stiffness, and damping are constant, the damping can not be reliably estimated using ambient vibration techniques. Because the damping can not be reliably estimated using ambient vibration techniques, damping estimation techniques were not incorporated into the dynamic testing system developed for this thesis.

2.3.3 Practical Considerations of Ambient Testing and Model Refinement

The previous sections outlined the theoretical background for ambient vibration testing and introduced numerical methods used to obtain the natural frequencies and mode shapes of a structure from experimental data. This section will introduce the practical aspects of ambient vibration testing and data interpretation. Subsequently the method used to refine the analytical model of the structure is briefly described.

2.3.3.1 Practical Considerations of Ambient Vibration Testing

When ambient vibration techniques are used to determine the frequencies and mode shapes of bridges, several factors must be considered. These are:

Low Excitation Levels

It is very difficult to obtain good vibration records when the ambient excitation is very small or the structure is very stiff. In these cases, you can obtain the best results by using transducers that are very sensitive or by providing random excitations at higher levels.

Seized Bearings and Expansion Joints

The movements associated with ambient vibrations are often so small that some elements of a structure, such as sliding bearings, pins, and expansion joints, do not permit movement. In these cases, the structure will exhibit different dynamic characteristics at low vibration levels than at larger vibration levels. This behaviour was observed during an ambient vibration study of Lions Gate Bridge in Vancouver (Buckland, 1990). You can sometimes overcome this

problem using forced vibration testing. You can also confirm the fixity of the expansion joints and bearings by ambient measurement and then temporarily adjust the bridge's dynamic model to reflect the immobility of the expansion joints.

Dominant Excitation at Specific Frequencies

If rotating machinery is attached to the structure or is operated nearby at a particular frequency, then the structure will responded at those frequencies. This causes peaks in the auto spectra which do not correspond to the natural frequencies. It is important to determine which dominant frequencies are caused by the operating machinery, to account for the corresponding peaks in the PSD. Otherwise, these peaks may be falsely identified as natural frequencies of the structure.

Influence of Vertical Excitation

Vehicle traffic is the main source of ambient excitation on bridges. The resulting excitation is dominant in the vertical direction, allowing the vertical modes to be readily identified. Many of these vertical modes also have lateral motions associated with them. The transverse components of vertical modes cause significant peaks in the PSDs associated with lateral signals, because the transverse and longitudinal modes are not significantly excited by the traffic. Therefore, it is important to identify the vertical modes of bridges clearly so their influence on the lateral PSDs can be considered when determining lateral modes.

Added Mass Effect

The added mass of bridge traffic may make it difficult to identify higher modes using ambient vibration tests. When traffic is used to excite bridges, you are measuring the modes and frequencies of the structure combined with vehicles causing the excitation. While the vehicles' mass do not usually affect the lower modes of the structure which have large modal masses,

they occasionally affect higher modes which have much smaller modal masses. Ambient vibration measurements should be taken when bridge traffic is light if the added mass of vehicles on the bridge makes it difficult to identify the structure's modes.

2.3.3.2 Analytical Model Refinement

After you have determined the dynamic characteristics of a bridge experimentally using ambient vibration data, you can refine the structure's analytical model. There are two general ways to refine an analytical model: automatically and manually.

Flesch and Kernbichler (1990b) reported that manually manipulating key parameters, such as mass and stiffness values of major members of the analytical model, quickly leads to sensible refinements. The key parameters are selected and varied by the user until a satisfactory correlation between the analytical and experimental characteristics is achieved. In the process of manually refining a series of dynamic models of bridges, the user gains valuable modeling experience and insight into the dynamic behaviour of structures. The experience can be utilized later to create appropriate models for other bridges.

In the field of mechanical engineering, a variety of algorithms have been developed to refine mathematical models automatically. The experimental results used for these algorithms are usually obtained from forced vibration tests. These tests can employ multiple shakers and systems capable of simultaneously recording data from several hundred sensors (Allemang, 1993), (Lally & Severyn, 1993). During these tests, the nature of the excitation can be carefully controlled and environmental influences can usually be eliminated.

Also, in contrast to forced vibration tests performed by mechanical engineers, data obtained from ambient vibration tests of large bridges is generally not as extensive for economic reasons.

Therefore, model refinement based on the manual modification of key parameters was incorporated into the bridge evaluation system developed for this thesis. For more information on the HBES's model refinement procedure, refer to section 3.3.5.

Chapter 3

Development of the Hybrid Bridge Evaluation System

The research described in this thesis was aimed at developing a system which would meet the following criteria.

1. The testing must be conducted without interruption to the normal operation of the bridge.

2. The system should perform well on a large variety of bridges.

3. Preliminary results should be available shortly after the testing.

4. The testing should be relatively inexpensive.

5. The test results should be useful for optimizing analytical models of bridges.

To meet these objectives, a dynamic testing system known as the Hybrid Bridge Evaluation System (HBES) that uses ambient vibration techniques was created.

This system combines commercially available hardware with a series of custom developed programs to accelerate and optimize acquiring and reducing ambient data. Also, part of the software can be used to quickly alter parameters to match the analytical model with experimental results.

In the following sections, I will briefly describe the HBES's hardware and software. I will also describe tests conducted on the Second Narrows Bridge shortly after this research program began. The lessons learned from these tests helped specify and assemble the HBES hardware and software.

3.1 Vibration Measurements on Second Narrows Bridge

In February and March of 1991, at the beginning of this research program, a series of tests were conducted on the Second Narrows Bridge. These tests were performed, in conjunction with a bridge evaluation project by the consulting company Buckland and Taylor Ltd. from North Vancouver, B.C., to identify the natural frequencies of the bridge.

In this section, I will describe how the natural frequencies of the Second Narrows Bridge were obtained. You will see how these tests were used to:

- Evaluate the suitability of available sensors for ambient vibration measurements.
- Determine the software requirements for efficient on-site ambient vibration analysis.
- Gain experience in planning and conducting tests of large structures.

3.1.1 Background on the Second Narrows Bridge

The Second Narrows Bridge, shown in Fig. 3.1, is located in Vancouver B.C.. It carries six lanes of traffic of the Trans Canada Highway across the Burrard Inlet.

The main span of the bridge is a cantilever deck truss with a total span of 335.3 m. It is comprised of two 116.5 m cantilevers and one 102.3 m suspended span. The anchor arm spans are 142.3 m on the north side and 142 m on the south side. An elevation view of the main span of the bridge is shown in Fig. 3.2.

The deck is made of a 0.13 m thick light weight concrete slab with a 0.05 m high density concrete overlay. The deck acts compositely with stringers at 1.8 m centers spanning between floor beams at approximately 13.7 m to 18.3 m spacing. The floor beams are supported by two haunched steel trusses.

On the north approach, four steel trusses span over the water from pier 10 to pier 14. North of pier 10 a series of concrete spans which where not tested as part of this study connect the structure to the north shore. The individual truss spans are approximately 86 m long and rise on a grade of 5 % from north to south. Each simply supported truss has an upper chord, which supports floor beams, stringers, and a cast in place deck.

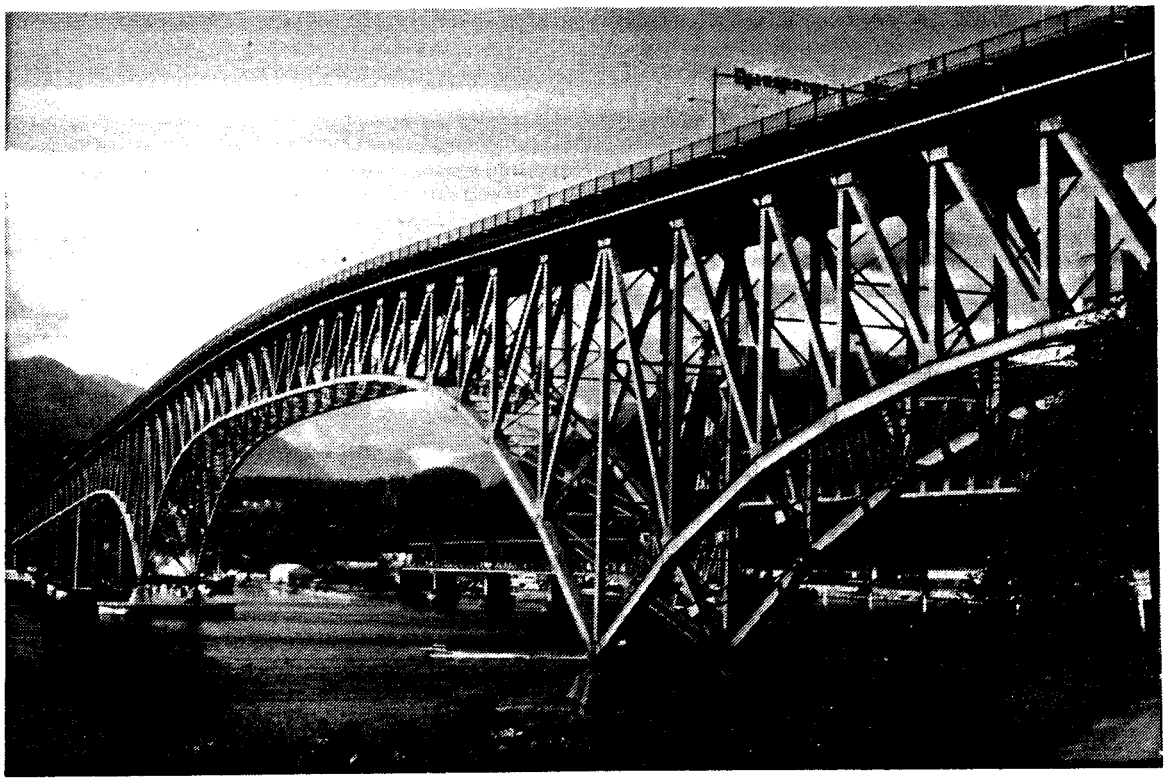

Fig. 3.1: View of the Second Narrows Bridge.

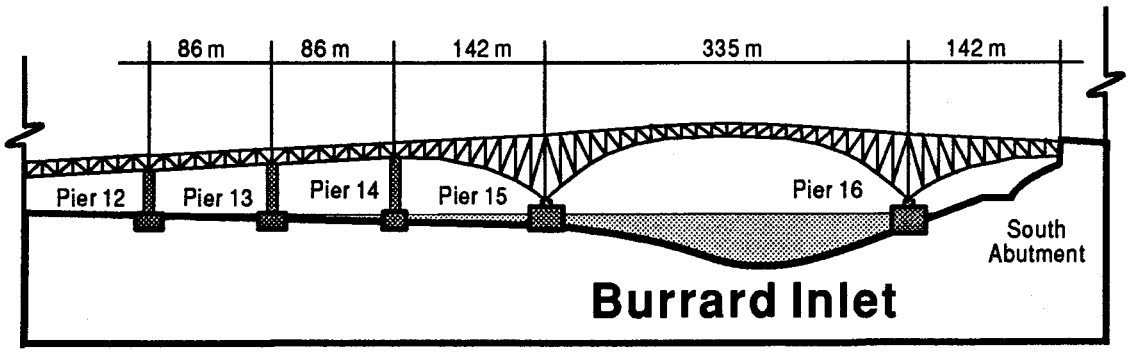

Fig. 3.2: Elevation View of the Second Narrows Bridge.

3.1.2 Vibration Test Data from Second Narrows Bridge

All of the vibration measurement equipment available at the Earthquake Laboratory of the Department of Civil Engineering was used to measure the ambient vibrations of the Second Narrows Bridge. For individual acceleration time histories and the corresponding power spectral densities the reader is refered to appendix A.

3.1.3 Data Analysis

Because the HBES software was not developed when the measurements were taken, a dual channel spectral analyzer (model: Zonic AND 3525) was used to analyse the measurements in the field. While the analyzer had many built in features, it did not contain some of the fundamental signal processing functions needed to process ambient vibration data and could only be used to inspect the data quickly. The computation of frequency domain functions was too time consuming to be done routinely in the field because the analyzer did not have an optional math processor. Therefore, the data had to be inspected and analysed in the office after the field work was completed. Any problems associated with individual readings did not become apparent until after the field testing was complete.

Early versions of the HBES software were used to compute the PSDs for all the recorded signals. The peaks in these PSDs were then used to identify possible natural frequencies of the structure. The natural frequencies could not be determined with great certainty as they could not be verified visually, because the corresponding mode shapes could not be computed from the recordings.

3.1.4 Results from Second Narrows Bridge Test

Although the testing equipment available at the time of the test was not suited for measuring the ambient vibrations, a limited amount of information was obtained and the dominant natural frequencies were identified.

The first three dominant frequencies identified from the transverse measurements of the main span of the Second Narrows Bridge were 0.26 Hz, 0.41 Hz, and 0.71 Hz. The first three dominant frequencies determined from vertical measurements of the main span were 0.38 Hz, 0.66 Hz, and 0.86 Hz. The vertical measurements of the approach trusses were used to establish the first three dominant frequencies as 0.45Hz, 0.65 Hz and 0.95 Hz.

The results of these measurements are described in more detail in a report to Buckland and Taylor (Felber & Stiemer, 1991).

3.1.5 Conclusions from the Second Narrows Bridge Study

Valuable experience was gained while measuring the Second Narrows Bridge. Many of the lessons learned were used to specify and assemble the HBES hardware and software. The most important lessons were:

1. Sensors should be capable of measuring the vertical vibrations caused by vehicle traffic and at the same time be sensitive enough to pick up smaller transverse vibrations. The sensors should be able to record vibrations in the frequency range of 0 - 20 Hz.

2. At least four sensors should be available to simultaneously record vibrations at different locations on the structure.

3. Signal conditioning equipment should exhibit as little drift as possible. Multiple signal amplification levels and filter options should be available.

4. Programmable data acquisition hardware capable of recording a minimum of four channels should be obtained. This hardware must be able to acquire long data records at various sampling rates.

5. Acquisition software specifically designed for ambient vibration data needed to be developed to conveniently record the large amount of data associated with ambient vibration studies.

6. Software suitable for in-situ inspection of ambient vibration data needed to be created. To identify natural frequencies and mode shapes in the field, the software should be able to automatically analyse all of the data as soon as it is acquired. The capability to display and animate the computed mode shapes for visual verification should also be available.

The experience gained from the measurements at the Second Narrows Bridge was used in the development of the Hybrid Bridge Evaluation System (HBES). The hardware and software of the HBES are described in the following sections.

3.2 HBES Hardware Description

After the tests at Second Narrows Bridge were completed, a study of the specifications for versatile ambient vibration measurement hardware was undertaken. The important specifications of each component were investigated and the hardware was obtained. The main components of the HBES ambient vibration measurement hardware are introduced in section 3.2.1. As part of the Colquitz River Bridge study (described in section 4.3) a series of pullback tests was conducted to verify the ambient vibration results. A special device was constructed for the controlled release of the pullback force. This device is described in section 3.2.2.

3.2.1 Measurement Hardware

Considerable effort was spent on selecting electronic hardware that would be versatile and suited for performing ambient vibration studies of a variety of bridges. Modular components, which could be easily transported to and from remote locations, were selected. The system had to be suitable for field work. In addition, the modular measurement equipment was designed so hardware could be added and individual components could be replaced without compromising the functionality of the overall system.

Fig. 3.3 shows a typical ambient vibration setup with all the measurement hardware components. This figure shows a sensor which converts the physical excitation into electrical signals. These signals are then transmitted to the signal conditioner by cable where they are amplified and filtered. The conditioned signals from all sensors are then converted from analog to digital information and stored on a computer. The data is transferred to a second computer for on site analysis. In addition, a spectrum analyzer can be used to monitor two of the analog signals. Fig. 3.4 shows a sensor mounted to the bottom flange of a steel beam. Fig. 3.5 shows a picture of the signal conditioner below the data acquisition computer. In this figure, the analog to

digital converter is placed to the left of the signal conditioner and the data analysis computer is located on the right. These individual components of the measurement equipment are described individually below. For specifications of the individual hardware components and a description of the test used to verify the suitability of the hardware for ambient vibration measurements, refer to Appendix A.

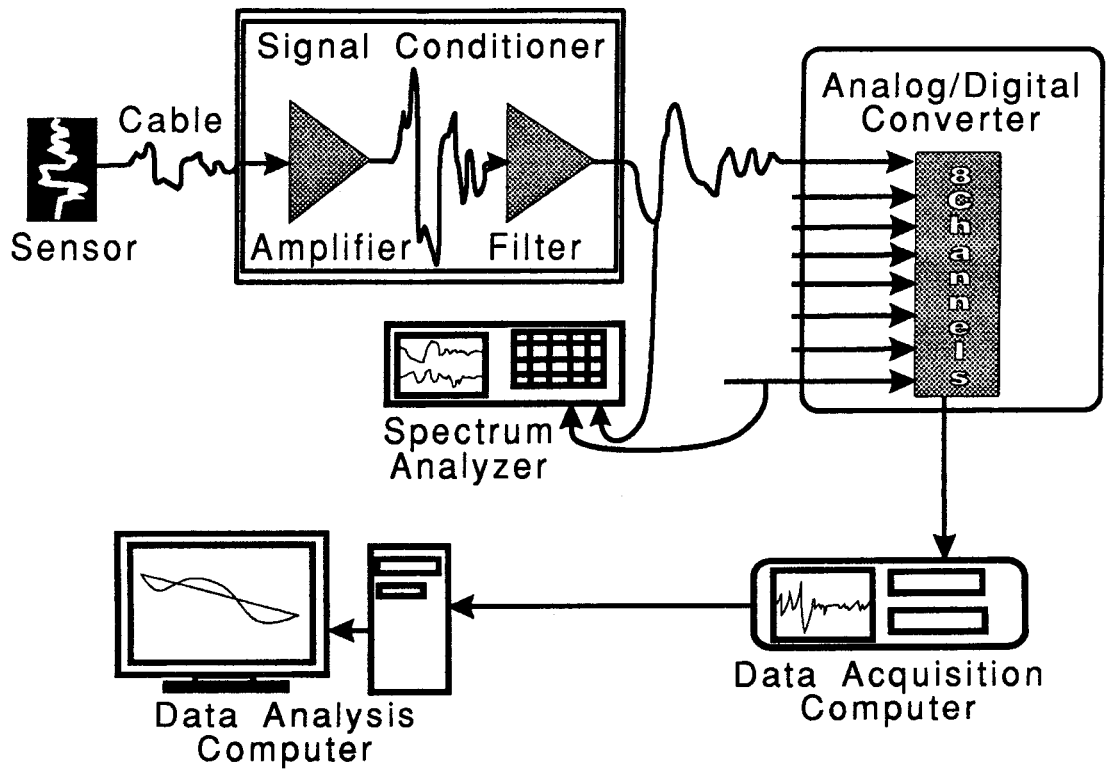

Fig. 3.3: Typical Recording Setup for Ambient Vibration Measurements

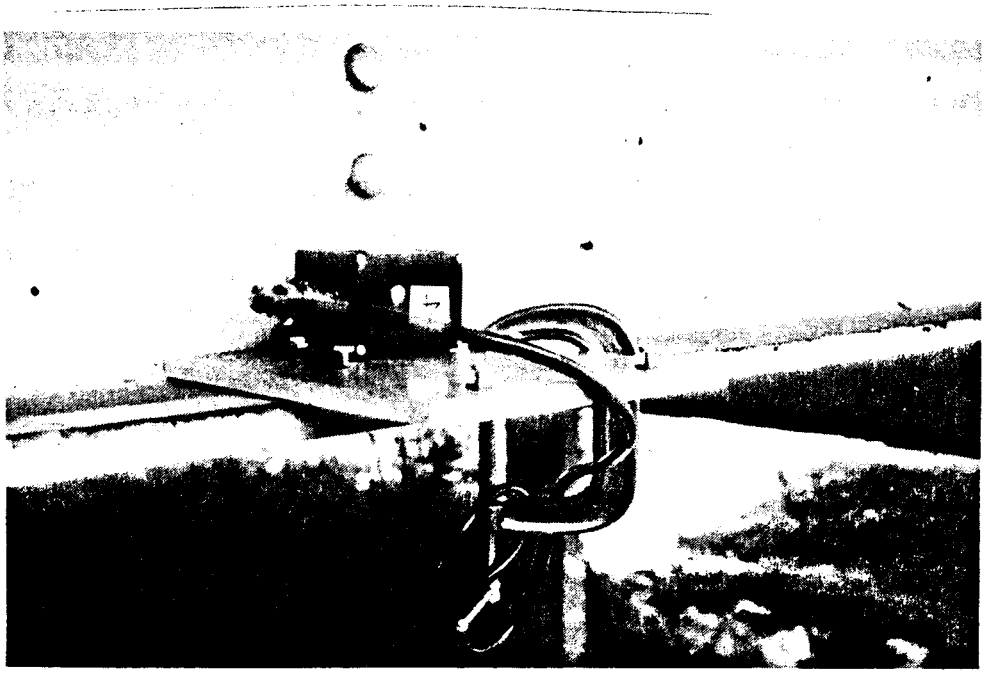

Fig. 3.4: HBES Sensor Attached to a Steel Beam

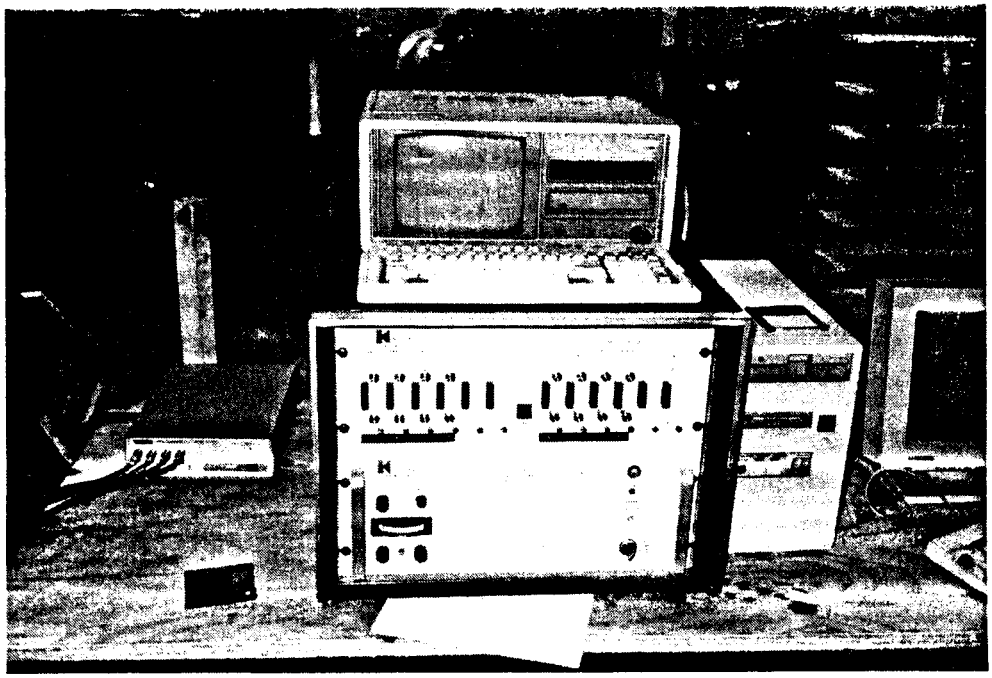

Fig. 3.5: Ambient Vibration Measurement Hardware

3.2.1.1 Sensors and Cables

The current HBES system has eight sensors. These sensors are mounted at various locations throughout the structure and are used to transform the structure's vibrations into electronic signals. These sensors are capable of measuring accelerations up to $\pm 0.5g$. Each sensor has a resolution of $0.2\mu g$, in the frequency range of 0 to 40 Hz.

Cables are used to transmit the electronic signals to a central recorder unit. The cables are shielded to minimize noise during the transmission.

3.2.1.2 Signal Conditioner

The signal conditioner improves the quality of the recording by removing undesired frequency components from the signals and by amplifying them. The amplifiers and filters for all channels are mounted in a portable signal conditioner. Each channels' signal can be independently amplified and filtered. Twelve different amplification levels ranging from 1 to 2000 are available. The low-pass filters can remove unwanted frequencies above 2.5 Hz, 5 Hz, 12.5 Hz, 25 Hz, or 50 Hz. The high-pass filters can remove all components below 0.1 Hz or 5Hz.

The portable signal conditioner is battery powered. It can be used continuously for approximately 20 hours before the batteries need to be recharged.

3.2.1.3 Analog/Digital Converter

The amplified and filtered analog signals must be converted to digital information before they are stored on the data acquisition computer. An analog to digital (A/D) converter with a resolution of 16 bits sequentially samples the analog signals from all of the channels and converts them into digital information. The A/D converter is controlled from the data acquisition

computer using a custom program called AVTEST. Using AVTEST, the A/D converter can be used to sample up to eight channels at frequencies between 0.2 Hz and 200 Hz. Between 1024 and 131072 points can be obtained for each channel.

For more information on AVTEST, see section 3.3.1.

3.2.1.4 Data Acquisition Computer

After the analog signals are converted to digital form, they are stored on the data acquisition computer's hard disk. The data is stored in binary form.

The data acquisition computer controls the A/D converter and stores ambient measurements on its hard disk using the program AVTEST. This computer is a portable IBM compatible computer (Compaq II). Its rugged design and size make it ideal for field work.

The Compaq II has a storage capacity of approximately 30Mb. This is sufficient storage, since during a regular day of testing, approximately 20Mb of data are collected.

3.2.1.5 Data Analysis Computer

After the data acquisition computer has obtained a set of recordings, the data is transferred to the data analysis computer.

The data analysis computer is another IBM compatible computer which runs the custom developed ambient vibration analysis programs, ULTRA and VISUAL. These programs are used to identify the structure's natural frequencies and mode shapes. The main advantage of having a separate data analysis computer is that preliminary results, obtained in-situ, can be used to assess the quality of the measurements while testing is in progress. Occasionally these results can be used to change the remaining test setups.

For more information on ULTRA and VISUAL see sections 3.3.2 and 3.3.3 respectively.

3.2.1.6 Spectrum Analyzer

In addition to the equipment above, the dual channel spectrum analyzer, which was used during the Second Narrows Bridge test, can be used to monitor signals. While the analyzer is not required to analyse or record signals, it is very helpful for on-line signal monitoring and trouble shooting. The analyzer can monitor up to two signals independently and compute PSDs as they are being recorded.

3.2.2 Quick Release Mechanism (QRM)

As mentioned in section 1.2, Douglas, Margakis, and Nath (1990) have performed quick release tests. Douglas used a hydraulic quick release while others, such as Lorenz (personal communication January 30, 1993), have blasted load carrying cables to instantly release the pullback load. While the blasting approach releases the load very quickly, it destroys the cable and requires special permits and safety measures.

To avoid the use of hydraulics and explosives, a special mechanical device called a Quick Release Mechanism (QRM) was developed as a part of this thesis. The QRM was developed to release loads up to 90 kN instantaneously for the dynamic testing at the Colquitz River Bridge.

Plan and elevation views of the QRM are shown in Fig. 3.6. The QRM consists of two rigid arms joined together with a large pin and a Sparcraft™ shackle. A Sparcraft shackle is a sailing shackle designed to quickly release a sail sheet under load on a boat. Although the shackle used for the QRM has a breaking strength of 90 kN, due to its geometry, the QRM has an overall safety factor of five under an applied load of 90 kN.

While loading, a safety pin is placed under the sliding link to prevent accidental release of the load. To release the load the safety pin is removed, the Sparcraft shackle is opened, and the release arm rotates. After the release arm has sufficiently rotated, the sliding link becomes free and the load is totally released.

A typical release force time history is shown in Fig. 3.7. As you can see from this figure, the release time for a 90 kN force is approximately 0.04 seconds. The small discontinuity of the release at about 72 kN is caused by the mechanics of the QRM. Since the discontinuity lasts about one hundredth of a second, it excites the modes well above the frequency range of interest. This discontinuity does not affect the excitation of the primary modes of bridges.

The advantage of the QRM over other methods, such as blasting, is that the release is controlled and safe. Because the rigging is not damaged during the release, the test can be repeated several times.

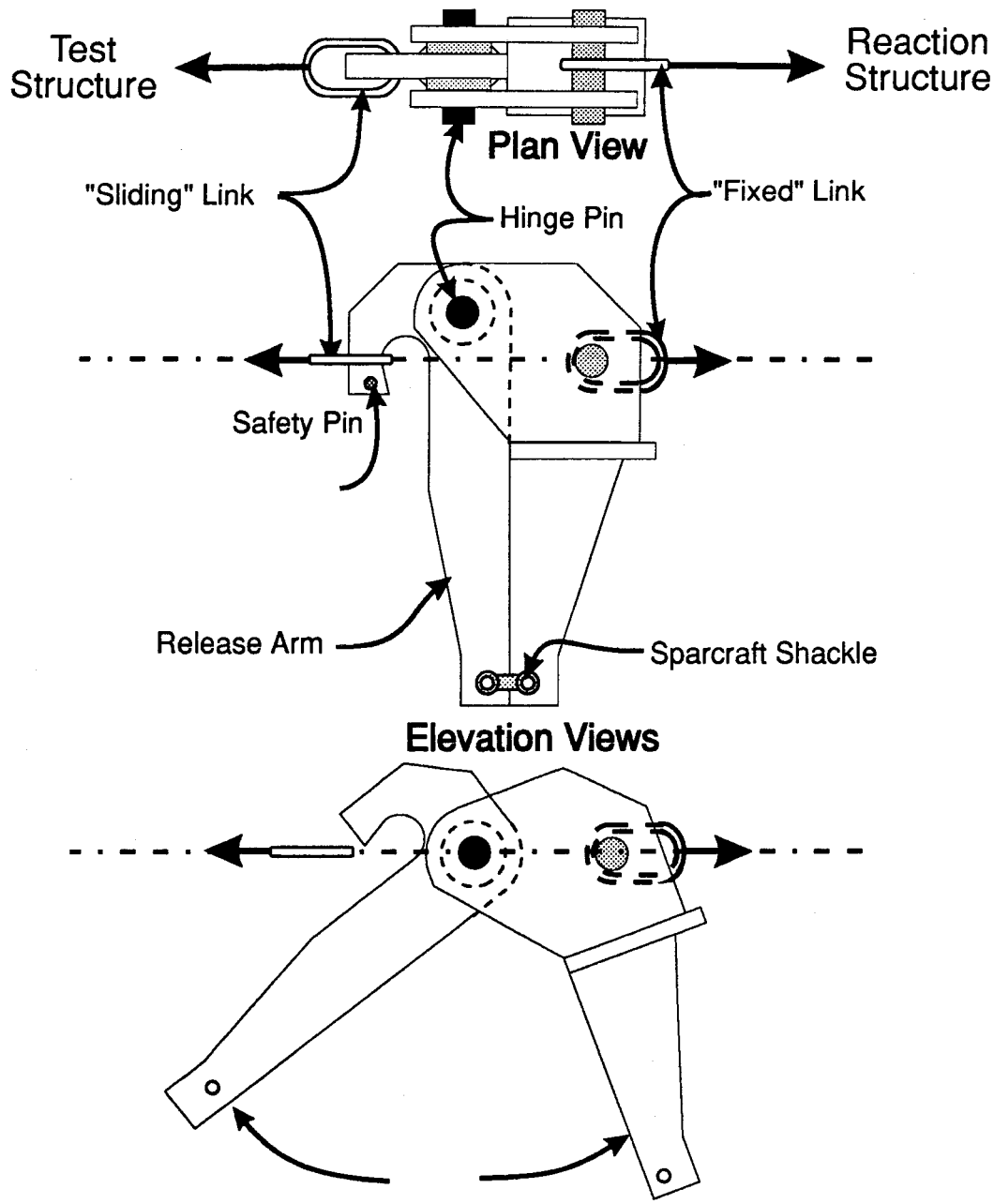

Fig. 3.6: Quick Release Mechanism.

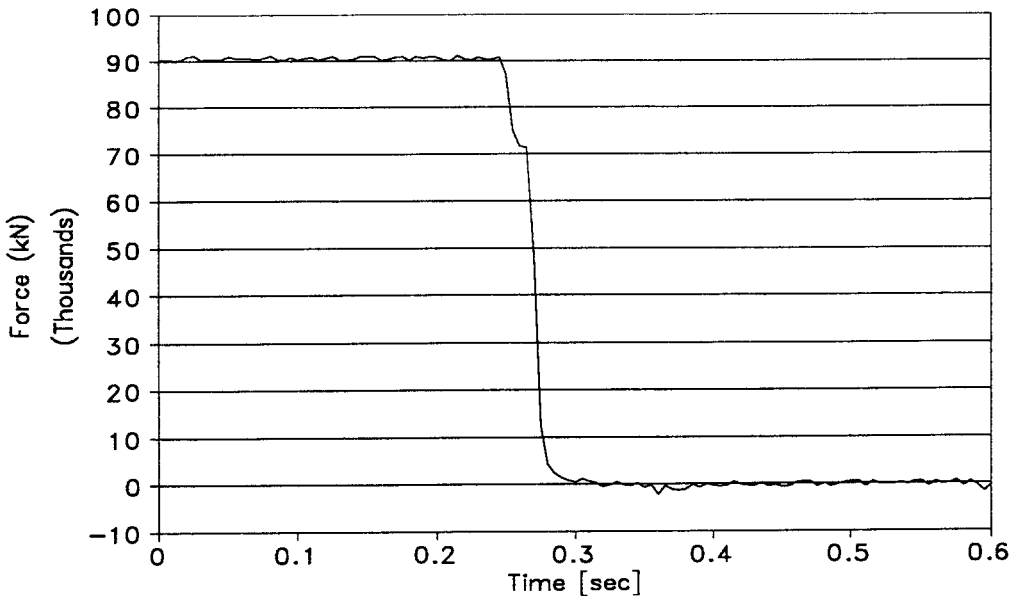

Fig. 3.7: Typical Release Force Time History of the QRM Developed at UBC.

3.3 HBES Software Description

Since the aim of this research was to develop a system that can be used to quickly evaluate the dynamic properties of bridges, a technique for reducing large amounts of data associated with ambient vibration testing needed to be developed. Concise representations of the important features of the data needed to be devised so the data could be visually verified at the site. This section introduces two refinements to the traditional ambient vibration analysis process which were incorporated in the HBES to make the data analysis and interpretation more efficient.

Four computer programs, AVTEST, ULTRA, VISUAL, AND SUBSAP, were developed to generally acquire ambient vibration records (AVTEST), reduce them to power spectra and modal ratio functions (ULTRA), assemble them into mode shapes (VISUAL), and update a dynamic

model's parameters (SUBSAP). In addition, a commercially available dynamic analysis program (SAP90) was used for the analytical modeling of structures. The main features of these programs are described in the sections below. Detailed information about each custom program is given in their user manuals in appendices B, C, D, and E.

3.3.1 Data Acquisition Software - AVTEST

Ambient vibrations are recorded onto the data acquisition computer using the custom program AVTEST. While commercial general purpose data acquisition software could have been used, AVTEST was developed to optimize the data acquisition procedure. Because ambient vibration testing involves the acquisition of large data records from many different test setups, the acquisition program had to address several quality control issues. The following features were developed and incorporated into AVTEST to enhance quality control.

- Command Line Structure:

  All of the options and commands regarding the setup of the acquisition are entered on a command line. The individual options that are most likely to change from test to test are at the end of the command line. You can use the "DOSKEY" feature in DOS (Microsoft, 1991) to quickly change the file name from test to test while all of the other settings remain the same. Little typing is required to run the program from test to test which makes running the program very quick and consistent.

- Calibration Records:

  Each of the sensors is checked with a calibration signal before and after the ambient vibration data is acquired. AVTEST records the calibration signals and graphically displays them for visual verification. ULTRA can be used to analyse these signals to

determine the sensors' natural frequency and damping. If these properties are the same before and after the data is acquired, it is highly probable the sensors were working during the test and the data can be relied upon.

- Signal Levels:

  After the initial calibration, the signal levels and their temporary maxima and minima are displayed for all channels. At this time, the amplification levels can be set for each channel so the signals are strong enough to be digitized with good resolution but without saturation.

- Data Display:

  While acquiring the data, the recorded signal levels are displayed graphically on the screen in real time. This feature allows the user to check signal levels and to detect abnormalities as soon as they occur.

For a detailed description of AVTEST's settings and operations, refer to the user's manual in Appendix B.

3.3.2 Data Reduction Software - ULTRA

After AVTEST records the data onto the data acquisition computer, the ambient vibration records must be analyzed to obtain the natural frequencies and mode shapes of the structure. The phase and transfer function for two signals must be computed to establish the relative modal amplitudes. In addition, auto spectra, cross spectra, and coherence are used to establish the natural frequencies.

Currently available commercial programs, which can compute the functions above, could not be used to automatically reduce large quantities of ambient vibration data automatically in the

field. The program ULTRA was developed to facilitate both manual and automatic reduction of ambient vibration data. This process is illustrated in Fig. 3.8. ULTRA can compute the individual power spectral densities, cross spectrum, transfer function, phase angle, coherence function, and the potential modal ratio function (defined in section 3.3.2.1.), for a pair of acceleration time histories.

The main features of ULTRA are described briefly below. Detailed information is presented in the user's manual in Appendix C.

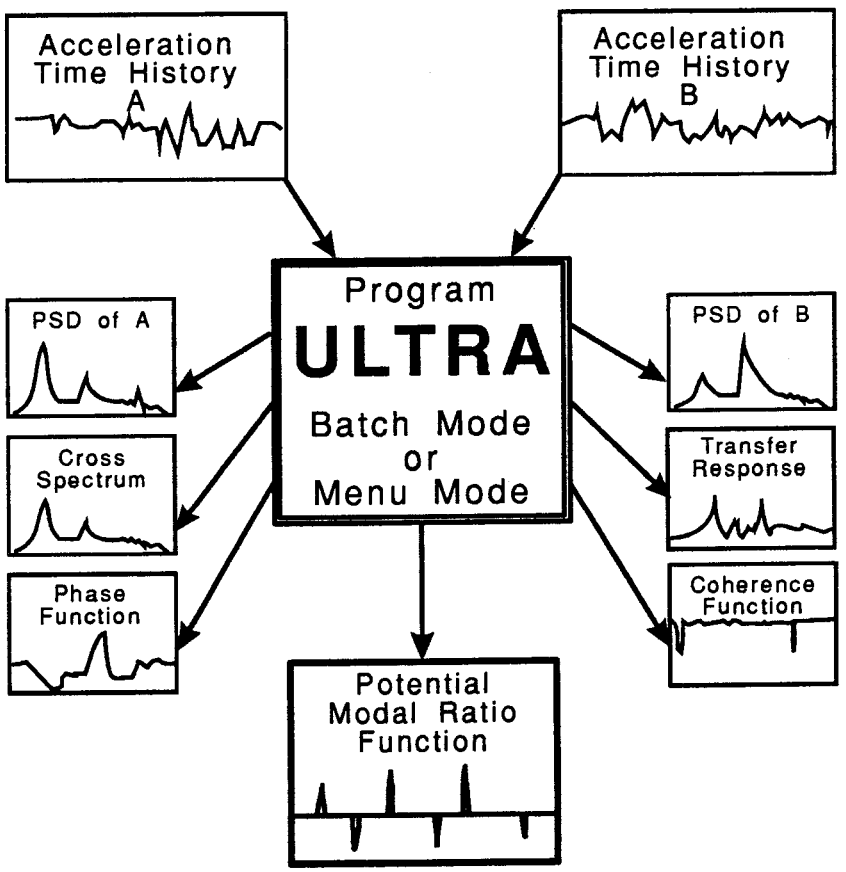

Fig. 3.8: Schematic of Data Reduction with ULTRA.

3.3.2.1 Determining Natural Frequencies and Mode Shapes

The aim of the data reduction is to identify natural frequencies and modal ratios. The modal ratio function was developed and implemented into ULTRA to help determine modal amplitude ratios. ULTRA simultaneously considers the information from the frequency response function as well as the phase angle and the coherence value to compute the modal amplitude ratio between two degrees of freedom at potential natural frequencies. This use of the potential modal ratio function and its implementation are described in detail below and its implementation is documented in Appendix C.

Determining Natural Frequencies

The natural frequencies of the structure are traditionally determined from the peaks of averaged PSDs. You can not assume that all of the structure's natural frequencies are represented in an averaged PSD of a single measurement location because this location may coincide with a node of a vibration mode. You need to consider the average PSDs of all measured locations to ensure all of the natural frequencies of a structure are identified. Since this may require examination of several dozen PSD plots, a new natural frequency indicator function based on a group of PSDs was developed for this thesis. This function called the Averaged Normalized Power Spectral Density (ANPSD), is defined as the average of a group of l normalized power spectral densities (NPSDs). The ANPSD functions are calculated using:

$$ANPSD(f_k) = \frac{1}{l}\sum_{i=1}^{i=l} NPSD_i(f_k) \tag{3-1}$$

where $NPSD_i(f_k)$ is defined as

$$NPSD_i(f_k) = \frac{PSD_i(f_k)}{\sum_{k=0}^{k=n} PSD_i(f_k)} \tag{3-2}$$

and f_k is the kth discrete frequency and n is the number of discrete frequencies.

The peaks of the ANPSD were used to determine the natural frequency estimates f_j for all the structures tested for this thesis.

Determining Mode Shapes

Mode shape vectors corresponding to individual natural frequencies are determined from individual modal ratios estimates $\hat{r}_{j_{il}}$. As discussed above, the modal ratio estimates are only defined at the natural frequencies f_j, where the phase angle of the transfer function is either near 0° or 180°. Near the natural frequencies, the coherence value $\gamma^2_{il}(f)$ should be near 1 for properly recorded signals.

A new function was defined to identify the frequencies f_p where the modal ratio estimates $\hat{r}_{j_{il}}$ can be equal to the transfer function ratios. These frequencies, f_p, are potentially equal to the natural frequencies, f_n, of the system. The visualization of the modes shapes described in the next section is used to verify which of the potential natural frequencies, f_p, are indeed natural frequencies, f_n. The new function $M_{il}(f)$ is called the Potential Modal Ratio (PMR) function and defined as:

$$M_{il}(f) = | T_{il}(f) | * PW_{il}(f) * CW_{il}(f) \tag{3-3}$$

Where $| T_{il}(f) |$ is the absolute value of the transfer function defined in Eqn. 2-36 and $PW_{il}(f)$ is the Phase-Window function defined as

$$PW_{il}(f) = \begin{cases} 1 & 0 \le \phi_{il}(f) \le \phi_c \\ 0 & \phi_c < \phi_{il}(f) < 180 - \phi_c \\ -1 & 180 - \phi_c \le \phi_{il}(f) \le 180 \end{cases} \tag{3-4}$$

$\phi_{ij}(f) =$ Phase Function (degrees)

$\phi_c =$ Modal-Cut-Off Angle (degrees)

and $CW_{il}(f)$ is the coherence-window function given by:

$$CW_{il}(f) = \begin{cases} 1 & \gamma_c^2 \le \gamma_{il}^2(f) \le 1 \\ 0 & 0 < \gamma_{il}^2(f) < \gamma_c^2 \end{cases} \tag{3-5}$$

$\gamma_{il}^2(f) =$ Coherence Function

$\gamma_c^2 =$ Coherence-Cut-Off

The Modal-Cut-Off angle is used to determine the sign of the potential modal ratio and to eliminate the transfer function values associated with phase angles that are not near 0° or 180°. The Coherence-Cut-Off value is set to eliminate the transfer function values associated with low coherence. The remaining values are then the potential modal ratios between two degrees of freedom for the measured frequency band.

Since the PMR function combines the information from the transfer functions magnitude and the coherence automatically, the time required to reduce the data is greatly decreased. The data is reduced more consistently, because the same criteria is used to determine the potential modal ratio of each individual pair of signals.

This process is illustrated using sample data from the Colquitz River Bridge test described in section 4.3. For two vertical signals recorded on opposite sides of the center span of the bridge, the frequency response, phase angle, and coherence were computed. Fig. 3.9 shows the transfer function for the two signals. The phase angle between the two signals is given in Fig. 3.10.

In this figure two horizontal lines corresponding to a modal cut-off angle of 20 degrees are drawn. The corresponding phase-window is shown if Fig. 3.11. The coherence for the pair of signals is shown in Fig. 3.12 with a horizontal line corresponding to a Coherence-Cut-Off value of 80%. The coherence-window is shown in Fig. 3.13. The PMR function which is obtained when the response function is multiplied by the phase window and the coherence window is shown in Fig. 3.14. This PMR function shows that the 20 degree phase angle and the 80% coherence criteria are only met in the range of 4 to 12 Hz. In particular, the potential modal ratio at 6Hz is roughly 0.5 and at 6.8Hz it is approximately -2. When a complete set of modal ratio functions are computed with respect to a common reference station, the mode shape vectors can be defined as described in section 3.3.3.

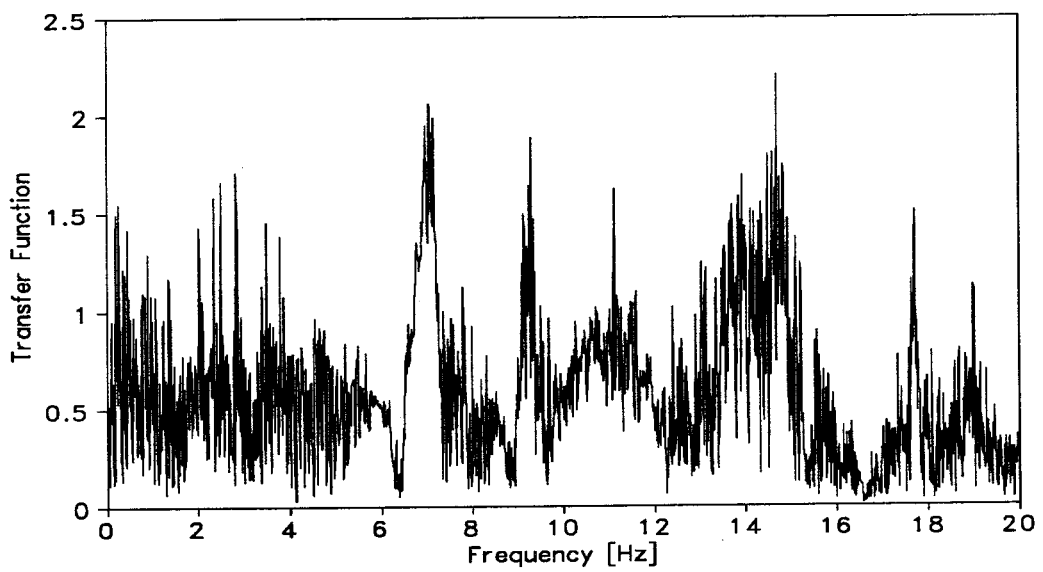

Fig. 3.9: Transfer Function of the Sample Data

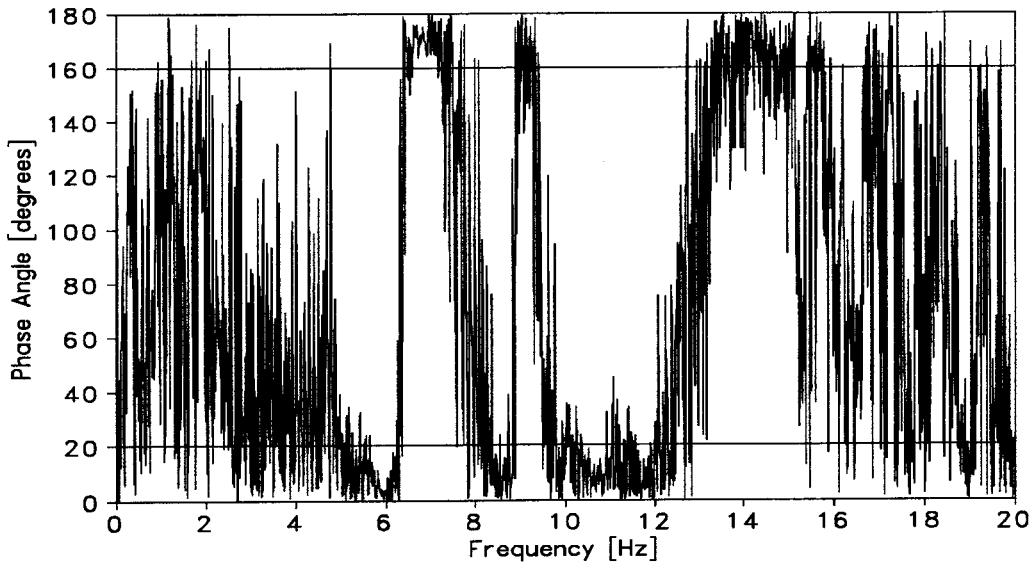

Fig. 3.10: Phase Angle of the Sample Data

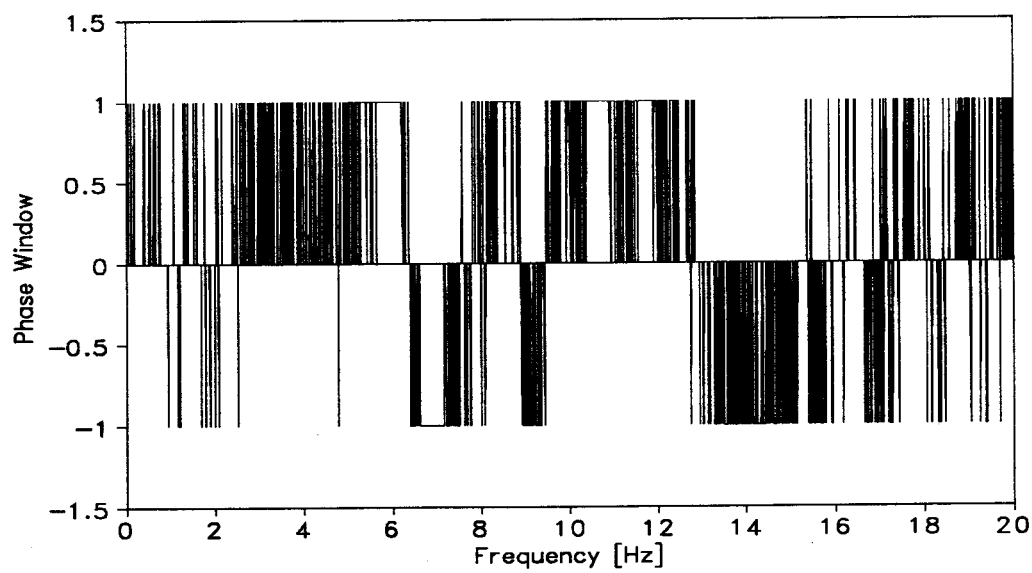

Fig. 3.11: Phase Window Function Corresponding to the Sample Data

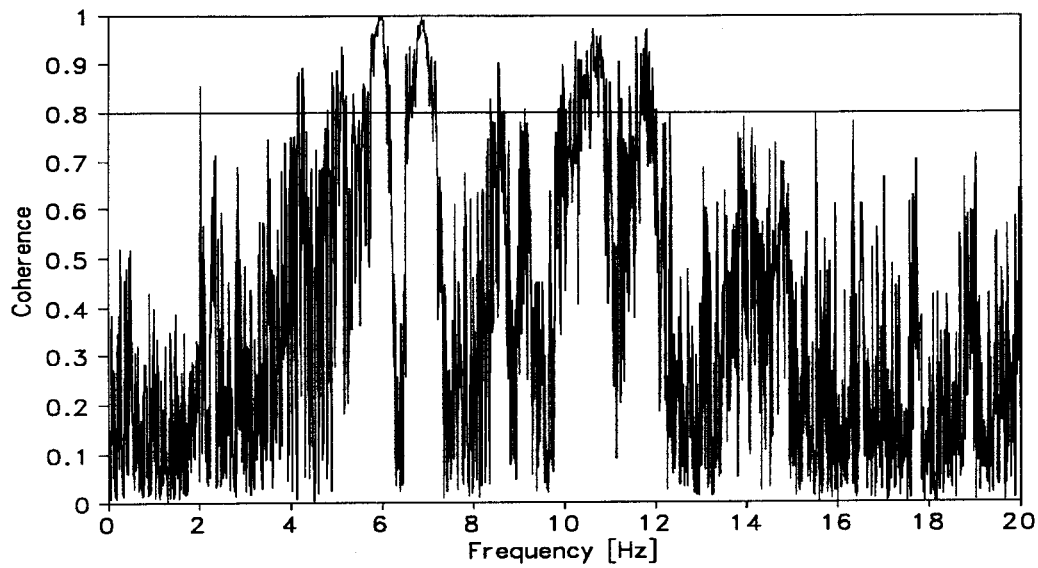

Fig. 3.12: Coherence Function of the Sample Data

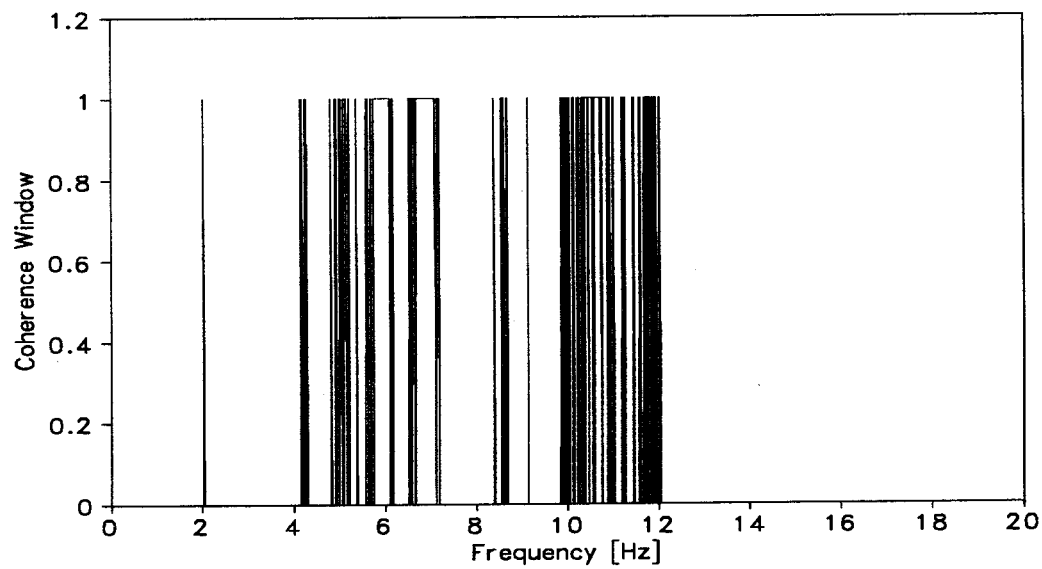

Fig. 3.13: Coherence Window Function Corresponding to the Sample Data

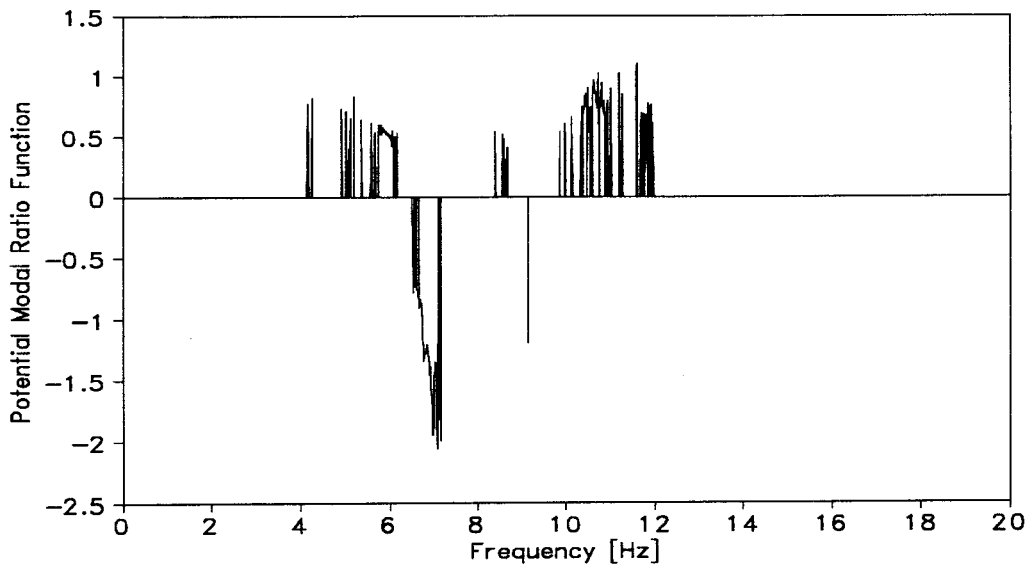

Fig. 3.14: Potential Modal Ratio Function of the Sample Data

3.3.2.2 Processing Records Automatically

When analyzing ambient vibration records, you must compute the PSDs for all of the obtained records. In addition, for each setup, PMRs must be computed for each combination of a roving sensor record and a reference sensor record. It would be too time consuming in the field to compute these functions using the interactive menu mode of ULTRA, therefore, ULTRA was designed to run in both interactive and batch mode. In batch mode the program can be used to automatically and consistently reduce large numbers of records. This option is used extensively in the field for the preliminary analysis of the data. In the office this option can be used to determine the effects of different Modal-Cut-Off angles and Coherence-Cut-Off values on the ensemble of Potential Modal Ratios. The use of this option is discussed in detail in Appendix C.

3.3.2.3 Removing Linear Trends Automatically

The frequency domain functions used for the data reduction are often computed as averages of functions based on segments of the data. Each segment can have a small offset and some linear drift due to the long recording times. ULTRA automatically removes any linear trend from the time domain data before it is used to compute frequency domain functions. This feature leads to cleaner looking spectra and improved results.

3.3.2.4 Verifying Instruments

ULTRA can be used to examine the calibration records taken by AVTEST before and after each test setup. It extracts the natural frequency and damping value of the sensor from the calibration record. These values can be used to evaluate the condition of the sensor before and after the testing. Because the manual examination of these calibration records is quite tedious, this feature saves a lot of time.

3.3.3 Data Interpretation Software - VISUAL

After all the natural frequencies f_j have been obtained from the ANPSD and all the PMR functions have been computed with respect to a reference coordinate, you can assemble the mode shapes φ_j. The PMRs are used by VISUAL to assemble and animate mode shapes. This process is illustrated in Fig. 3.15. Two data files defining the geometry of the structure and the locations of all the measurements are used by VISUAL in conjunction with the PMR files. The program can then be used to assemble the PMRs at a selected frequency into a shape which can be displayed and animated. At the frequencies corresponding to the natural frequencies of the structure these animated shapes correspond to mode shapes. For the example illustrated in Fig. 3.15, the PMRs for a simply supported beam are used to obtain the first three

mode shapes. Ambient vibration readings were obtained from a total of seven coordinates and the reference readings were made at a node near one end (node number 1). The jth mode shape vector is assembled using

$$\{\varphi_j\}^T = \{M_{11}(f_j), M_{12}(f_j), M_{13}(f_j), M_{14}(f_j), M_{15}(f_j), M_{16}(f_j), M_{17}(f_j)\} \tag{3-6}$$

This method of mode shape vector assembly automatically scales the modes shape vector with respect to the reference location, where $M_{11}(f_j) = 1$. The mode shapes corresponding to the natural frequencies, f_1, f_2 and f_3 can then be printed or stored to a file.

Occasionally, peaks occur in the PSDs and ANPSD, which do not correspond to natural frequencies of the structure. Since all PMRs have been computed using the same Modal-Cut-Off values and Coherence-Cut-Off values, at frequencies, f_k, not corresponding to natural frequencies of the structure, these criteria will generally not be met for all the computed PMR values. A number of the PMR values will be zero and the resulting shape will look very unnatural. The more restrictive the phase and coherence criteria are set, the more PMRs will be zero. As you can interpret from Fig. 3.15, at frequencies f_k, which do not correspond to natural frequencies, the resulting shape does not look like a mode shape.

By identifying the modes associated with the natural frequencies of a structure visually, you can eliminate data abnormalities and gain a better understanding of the dynamic behaviour of the structure.

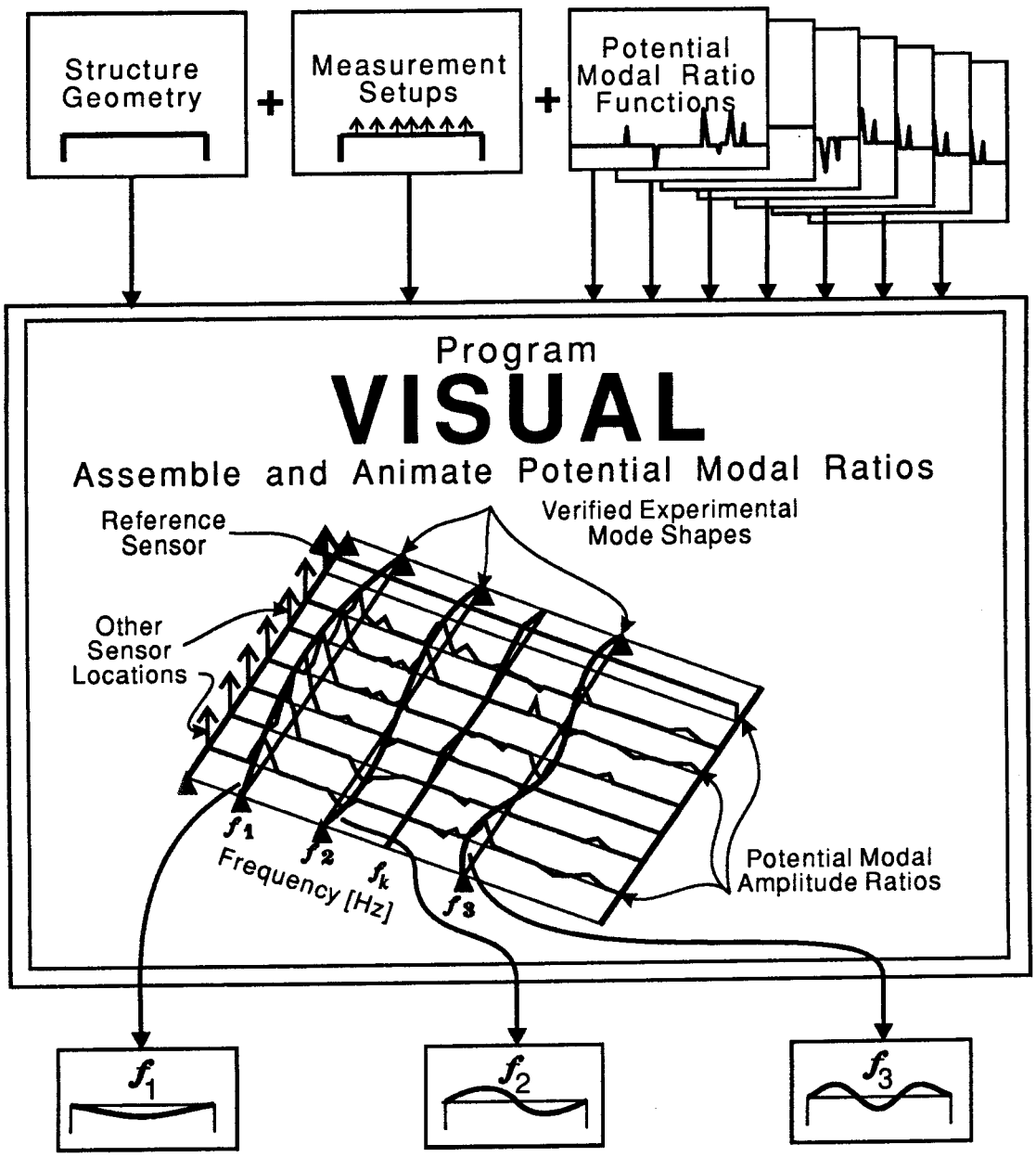

Fig. 3.15: Schematic of Data Interpretation with Visual.

3.3.4 Dynamic Analysis Software - SAP90

Dynamic analysis used for the HBES should be capable of performing modal analysis to identify the natural frequencies and mode shapes of a dynamic model. There are many commercially available programs on the market which perform modal analysis. The major differences between these packages are their program structure, memory requirements and pre- and post-processing features. The SAP90 (Computers & Structures Inc. 1992) program was included in the HBES because it was available in the Civil Engineering Department.

SAP90 has all the options required to perform linear elastic dynamic modal analysis of bridges. However, it does not have features for the convenient manipulation of individual model parameters. This drawback was overcome by writing a small program called SUBSAP which can be used in combination with SAP90 to provide a convenient way of varying key parameters. The parameter modification with SUBSAP is described in more detail in the following section.

3.3.5 Parameter Updating Software - SUBSAP

A dynamic model of the structure is usually constructed, parallel to the field work. Some of the key parameters of the model such as material stiffness and mass may not be known with certainty, however, best estimates can be used to develop a preliminary model. A dynamic analysis program is then used to obtain the natural frequencies and modes of the mathematical model.

After both experimental and analytical frequencies and mode shapes have been obtained, they need to be compared to determine how well the dynamic model matches the existing structure. At this point the key parameters of the mathematical model can be updated until the match of frequencies and mode shapes is satisfactory. After a match has been achieved, the dynamic

base line model is verified and can be used for analytical studies with more confidence.

The program SUBSAP simplifies the process of manually updating key variables in a dynamic model. A standard SAP90 input file is created and the key parameters to be varied are replaced by tokens. This information is then saved in a "token" file with the extension "inp". A small "variable" file with the extension "var" is also created which contains the numerical values corresponding to the tokens. SUBSAP is run prior to running SAP90 to create a SAP90 input file from the "token" and the "variable" file. After the SAP90 run is complete, the results can be interpreted and any necessary parameter changes can be quickly performed by editing the small "variable" file. Another SAP90 run can be performed to evaluate the changes. More detail on the use of SUBSAP is given in appendix E.

3.3.6 Programming Methodology

3.3.6.1 Object Oriented Programing

While the programs AVTEST and SUBSAP were developed in ANSI C (Kernighan & Ritchie, 1988), the programs ULTRA and VISUAL were developed using the object oriented language C++ (Stroustrup, 1986). AVTEST and SUBSAP are small programs which were written to perform predefined tasks. ULTRA and VISUAL, on the other hand, were continuously developed and refined throughout the early stages of this research and, therefore, had to be structured to facilitate expansions and modifications.

An object-oriented language such as C++ readily facilitates program expansion and reduces the amount of coding. The fundamental concept behind object oriented programming is the connection of the data and the methods (functions and routines) which operate on it. The

logical connection between data and methods is achieved through the declaration of classes. The word "class" is used in C++ to define memory structures that encapsulate both data and methods.

Object oriented programming, when applied effectively, will group the data and the corresponding methods in a number of classes which are often similar to the mental abstractions which we deal with on a daily basis. For example, some abstractions are time histories, or spectra. If the structure of the program emulates the structure of the abstraction which we use to describe the physical problem, the program will generally be much easier to understand and modify. This concept will be briefly illustrated using the class structure adopted for the program ULTRA. For the specifics of the individual classes of ULTRA, refer to Felber & Stiemer (1992).

ULTRA deals with vibration signals in the time domain and spectra in the frequency domain. In both domains the information can be represented as large series of data combined with some auxiliary information. Thus, both signals and spectra require methods that can manipulate large arrays of data. These large arrays form the basis of the Series class. The Series class encapsulates the data and methods associated with large series of equally spaced numbers.

The two other classes which form part of the programs class structure are the Signal class and the Spectra class. As the name implies the Signal class encapsulates all the information associated with a particular signal. This information can include the data and time of the recording, instrument location, and settings. Most importantly, the data structure of the Signal object has a pointer to a Series object that is used to store and manipulate the digitized signal.

The Spectra class is used to group information associated with a spectra or frequency domain function. Similar to the Signal class, the Spectra class has a pointer to a Series object that

contains the data. Other information regarding spectra is stored in the Spectra object. This information includes pointers to one or more signals from which the spectral function was calculated.

The relationship between the three classes is illustrated in Fig. 3.16. As you can see from this figure, the Series class is used by both the Signal and the Spectra class. The source code associated with the Series class is reused by the Signal and Spectra class. For example, the same routine of the series class can be used to display time histories or spectra on screen. Any modifications to the series class are automatically implemented in the other two classes. Therefore, a lot of code duplication, typical of conventional programing, is avoided.

These features of object oriented programming were ideally suited for the on going development of the programs ULTRA and VISUAL.

For more information on programming in C++, refer to Stroustrup(1986).

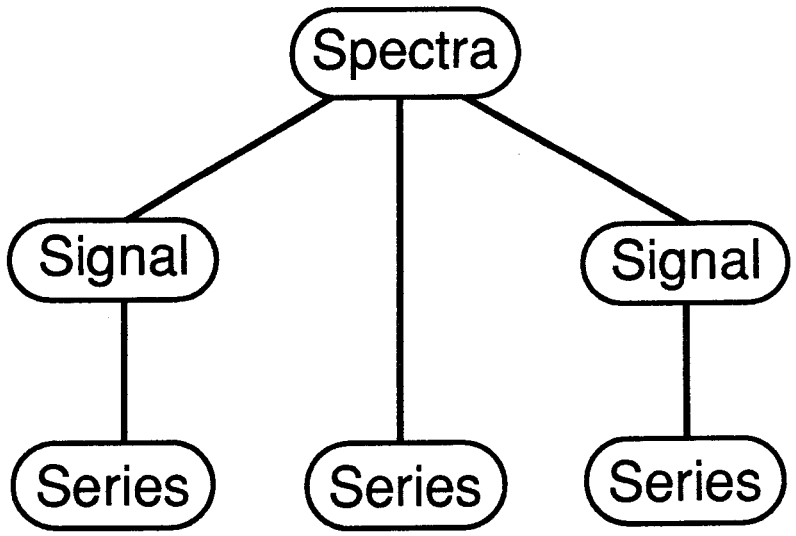

Fig. 3.16: Relationship Between the Series, Signal, and Spectra Classes.

3.3.6.2 Extended Memory Data Storage

During execution, both ULTRA and VISUAL use extended memory to store the large amounts of data they process. The extended memory is accessed using huge virtual array drivers developed by Quinn-Curtis (1991). With the use of these drivers and 2Mb of extended memory ULTRA can be used to analyse pairs of data records containing up to 131072 points each. Using the same hardware, VISUAL can be used to animate measured mode shapes of structures with more than 200 coordinates. For more information on the implementation of huge Virtual Arrays refer to Quinn-Curtis.

3.4 Software and Hardware Interaction

This section discusses the interaction between the individual software and hardware components of the HBES.

3.4.1 Interaction between AVTEST, ULTRA, VISUAL, and the Measurement Hardware

The interaction between the programs AVTEST, ULTRA, VISUAL, and the measurement hardware is shown schematically in Fig. 3.17. As you can see from this figure, AVTEST is used to control the A/D converter and to obtain the time histories which are then stored on the hard disk of the Data Acquisition Computer. Between recordings, these time histories are transferred to the Data Analysis Computer. There the program ULTRA is used to reduce pairs of time histories. ULTRA can be used to compute and display a variety of spectra, which can be printed or stored to file. The PSDs and Potential Model Ratios are commonly stored on the hard disk of the Data Analysis Computer. Small files describing the structure's geometry and the measurement setups, created with an ASCII editor, are then used by the program

VISUAL to verify the natural frequencies and mode shapes. The displayed mode shapes can again be printed or stored to a file. For more information on the operation of the individual programs and the file formats, refer to Appendices B, C, and D.

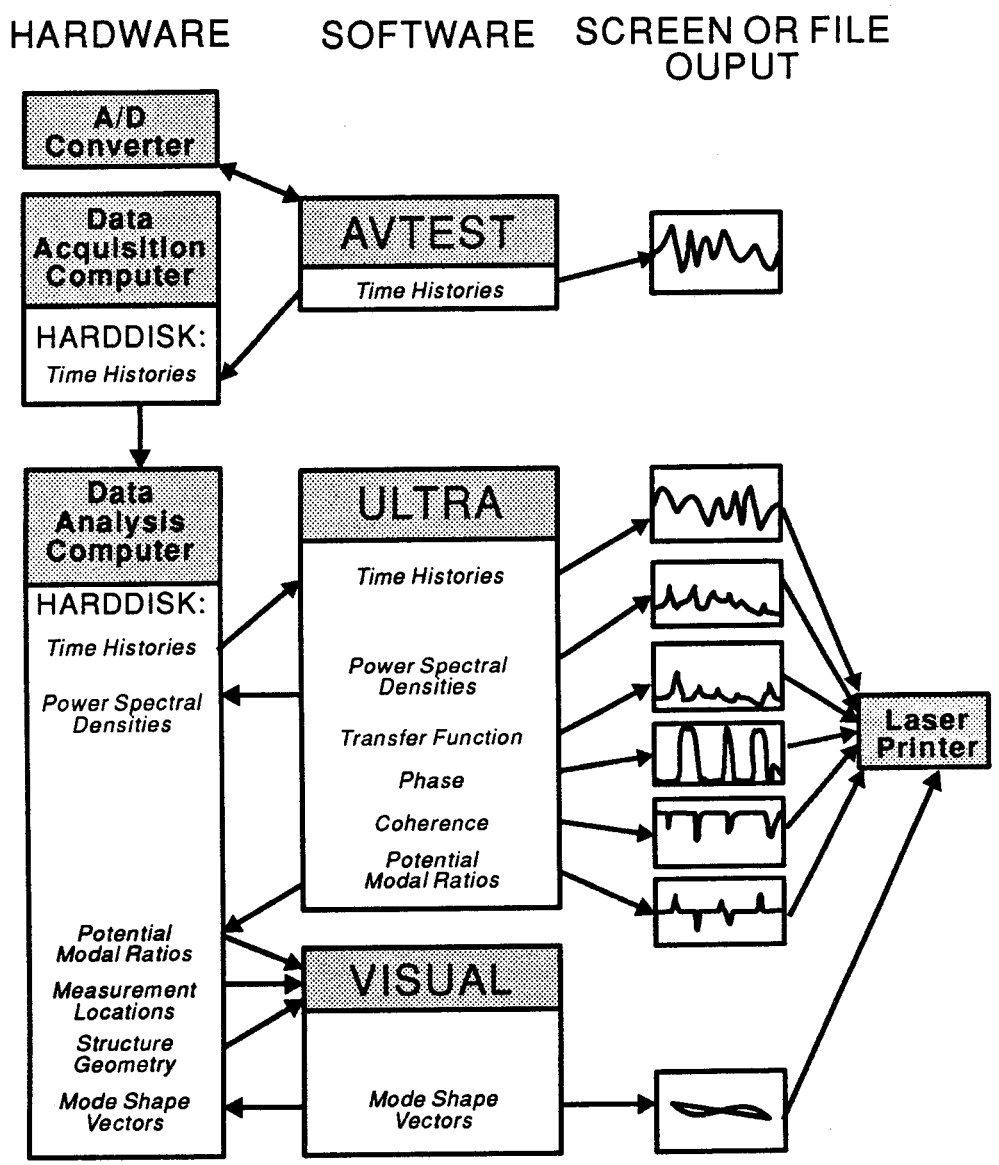

Fig. 3.17: Interaction of AVTEST, ULTRA, VISUAL, and the Measurement Hardware

3.4.2 Interaction between SUBSAP and SAP90

The program SUBSAP is used in combination with SAP90 to quickly tune analytical models to correlate with the experimentally obtained natural frequencies and mode shapes. This process is illustrated in Fig. 3.18. First, a standard SAP90 input file describing the structure is prepared. Then the parameters to be refined are replaced by a series of tokens and the new file is stored as a token file. A variable file containing the numerical values for the tokens is created. Then, the program SUBSAP is used to create a SAP90 input file which has all the tokens replaced with numerical values. This file is then used by SAP90 to compute the frequencies and mode shapes of the model. These analytically derived frequencies and mode shapes are then compared to the experimentally determined values. If the difference between these is too large, the values in the variable file are modified and another analysis is performed. This process is repeated until a good correlation between the experimentally determined and analytically derived dynamic characteristics is achieved.

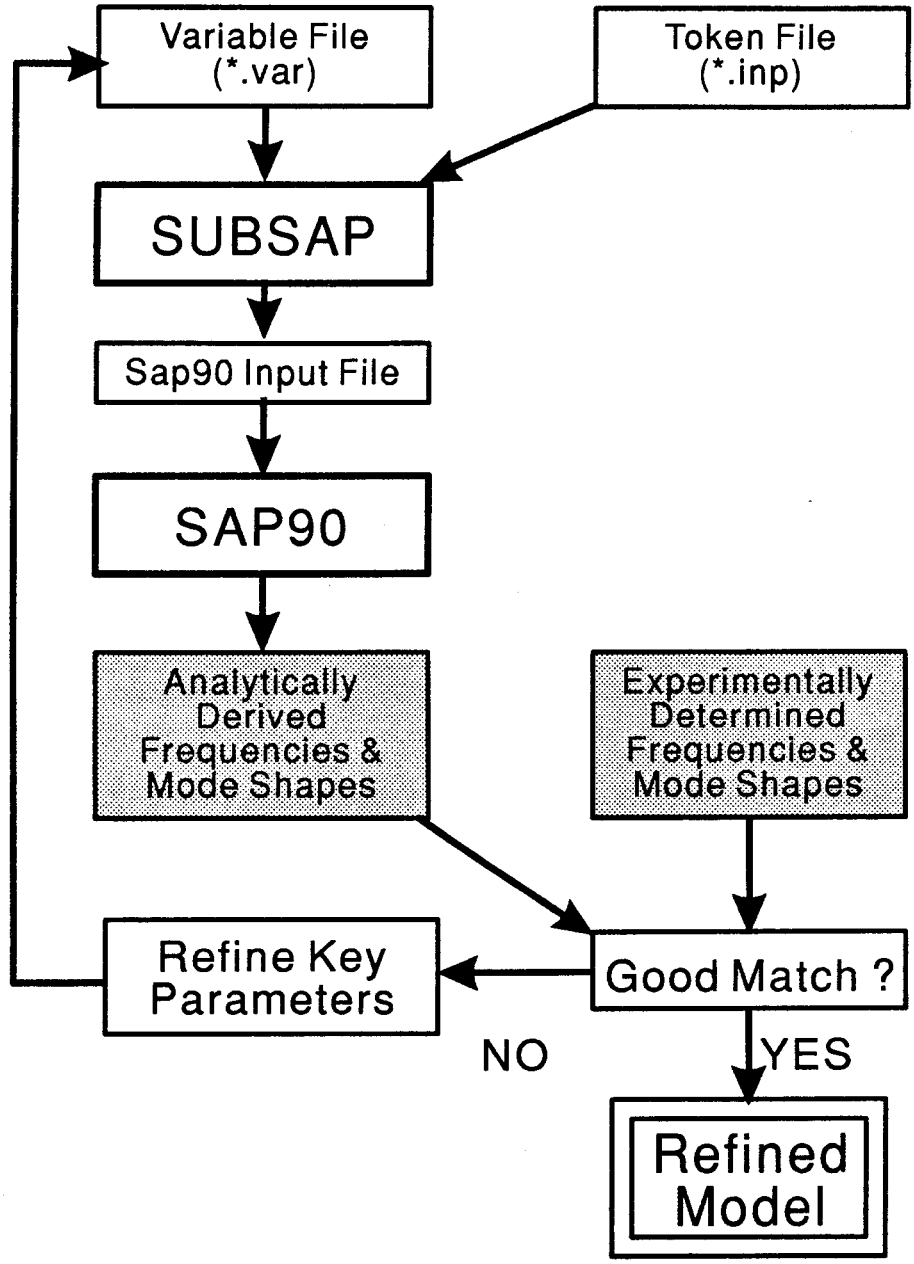

Fig. 3.18: Interaction of SUBSAP and SAP90

Chapter 4

Evaluation of the Hybrid Bridge Evaluation System

Many tests were conducted to verify the performance of the hybrid bridge evaluation system (HBES) throughout its development. The custom programs, AVTEST, ULTRA, VISUAL, and SUBSAP were individually tested before it was implemented into the HBES. Several full sized bridges were tested to evaluate the HBES as a system.

In this chapter I will describe these tests and the experience gained from each test.

4.1 Preliminary Verification of HBES Software

Each program written for the HBES was tested before they were implemented. These tests are briefly described in the sections below.

4.1.1 Verifying the Data Acquisition Software - AVTEST

The data acquisition software, AVTEST, was tested by comparing its performance to another working system. Signals produced by a signal generator were recorded simultaneously by the spectrum analyzer and the A/D converter (which is controlled by the AVTEST). The two sets of signals were compared to each other in the time and frequency domains. The data acquired by the A/D converter matched the data acquired by the spectrum analyzer. In particular the dominant spectral frequencies obtained from processing both sets of records agreed within $\pm\Delta f$. The performance of AVTEST was verified.

4.1.2 Verifying the Data Analysis and Interpretation Software - ULTRA & VISUAL

The data analysis and interpretation programs, ULTRA and VISUAL, were verified with the numerically generated responses of the three degree of freedom system, described in section 2.1.2, to ground motions with white noise characteristics.

The accelerations for the three degrees of freedom were computed using MODAL, a program developed by Dr. Ventura (1985). Each computed acceleration record consisted of 16384 points with a time increment of 0.025 seconds.

Using ULTRA, the PSDs of these records were computed and then normalized and averaged to obtain the ANPSD function. Fig. 4.1 shows the ANPSD. The natural frequencies were estimated from the highest ANPSD values of each peak. The system's natural frequencies were estimated as $\hat{f}_1 = 2.607Hz$, $\hat{f}_2 = 7.148Hz$, and $\hat{f}_3 = 9.678Hz$.

ULTRA was also used to compute the potential modal ratio functions. VISUAL then used these functions to assemble the mode shapes. The mode shapes were visually verified and stored in a file.

Table 4.1, below, compares the known dynamic characteristics of the three degree of freedom system to the estimates obtained with ULTRA and VISUAL. Because the mode shapes are dimensionless, the numerical and analytical shapes were scaled with respect to the first degree of freedom. The differences were computed with the remainder of the mode shape. The difference in these estimates was defined as:

$$\text{Difference} = \frac{|\text{Numerical Value} - \text{Known Value}|}{\text{Known Value}} * 100 \quad \text{in } \% \tag{4-1}$$

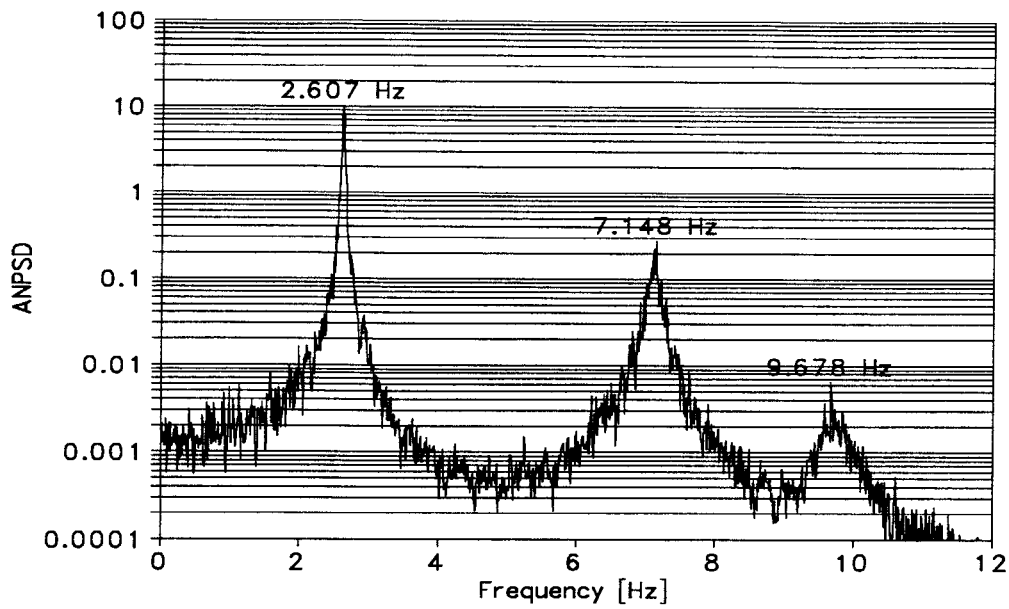

Fig. 4.1: ANPSD for the Three Degree of Freedom System Example

As you can see from Table 4.1, the natural frequencies obtained from the ANPSD peaks closely matched the natural frequencies of the system. The first and second mode shapes were estimated with an error of less than 1%, and the third mode shape was estimated with an error of less than 5%.

The modal ratios of the third mode, estimated using Eqn. 2-34, did not match the analytical mode as well as the estimates for the lower modes. As you can see in the ANPSD plot in Fig. 4.1, the peaks of the first two modes were much larger than the peak of the third mode. The structure's response was dominated by the first and second mode. A portion of the response at the third natural frequency was associated with the first two mode shapes and, therefore, the third mode shape was not as clearly identified.

Overall, the three degree of freedom system's frequencies and mode shapes were determined with only a small difference to the analytical mode shapes. Thus, a person who has a good background in structural dynamics could use ULTRA and VISUAL to determine frequencies and mode shapes reliably.

Table 4.1
Analytical Derived and Numerically Obtained Dynamic Characteristics of the Three Degree of Freedom System Example

Dynamic Characteristic	Analytical Value	Numerical Estimate	Error
f_1	2.605 Hz	2.607 Hz	0.08%
f_2	7.118 Hz	7.148 Hz	0.42%
f_3	9.723 Hz	9.678 Hz	0.46%
ϕ_{11}	1.000	1.000	N/A
ϕ_{12}	1.732	1.742	0.57%
ϕ_{13}	2.000	2.014	0.70%
ϕ_{21}	1.000	1.000	N/A
ϕ_{22}	0.000	0.000	N/A
ϕ_{23}	-1.000	-1.004	0.40%
ϕ_{31}	1.000	1.000	N/A
ϕ_{32}	-1.732	-1.699	1.91%
ϕ_{33}	2.000	2.086	4.30%

4.1.3 Verifying the Parameter Updating Software - SUBSAP

The parameter updating program SUBSAP, was tested using input and variable files. A typical input file was generated for the commercial program SAP90. A number of parameters in the SAP90 file were replaced with tokens (i.e. $INT1, $REAL1, $REAL2, etc...). After the SAP90 file was saved, a variable file was created that contained the values of these tokens.

The SUBSAP program then replaced the tokens in the SAP90 file with the proper values in the variable file. The updated SAP90 input file was inspected visually and all of the parameters in the SAP90 were updated correctly.

4.2 Study of the Shipshaw Bridge Vibration Data

The damage at one of the abutments of the Shipshaw Bridge during the moment magnitude (defined in Bolt, 1988) 6.0 Saguenay earthquake in 1988 has been the subject of recent investigations by researchers at the Department of Civil Engineering at Ecole Polytechnique in Montreal (Filiatrault, Tinawi & Massicotte, 1993c). As part of these investigations, a series of tests were conducted on the bridge to determine its dynamic characteristics at low amplitude vibrations. These tests were conducted using the hardware of the Quebec Ministry of Transportation (Filiatrault, Tinawi, Felber, Ventura & Stiemer, 1993a). The HBES software was used to analyse the Ministry's vibration data. The following sections briefly describe the Shipshaw Bridge and the results from the data analysis.

4.2.1 Objectives of the Shipshaw Bridge Study

The data from the Shipshaw Bridge provided an ideal opportunity to evaluate the HBES data reduction and interpretation software, ULTRA and VISUAL. The objectives of this project were to:

- Identify the principal modes of the Shipshaw Bridge from data obtained by the Quebec Ministry of Transportation,
- Evaluate the HBES' Data Reduction Program ULTRA,
- Evaluate the HBES' Data Interpretation Program VISUAL

4.2.2 Background on the Shipshaw Bridge

The Shipshaw Bridge was built in 1972 to cross the Saguenay River near Jonquiere, Quebec. It is a 183 m long, four-span, cable stayed bridge, consisting of a double-leg steel tower, double-plane fan type cables, and two steel box girders supporting the deck. Each span is equal in length and is supported by the cable anchorages, the steel tower, and the bearing supports at the abutments. The composite concrete steel deck is 11 m wide topped with a 165mm thick concrete road slab. The bridge includes thirty-six standard 65mm diameter galvanized strand cables. An elevation view of the Shipshaw Bridge is shown in Fig. 4.2. For more details of the bridge's composition, refer to Filiatrault, Tinawi & Massicotte (1993b).

Fig. 4.2: View of the Shipshaw Bridge

On November 25, 1989, the Shipshaw Bridge was subjected to the Saguenay earthquake, centered approximately 40 km southeast of the bridge (Mitchell, Tinawi & Law, 1990). A ground response instrument located approximately 15 km from the Shipshaw Bridge recorded the strong motions of the 6.0 moment magnitude earthquake. The peak ground acceleration recorded at this site was 0.13 g. There was significant damage to one of the four anchorage plates connecting the steel box girders of the deck to one of the abutments. The study by Filiatrault, Tinawi and Massicotte (1992b) concluded that the earthquake caused the failure of the anchorage plate.

4.2.3 Dynamic Analysis

The dynamic behaviour of the Shipshaw Bridge was modeled by Filiatrault et al. (1993b) with a three-dimensional linear elastic model. The first six modes of vibration computed from this model are compared to the results obtained with ULTRA and VISUAL in section 4.2.6.

4.2.4 Vibration Test Data

Bridge accelerations and vibrations were measured using the Quebec Ministry of Transportation's mobile accelerometer-based dynamic instrumentation and data acquisition system. Bridge accelerations were induced by driving a truck along the bridge deck. Vibrations were also induced by suddenly stopping the truck on the bridge.

The bridge was closed to traffic each time a test was performed. The bridge only has two lanes. The sensors had to be installed and the mobile unit had to be positioned on the bridge to record the data.

In addition to the truck-induced vibrations, ambient vibrations were also recorded. The ambient data was unsuitable for analysis because of its low resolution.

A total of eight tests were performed. Fig. 4.3 shows where the accelerometer was placed during the tests. The arrows in this figure indicate the location and direction of individual measurements. The bold numbers identify the sensor locations. The location and orientation for each sensor is given in Table 4.2. The individual acceleration records consisted of 8192 points sampled at 200 Hz.

After the records in Table 4.2 were visually inspected, it was apparent that only some of the measurements could be used to determine the natural frequencies and mode shapes of the bridge. The data corresponding to the sensor numbers and locations printed in **bold** in the Table could not be used due to test malfunctions and errors. Data abnormalities were found in the records printed in ***bold italics***. In particular:

- Because the signal of the reference sensor (#5) was not recorded properly during test number 5, the other measurements taken during this test had limited use.
- Large drifts occurred in some records (see Fig. 4.4)
- Some records displayed abrupt jumps of acceleration levels (see Fig. 4.5)
- The data was sampled too quickly and the signals were too short to provide good resolution in the frequency domain.
- Sensors behaved erratically: some sensors malfunctioned during one setup but performed well during the next setup without proper explanation.

These problems emphasize the need for detailed test planning and on-site data quality control.

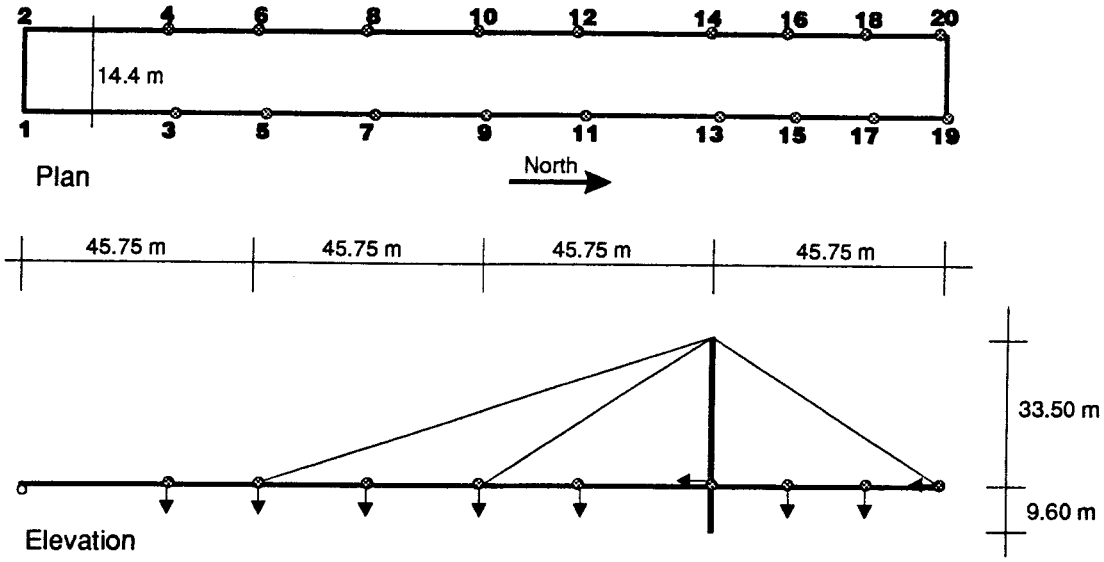

Fig. 4.3: Sensor Locations for the Shipshaw Bridge

Table 4.2: Sensor Locations for the Shipshaw Bridge Tests

Test #	Test Type	Sensors Number	Locations: V = Vertical, L = Longitudinal.
1	Rolling	***2, 3,*** 4, 5, 6, 7, 8	***4V, 6V,*** 8V, 10V, 12V, 16V, 18V
2	Rolling	***2, 3, 4, 5,*** 6, 7, **8**	***4V, 6V, 8V, 10V,*** 12V, 16V, **18V**
3	Breaking	2, 3, ***4***, 5, 6, 7, ***8***	4V, 6V, ***14L,*** 10V, 12V, 16V, ***20L***
4	Breaking	2, 3, 4, 5, 6, 7, 8	4V, 6V, 14L, 10V, 12V, 16V, 20L
5	Rolling	2, 3, 4, **5, 6,** 7, 8	3V, 5V, 7V, **10V, 11V,** 15V, 17V
6	Rolling	2, 3, 4, 5, 6, 7, 8	3V, 5V, 7V, 10V, 11V, 15V, 17V
7	Breaking	2, 3, 4, 5, **6,** 7, 8	3V, 5V, 13L, 10V, **11V**, 15V, 19L
8	Breaking	2, 3, 4, 5, **6,** 7, 8	3V, 5V, 13L, 10V, **11V**, 15V, 19L

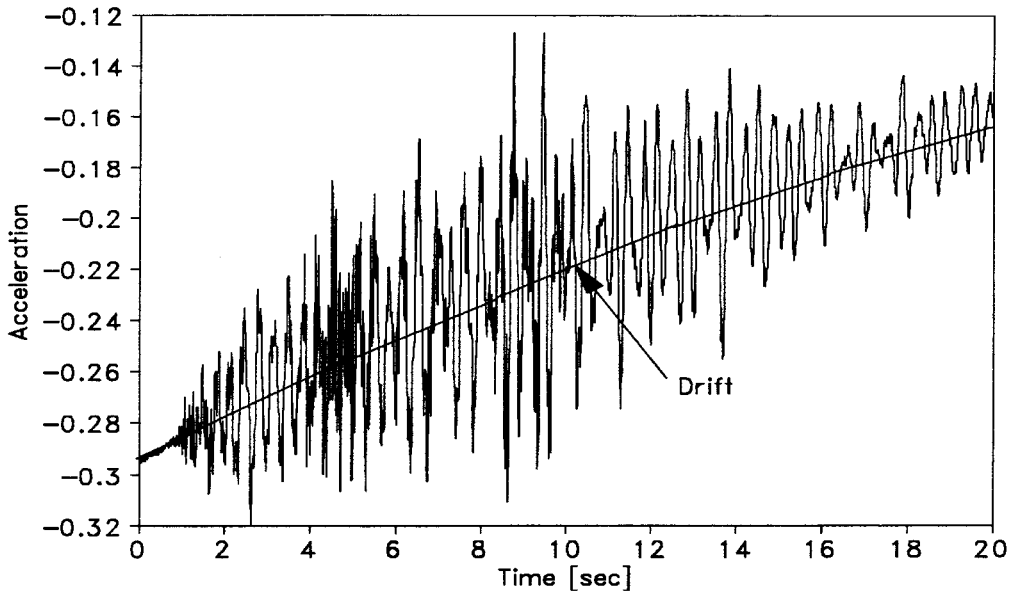

Fig. 4.4: Acceleration Record for Sensor No. 6 During the 5th Test of the Shipshaw Bridge

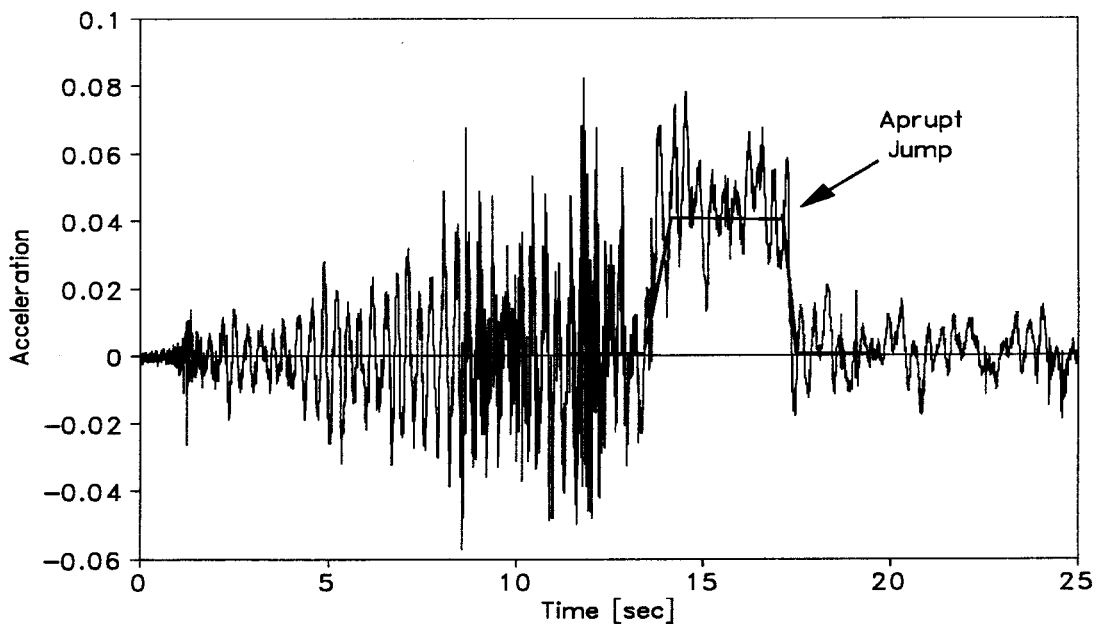

Fig. 4.5: Acceleration Record for Sensor No. 3 During the 2nd Test of the Shipshaw Bridge

4.2.5 Data Analysis

The data from the Quebec Ministry of Transportation's test was analysed using ULTRA and VISUAL. ULTRA computed the phase, transfer function, cross-spectra, and coherence functions for each pair of signals and used these functions to determine the PMR modal ratio functions. (The phase had to be (0° ± 20°) or (180° ± 20°) to be considered as a potential mode shape.) The PMRs were used by VISUAL to animate the mode shapes at the various frequencies. The mode shapes that were calculated with ULTRA and VISUAL are described below.

4.2.6 Results

Table 4.3 and Fig. 4.6, below, summarize the frequencies and mode shapes of the Shipshaw Bridge calculated from the experimental data and determined analytically by Filiatrault prior to the interpretation of the experimental data. As you can see, the analytical results closely correlate with the experimental results obtained with ULTRA and VISUAL. The average of the frequency differences for the first six modes was only 4.3 % (Table. 4.3). The experimentally determined modes in Fig. 4.6 closely match the analytically derived mode shapes.

The difference between analytically derived and experimentally determined frequencies was defined as

$$\text{difference} = \frac{|f_a - f_e|}{f_e} * 100 \quad \text{in } \% \tag{4-2}$$

where f_a is the analytical frequency and f_e is the experimental frequency.

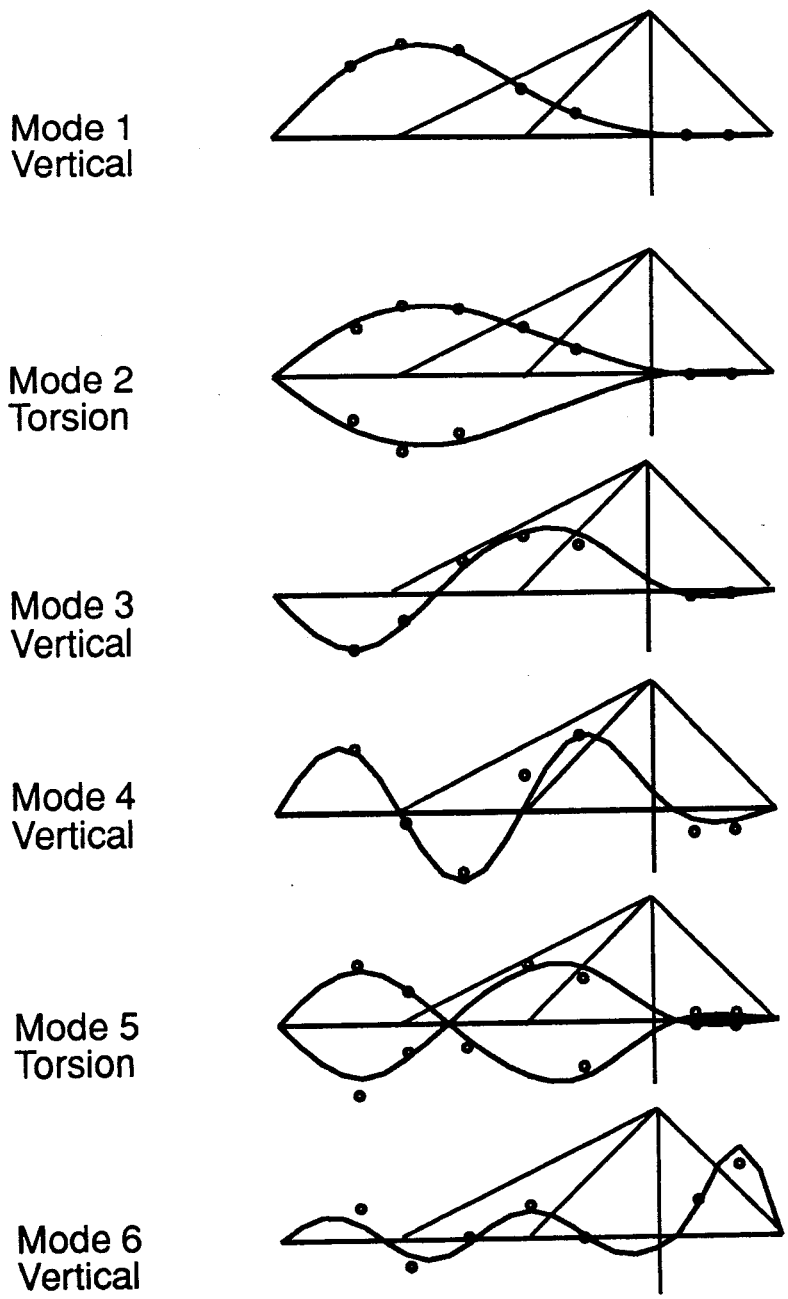

Fig. 4.6: Computed and Measured Mode Shapes of the Deck of the Shipshaw Bridge.

Table 4.3: Experimentally Determined and Analytically Derived Frequencies of the Shipshaw Bridge

Mode Number	Description of Mode Shape	Experimentally Determined Frequency [Hz]	Analytical Derived Frequency [Hz]	Difference [%]
1	1st Vertical Mode of Deck	0.58	0.56	3.4
2	1st Torsional Mode of Deck	1.03	1.10	6.8
3	2nd Vertical Mode of Deck	1.17	1.17	0.0
4	3rd Vertical Mode of Deck	1.76	1.82	3.4
5	2nd Torsional Mode of the Deck	2.05	2.11	2.9
6	4th Vertical Mode of Deck	2.44	2.21	9.4

4.2.7 Performance of the HBES Software

Because the Quebec Ministry of Transportation provided the data and the researchers at Ecole Polytechnique created the dynamic model, ULTRA and VISUAL were the only parts of the HBES used in the Shipshaw bridge study.

The ASCII data input option of ULTRA was used to process fifty-six records, that contained 8192 points each, from the Shipshaw Bridge. ULTRA's data manipulation options were used to remove constant and linear trends from these records before the PSDs and PMRs were computed. Overall, the program was very effective for reducing the Shipshaw data. All of the records were processed in one day.

The modal ratio functions created by ULTRA were assembled into mode shapes using VISUAL. The undeformed shape of the stick-model used to represent the structure could be viewed from

any angle with the 3-D plotting features of VISUAL. After a good view of the structure was found, the mode shapes were animated. The first six mode shapes of the Shipshaw Bridge were determined in less than one hour.

Two limitations of VISUAL were discovered when the Shipshaw data was interpreted. A memory problem was encountered when more than 15 modal ratio files were used. Also, the numerical values of the mode shape vectors could not be extracted conveniently. The memory problem was eliminated by integrating extended memory drivers into VISUAL (described in section 3.3.6.2). An option to store the mode shape information in a file was also added to VISUAL so numerical values could be extracted later.

Overall, ULTRA and VISUAL analysed the Shipshaw Bridge's data effectively in an office environment.

4.2.8 Conclusions of the Shipshaw Bridge Study

In spite of the limitations of the data, the primary modes of vibration of the Shipshaw Bridge were clearly identified. The frequencies and mode shapes obtained with ULTRA and VISUAL closely matched the analytically calculated frequencies and mode shapes.

This study clearly demonstrated how effectively ULTRA and VISUAL analyse data. The 56 acceleration records, consisting of 8192 points each, were analysed in less than one day. The first six natural frequencies of the bridge were identified and the corresponding mode shapes were determined. Traditionally, this process might have taken a few weeks.

The experience gained from examining the data of the Shipshaw bridge was used to plan and execute the tests of the Colquitz River Bridge discussed in the following section. A "quality

control" program was implemented into HBES after this study to avoid the shortfalls of the Shipshaw data. Many typos and small bugs in the early versions of the HBES programs were also eliminated.

4.3 Study of the Colquitz River Bridge

A series of dynamic tests were performed on the Colquitz River Bridge, near Victoria, at the end of August, 1992. This bridge was selected because it is typical of many bridges in B.C.. It is located in an area of high seismic risk and the site is very accessible.

Ambient vibration tests were performed to determine the dynamic characteristics of the bridge. In addition, pullback tests were performed to verify the results from the ambient tests. The data from both the ambient and the pullback tests was analyzed to determine the frequencies and mode shapes of the bridge. These experimentally determined dynamic characteristics were used to tune computer models. A detailed description of the testing and the subsequent analysis is given in the following sections.

4.3.1 Objectives of the Colquitz River Bridge Study

The objectives of the tests on the Colquitz River Bridge were to:

- Assess the performance of the HBES hardware under field conditions.
- Evaluate the applicability of the HBES software for in-situ data interpretation.
- Perform extensive ambient vibration tests of a bridge by measuring its motions at a large number of locations.
- Use pullback tests to verify the ambient vibration results.
- Determine the structure's principal modes of vibration.
- Create improved computer models that correlate with the experimental results.

The tests on the Colquitz River Bridge were the first opportunity to use and evaluate all of the components of the HBES.

4.3.2 Background on the Colquitz River Bridge

The Colquitz River Bridge, shown in Fig. 4.7, was built in the late 1950s. It supports two lanes of north bound traffic of the Trans Canada Highway near Victoria, British Columbia. As shown in Fig. 4.8, the bridge is a 82.68 m long, five span continuous overpass. The deck consists of a 0.165 m thick concrete slab with a 0.06 m wearing surface. The deck is supported by six continuous steel girders which rest on two pier concrete bents. Each bent has two orthogonal columns with a width of 0.914m. These columns support 0.914 m wide and 1.219 m high cap beams. In the longitudinal direction, the central two bents restrain the bridge through fixed bearings. The other two bents and the abutments have 0.240 m high rocker bearings which allow the bridge to move longitudinally. The steel bearings restrain the steel girders at all the bents and the abutment in the transverse direction.

4.3.3 Dynamic Base Model of the Colquitz River Bridge

SAP90 was used to develop and analyse a "base model" of the bridge. This model was used to determine the location of sensors. The model was created using "as built" drawings of the bridge. The "base model" assumes the following:

- The abutments and the column footings are fixed. (No soil springs.)
- The columns behave as if they are unrestrained by the soil.

- The deck is modeled as a series of shell elements with a 0.18 m thickness. The girders are modeled as beam elements with their center line at the top flange location. To account for the increase in stiffness, due to the assumed composite action of the girders and deck, the moments of inertia of the girders is increased.

- Stiffening diaphragms between the girders are not modeled.

- Bearings are idealized to behave as they are shown on the drawings.

- Short links with the stiffness of the stringers are used to account for the difference in elevation between the top of the bents and the deck level.

Some of the material and geometric properties of the base model are listed in Table 4.4. A plot of the undeformed model is shown in Fig. 4.9.

The "base model" has a total of 244 three-dimensional beam elements that are used to model the steel girders, the concrete piers, and the concrete cap beams. The deck was modeled using 126 shell elements. Fig. 4.10 shows the principal modes of vibration and the frequencies computed for the "base model". These mode shapes were used to determine the sensor locations described in the following section.

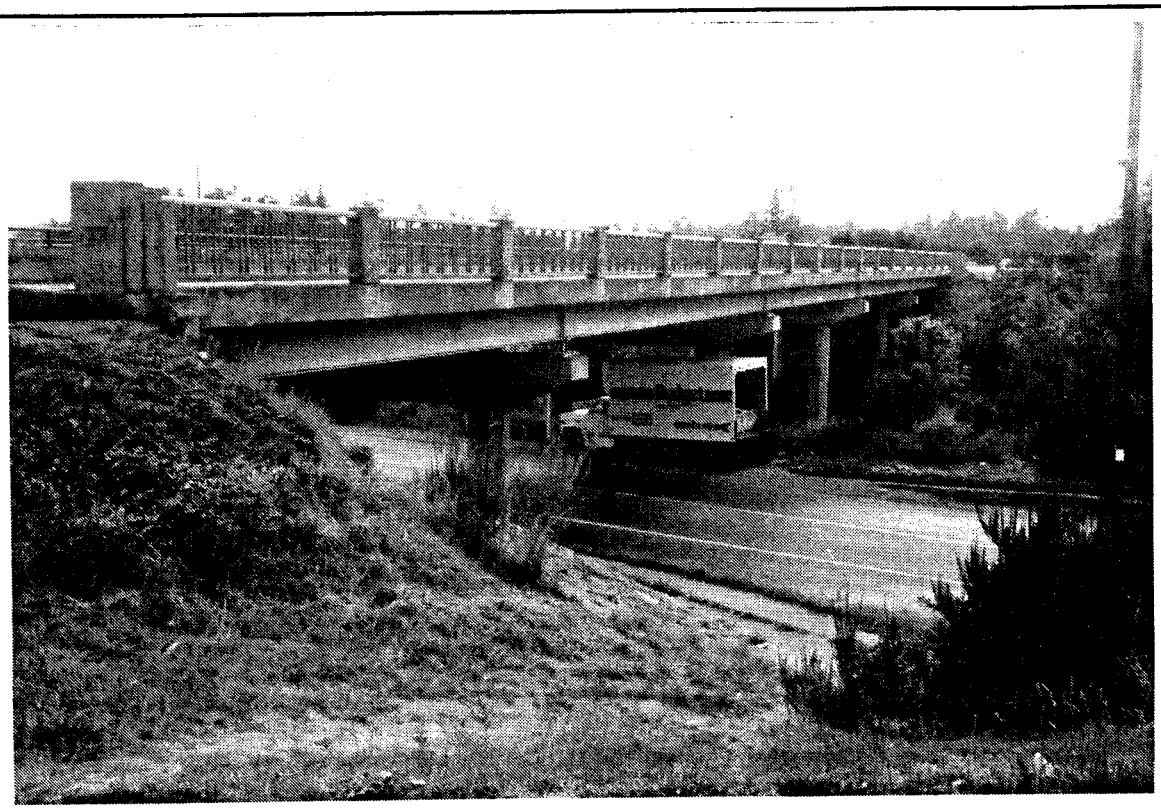

Fig. 4.7: View of the Colquitz River Bridge

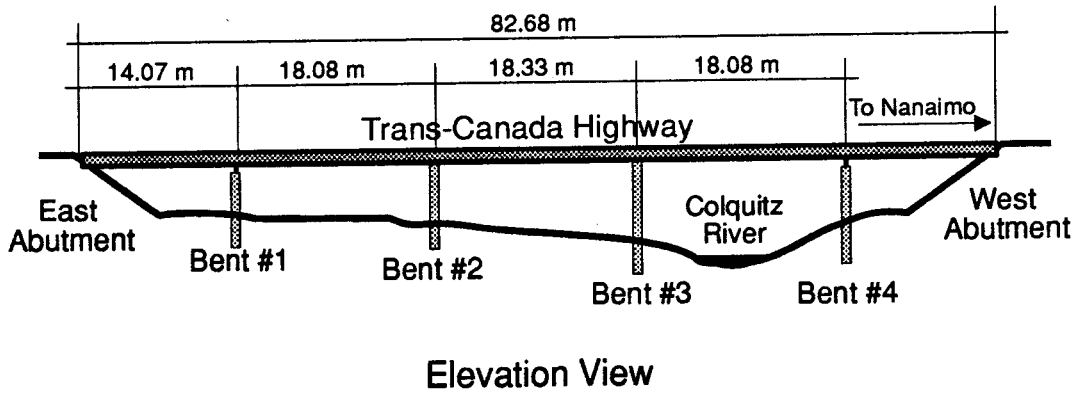

Fig. 4.8: Colquitz River Bridge Elevation

Table 4.4: Key Element Properties for the "Base Model" of the Colquitz River Bridge

Property	Deck (Shell)	Girder (3D-Beam)	Pier (3D-Beam)	Cross-Head (3D-Beam)
Elastic Modulus MPa	26540	200000	26540	26540
Shear Modulus MPa	12490	76900	12490	12490
Area m^2	N/A	0.027	0.697	1.114
Moment of Inertia m^4 Strong Axis Weak Axis	N/A	0.00311 0.000103	0.038 0.038	0.138 0.078
Unit Mass	2400 kg/m^3	210 kg/m	1673 kg/m	2674 kg/m
Thickness	0.18 m	N/A	N/A	N/A

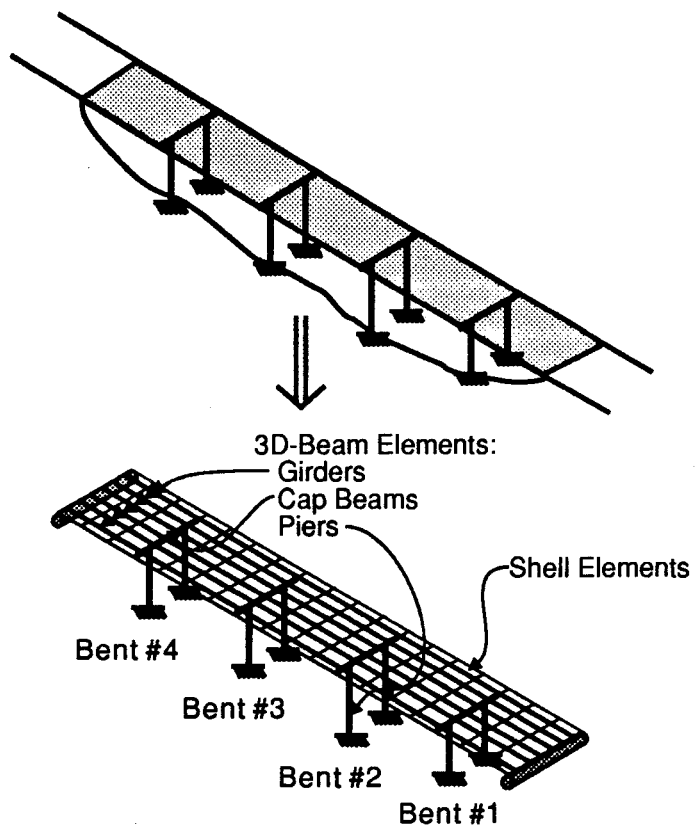

Fig. 4.9: "Base Model" of the Colquitz River Bridge

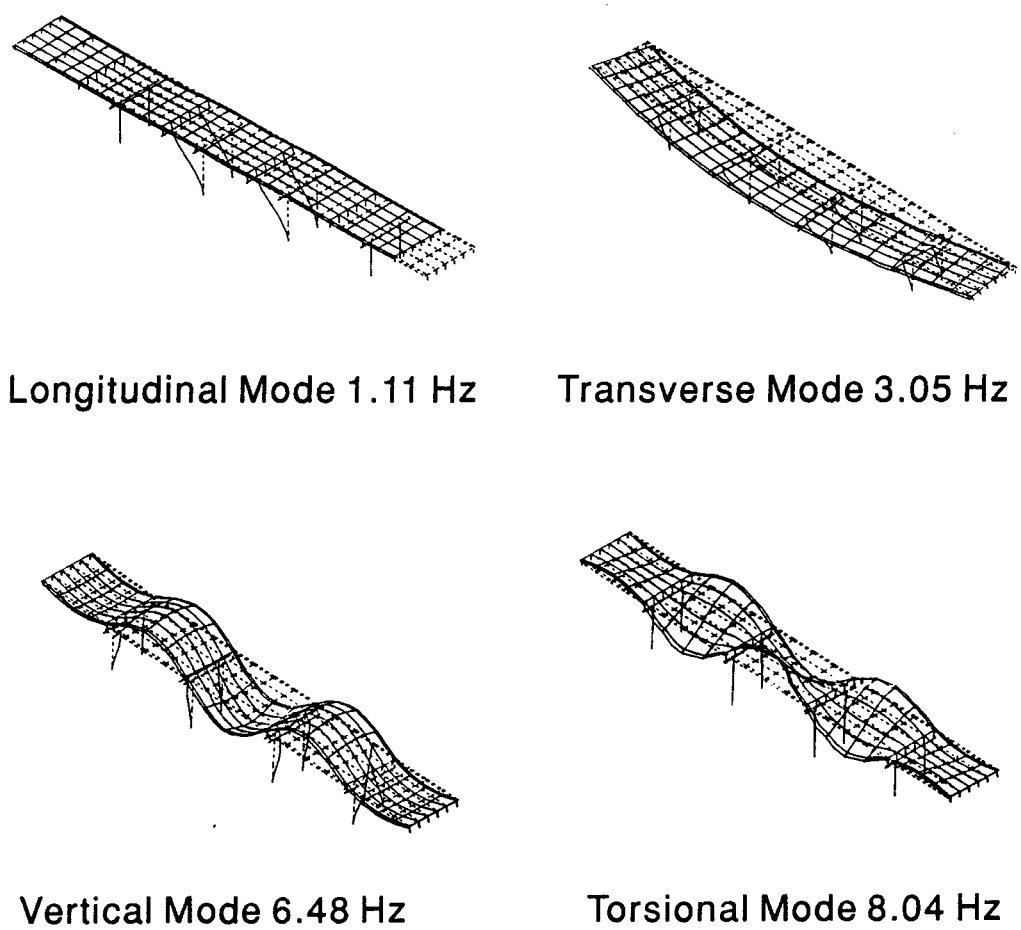

Fig. 4.10: Principal Analytical Modes of the Colquitz River Bridge ("Base Model")

4.3.4 Vibration Test Data

4.3.4.1 Ambient Vibration Test Data

Sensor Locations

Sensor locations were selected at the bents and along the two exterior bridge girders based on the results described in section 4.3.3. These locations were identified using odd numbers for the northern half of the bridge and even numbers for the southern half, as illustrated in Fig. 4.11. This numbering convention was used for all of the tests. The vertical ambient vibrations were recorded at locations 1 - 38. The vibrations were measured at 38 locations to adequately define the higher modes of the deck in the vertical direction. The transverse measurements were limited to the odd numbered locations between 1 - 37. The longitudinal vibrations were measured at bent No. 2 (locations 15, 16, 41, and 42) and bent No. 4 (locations 31, 32, 45, and 46). A total of 156 ambient vibration records were obtained. The individual test setups are described in Appendix F.

More data was collected at the Colquitz River Bridge than is traditionally taken in other ambient vibration studies. For example, while 156 records were taken at the Colquitz River Bridge, Muria-Vila, Gomez, & King (1991) studied the cable stayed Tampico bridge with 34 ambient vibration records.

The large number of records obtained at the Colquitz River Bridge was used to define the structure's mode shapes in detail. Because the HBES was designed to handle large sets of ambient vibration data, this comparatively large data set was obtained and analysed easily.

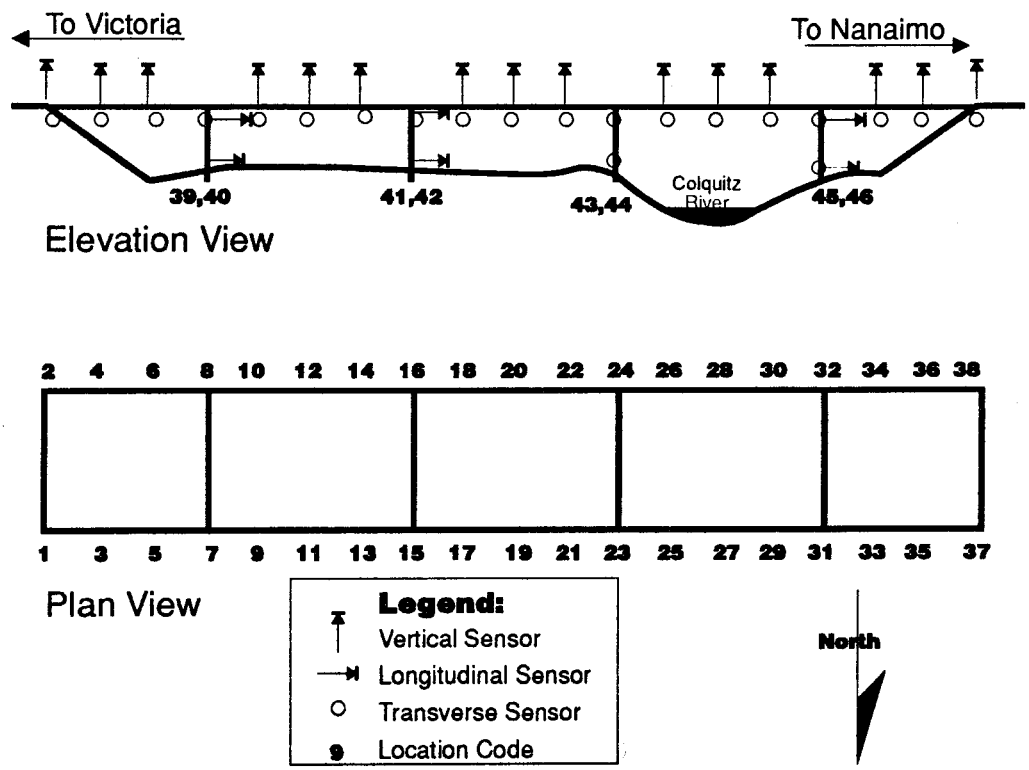

Fig. 4.11: Numbering Convention for Sensor Locations during Colquitz River Bridge Tests.

Data Quality Control Program

A quality control program was implemented to obtain reliable data with the HBES. Quality control was achieved by using the following procedure for each measurement setup:

Step 1 Install sensors at desired locations and connect them to the signal conditioner using colour coded cables.

Step 2 Send a calibration signal to the sensors and visually inspect the calibration records for abnormalities. Proceed with test if calibration is acceptable.

Step 3 Amplify the signals to match the conversion range of the A/D converter using the signal conditioner.

Step 4 Start recording the signals and monitor the signal levels for saturation.

Step 5 Repeat the calibration of the sensors and inspect the calibration record again.

Step 6 Copy the records from the acquisition computer to the analysis computer and inspect the data for drifts and other abnormalities using ULTRA.

Following these steps the proper function of each sensor before and after each setup was insured. The quality of each record was verified shortly after each setup was completed. If any abnormalities occurred in the recorded data, such as saturation, the records were retaken before the sensors were relocated. A portion of a typical vertical vibration record obtained at location No. 20 is shown in Fig. 4.12. This record does not show any drifting and the corresponding PSD in Fig. 4.13 shows there is very little frequency content in the signal up to approximately 5 Hz. The peak near 6 Hz clearly identifies a natural frequency of the structure (discussed in more detail in section 4.3.5.1.)

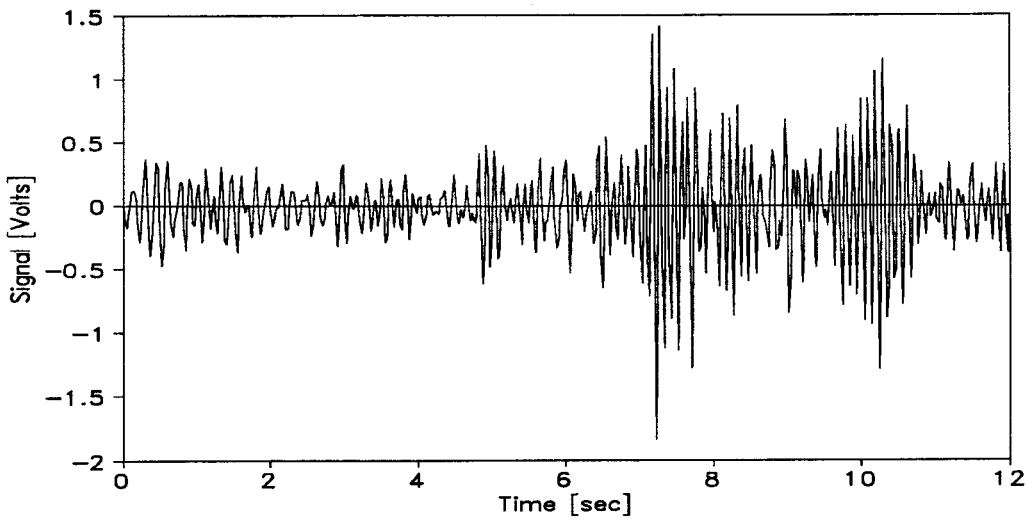

Fig. 4.12: Portion of Vertical Ambient Vibration Signals from Location No. 20 of the Colquitz River Bridge

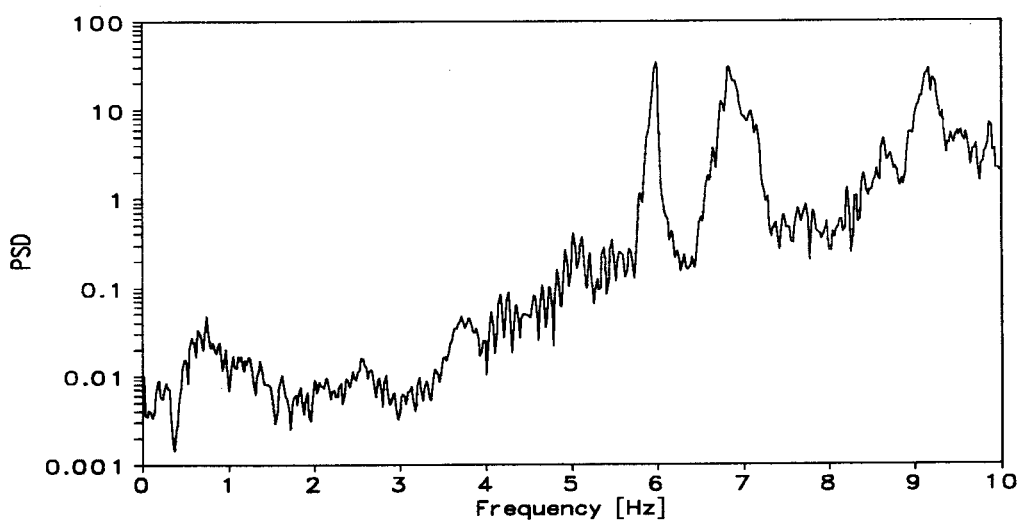

Fig. 4.13: PSD of Vertical Ambient Vibration Signals from Location No. 20 of the Colquitz River Bridge

4.3.4.2 Pullback Tests

Several pullback tests were conducted to verify the ambient vibration test results. These tests were used to identify the dynamic characteristics of the bridge in the transverse and longitudinal directions. Pullback tests consisted of loading the bridge at a selected location with approximately twenty thousand pounds of force and then releasing the load very quickly to induce free vibrations.

Pullback tests are generally more expensive than ambient vibration tests, because an anchor structure usually needs to be constructed. In this project, the proximity of an abandoned railway pier provided an excellent anchor structure for pullback testing, which made this test relatively inexpensive.

Transverse Pullback Tests

During the transverse pullback tests, wire ropes were attached to the abandoned railway piers and a chain block was connected to the Quick Release Mechanism (QRM) introduced in section 3.2.2. The bridge was pulled laterally at the top of the northern pier of bent No. 3 using the chain block. The load was then released with the QRM.

Fig. 4.14 shows a schematic of the test setup. The structure's free vibrations were recorded at the reference locations of the ambient tests and at the pier where the load was applied. This pier was instrumented at the top of the cap beam and on the bottom flange of the exterior girder just above the fixed bearing.

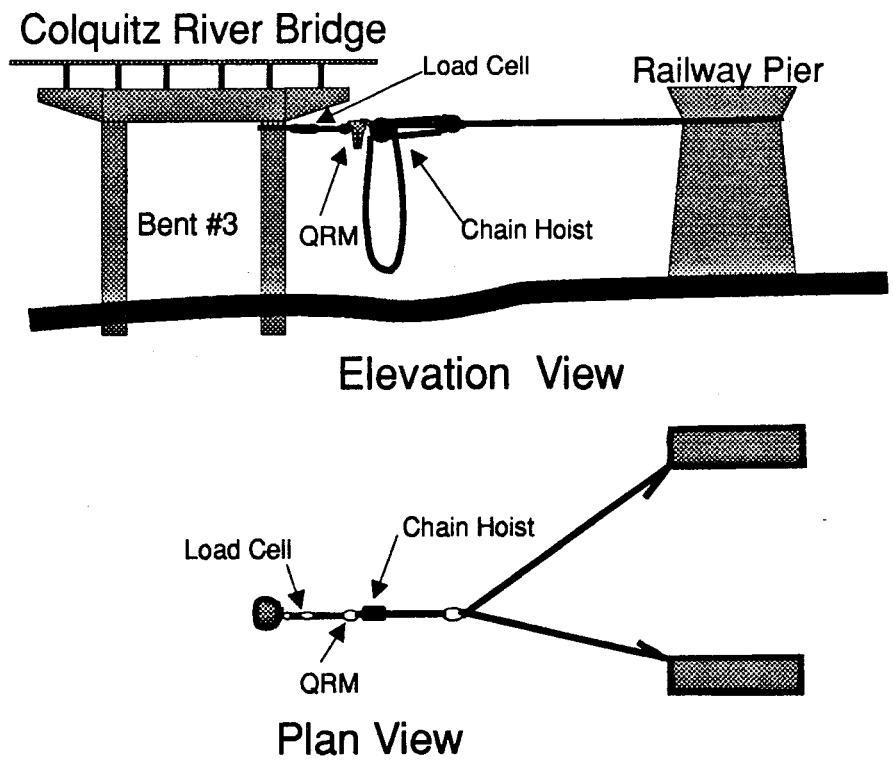

Fig. 4.14: Transverse Pullback Test Setup for the Colquitz River Bridge

The instruments on top of the pier and on the girder were later used to determine if the bearing slipped transversely during the release. These records were also used to determine the damping associated with the first transverse mode (see section 4.3.5.2).

Longitudinal Pullback Tests

In addition to the transverse pullback tests, longitudinal pullback tests were performed to determine the first longitudinal mode of the deck. For these tests, wire ropes were attached to the top of the expansion bents on one side and to the QRM and chain block which were attached to a fixed bent on the other side. This setup could be used to excite the deck longitudinally without using tiebacks. Fig. 4.15 shows a schematic of this setup.

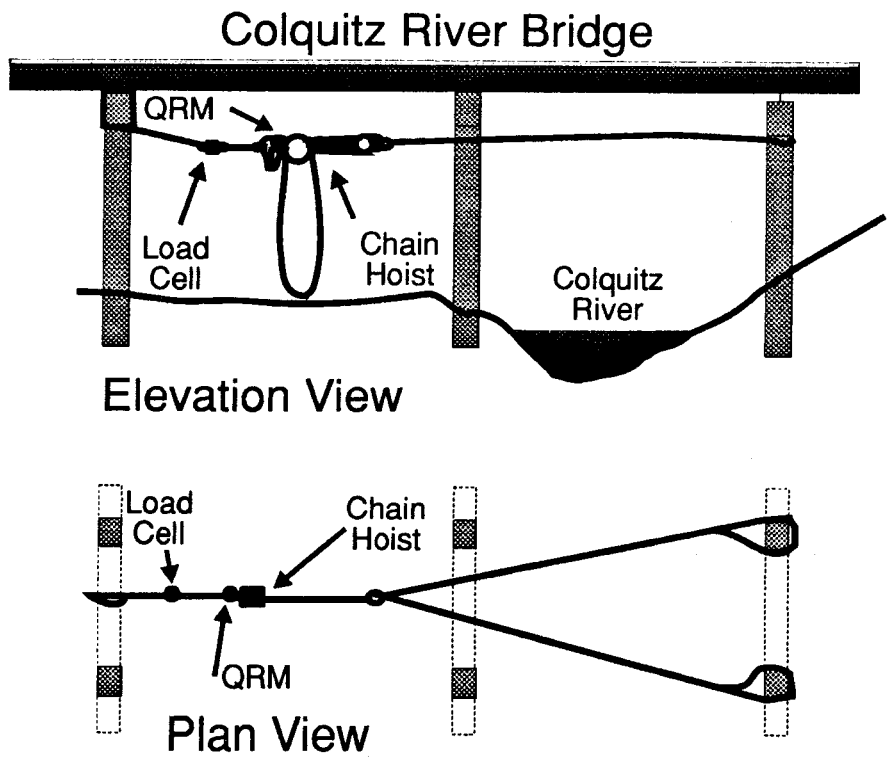

Fig. 4.15: Longitudinal Pullback Test Setup for the Colquitz River Bridge

The sensors were placed alternately at the top and bottom of each pier of the expansion bent and the fixed bent. The data obtained from these tests was used to determine the damping associated with the first longitudinal mode (see section 4.3.5.2).

4.3.5 Test Data Analysis and Results

Unlike the analysis of the Shipshaw data, all the data records for the Colquitz River Bridge were processed on site shortly after they were obtained. Natural frequency and mode shape information was calculated while testing was in progress. The results from a preliminary analysis, identifying the important dynamic characteristics of the structure, were presented in

a report (Felber, Ventura, Yee and Stiemer, 1992) to the Ministry of Transportation and Highways of B.C. only four days after the returning from the site. The following sections will present the results from a more complete data analysis.

4.3.5.1 Ambient Vibration Test Results

The natural frequencies determined from the ambient vibration data analysis are summarized in Table 4.5. A detailed discussion of these results is given in the following sections.

Vertical Modes

Power Spectral Densities (PSDs) were computed for all the vertical motions recorded on the bridge. These PSDs were then normalized and averaged to produce plots of the averaged normalized PSDs (ANPSD). The ANPSD for all of the vertical signals is shown in Fig. 4.16. As you can see from this figure, the bridge's dominant peaks range from 6 Hz to 10 Hz.

Table 4.5: Experimentally Determined Modal Frequencies of the Colquitz River Bridge

Mode Number	Description of Mode Shape	Frequency [Hz]	Period [sec.]
1	1st Longitudinal	1.66	0.60
2	1st Transverse	2.81	0.36
3	2nd Transverse	3.20	0.31
4	1st Deck Vertical	5.95	0.17
5	3rd Transverse	6.67	0.15
6	1st Deck Torsion	6.83	0.15
7	2nd Deck Vertical	7.14	0.14
8	2nd Deck Torsion	7.85	0.13
9	3rd Deck Vertical	8.70	0.11
10	3rd Deck Torsion	9.20	0.11
11	4th Transverse	14.7	0.07

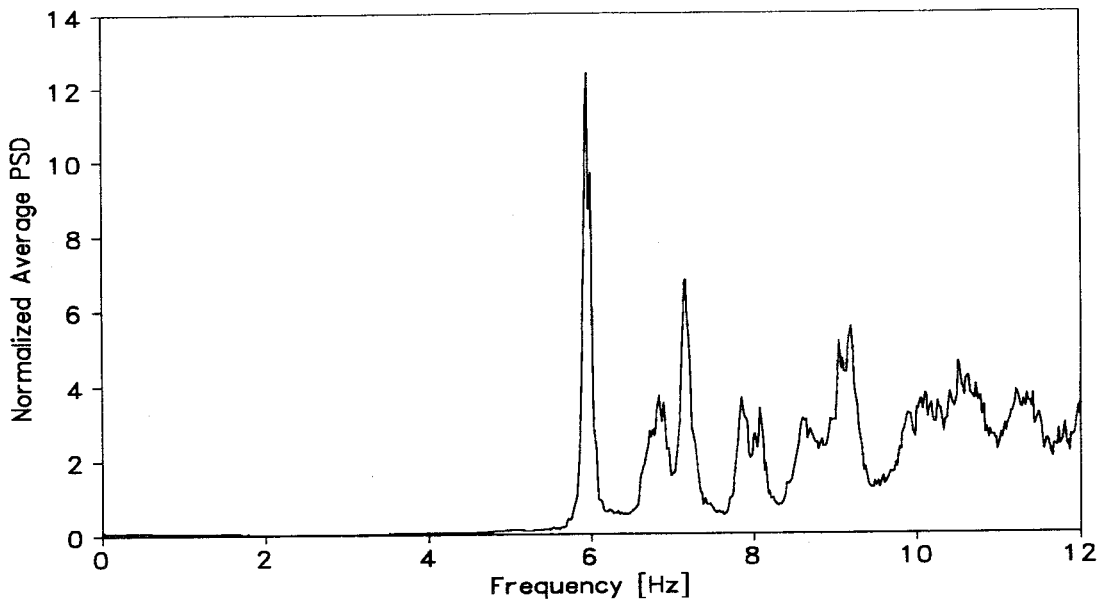

Fig. 4.16: Vertical ANPSD for the Colquitz River Bridge

Signals from sensors on either side of the deck were added to produce a series of signals in which the vertical translational modes were enhanced. The computed ANPSD for these signals is shown Fig. 4.17. The first three peaks of this spectrum were used to identify the vertical translational frequencies as 5.95 Hz, 7.17 Hz, and 8.63 Hz. Elevation views of the corresponding mode shapes are shown in Fig. 4.18. The measurement locations are shown as dots and the inferred smoothed mode shape is drawn as a dashed line.

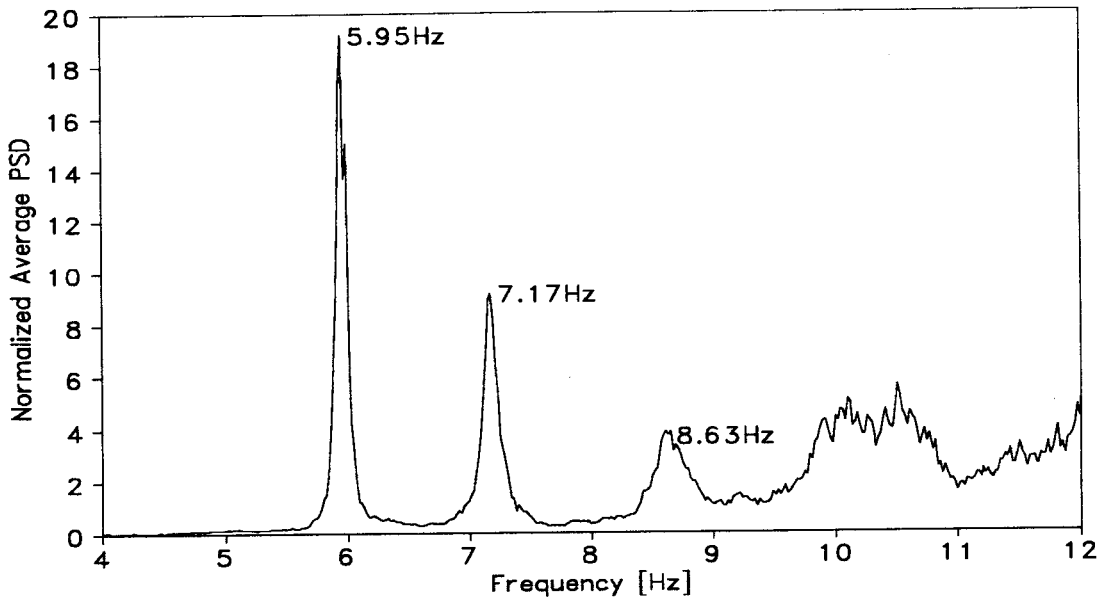

Fig. 4.17: Vertical Translation Enhanced ANPSD for the Colquitz River Bridge

To enhance the vibration's torsional components, a new set of signals was created by subtracting the acceleration time histories from opposite sides of the deck. These new signals were then used to compute the ANPSD shown in Fig. 4.19. The first three peaks of this spectrum identify the torsional modes of the deck as 6.8 Hz, 7.85 Hz, and 9.2 Hz. Elevation views of the torsional mode shapes corresponding to the frequencies are shown in Fig. 4.20. The measurement locations on the south side of the deck are shown with rectangles, while the measurement locations on the north side of the bridge are shown with dots. The dotted line shows the inferred mode shape on the south side and the dashed line shows the inferred shape on the north side of the deck.

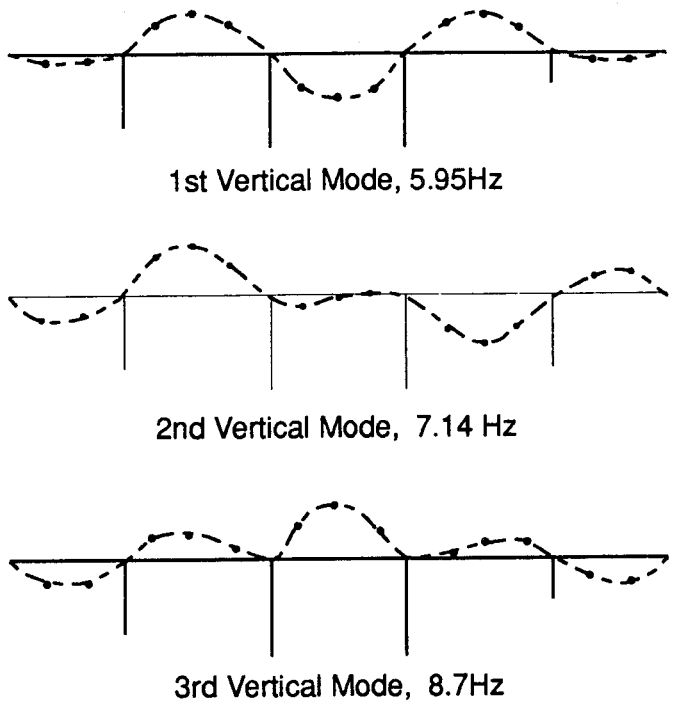

Fig. 4.18: Measured Vertical Mode Shapes of the Colquitz River Bridge

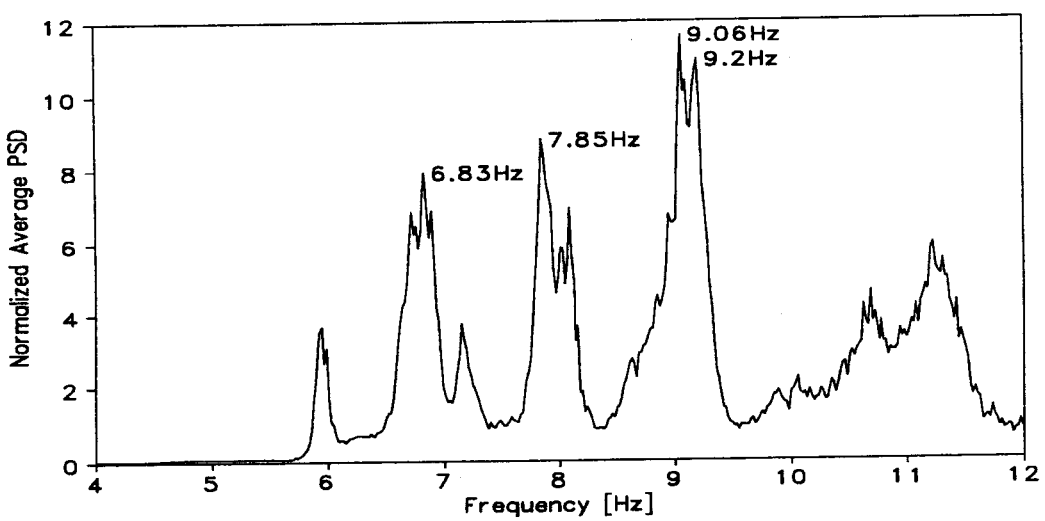

Fig. 4.19: Torsion Enhanced Vertical ANPSD for the Colquitz River Bridge

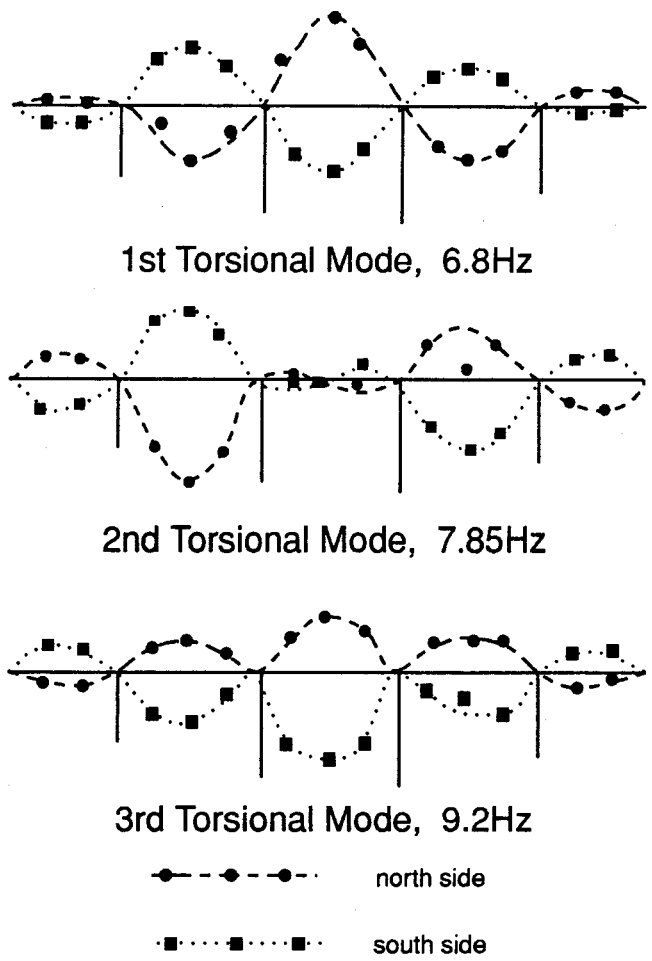

Fig. 4.20: Measured Torsional Mode Shapes of the Colquitz River Bridge

Transverse Modes

The ANPSD of the traverse signals were computed to identify the transverse modes of the deck. From the peaks of this spectrum, shown in Fig. 4.21, the first two transverse modes were identified as 2.81 Hz and 3.2 Hz. After examining the PSDs from the transverse vibration records along the length of the bridge deck, it was apparent that the peak at 2.81Hz is associated with an overall transverse mode of the deck. This mode was more pronounced between bent

No. 2 and the west abutment. The peaks at 3.2 Hz were the most dominant between the east abutment and bent No. 2. The relative strength of the power spectral peaks along the length of the deck, for the frequency band from 2 Hz to 6 Hz, is illustrated in Fig. 4.22. The peaks of the ANPSD at 6.67 Hz, 9.96 Hz, 11.97 Hz and 14.7 Hz correspond to modes that have both transverse and vertical components.

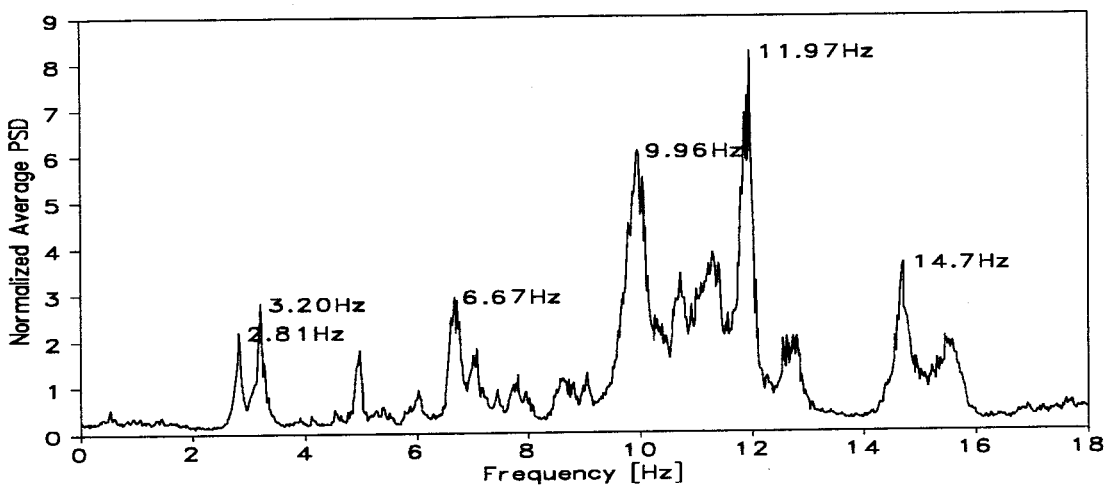

Fig. 4.21: Transverse ANPSD for the Colquitz River Bridge

After analyzing the modes for these frequencies, I concluded that the peak at 6.67 Hz corresponded to the 3rd transverse mode and that the peak at 14.7 Hz corresponded to the 4th transverse mode. The other two peaks appeared to be associated with modes which are dominated by vertical movement.

Plan views of the transverse mode shapes associated with the four identified frequencies are shown in Fig. 4.23. In this figure the computed modal ratios corresponding to the measurement locations are identified as dots. The smoothed mode shapes inferred are drawn as dashed lines.

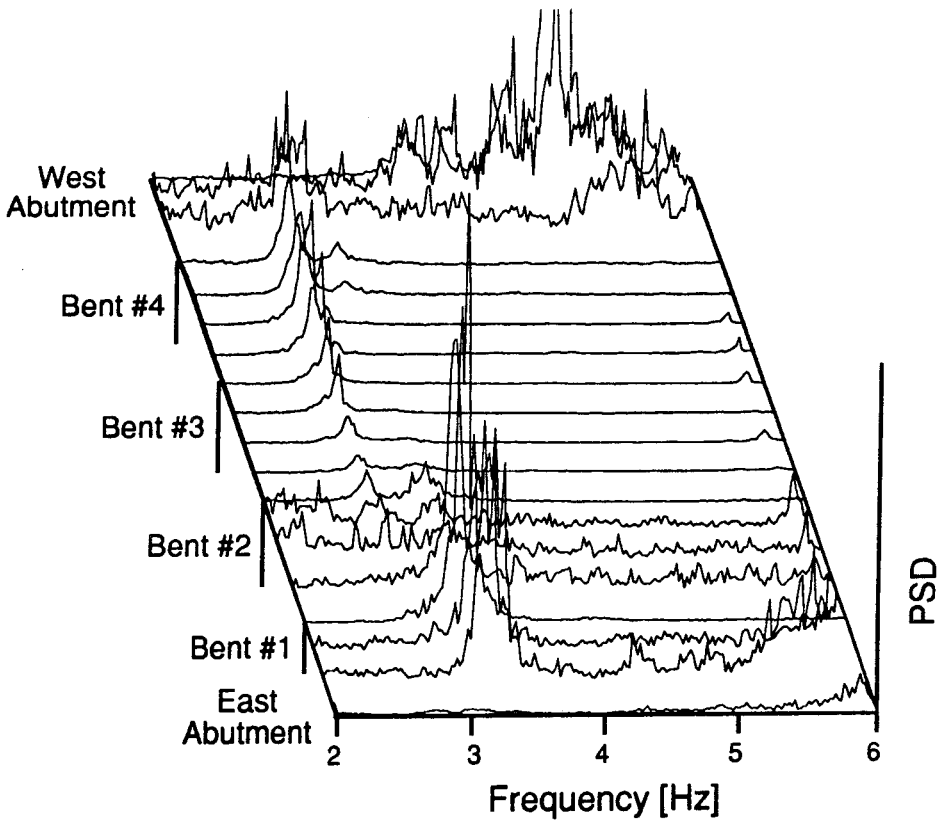

Fig. 4.22: Transverse PSD Distribution Along the Length of the Colquitz River Bridge

The transverse modes are not as well defined as the vertical and torsional mode shapes of the deck, shown previously. To enhance the definition of the transverse modes, the following improvements are suggested. When these measurements were conducted only 4 sensors were available as part of the HBES. One of these sensors was used as a vertical reference station and another as a transverse reference station. The remaining two transducers were roved along the length of the bridge. While this approach theoretically produces reliable results, the higher transverse modes could not be positively identified. If two or more reference stations are used, the data can be independently recorded with respect to each reference. The resulting mode shapes can then be compared.

In addition, certain modes may have nodes at a particular reference station and these modes can, therefore, not be identified if the data was reduced with respect to only that reference location. To improve the results of transverse ambient vibration studies of similar structures, more reference sensors and roving sensors should be used. Transverse measurements should be taken during periods of very light traffic so that the vertical modes have less ambient excitation.

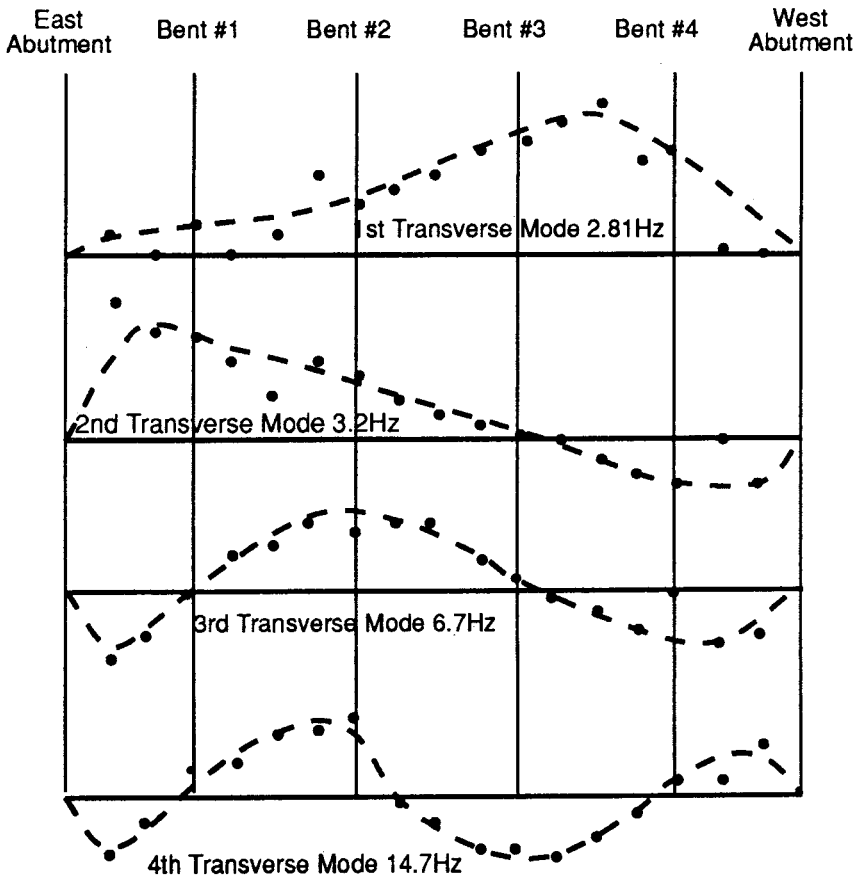

Fig. 4.23: Transverse Mode Shapes of the Colquitz River Bridge

Longitudinal Mode

The ANPSD for the longitudinal direction is shown in Fig. 4.24. From the first peak of this ANPSD, the bridge's first longitudinal mode was identified as 1.66 Hz. The other two large peaks in this spectrum at 5.9 Hz and 6.71 Hz correspond to the deck's first vertical and torsional modes respectively. As the deck flexes up and down, its underside contracts and expands. This motion causes the bents to move longitudinally. It is assumed that the deck translates in rigid motion with the top of the bent. Fig. 4.25 illustrates the first longitudinal mode shape of bent No. 2.

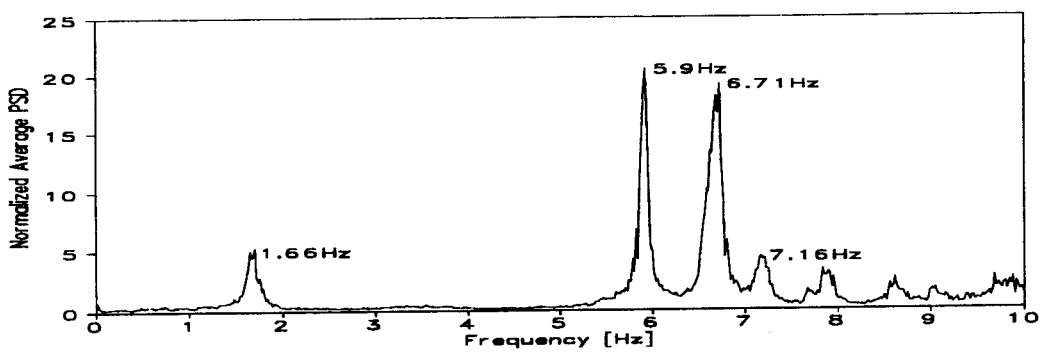

Fig. 4.24: Longitudinal ANPSD for the Colquitz River Bridge

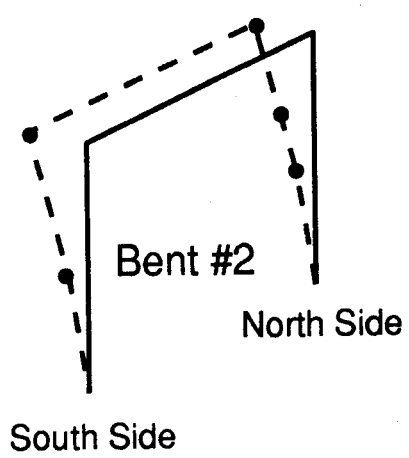

Fig. 4.25: First Longitudinal Mode Shapes of Bent No. 2 of the Colquitz River Bridge

4.3.5.2 Pullback Test Results

The data obtained from the transverse and the longitudinal pullback tests was analysed to determine the primary natural frequencies and the critical damping values for the Colquitz River Bridge. In addition, I investigated slippage of the bearings during the pullback test. The analysis of this data is discussed in the following sections.

Frequency and Damping Analysis

Determination Transverse Frequencies and Damping

The pullback tests were performed to verify the natural frequencies from the ambient vibration tests and to determine the damping values of the principal lateral modes. A typical acceleration record from a transverse pullback test is shown in Fig. 4.26. This acceleration record, was recorded at 200 samples per second with the analog low-pass filters set at 50 Hz. The PSD of this signal, shown in Fig. 4.27, revealed the first frequency was excited at 2.8 Hz. Additional large peaks occurred at 6.7 Hz, 9.2 Hz and 14.6 Hz.

As you can see from both the acceleration record and the PSD, the principal mode was not the only mode excited by the pullback test. The time history had to be digitally filtered, using ULTRA, to remove the higher frequency components. The filtered records were then used to estimate the damping for the first mode.

The frequency response function corresponding to the digital filter is shown in Fig. 4.28. After this filter was applied to the signal, the acceleration record shown in Fig. 4.29 was obtained. The PSD for the filtered acceleration record is shown in Fig. 4.30. This PSD shows all of the signal's high frequency components have been virtually eliminated and the

response of the second excited mode (6.7 Hz) has been reduced significantly. While the filtered signal still contains some high frequency components, it can now be used to estimate damping using the logarithmic decrement method (Clough and Penzien 1975).

The damping value for the deck's first transverse mode was estimated using two filtered transverse acceleration records from the top of bent No. 3. The record from the second transverse test is shown in Fig. 4.31 and the record from the third transverse test is shown in Fig. 4.32. The critical damping values, based on the single cycle logarithmic decrement (Clough & Penzien, 1975), were computed for the first ten cycles of each decay. These values are summarized in Table 4.6. The average critical damping value for the first transverse mode obtained from the two filtered records was 2.6 %.

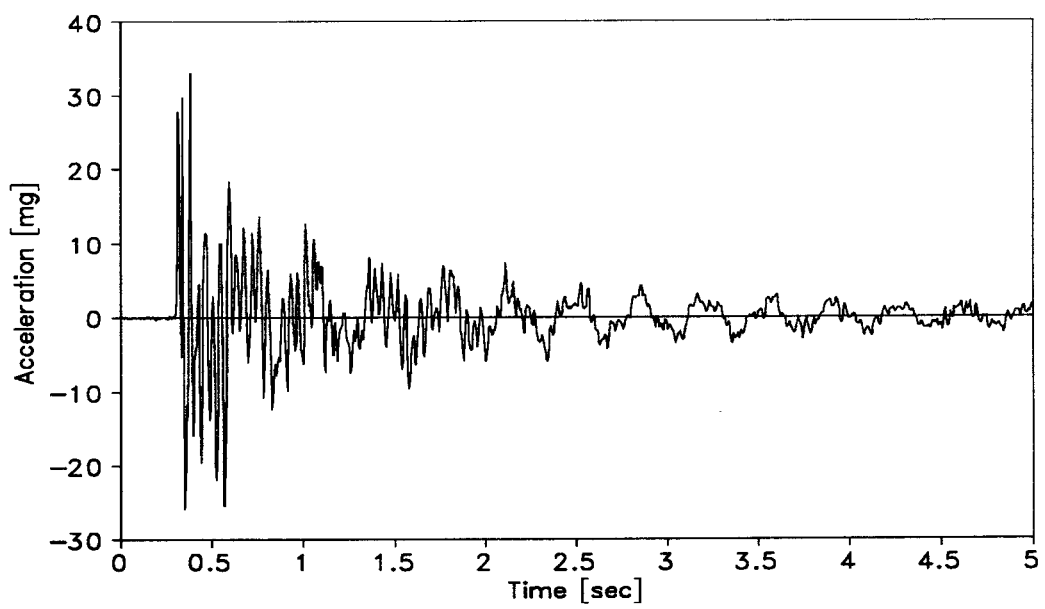

Fig. 4.26: Unfiltered Transverse Pullback Test Acceleration Response

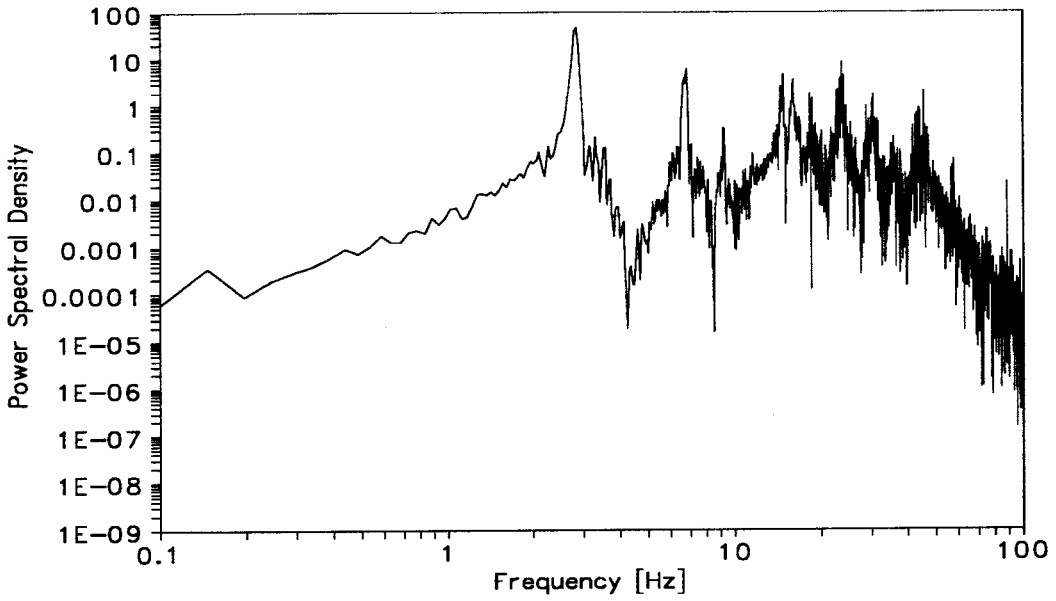

Fig. 4.27: PSD of the Unfiltered Transverse Pullback Test Acceleration Response

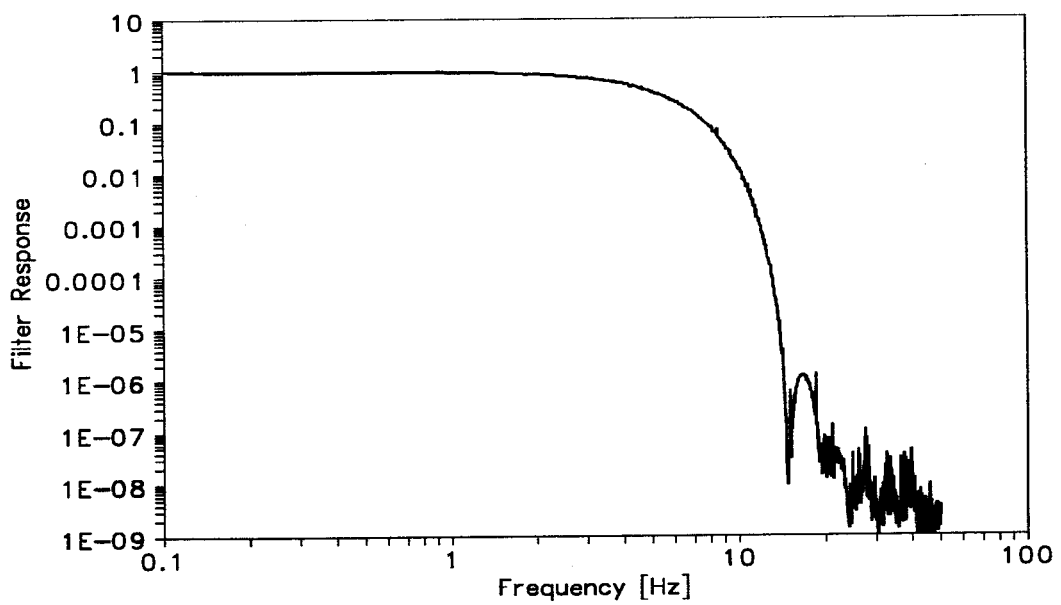

Fig. 4.28: Filter Response

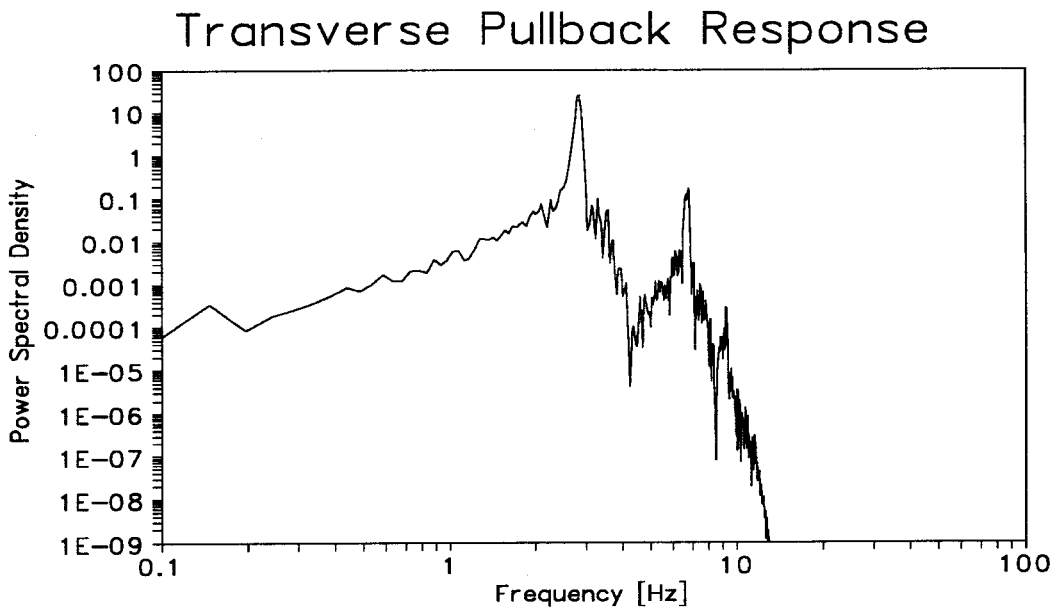

Fig. 4.29: PSD of the Filtered Transverse Pullback Test Acceleration Response

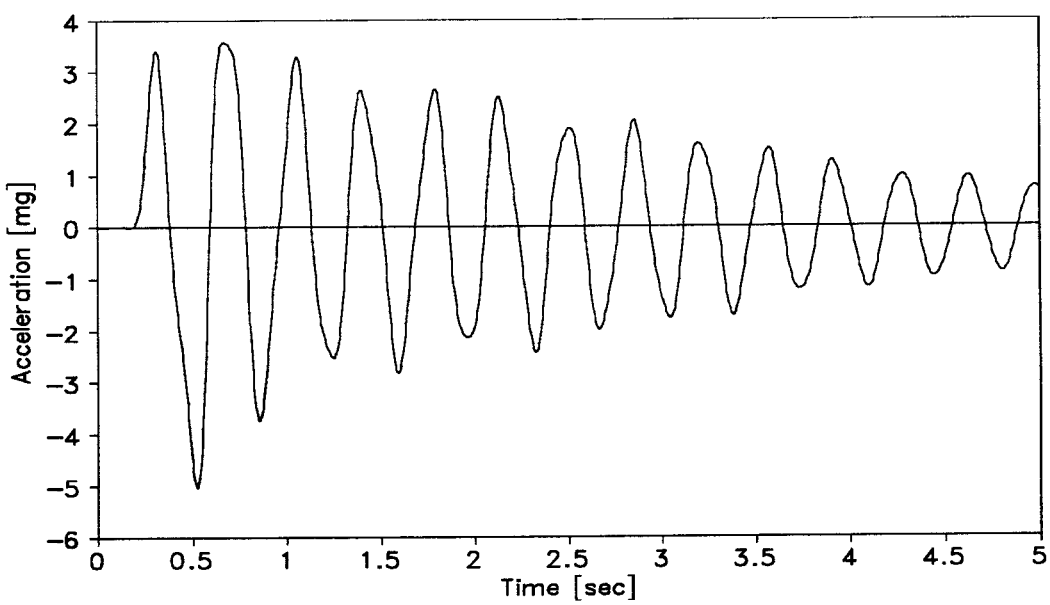

Fig. 4.30: Filtered Transverse Pullback Test Acceleration Response

Table 4.6: Damping Estimates from the First Ten Cycles of the Transverse Pullback Test of the Colquitz River Bridge
[% of critical damping]

Cycle	Second Test	Third Test
1	5.04	5.72
2	2.47	3.75
3	0.51	0.97
4	2.86	1.18
5	3.06	1.27
6	3.05	1.97
7	2.31	1.72
8	2.95	1.66
9	4.02	3.19
10	2.76	2.40
Average	2.90	2.38

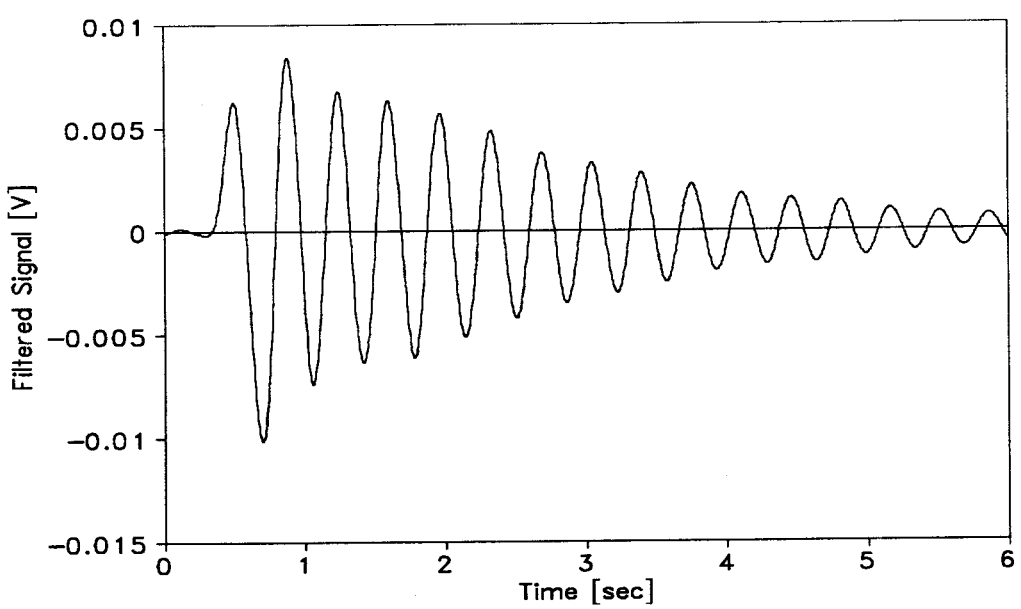

Fig. 4.31: Filtered Transverse Signal on Top of Bent No. 3 for Pullback Test No. 2

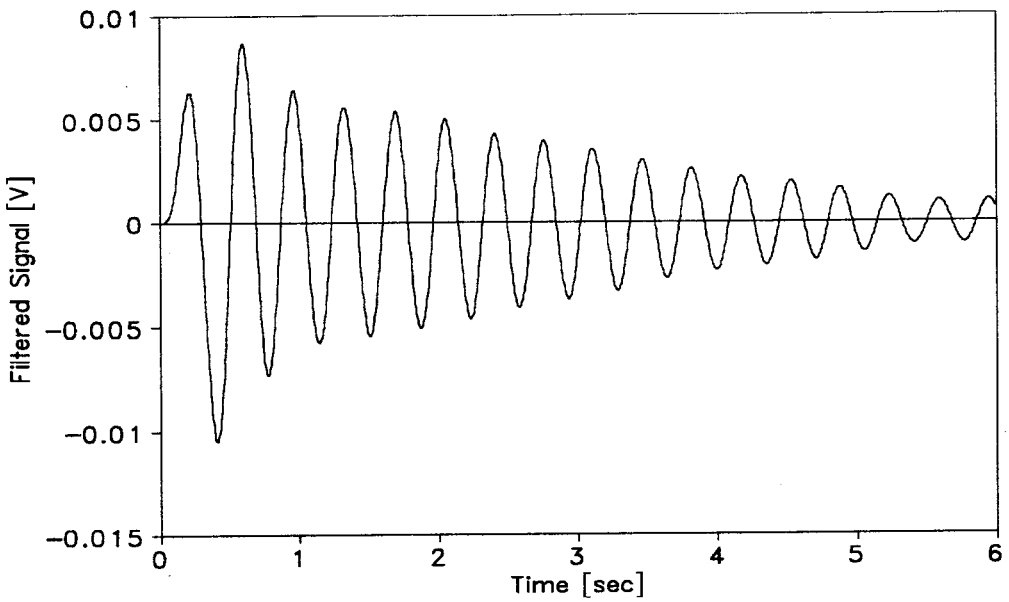

Fig. 4.32: Filtered Transverse Signal on Top of Bent No. 3 for Pullback Test No. 3

Determining Longitudinal Frequency and Damping Estimates

Five longitudinal tests were performed on the Colquitz River Bridge. During the first test, the sensors were placed on bent No. 4. This bent was an expansion bent and, therefore, did not move longitudinally with the deck. The release did not occur in the second and the third tests due to communication problems. The longitudinal frequencies and damping estimates, below, were obtained from the fourth and fifth longitudinal pullback tests. During these tests the sensors were mounted on the fixed bent No. 2.

During the longitudinal pull back test, a 90 kN force was applied at the center of the cross head of bent No. 2. The acceleration response caused by the quick release of the force, was measured at both ends of the cross head. These two signals were added together to remove some of the noise.

The PSD was computed for the unfiltered added signals from the fourth pullback test and is shown in Fig. 4.33. The first main peak of this PSD identifies the frequency of the first longitudinal mode as 1.66 Hz. The other two dominant peaks correspond to the first vertical and first torsional modes of the deck. These two modes were excited because the force was not applied concentrically to the center of the deck. In addition, some of the measured response is due to ambient motions, as discussed in the next section.

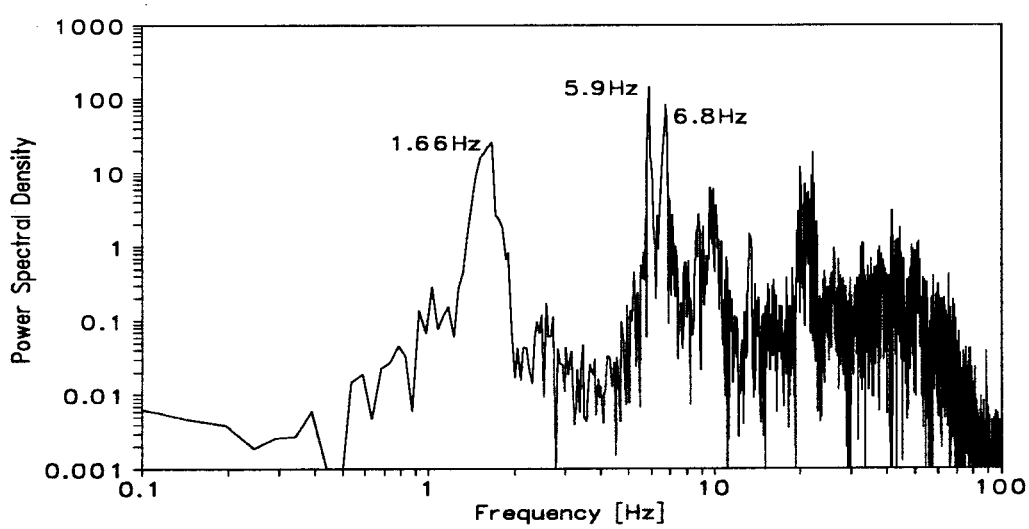

Fig. 4.33: PSD of Added Longitudinal Signal from Top of Bent No. 2 Pullback Test No. 4

To estimate the damping using the logarithmic decrement method, both signals were filtered to remove frequency components above 2 Hz. The records obtained from adding and filtering the signals from the fourth and fifth longitudinal pullback test are shown in Fig.

4.34 and Fig. 4.35 respectively. These records were used to compute the critical damping values based on the single cycle log decrement for the first ten cycles of each decay signal and the corresponding values are given in Table 4.7. The average critical damping value for the first longitudinal mode obtained from the two filtered records was 4.3 %.

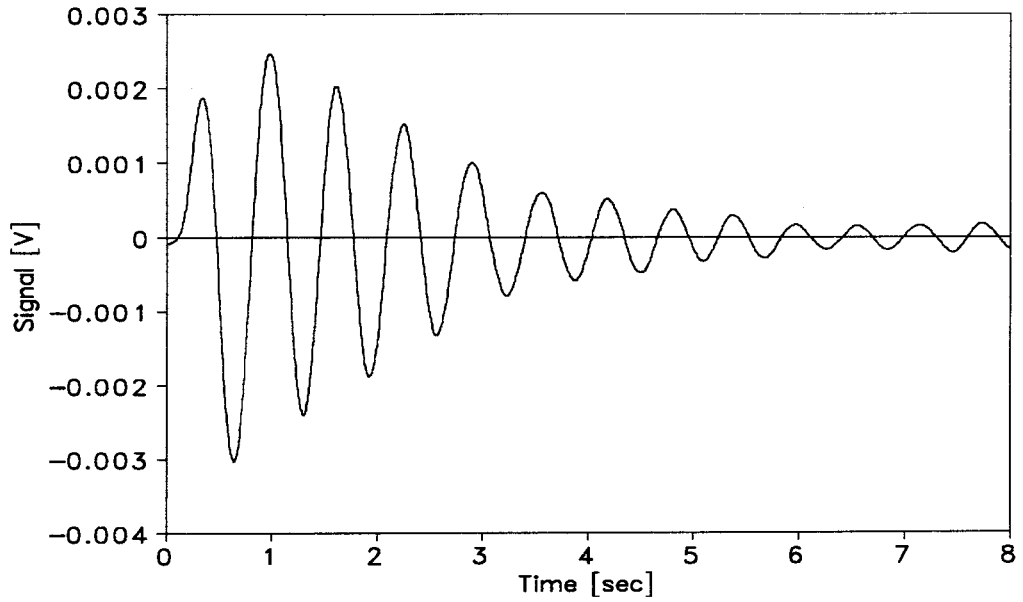

Fig. 4.34: Filtered Added Longitudinal Signal from Top of Bent No. 2 Pullback Test No. 4

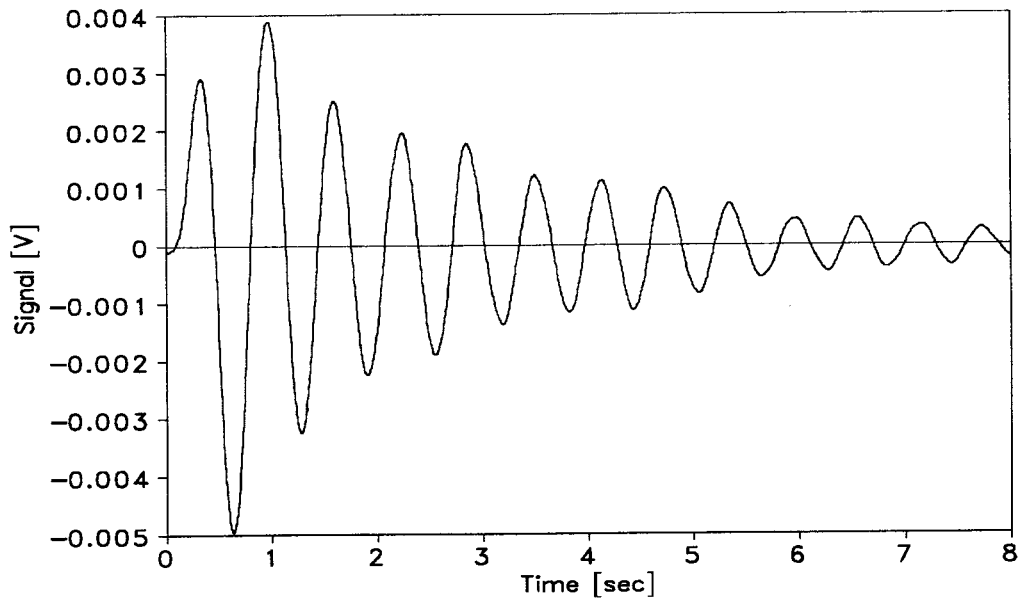

Fig. 4.35: Filtered Added Longitudinal Signal from Top of Bent No. 2 Pullback Test No. 5

Table 4.7: Damping Estimates from the First Ten Cycles of the Longitudinal Pullback Test of the Colquitz River Bridge
[% of critical damping]

Cycle	Fourth Test	Fifth Test
1	3.71	6.75
2	3.83	5.84
3	5.59	2.63
4	8.16	5.18
5	5.04	2.71
6	3.11	0.44
7	6.06	4.73
8	2.53	6.76
9	8.02	2.74
10	-0.09	2.45
Average	4.59	4.02

Discussion of Damping Value Determination

As you could see from the test results in the previous section, there is considerable variation between the damping value estimates for the transverse and longitudinal pullback test. The main source of this variation can be attributed to the fact the motions from the pullback test were not significantly larger than the ambient vibrations. Because the available chain block had a capacity of only 90 kN, the induced free vibration amplitude was not very large.

Prior to the release of the 90 kN force, a static displacement of approximately 1 mm was observed at the top of the piers of bent No. 3. While attempts were made to measure free vibration decay when there was little or no traffic, there was still significant ambient movement of the structure prior to the release and during the free decay period. This means that part of the measured accelerations from the quick release tests was due to ambient vibrations. If the free decay signal had been several orders of magnitude larger than the ambient signal, the free decay signal would not have been significantly affected. However, since the free decay and the ambient signal were of the same order of magnitude, the results were distorted.

Since the second and third longitudinal pullback test recordings were made without a release taking place, these records provide a measure of the typical ambient vibration levels. One of the signals observed during test number two on top of bent No. 2 was filtered to remove the high frequency components and is shown in Fig. 4.36. The characteristics of the digital filter used for this purpose were illustrated previously in Fig. 4.28. The free decay signal from the same location from test number four has been filtered exactly the same and is shown in Fig 4.37. Both of these figures are drawn to the same scale to compare their

relative amplitude. As you can see, the ambient level is approximately 10 % of the maximum free decay amplitude. However, after five free decay cycles the ambient level is approximately 25 % or more of the decay signal.

Since the acceleration levels due to the free decay were not significantly larger than the ambient vibrations, the free decay signal was polluted considerably by the ambient vibrations and the damping estimates, which were based on a method which assumes a clean decay signal, showed large variations. For both damping estimates, the standard deviations are large when they are compared to the mean value. For the first transverse mode, the mean estimate of critical damping is 2.6 % with a standard deviation of 1.3 %. The mean critical damping estimate for the first longitudinal mode is 4.35 % with a standard deviation of 2.2 %.

For future pullback tests it is recommended that higher forces are applied to induce much larger displacements and to reduce the variability in the damping estimates.

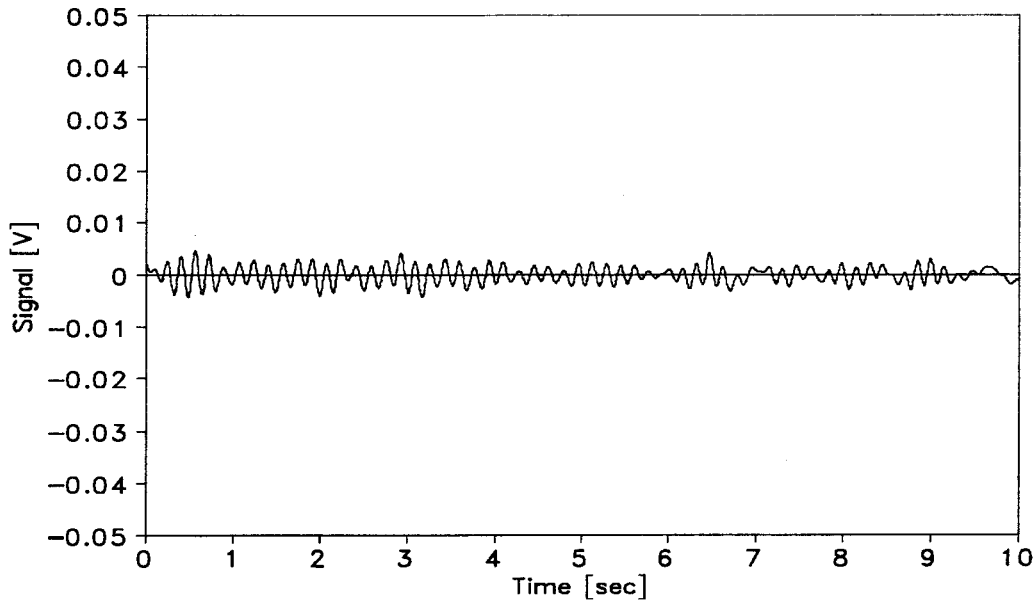

Fig. 4.36: Filtered Longitudinal Signal from Top of Bent No. 2 Pull back Test No. 2

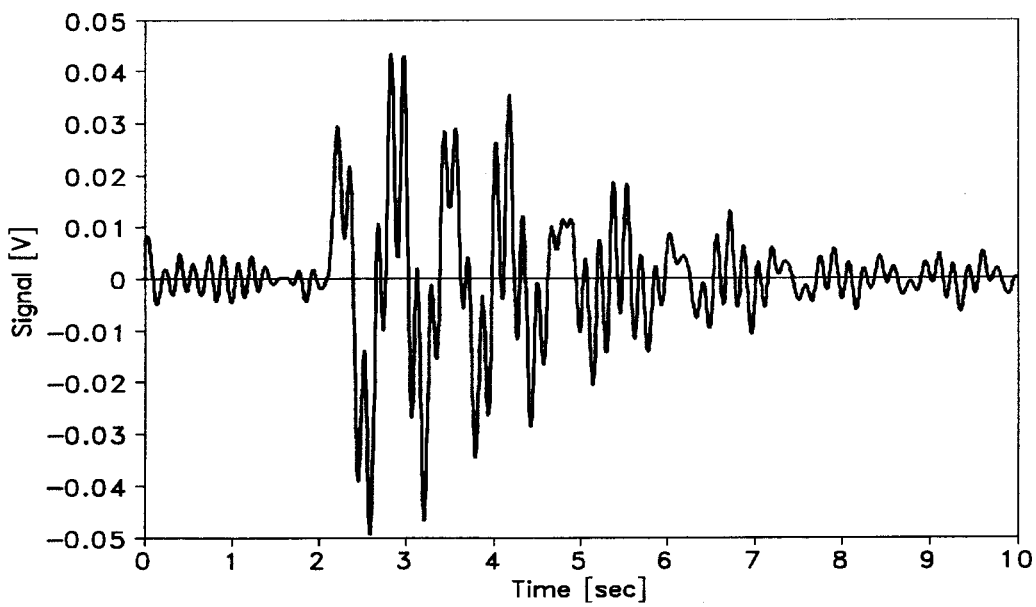

Fig. 4.37: Filtered Longitudinal Signal from Top of Bent No. 2 Pull back Test No. 4

Lateral Response of Bearings

Because the force causing the initial deformation for the transverse tests was applied just below the cap beam of bent No. 3, there was concern that the cap beam might move relative to the girders during the release. The gravity load was calculated as 180 kN per girder, therefore the total normal force for the six girders was 1080 kN. For slip to occur under the 90 kN load, the coefficient of friction would have to be 0.08 or less. Because the value for steel to steel friction is approximately 0.3, the bearings were not expected to slip.

To confirm this, sensors were placed on both the bottom flange of the exterior girder and the top of the bent for the transverse test. The signals obtained below and above the bearing were plotted against each other to investigate if slip had occurred during the test. This plot is shown in Fig. 4.38.

From this figure you can see, the accelerations recorded on top of the cap beam and the bottom flange of the girder agreed. The cap beam did not slip.

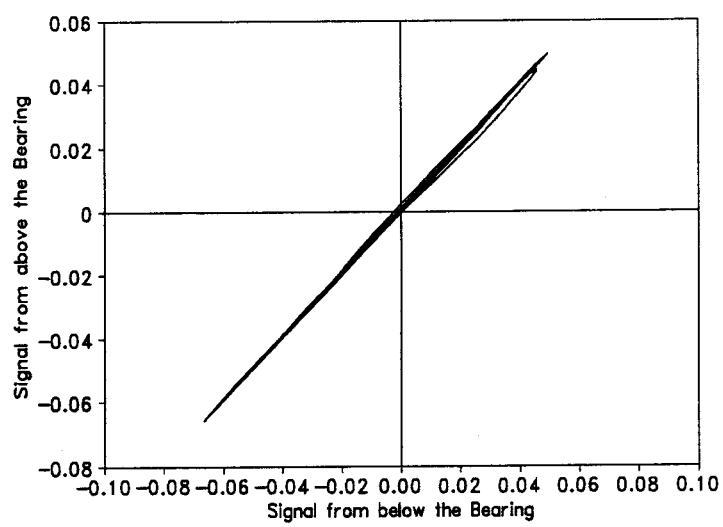

Fig. 4.38: Comparison of Signal Below the Rocker Bearing with the Signal Above the Bearing at Bent No. 2

4.3.6 Model Refinement

The analytical model could be refined after all of the experimental frequencies and mode shapes were determined. The main purpose of this refinement was to correlate the analytical frequencies obtained from the SAP90 model as closely as possible to the results from the ambient and pullback test.

The "base-model", introduced in section 4.3.3, was very detailed as it had 1464 degrees of freedom, 244 beam elements, and 126 shell elements. To arrive at a practical refined model, emphasis was placed on the variation of key parameters and the inclusion of only those additional elements which have considerable influence on the bridge's dynamic behaviour.

The "base-model" was modified to get an improved correlation between the experimental and analytical frequencies. The final "refined model" takes into account all of the main features of the deck and includes springs which model seized bearing restrainer bolts, as discussed in section 4.3.6.2. I found the mass and stiffness contributions of the sidewalk and parapet significantly influenced the vertical dynamics of the deck. This effect is illustrated through the use of an additional model called the "mass-refined" model which only accounts for the additional mass of the sidewalk and the parapet. These individual refinements are discussed in detail in the following sections.

In engineering practice, "stick models" are usually developed for dynamic analysis of bridges, mainly due to economic reasons. It is unlikely that a practicing engineer would routinely create a model as sophisticated as the "base-model" created in this study. A simple stick model was created from the "as built" drawings to evaluate the suitability of the models typically used in practice.

4.3.6.1 Stick Model

The "stick model" of the Colquitz River Bridge was created using only 3D-beam elements. The bridge deck was modeled as a line of beam elements with the vertical and transverse stiffness properties of the composite deck. The mass of the deck element was accounted for by using lumped masses at 4.57 m on centre. The bents were modeled with 3D-beam elements which have the same properties as the bents in the "base model". The "stick model", shown in Fig. 4.39, consists of:

18 3D-beam Elements for the deck

32 3D-beam Elements for the bents

17 Lumped Mass Elements

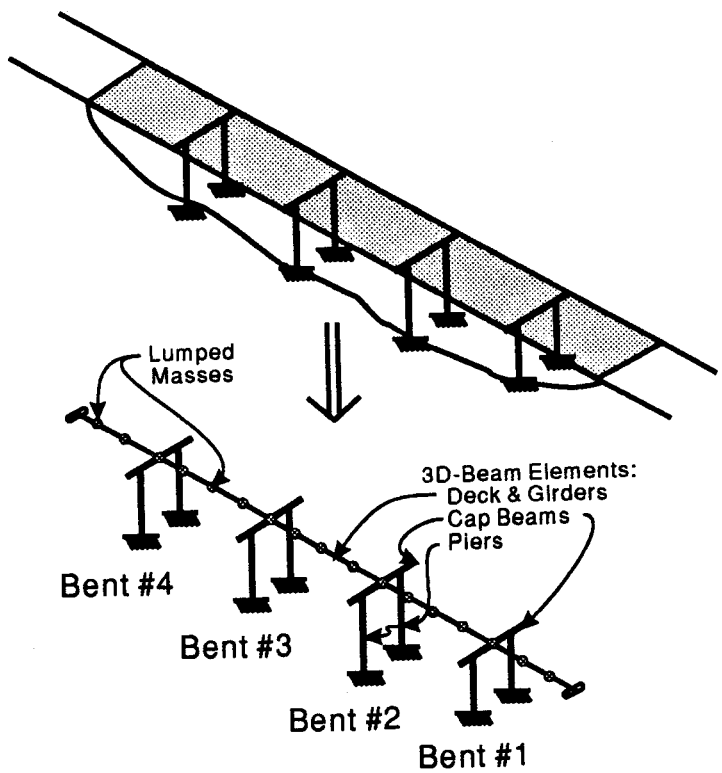

Fig. 4.39: "Stick Model" of the Colquitz River Bridge.

The first longitudinal mode, first transverse mode, and first three vertical modes of the stick model are shown below in Fig. 4.40. Torsional modes were not computed, because the torsional inertia of the deck was not modeled.

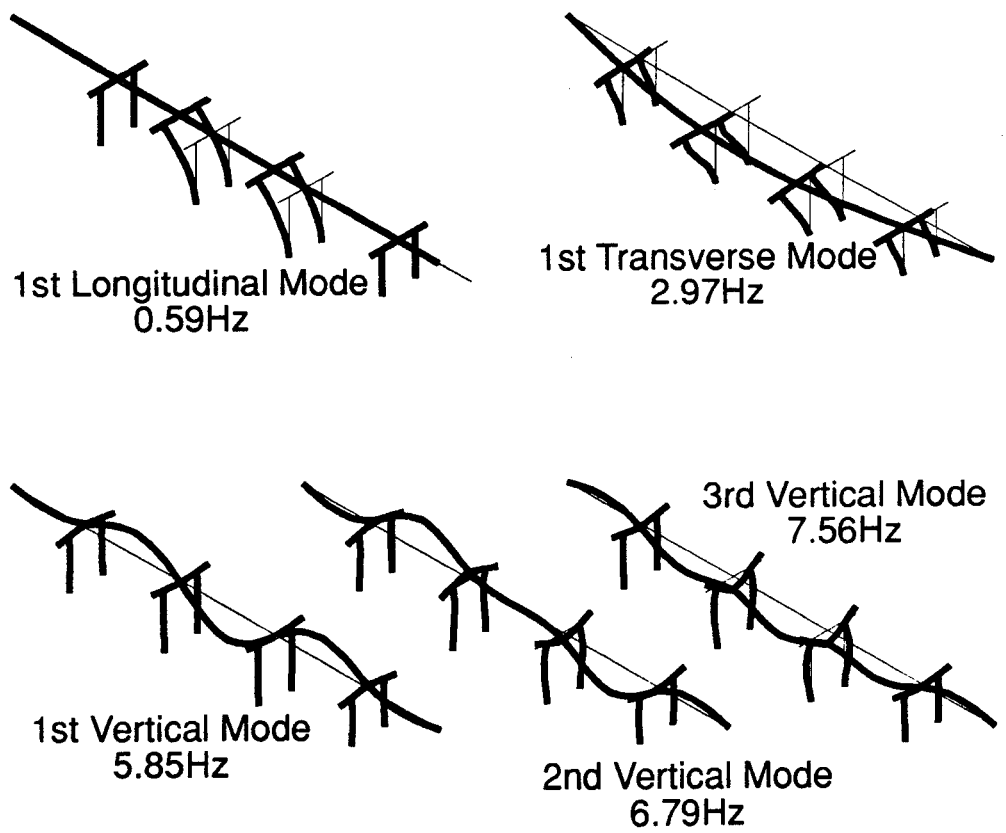

Fig. 4.40: Lateral and Vertical Modes of the "Stick Model" of the Colquitz River Bridge

The results of this "stick model" are compared to the results of the base model in following section 4.3.7.

4.3.6.2 Refined Model

The "base model" was refined in three steps; the model was modified first to adjust the vertical modes, then it was modified to improve the transverse modes and finally the longitudinal mode was adjusted, as follows:

Model Refinement - Vertical Modes

The dynamic "base model" of the Colquitz River Bridge was first modified to match the six experimentally determined vertical modes. A cross-section of the bridge deck is shown in Fig. 4.41. As you can see from this figure, the flexural stiffness of the deck about the X-Axis, depends on the composite action of the W840x210 steel girder and the 0.165 m thick concrete slab. In the transverse direction, the flexural stiffness depends on the composite action of the diaphragms and the deck.

The concrete deck was modeled as a series of shell elements. The girders and diaphragms were modeled as 3D-beam elements. The increase in stiffness due to the composite action was accounted for through the use of an effective moment of inertia of the beam elements. The effective moment of inertia about the X-Axis, I_{eff}, was computed for the girders as:

$$I_{eff} = I_{\circ} - I_{slab} \tag{4-3}$$

where $I_{\circ}$ is the composite section's moment of inertia, and I_{slab} is the slab's moment of inertia.

According to the "as built" drawings, the wearing surface thickness varies from approximately 0.05 m to 0.09 m. Because the wearing surface contributes both mass and stiffness to the deck, it was included in the refined model.

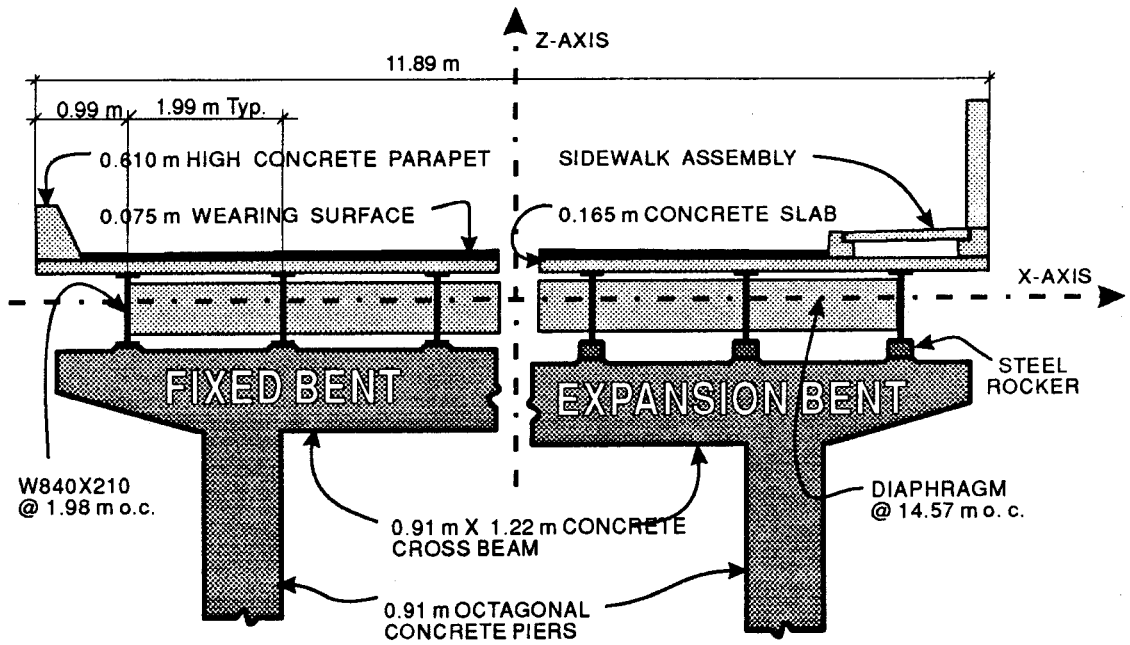

Fig. 4.41: Cross-Section of the Deck of the Colquitz River Bridge

Effective moments of inertia were computed for the girder about the X-Axis and for the diaphragm, using a similar approach, about the Y-Axis to investigate the effect of deck thickness varying from 0.152 m to 0.229 m. As you can see in Table 4.8, an increase in the deck thickness from 0.152 m to 0.203 m represents a 13 % ([79-70]/70) increase in effective moment of inertia of the girders. The best match with the experimental vertical frequencies was obtained using a 0.21 m deck thickness. This corresponds to a wearing surface thickness of 0.045 m (0.021-0.165 m).

Table 4.8 : Variability of Effective Moments of Inertia of Beam Elements for the Refined Model of the Colquitz River Bridge		
Deck Thickness [meters]	Effective Moment of Inertia [m^4]	
	Girder	Diaphragm
0.152	0.0070	0.0022
0.178	0.0075	0.0026
0.203	0.0079	0.0031
0.229	0.0083	0.0037

When the additional mass of the sidewalk assembly and the parapet was included in the model, the match between experimental and analytical frequencies deteriorated. This deterioration mostly affected the frequencies associated with torsional modes of the deck.

After examining the drawings more closely, it was determined that the sidewalk and the parapet form an integral part of the deck and, therefore, contribute to the deck's flexural stiffness. The additional portion of the deck was accounted for, in the model, by increasing the moment of inertia of the exterior girders about the X-Axis. After the moment of inertia was increased, the correlation between experimentally determined and analytically derived frequencies improved. The model used to represent the stiffness and mass of the deck is shown schematically in Fig. 4.42.

The "base model" included short beam elements to account for the difference in elevation between the top of the pier and the bridge deck. These members were eliminated from the "refined model" to reduce the complexity of the model.

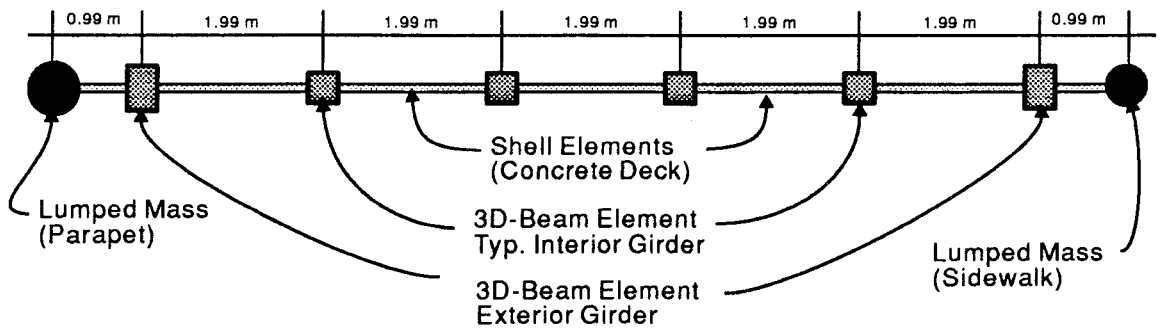

Fig. 4.42: Cross-Section of the Model used to Represent the Behaviour of the Colquitz River Bridge Deck about the X-Axis.

The first six vertical modes of the refined model are shown in Fig. 4.43. These modes compare well with the experimentally obtained modes shown in section 4.3.5.1.

Model Refinement - Transverse Mode

In the transverse direction, the results were only correlated for the first mode. As discussed in section 4.3.5.1, the higher modes could not be determined with enough certainty in the transverse direction to justify correlating them with an analytical model. The frequency of the first experimentally determined transverse mode was 2.81 Hz and the analytical frequency of the "refined model", which included the mass of the sidewalk and parapet, was 2.91 Hz. Because the difference between the experimental and analytical frequencies was only 3.6 %, further refinements to the model were not necessary.

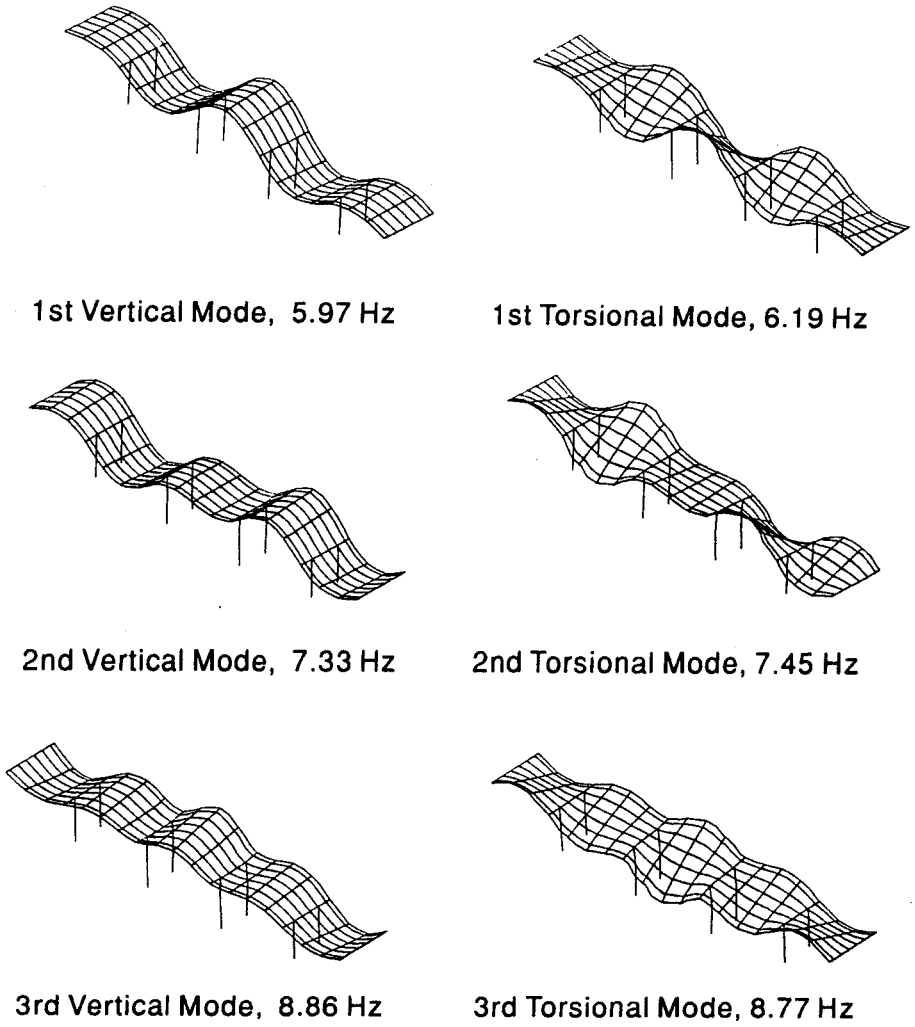

Fig. 4.43: Vertical Mode Shapes of the Refined Model of the Colquitz River Bridge

Model Refinement - Longitudinal Mode

During the testing, it was discovered that seven of the eight bolts restraining the movement of the girders at the rocker bearings located at the abutments were seized in their slotted holes and one of the bolts was missing its nut. This restrained the deck's longitudinal motion to

such an extent that the bolts had to be included in the computer model to obtain good correlation between the computed and experimental longitudinal modes. A picture of a typical seized restrainer bolt is shown in Fig 4.44.

This section outlines how the spring's stiffness was determined and used to model the seized bolts. Also, the bolts' maximum longitudinal capacity is computed and compared to the column's longitudinal capacity to determine the significance of this restraint under larger vibrations.

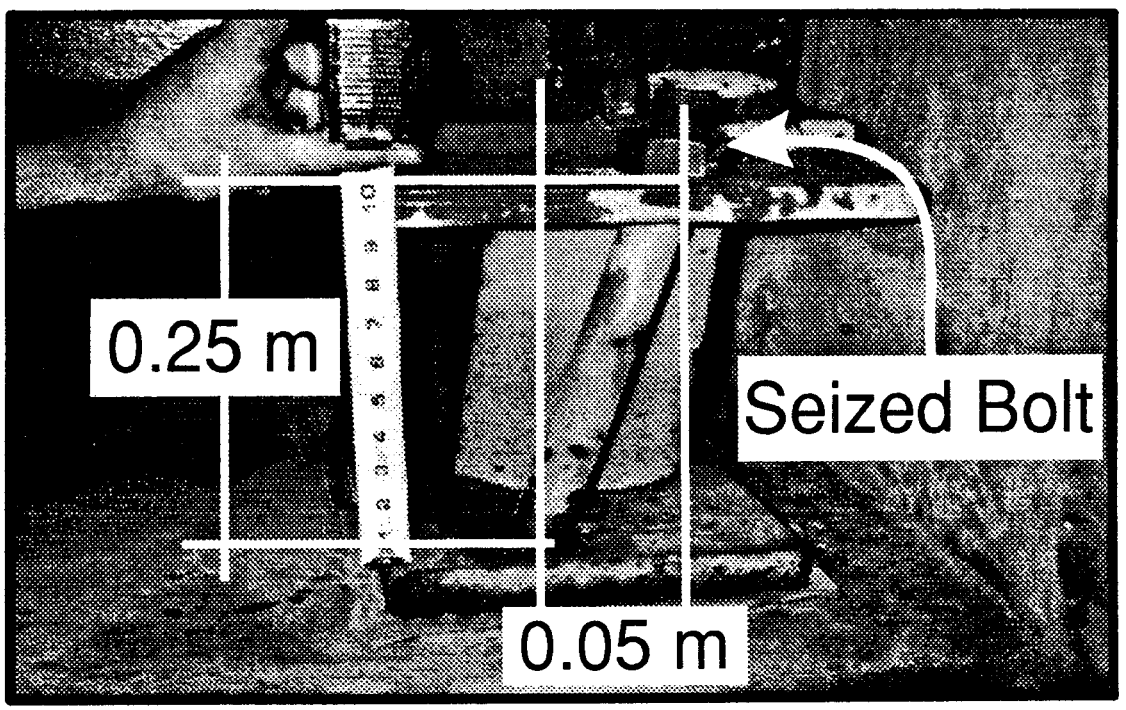

Fig. 4.44: Typical Seized Bearing Restrainer Bolt of the Colquitz River Bridge.

Stiffness and Strength of Seized Bolts

The longitudinal restraint from a seized bolt was modeled by an equivalent linear spring with a stiffness value, k, based on the flexural rigidity of a 0.032 m diameter bolt. Because the bolts were welded to the base plate and wedged against the slotted hole, two boundary conditions were investigated to bound the stiffness: fixed-fixed and fixed-pinned.

The upper bound of the flexural stiffness was calculated using the fixed-fixed case as

$$k = \frac{12EI}{L^3} = \frac{12E\pi R^4}{4L^3} = \frac{12*200000*\pi*0.016^4}{4*0.25^3} = 7.91 \ MN/m \tag{4-4}$$

where E is the modulus of elasticity, I is the moment of inertia, R is the radius of the bolt and L is the length of the bolt subjected to bending moments.

The lower bound of the flexural stiffness was calculated using the fixed-pinned case as:

$$k = \frac{3EI}{L^3} = \frac{3E\pi R^4}{4L^3} = \frac{3*200000*\pi*0.016^4}{4*0.25^3} = 1.98 \ MN/m \tag{4-5}$$

Because all of the bolts were considerably inclined as shown in Fig. 4.44, the horizontal component of the axial bolt stiffness in the deck's longitudinal direction could be considered as well. The horizontal stiffness component, k_a, for a bolt of cross sectional area A inclined at an angle $\alpha = 10°$ is:

$$k_a = \sin^2\alpha \frac{EA}{L} = \sin^2 10 \frac{200000*\pi*0.016^2}{0.25} = 19 \ MN/m \tag{4-6}$$

The flexural stiffness attributed to all seven seized restrainer bolts would therefore be between 13.8 MN/m and 55.3 MN/m. If you also considered the horizontal component of the axial stiffness, their combined stiffness could be higher.

The maximum longitudinal capacity of the bolts is a function of the bolt's flexural and axial capacities. The longitudinal capacity of the bolts is computed below. The nominal plastic moment capacity, M_p, of each bolt assuming a yield strength, f_y, of 400 MPa is computed as:

$$M_p = fy\frac{4R^3}{3} = 400*\frac{4*0.016^3}{3} = 2.2 \ \ kNm \tag{4-7}$$

The longitudinal resistance, P, from seven bolts with plastic hinges at both ends is:

$$P = 7\left(\frac{2M_p}{L}\right) = 14\left(\frac{2.2}{0.25}\right) = 123 \ \ kN \tag{4-8}$$

The nominal axial capacity, F_a, of the restrainer bolts is:

$$F_a = f_y \pi R^2 = (400)\pi(0.016)^2 = 321 \ \ kN \tag{4-9}$$

Because the bolts were bent in opposite directions at the two abutments, only three or four bolts can provide resistance to longitudinal movement through axial load capacity. The longitudinal restraint, P_a, from the axial component of three bolts is:

$$P_a = 3F_a \sin(10) = 3(321)\sin(10) = 167 \ \ kN \tag{4-10}$$

To evaluate the significance of the longitudinal restraint of the seized bolts, the seized bolts' stiffness and strength are compared to the concrete bents stiffness and strength.

Stiffness and Strength of Concrete Bents

The bending stiffness of the octagonal piers is based on the gross moment of inertia of the concrete cross-section and the modulus of elasticity, E_c. This is given by Collins and Mitchell (1991) as

$$E_c = w_c^{1.5} 0.043\sqrt{f'_c} \tag{4-11}$$

where w_c is the unit weight of concrete [in kg/m^3] and f'_c is the concrete compressive strength [in MPa].

Since testing was not performed to determine the concrete strength, elastic moduli, E_c, were computed for compressive strength, f'_c, values of 28 MPa and 35 MPa. The resulting moduli are

$$E_{c28} = 2400^{1.5} 0.043\sqrt{28} = 26750 \ MPa \tag{4-12}$$

$$E_{c35} = 2400^{1.5} 0.043\sqrt{35} = 29900 \ MPa$$

Using the concrete section evaluation program RESPONSE (Felber, 1990), the octagonal column's uncracked moment of inertia was calculated as $0.0384m^4$. The longitudinal stiffness was provided by the four piers acting as cantilevers. The lengths, L_i, of the piers of bent #2 and bent #3 were determined as 6.7 m and 9.1 m, respectively. Using these lengths and an elastic modulus of 28,000 MPa, the combined stiffness, K_{bents}, of the two bents in the longitudinal direction of the deck was estimated as:

$$K_{bents} = \Sigma \frac{3EI}{L_i^3} = 2(3*28000*0.0384)\left(\frac{1}{6.7^3} + \frac{1}{9.1^3}\right) = 30 \ MN/m \tag{4-13}$$

The program RESPONSE, was also used to calculate the column's moment capacity. The moment capacities for various axial load levels for two concrete compressive strengths, 28 MPa and 35 MPa, are shown in Fig. 4.45 . The axial load in the piers due to the dead weight of the structure was 960 kN. For this axial load, a moment capacity of 1,070 kNm was obtained from Fig. 4.45. As you can see from this figure, at this axial load level, the concrete strength has little effect on the moment capacity of the section. Using the moment capacity of 1,070 kNm, the maximum longitudinal load, $P_{h\,\max}$, which can be applied to the top of the bents is computed as:

$$P_{h\,\max} = 2*Mp\left(\frac{1}{L_1}+\frac{1}{L_2}\right) = 2*1070\left(\frac{1}{6.7}+\frac{1}{9.1}\right) = 555\ kN \tag{4-14}$$

The pier's longitudinal stiffness is used in the following section to verify the equivalent spring stiffness of the bolts. The longitudinal capacity is used to compare the capacity of the bolts and the bents.

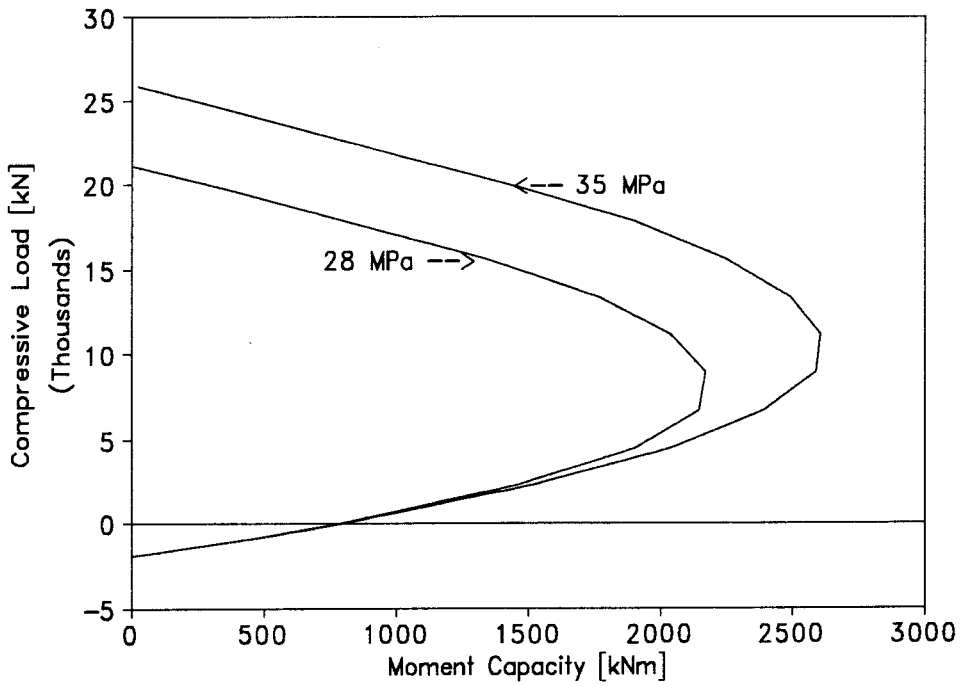

Fig. 4.45: Moment Capacity of the Concrete Piers of the Colquitz River Bridge for 28 MPa and 35 MPa Concrete.

Dynamic Model Refinement

The first longitudinal mode, determined by the "base model", had a natural frequency of 1.12 Hz. Experimental data obtained during the ambient vibration study and the pull back tests indicated that the first longitudinal mode was 1.66 Hz. The difference can be attributed to the effects of the seized restrainer bolts not included in the "base-model".

The seized bolts were modeled in the "refined-model" as equivalent linear springs. The stiffness of these springs required to correlate to the experimental frequency was computed by approximating the bridge as a single degree of freedom system. The natural frequency of a single degree of freedom system was calculated using:

$$f = \frac{1}{2\pi}\sqrt{\frac{k}{m}} \tag{4-15}$$

Since the mass, m, can be computed with sufficient accuracy, the stiffness can be derived from the experimental results. The mass of the bridge deck and the two cross heads was computed as 776 tonnes and the longitudinal stiffness of the structure was then computed as

$$K_{total} = m(f_{\exp}2\pi)^2 = 776(1.66*2*\pi)^2 = 84.4 \ \ MN/m \tag{4-16}$$

Using the bent stiffness computed in Eqn. 4-13, ($K_{bents} = 30 \ \ MN/m$), the effective stiffness of the bolts, K_{bolts}, was computed as:

$$K_{bolts} = K_{Total} - K_{Piers} = 84.4 - 30 = 54.4 \ \ MN/m \tag{4-17}$$

The stiffness calculated for the seven bolts with fixed-fixed boundary conditions using Eqn.4-4 is 55.3 MN/m, which compares well with the effective bolt stiffness given above (54.4 MN/m). After linear springs were included in the refined model, to account for the longitudinal stiffness provided by the seized bolts, the longitudinal frequency of the model correlated very well with the experimental results.

Simple idealized load-deformation curves were constructed for the longitudinal direction to determine whether the increased stiffness attributable to the seized bolts would affect the longitudinal behaviour of the structure during a seismic event. Fig. 4.46 shows idealized

load deformation curves for the restrainer bolts and the concrete piers and a curve for the combined action of the piers and bolts. From this figure you can see that up to a force level of approximately 450 kN, the coupled behaviour is dominated by the stiffness of the bolts. After this force level is exceeded, the stiffness drops dramatically. Because this force level corresponds to about 70% of the capacity of the piers, one can conclude that the effects of the restrainer bolts should be included in the dynamic model of the bridge.

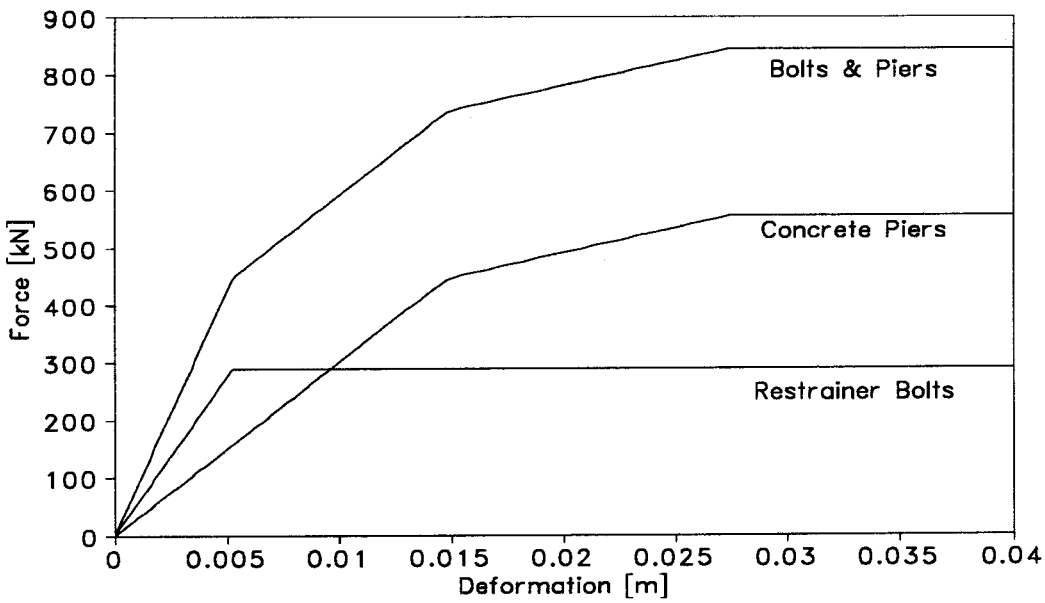

Fig. 4.46: Longitudinal Load Deformation Curve of the Colquitz River Bridge.

Summary of Refinements

Six refinements were made to the base model:

1. The diaphragms and their composite action were added to the model.

2. The mass and stiffness effect of the wearing surface was accounted for.

3. The mass of the parapet and the sidewalk was added to the model.

4. The increase in stiffness of the exterior composite girders due to the sidewalk assembly and the parapet was accounted for.

5. The short beam elements that account for the difference in elevation between the deck and the cross-head were removed.

6. The seized bearing restrainers were modeled by equivalent linear springs.

The refined model had a total of 1172 degrees of freedom and used 261 3D-Beam elements, 126 shell elements, and 4 springs.

4.3.6.3 Mass-Refined Model

The only difference between the "refined model" and the "mass refined model" is, that the stiffness of the exterior girders was not increased to account for the effect of the parapet or sidewalk assembly in the "mass refined model". The mass refined model was included in this discussion because it illustrates how a single refinement can significantly affect a model. Compared to the experimentally obtained mode shapes, the vertical modes shapes of the "mass-refined model" are quite unsymmetric. This is due to the difference in the lumped masses used to represent the sidewalk and the parapet wall. The vertical and torsional modes of the deck predicted by the "mass refined model" are shown in Fig. 4.47. The "mass refined" model is discussed in more detail in the following section.

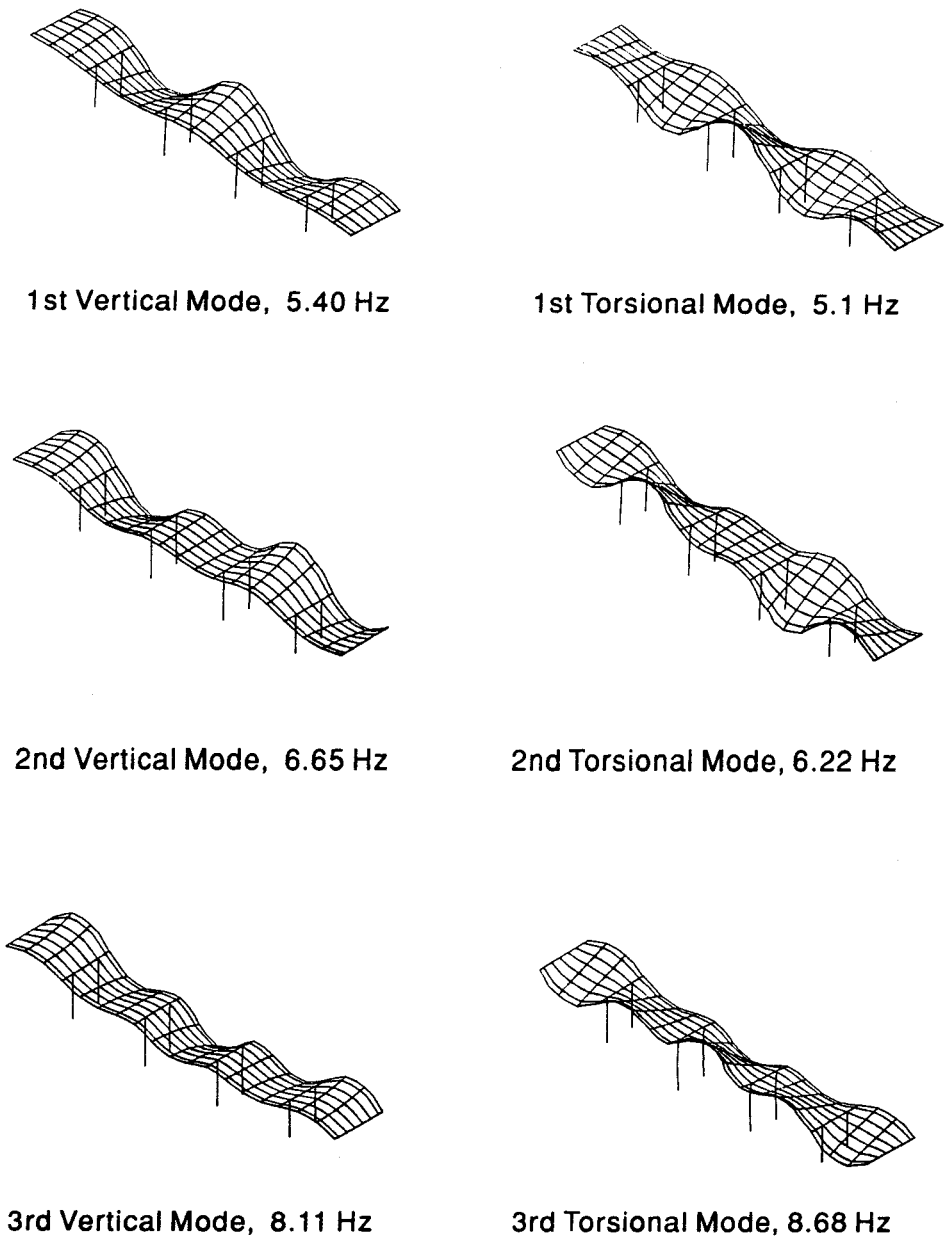

Fig. 4.47: Vertical Mode Shapes of the "Mass Refined" Model of the Colquitz River Bridge.

4.3.7 Comparison of Analytical and Experimental Results

In this section, I will compare the frequencies obtained from the tests described at the beginning of this chapter with the analytical frequencies of the four dynamic models described in the section 4.2. Table 4.9 summarizes all of the frequencies for tests and each of the models.

Figure 4.48 shows a plot of the analytically obtained frequencies for each mode against the experimental frequencies. The line in this plot indicates a perfect correlation between experimental and analytical frequencies. Analytical frequencies plotted above the line indicate the model is too stiff or has insufficient mass. If points lie below the line the model is too flexible or has too much mass.

The absolute value of the difference between the experimental frequencies and the analytical frequencies for all four models, calculated using Eqn. 4-2, are given in Table 4.10 and illustrated graphically in Fig. 4.49. A discussion of these results follows.

Table 4.9: Experimentally Determined and Analytically Derived Frequencies of the Colquitz River Bridge

Description of Mode Shape	**Experimentally Determined Frequency [Hz]**	**Analytically Derived Frequency [Hz] Model:**			
		Base	**Stick**	**Mass-Refined**	**Refined**
1st Longitudinal	1.66	1.11	0.58	1.67	1.67
1st Transverse	2.81	3.03	2.98	2.91	2.91
1st Deck Vertical	5.95	6.48	5.85	5.40	5.97
1st Deck Torsion	6.83	8.04	N/A	5.10	6.19
2nd Deck Vertical	7.14	7.86	6.78	6.65	7.33
2nd Deck Torsion	7.85	9.00	N/A	6.22	7.45
3rd Deck Vertical	8.70	9.25	7.54	8.11	8.86
3rd Deck Torsion	9.20	10.03	N/A	8.68	8.77

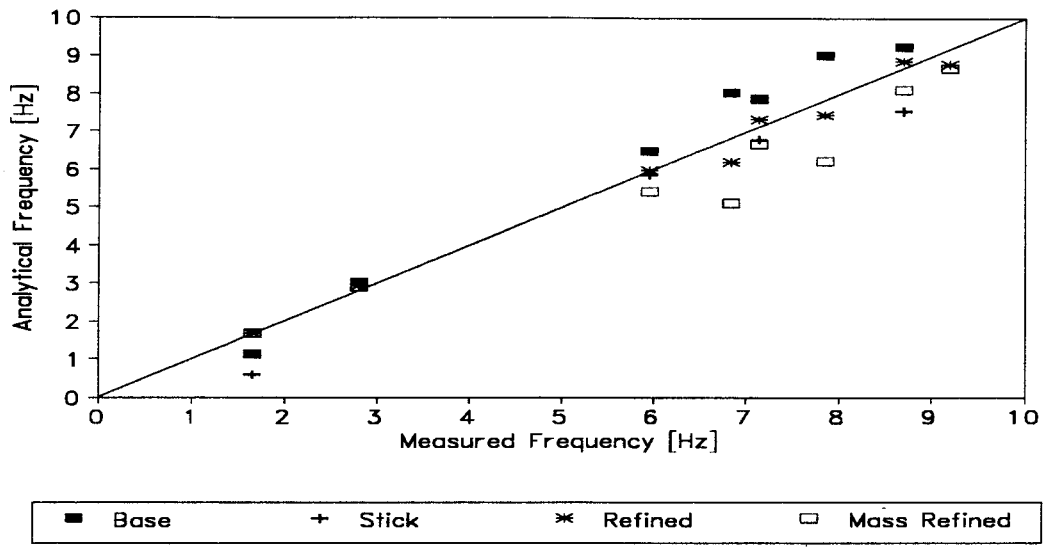

Fig. 4.48: Comparison of Experimentally Determined and Analytically Derived Frequencies of the Colquitz River Bridge

Table 4.10: Difference Between Experimentally Determined and Analytically Derived Frequencies of the Colquitz River Bridge

Description of Mode Shape	**Frequency Difference Model:**			
	Base	**Stick**	**Mass-Refined**	**Refined**
1st Longitudinal	30.1%	65.1%	0.6%	0.6%
1st Transverse	8.2%	6.4%	3.6%	3.6%
1st Deck Vertical	8.9%	1.7%	9.2%	0.3%
1st Deck Torsion	17.7%	N/A	25.3%	9.4%
2nd Deck Vertical	10.1%	5.0%	6.9%	2.7%
2nd Deck Torsion	14.6%	N/A	20.8%	5.1%
3rd Deck Vertical	6.3%	13.3%	6.8%	1.8%
3rd Deck Torsion	9.0%	N/A	5.6%	4.7%
Average Difference	13.1%	18.3%	9.9%	3.5%

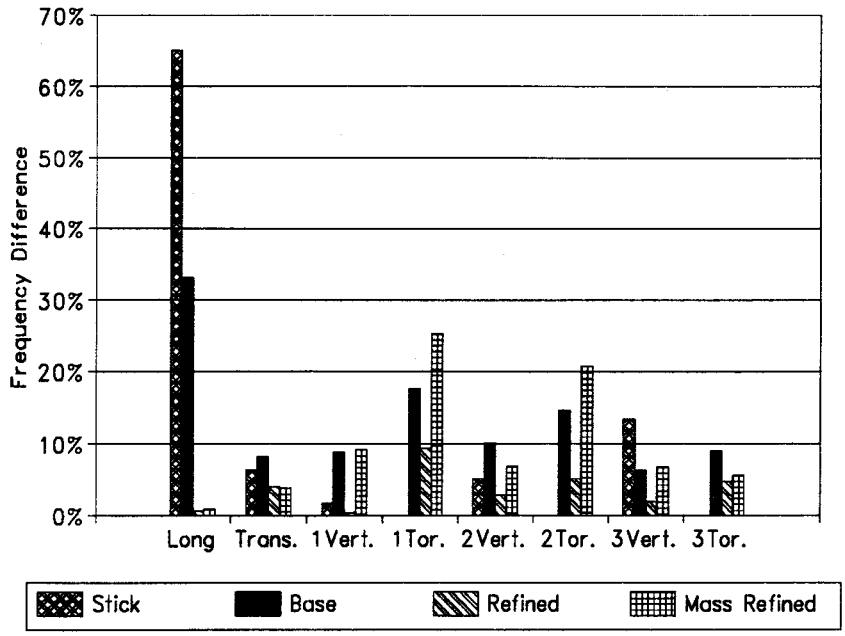

Fig. 4.49: Difference Between Experimentally Determined and Analytically Derived Frequencies of the Colquitz River Bridge

The "base model" underestimates the first longitudinal mode by 30 %, because the seized bearing restrainer bolts were not included in the model. Since the mass of the wearing surface, sidewalk, and parapet was ignored, the vertical and torsional deck frequencies are overestimated by 6 % to 15 %.

The "stick model" underestimates the longitudinal frequency by 65 % because the seized bearing restrainers were not included in the model. The transverse behavior was modeled well with a difference of only 6 %. The "stick model's" first and second vertical modal frequencies were only 2 % and 5 % (respectively) lower than the measured frequencies.

The frequencies of the "refined model" match all eight experimentally determined frequencies with an average difference of 3.5 %. The longitudinal frequencies were correlated by adjusting

the longitudinal springs which represent the seized bearing restrainer bolts. By properly accounting for the mass and stiffness distribution of the deck, the vertical and torsional modal frequencies show differences ranging from 0.3 % to 9.4 %. After the mass of the deck was accounted for properly, the difference for the first transverse mode was only 3.6 %. Attempts were not made to improve the correlation for this mode.

The lateral frequencies derived from the "mass refined model" matched the experimentally determined frequencies well. Because the stiffening effect of the sidewalk and the parapet was ignored, the vertical and, in particular, the torsional frequencies were underestimated considerably. The difference for the vertical frequencies ranged from 7 % to 9 % and for the torsional frequencies the differences ranged from 6 % to as high as 25 %. The differences were larger for the torsional modes because the exterior girders contribute the most to the torsional stiffness of the deck.

4.3.8 Performance of the HBES Hardware and Software

The Colquitz River Bridge study provided the first opportunity to test all of the components of the HBES under field operating conditions. The performance of the HBES's measurement hardware and software is discussed below.

4.3.8.1 Hardware Performance

The HBES sensors, signal conditioner, and A/D converter were used to consistently obtain high resolution ambient vibration data (as described in section 4.3.4.) in the field.

While four channels could be used to identify the Colquitz Bridge's vertical and longitudinal modes of vibration, the transverse mode shapes could not be clearly identified. With four

channels, only one reference station could be used for the transverse measurements. All of the data had to be reduced with respect to a single reference. As described in section 4.3.5.1, the higher transverse mode shapes could not be clearly identified using only one reference station.

To overcome this limitation, four additional sensors and conditioning cards were procured for the HBES. The enhanced eight channel system can collect more information simultaneously and, therefore, the dynamic characteristics of structures can be determined in more detail.

4.3.8.2 Software Performance

The performance of the HBES programs, AVTEST, ULTRA, VISUAL, and SUBSAP is described in this following section.

Performance of the Program AVTEST

AVTEST was effectively used to acquire 156 ambient vibration records with 32,768 points each. From the pullback tests, 35 transient vibration records with 4,096 points each were collected.

While the quality of these individual acceleration time histories were suitable to reliably determine dynamic characteristics of the structure, the data could have been affected by the following factors:

- Sensor malfunction,
- Cable malfunction,
- Signal drift,
- A/D converter saturation,
- Low signal strength.

The first two problems were avoided using AVTEST's calibration feature to verify the operation of the installed sensors before and after each test setup. The remaining problems were avoided by monitoring all the channels displayed by AVTEST in real time, during each test.

In the field, the following problems affecting the data quality were identified using AVTEST.

- Disconnected sensors
- Incorrect sensor orientation
- Cable faults
- A/D converter saturation
- Drift due to system warm up at the beginning of the test.

Whenever any of these problems occurred, they were visually identified and remedied in the field.

The tests at the Colquitz River Bridge indicated that the interface of the program is well suited for the field testing environment.

Performance of the Program ULTRA

The time required to acquire data from a typical test setup at the Colquitz River Bridge was approximately 15 minutes. After the data for each setup was transferred from the data acquisition computer to the analysis computer, it was reduced using ULTRA while the data for next test setup was being acquired. The automatic data reduction features of ULTRA were used to compute the potential modal ratios of all the sensors with respect to the reference sensor. Because ULTRA was specifically developed to process long ambient vibration records, the potential modal ratios from a test setup could be processed on a 33 MHz PC computer with a

80486 processor in less than 2 minutes. After the automatic data processing was completed, there was enough time to identify the structure's dominant frequencies from peaks in the computed PSDs using the interactive mode of the program.

Performance of the Program VISUAL

VISUAL was used to assemble, display and animate the bridge's mode shapes on-site. While the testing was in progress, some of the modal ratio functions were computed and used to generate the mode shape vectors for the part of the structure which had already been measured. These partial mode shapes were then displayed and animated. The bridge's primary modes were identified and verified at the site.

After all the test data had been collected and reduced, VISUAL was used to assemble the complete mode shape vectors. The numeric values of the mode shape vectors were written to file for further analysis. Since VISUAL was used to display partial and complete 3-D mode shape vectors at the site, the test crew developed a good understanding of the structure's dynamic behaviour before leaving the site.

Performance of the Program SUBSAP

After all the experimental data had been analysed at the office, SUBSAP was used with SAP90 to refine the analytical models of the Colquitz River bridge. Parameters such as moments of inertia, lumped masses, and spring stiffnesses were varied.

The file of variables (called tokens) used for refining the Colquitz model was only 23 lines long. SUBSAP replaced all of the tokens in the input file with the appropriate values. The

input file for the Colquitz River Bridge model was 690 lines long. Using SUBSAP only the small variable file had to be manipulated to correlate the models. The use of SUBSAP did not only speed up the process but also ensured that all of the tokens were changed consistently.

Using SUBSAP and SAP90 the model of the Colquitz River Bridge was refined until there was an average difference of 3.5 % between eight analytical and experimental frequencies. This difference was deemed small enough for practical purposes.

4.3.9 Conclusions of the Colquitz River Bridge Study

The Colquitz River Bridge study demonstrated how the HBES could be used effectively to optimize dynamic models using dynamic characteristics obtained from field testing.

All of the components of the HBES were tested in the Colquitz River Bridge study. These tests provided the opportunity to assess the performance of the individual components and their interaction. During the study, all the hardware and software components generally performed quite well. Using the HBES, software preliminary results could be obtained on site and reported within days after the test. After the tests only minor modifications needed to be made to the software programs to enhance their performance. The HBES was expanded to an eight channel system since I found a four channel system was limiting.

The results from pullback tests were used to verify the primary lateral frequencies obtained from the ambient vibration data. Since the force level used for the pullback test only caused deflections of approximately 1mm, the damping value estimates were affected by the ambient vibrations of the structure. To improve the damping estimates, pullback forces that can generate large displacements are recommended for future tests.

The dynamic model generated using SAP90 was easily refined with SUBSAP. A simple "stick model" of the structure gave reasonably good approximations of the fundamental transverse and vertical modes. In the longitudinal direction, the seized bearing restrainer bolts needed to be modeled correctly before a good match could be attained. For the more complex models, which accounted for the three dimensional distribution of mass and stiffness in the bridge deck, the accurate modeling of the sidewalk and the parapet was paramount to obtaining a good correlation particularly for the torsional modes. The "refined model's" frequencies correlated with the experimental frequencies with an average difference of only 3.5 % for eight modes.

4.4 Study of the Squamish Wharf

The HBES was also used to measure the ambient vibrations of a vertically piled wharf in Squamish, British Columbia. This test was conducted as part of a Masters Thesis at UBC, which explores the current modeling techniques used for wharf structures (Yee, 1993).

The following section briefly describes the wharf, test setup, and results. For more information on the entire study, refer to Yee.

4.4.1 Objectives of the Squamish Wharf Study

The objectives of this study were to:

- identify natural frequencies and modes of the Squamish Wharf,
- evaluate the hardware's ability to measure very small ambient vibrations.

The Squamish Wharf provided an excellent opportunity to measure the HBES's ability to determine the dynamic characteristics of a structure which is much stiffer than the Colquitz River Bridge. This structure was only excited by natural sources such as wind, tidal currents, waves, and micro tremors.

4.4.2 Background on the Squamish Wharf

The Squamish Wharf is a vertically piled wharf designed in 1987 and constructed in 1988. The main wharf apron is 153 m long and 32 m wide with a mass of 10600 tonnes. The support system consists of prestressed octagonal hollow core concrete piles, cast integrally with concrete pile caps. These piles and pile caps form 21 pile bents, spaced at 7.6 m centers, and are designed to resist lateral loads. The diaphragm spanning the pile caps is comprised of precast, prestressed

concrete double tee beams topped with a 0.15 m thick cast-in-place concrete slab. The wharf is isolated from the shore with an 7.5 m wide transition span which is fixed on the shore side and rests on a low friction sliding bearing on the wharf apron. The wharf's elevation and plan views are shown in Figure 4.50.

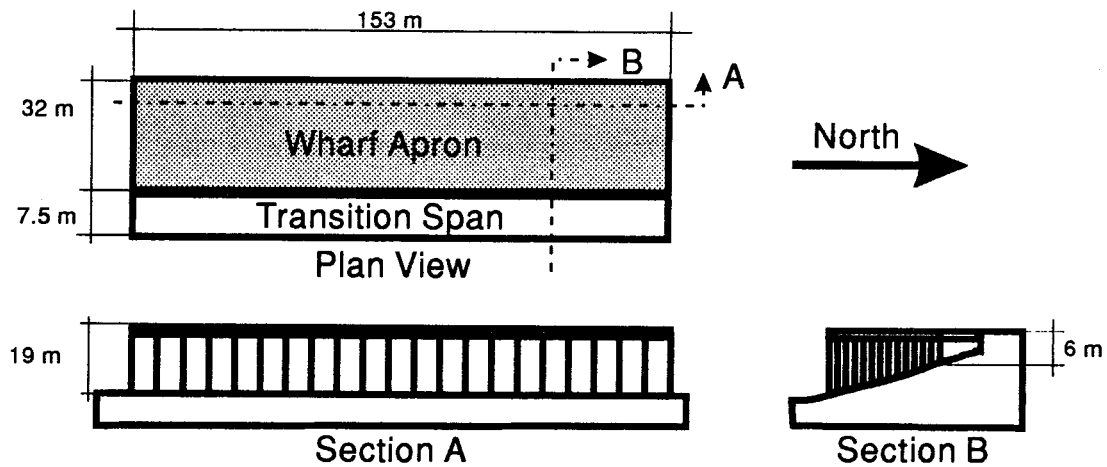

Fig. 4.50: Elevation and Plan Views of the Squamish Wharf

4.4.3 Wharf Measurement Setup

Sensors were placed around the wharf's perimeter. These locations are shown in Fig. 4.51. The signal conditioner's highest level of amplification was used to record the accelerations because the ambient vibrations were so small. The data quality control measurements discussed in section 4.3.4.1 were also used for these tests.

For more information on the test setups, refer to Appendix F.

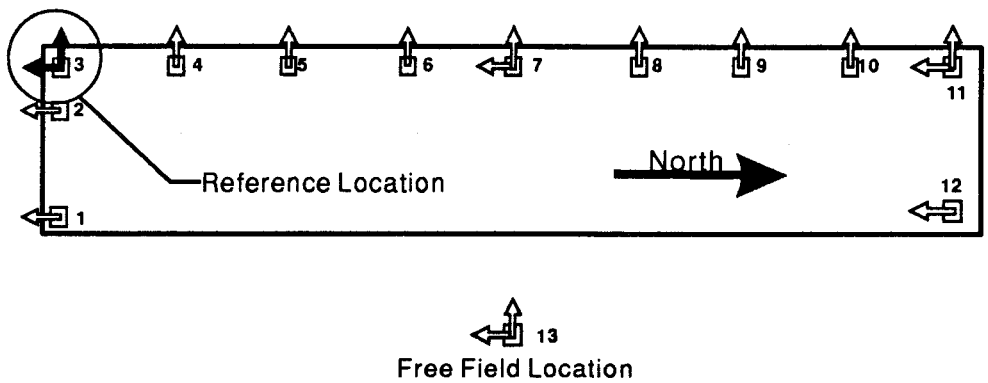

Fig. 4.51: Sensor Locations on Wharf Apron for Ambient Vibration Measurements

4.4.4 Experimental Results

Because the wharf was excited by weak natural sources, such as wind and waves, the accelerations recorded were quite small. A typical transverse acceleration time history had accelerations of less than 0.025 mg (0.25 mm/s^2). This is shown in Fig. 4.52.

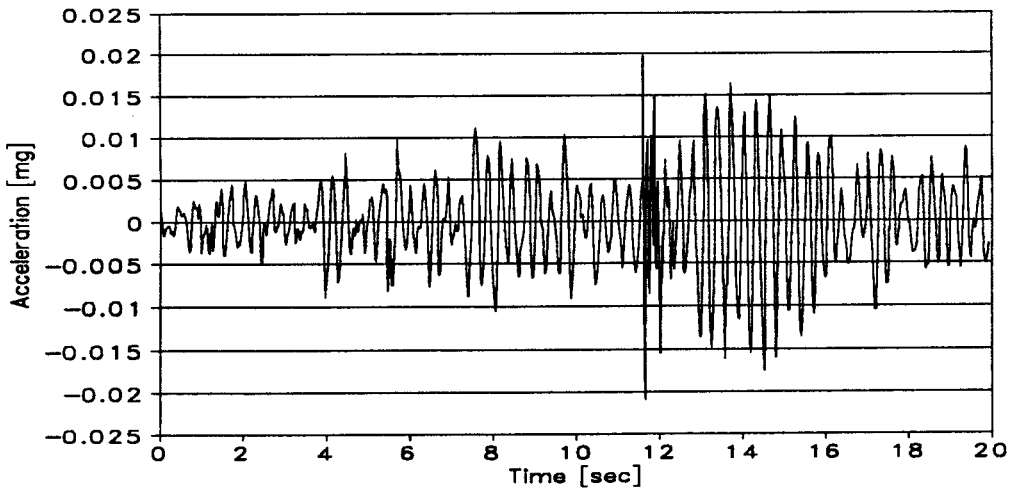

Fig. 4.52: Typical Transverse Acceleration Time History from Wharf Measurements

ULTRA and VISUAL were used to determine the frequencies and mode shapes from these acceleration time histories. The frequencies and mode shapes are summarized in Table 4.11 and are individually described in the following sections.

Table 4.11: Experimentally Determined Frequencies of the Squamish Wharf

Description of Mode Shape	**Frequency [Hz]**	**Period [sec]**
Overall Site Ground Motion	0.3	3.3
1st Rigid Body Mode	2.1	0.48
2nd Rigid Body Mode	3.3	0.30
1st Bending Mode	7.9	0.13
2nd Bending Mode	11.3	0.09
3rd Bending Mode	18.9	0.05

4.4.4.1 Overall Site Ground Mode

An overall site mode was identified at a frequency of 0.3 Hz. For this mode, the wharf apron and the free field station moved together in the east-west direction. This wharf mode is illustrated in Fig. 4.53, where the deformed wharf apron is shaded gray and the undeformed wharf apron is outlined in black.

4.4.4.2 Predominantly Rigid Body Modes of the Wharf Apron

Two modes of the wharf apron with predominant rigid body motions of the apron were also identified. The modes, shown in Fig. 4.54, corresponded to north-south translation at 2.1 Hz and rotation at 3.3 Hz. This translation mode shows rotation coupled with flexing of the deck.

The rotation is due to the non-uniform pile lengths and their distribution of stiffness. The flexing is due to the relatively large stiffness of the piled substructure compared to the flexural stiffness of the deck.

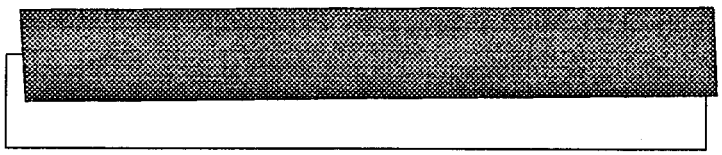

Overall Site Mode, 0.3Hz

Fig. 4.53: Plan View of the Overall Site Ground Mode of the Squamish Wharf

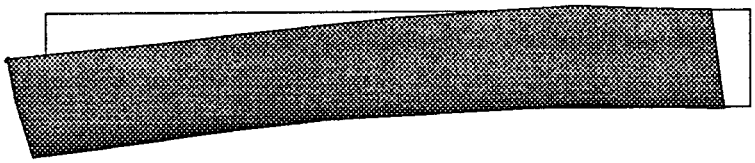

N-S Translational Mode, 2.1Hz

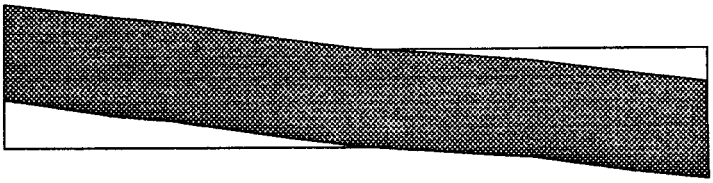

Rotational Mode, 3.3Hz

Fig. 4.54: Plan Views of the Predominantly Rigid Rigid Body Modes of the Squamish Wharf

4.4.4.3 Flexural Modes of the Wharf Deck

The first three flexural modes of the wharf apron were identified at 7.9 Hz, 11.3 Hz and 18.9 Hz. These modes are shown in Fig. 4.55.

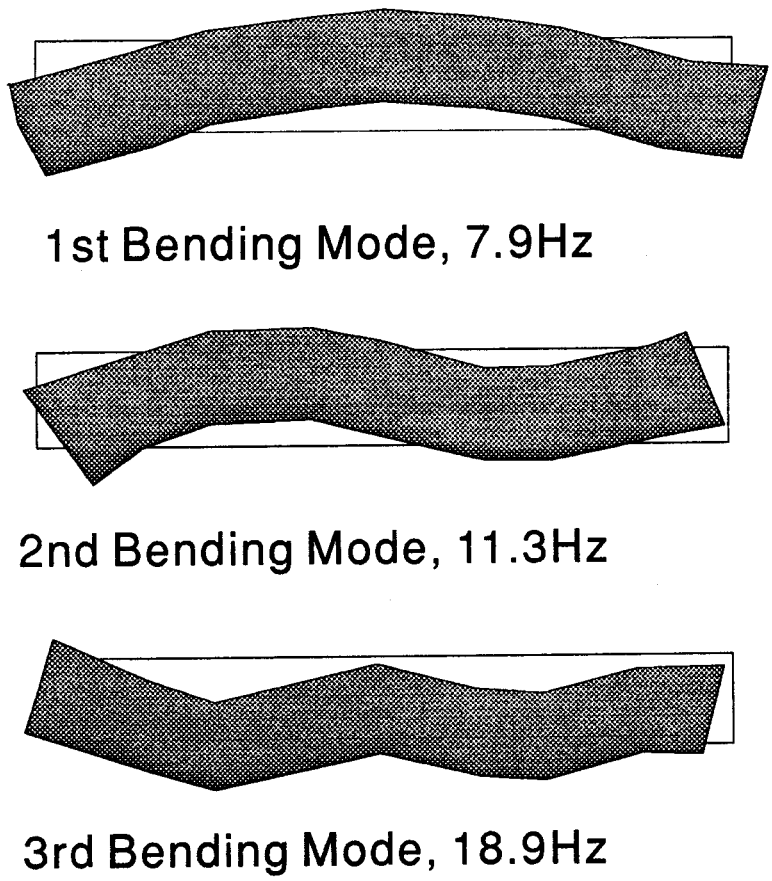

Fig. 4.55: Plan Views of the Flexural Modes of the Squamish Wharf

4.4.5 Performance of the HBES Hardware

The Squamish Wharf test was used to determine the limits of the HBES ambient vibration hardware. The ambient vibrations encountered on this structure were so small, I had to use

the maximum amplification level of the signal conditioning equipment, a gain of 2000. At this gain level, the measurement equipment's sensitivity is 5000 V/g. For a voltage range of ±1 Volt, the acceleration range is ±0.200 mg.

You can appreciate in this study the effectiveness of the HBES measurement hardware and data quality control program. Even though the typical ambient vibrations were 0.025 mg, the HBES hardware was able to record the data with enough resolution to determine the primary modes of the wharf.

4.4.6 Conclusions of the Squamish Wharf Study

The HBES successfully determined the fundamental dynamic characteristics of the Squamish Wharf. Even though the wharf's acceleration response to wind and wave excitation was very small (0.025 mg), the HBES helped to identify six natural frequencies and mode shapes. This test demonstrates how the HBES hardware and data quality control functions can be used to evaluate structures subjected to very low excitation levels.

Chapter 5

Summary of the Features of the Hybrid Bridge Evaluation System

The dynamic characteristics of bridges and other large civil engineering structures can be efficiently evaluated using the Hybrid Bridge Evaluation System (HBES). This system is relatively inexpensive. It uses ambient vibration measurements which do not disrupt the normal operation of the structure.

Unlike traditional systems, the HBES can be used to analyse all of the measurements in the field. You can determine the structure's natural frequencies and modes of vibrations in the field. You can verify that you have recorded usable test data and, if necessary, make adjustments to the measurements while you are at the test site. You can thereby assess any unanticipated or unusual dynamic behaviour of the structure without making a return trip to the site to collect additional data.

The HBES integrates state of the art hardware with custom developed software to acquire, reduce, and interpret vibration data. Data from force-balanced accelerometers is amplified and filtered by a signal conditioner and then converted to digital information. The software includes several programs. Program AVTEST was developed to acquire the digital information and store it to a disk. Data reduction is performed by ULTRA, a program developed to determine natural frequencies and modes of vibration. These modes can then be animated and displayed with the program VISUAL. SAP90 models can then be quickly modified using the SUBSAP program

in conjunction with SAP90 to improve the correlation between analytical and experimental dynamic characteristics. These refined models can then be used to predict the small amplitude behaviour of the structures more reliably.

The hardware assembled for the HBES has been used for both ambient vibration and pullback tests on a variety of structures. The sensors with their signal conditioner cards have been effectively used to measure accelerations levels ranging from 0.02mg to 0.2g. Because the sensors and the data acquisition hardware have been specifically selected for ambient vibration testing, data can be consistently obtained at a high resolution. The modular design of the measurement hardware facilitates ease of transportation and on site installation. The quick release mechanism (QRM) developed for pullback testing can be used to safely release loads up to 90 kN.

The program AVTEST was specifically developed to conveniently acquire the 20 Mb of data associated with a typical day of ambient vibration testing. The program can be used to visually monitor the data for problems associated with the signal level, drift, and saturation. In addition, the proper operation of the measurement chain before and after each test is verified by the program. With these features, the data quality can be assessed already in the field and if necessary corrective action can be taken immediately.

The potential modal ratio (PMR) function, which combines the information from the frequency response, phase, and coherence functions, was developed specifically to streamline the reduction of ambient vibration data. This PMR function and other ambient vibration data specific features, such as drift removal, were implemented in ULTRA. When ULTRA was used in batch mode, many pairs of ambient vibration records could be processed automatically to compute the modal

ratios between sensor locations required to define individual mode shapes. In addition, in the interactive mode, ULTRA's many signal conditioning options were used to study individual measurements in detail.

The program VISUAL automatically assembles the mode shape vectors using the computed modal ratio functions. During the field tests, VISUAL served as an important tool for the visualization of those portions of the mode shapes which had already been defined by measurements. Since three dimensional mode shapes can be displayed from any angle, a very good understanding of the dynamic behavior of the test structures can be developed by the user. The animation feature can also be used effectively for the presentation of the experimental results.

After the natural frequency and mode shapes are identified from experimental results, the analytical dynamic models can be refined. This refinement is achieved through the modification of key parameters such as mass and stiffness values. For this process, the program SUBSAP is used to conveniently modify the key parameters in the input files for the dynamic analysis program SAP90. Using this approach, dynamic models can be refined and correlated with experimentally obtained dynamic characteristics.

The emphasis of this project was placed on the development of a practical system which can be used to quickly evaluate the dynamic characteristics of existing bridges and to facilitate the improvement of dynamic models. The solid performance of the HBES software and hardware has proven that this system meets these requirements and can now be used to study a variety of civil engineering structures.

Conclusions

The following conclusions can be drawn from this research:

1. The Hybrid Bridge Evaluation System (HBES), developed as a part of this thesis, can be used effectively to determine the dynamic characteristics of a variety of structures.

2. The average normalized power spectral density (ANPSD) function, introduced as a part of this thesis, proved to be a powerful tool for the identifying natural frequencies. Traditionally, the information contained in a series of power spectral density plots was used to determine the natural frequencies of a structure. The ANPSD reduces the information contained in a series of power spectral densities into a single function.

3. The potential modal ratio function (PMR), which was developed and implemented into the HBES software, successfully automates the reduction of ambient vibration data. This function combines the information contained in the transfer function, coherence function, and phase relationships computed for each pair of measurements.

4. The integration of the program ULTRA which computes the PMR functions on site, and the program VISUAL, which assembles the experimentally determined mode shapes using the PMR functions, facilitates quick visual inspections of the structure's dynamic characteristics. This capability can be used to ascertain the objectives of a dynamic testing study have been met before leaving the site. Thus, expensive return visits to obtain additional measurements can be avoided.

5. The manual updating of parameters used to improve analytical models proved to be very effective. In particular, the experimentally determined natural frequencies of the Colquitz River Bridge could be correlated with the analytically derived frequencies with an average difference of only 3.5%.

6. The HBES's measurement equipment can reliably obtain ambient vibration records on a variety of structures. The tests conducted as a part of this thesis on a highway overpass and a relatively stiff wharf structure demonstrated that the system's hardware is capable of determining the dynamic characteristics of structures with ambient vibration levels ranging from 0.02 mg to 0.2 g.

7. When compared to forced vibration tests, which usually require interruptions in the operation of the structure, ambient vibration testing methods implemented in the HBES provide an inexpensive alternative.

8. The object oriented programming language C++ adopted for the coding of the data reduction and interpretation programs provided the necessary flexibility necessary for ongoing program development. The programs can be easily updated in the future should the need arise.

9. The quick release mechanism (QRM) developed for the pullback tests conducted at the Colquitz River Bridge, could be repeatedly employed for the controlled and safe release of a 90 kN pullback force. The natural frequencies obtained from the pullback tests and the ambient vibration tests agreed well.

10. The damping values for the principal lateral modes of the Colquitz River Bridge, obtained from the pullback test, varied significantly because the pullback force was too small. The 90 kN force that could be safely applied with the QRM did not excite the Colquitz River Bridge significantly above the ambient levels.

Future Applications

1. The system can now be used to complement the retrofit studies of existing bridges. The experimental dynamic characteristics obtained with the HBES can be used to refine linear elastic dynamic models used in retrofit studies. After the retrofit of the bridge has been completed, the dynamic characteristics can be determined again to determine if the retrofit achieved the desired change in the bridge's behavior.

2. The system can also be used to systematically take dynamic signatures of new bridges. This information can be stored on file and used later to assess how the bridge's dynamic characteristics have changed over time.

3. In the future, a series of optically based sensors could be added to the HBES to measure displacements directly. Currently accurate optic based sensors are expensive but in five to ten years their use may become economical.

List of References

Allemang, R. J. (1983). Experimental Modal Analysis. Modal Testing and Model Refinement, ASME, 59, (pp. 1-29)

Allemang, R. J. (1993). Modal Analysis - Where Do We Go From Here?. Proceedings of the 11th International Modal Analysis Conference [keynote paper], Kissimee, Florida.

Abdel-Ghaffar, A. M., & Housner G. H. (1977). An Analysis of the Dynamic Characteristics of a Suspension Bridge by Ambient Vibration Measurements. Earthquake Engineering Research Laboratory, California Institute of Technology, Report No. EERL77-01, Pasadena, California.

Abdel-Ghaffar, A. M., & Scanlan R. H. (1985). Ambient Vibration Testing of the Golden Gate Bridge: I. Suspended Structure. Journal of Engineering Mechanics, 111, (pp. 463-482).

Agardh, L. (1991). Modal Analyses of Two Concrete Bridges in Sweden. Journal of the International Association for Bridge and Structural Engineering, 1(4), (pp 35-39).

Aktan, A. E., Baseheart, T. M., Shelley S. & Ho I.-K. (1990). Forced Excitation and Identification of a Mid-Rise Building to Evaluate Vulnerability. Proceedings of the Fourth U.S. National Conference on Earthquake Engineering, 2, (pp. 747-756). Palm Springs, California, 1990.

Astaneh-Asl, A. (1992, June). Seismic Evaluation and Retrofit of the Bay Bridge. Seismic Design and Retrofit of Bridges, Seminar Proceedings, (pp. 1-31). UC Berkeley, Califonia.

Bendat, J. S., & Piersol, (1986). Random Data Analysis and Measurement Procedures (2nd ed). New York: John Wiley & Sons.

Berry, J. E. (1992). How 8-Bit Data Collectors Can Miss Important Machine Vibration Problems. Sound and Vibration, 26(5), pp. 6, 8, 10.

Biswas, M., Pandey, A. K., & Samman M. M. (1990). Modal Technology for Damage Detection of Bridges. In A. S. Nowak (Ed.) Bridge Evaluation, Repair and Rehabilitation (pp. 161-174). Netherlands: Kluwer.

Bollo, M., Mahin, S. A., Moehle J. P., Stephen, R.M., & Qi X. (1990). Observations and Implications of Tests on the Cypress Street Viaduct test Structure. Earthquake Engineering Research Center UC Berkeley, Report No. UCB/EERC-90/21. Berkeley, California.

Bolt, B. A. (1988) Earthquakes. New York: W. H. Freeman.

Borland International Inc. (1991). Borland C++ Version 2.0 Programmer's Guide. Scotts Valley, California: Author.

Bracewell, R. N., (1986). The Fourier Transform and Its Applications. (2nd ed. rev.) New York: McGraw-Hill.

Brownjohn, J. M. W. (1988). Assessment of Structural Integrity by Dynamic Measurements. Doctoral dissertation, University of Bristol, United Kingdom.

Brownjohn, J. M. W., Dumanaoglu A. A., Severn R. T, & Blakeborough A. (1989). Ambient Vibration Survey of the Bosporus Suspension Bridge. Earthquake Engineering and Structural Dynamics, 18, (pp. 263-283).

Buckland, P. G., Hooley, R., Morgenstern, B. D., Rainer, J. H., & van Selst, A. M. (1979). Suspension Bridge Vibrations: Computed and Measured. Journal of the Structural Division ASCE, 105, (pp. 859-874).

Buckland, P. G. (1990). Assessment and Rehabilitation of Suspension Bridges. In Harding, J. E., Parke, G. A. R., & Ryall, M. N. (Eds.), Bridge Management Inspection, Maintenance, Assessment and Repair, (pp. 475-487). London: Elsevier.

Cantieni, R., & Pietrzko, S. (1993). Modal Testing of a Wooden Footbridge Using Random Excitation. Proceedings of the 11th International Modal Analysis Conference, 2, (pp. 1230-1236). Kissimee, Florida.

Caughey, T. K., & O'Kelly, M. E. J. (1965). Classical Normal Modes in Damped Linear Dynamic Systems. Journal of Applied Mechanics, 32, (pp. 583-588).

Clough, R. W., & Penzien, J. (1975). Dynamics of Structures. New York: McGraw Hill.

Collins, M. P., & Mitchell D. (1991). Prestressed Concrete Structures. Englewood Cliffs, New Jersey: Prentice Hall.

Computers and Structures Inc. (1992). SAP90 User's Manual. Berkeley, California: Author.

Cooley, J. W., & Turkey, J. W. (1965). An Algorithm for the Machine Calculation of Complex Fourier Series. Mathematics of Computation, 19, (pp. 297-301)

Diehl, J. G. (1991). Ambient Vibration Survey: Application Theory and Analytical Techniques, Application Note No. 3. Pasadena, CA.: Kinemetrics.

Douglas, B. M., & Reid, W. H. (1982). Dynamic Tests and System Identification of Bridges. Journal of the Structural Division ASCE, 108, (pp. 2295-2312).

Douglas, B. M., Maragakis, E. A., & Nath, B. (1990). Static Deformations of Bridges from Quick Release Dynamic Experiments. Journal of Structural Engineering, 116, (pp. 2201-2213).

Ewins, D. J. (1984). Modal Testing: Theory and Practice. New York: John Wiley and Sons.

Felber, A. J. (1990). RESPONSE: A Program to Determine the Load Deformation Response of Reinforced Concrete Sections. Master's Thesis, University of Toronto.

Felber, A. J. & Stiemer, S. F. (1991). Results of Ambient Vibration Measurements of the Second Narrows Bridge. (Available from A. Felber, Department of Civil Engineering, University of British Columbia, Vancouver, British Columbia.)

Felber, A. J. & Stiemer, S. F. (1992). An Object Oriented Programming Approach to Ambient Vibration Data Analysis For Bridges. 1992 Annual Conference of the Canadian Society for Civil Engineering, (pp. 375-384). Quebec, Quebec, Canada.

Felber, A. J. & Stiemer, S. F. (1993). An Object Oriented Approach to Ambient Vibration Measurement Analysis. Journal of Computing in Civil Engineering, 7, (pp. 420-438).

Felber, A. J., Ventura, C. E., Yee, S., & Stiemer, S. F. (1992). Colquitz River Bridge Dynamic Test - Preliminary Results. (Available from A. Felber, Department of Civil Engineering, University of British Columbia, Vancouver, British Columbia.)

Filiatrault, A., Tinawi, R., Felber, A. J., Ventura, C. E., & Stiemer, S. F. (1993a). Modal Analysis and Testing of the Cable-stayed Shipshaw Bridge in Jonquiere, Quebec. Proceedings of the 11th International Modal Analysis Conference, 1, (pp. 14-20). Kissimee, Florida.

Filiatrault, A., Tinawi, R., & Massicott, B. (1993b). Damage to a Cable Stayed Bridge During the 1988 Saquenay Earthquake, Part I: Pseudostatic Analysis. Journal of Structural Engineering, 119, (pp. 1432-1449).

Filiatrault, A., Tinawi, R., & Massicott, B. (1993c). Damage to a Cable Stayed Bridge During the 1988 Saquenay Earthquake, Part II: Dynamic Analysis. Journal of Structural Engineering, 119, (pp. 1450-1463).

Flesch, R. & Kernbichler, K. (1990a). Diagnostic Dynamic Testing of Bridges on Brenner Motorway. In Harding, J. E., Parke, G. A. R., & Ryall, M. N. (Eds.), Bridge Management Inspection, Maintenance, Assessment and Repair, (pp. 327-338). London: Elsevier.

Flesch, R. G. & Kernbichler, K. (1990b). A Dynamic Method for the Safety Inspection of Large Prestressed Bridges. In A. S. Nowak (Ed.) Bridge Evaluation, Repair and Rehabilitation (pp. 175-185). Netherlands: Kluwer.

Green, M. F., & Cebon, D. (1993). Modal Testing of Two Highway Bridges. Proceedings of the 11th International Modal Analysis Conference, 2, (pp. 838-844). Kissimee, Florida.

Hart, G. C., & Yao J. T. P. (1977). System Identification in Structural Dynamics. Journal of the Engineering Mechanics Division ASCE, 103, (pg. 1089-1104).

Hudson, D. E. (1964). Resonance Testing of Full-Scale Structures. Journal of the Engineering Mechanics Division ASCE, 90(EM3), (pp. 1-19).

Hudson, D. E. (1977). Dynamic Tests of Full-Scale Structures. Journal of the Engineering Mechanics Division ASCE, 103, (pp. 1141-1157).

Jennings P. C., Matthiesen R. B., & Hoerner J. B. (1972). Forced Vibration of a Tall Steel Frame Building. Earthquake Engineering and Structural Dynamics, 1, (pp. 107-132).

Kernighan, B. W., & Ritchie, D. M. (1988). The C Porgramming Language. (2nd ed. rev.) Englewood Cliffs, New Jersey: Prentice Hall.

Kinemetrics (1991). Operation Instructions For FBA-11 Force Balance Accelerometer. Pasadena, CA.: Author.

Kinemetrics (1992). Operation Instructions For Vibration Survey System Model VSS-2. Pasadena, CA.: Author.

Lally, M. J., & Severyn A. J. (1993). New Concepts in Multi-channel Management for Large Scale Modal Analysis. Proceedings of the 11th International Modal Analysis Conference, 1, (pg. 382-386). Kissimee, Florida.

T. Y. Lin International (1990). Golden Gate Bridge Seismic Evaluation. San Francisco, California: Author.

Luz, E., Gurr-Beyer, C., & Stoecklin, W. (1984). Experimental Investigations of Natural Frequencies and Modes of the HDR Nuclear Power Plant by Means of Microtremor Excitation. Proceedings of the 8th World Conference on Earthquake Engineering, 5, (pp. 977-984). San Francisco, California.

Luz, E. (1986). Bestimmung von Bauwerksparametern und -zustaenden mit Hilfe von Schwingungsmessungen unter stochastischer Anregung. Materialprufung, 28, (pp. 177)

Luz, E. (1987, August). Experimental Modal Analysis of Large Scale Structures. Proceedings of International Conference on Mechanical Dynamics, (pp. 257-262). Shenyang, China.

Maia, N. M. M. (1990). Reflections on Some SDOF Modal Analysis Methods. Proceedings of the 8th International Modal Analysis Conference, 1, (pp. 658-666). Kissimee, Florida.

Mathesion, R. B., Benya, J. S. & R. D. Shanman (1970, April). Forced Vibration Tests of a Steel Frame Building. ASCE National Structural Meeting Preprint, (pp. 1-16). Portland, Oregon.

Messmer, I. C. (1991, April). Solicitor General's Reply. The BC Professional Engineer. (p. 31.)

Microsoft (1991). Microsoft MS-DOS Operating System version 5.0, User's Guide and Reference. Redwood, Washington: Author.

Mitchell, D., Tinawi, R. & Law, T. (1990). Damage caused by the November 25, 1988 Saguenay Earthquake. Canadian Journal of Civil Engineering, 17, (pp. 338-365).

Muria-Vila, D., Gomez, R. & King, C. (1991). Dynamic structural properties of cable-stayed Tampico bridge. Journal of Structural Engineering, 117, (pp. 3396-1416).

Natke, H. G. (1982). Die systematische Anpassung von Rechenmodellen an Versuchswerte als Verfahren zum Nachweis des Dynamischen Systemverhaltens. Der Bauingenieur, 57, (pp. 287-292).

Ngok, M. T. (1982). The Determination of Structural Dynamic properties of Three Buildings in Vancouver B.C. from Ambient Vibration Surveys April. Master's Thesis, University of British Columbia.

Nielson, N. N. (1964). Dynamic Response of Multistory Buildings. Doctoral dissertation, California Institute of Technology.

Okauchi, I., Miyata, T., Tatsumi, M. & Kiyota, R. (1992). Dynamic Field Tests and Studies on Vibration Characteristics of Long Span Suspension Bridges. JSCE Journal of Structural Engineering and Earthquake Engineering, 9, (pp. 89-100).

Panzeri, P., & Pezzoli, P. (1989). Analisi dinamica di un ponte ad arco. Ingegneria Sismica, 3. Bergamo, Italy.

Quinn-Curtis (1991). Huge Virtual Array & Nummerical Toolbox for Borland/TurboC. Needham, Massachusetts: Author.

Rainer, J. H. & Pernica, G. (1979). Dynamic testing of a modern concrete bridge. Canadian Journal of Civil Engineering, 6, (pp. 447-455).

Ramirez, R. W., (1985). The FFT Fundamentals and Concepts. Englewood Cliffs, New Jersey: Tektronix.

Rubin, S. (1980). Ambient Vibration Survey of Offshore Platform. Journal of the Engineering Mechanics Division, 106, (pp. 425-441).

Staker, C. H. (1990). Graphics: Key to Usefulness of Structural Dynamics Technology. Proceedings of the 8th International Modal Analysis Conference, Kissimee, 2, (pp. 992-998). Kisssime, Florida.

Stroustroup, B. (1986). The C++ Porgramming Language. Reading, Massachusetts: Addison-Wesley.

Topf, U. A. (1970). Structural dynamic properties from ambient vibrations. Master's Thesis, University of British Columbia.

Trifunac, M. D. (1972). Comparison between ambient and forced vibrations experiments. Earthquake Engineering and Structural Dynamics, 1, (pp. 133-150).

Ventura, C. E. (1985). Dynamic Analysis of Nonclassically Damped Systems, Doctoral dissertation, Rice University, Texas.

Weaver, W., Timoshenko, S. P., & Young, D. H. (1990). Vibration Problems in Engineering (5th ed.). New York: John Wiley and Sons.

Werner, S. D., Beck, J. L., & Nisar, A. (1990). Dynamic tests and seismic excitation of a bridge structure. Proceedings of the Fourth U.S. National Conference on Earthquake Engineering, 1, (pp. 1037-1046). Palm Springs, California.

Wilson, J. C., & Liu, T. (1990). Experimental determination of modal frequencies and mode shapes of a cable stayed Bridge. Proceedings of the Fourth U.S. National Conference on Earthquake Engineering, 2, (pp. 542-552). Palm Springs, California.

Wilson, J. C., & Liu, T. (1991). Ambient vibration measurements on a cable-stayed bridge. Earthquake Engineering and Structural Dynamics, 20, (pp. 723-747).

Yamada, K., Yamamoto, N. & Akiyama, H. (1988). Full-scale dynamic test of long span bridges. Proceedings 4th U.S.-Japan workshop on bridge engineering. San Diego, California.

Yee, S. Y. G. (1993). Experimental dynamic verification of open piled wharf models. Unfinished Master's Thesis, University of British Columbia.

APPENDIX A: Measurement Hardware Selection and Specifications

After the tesing at the Second Narrows Bridge, many aspects of measuring and recording ambient vibrations were investigated to determine the specifications for the measurement hardware . This investigation and its influence on the choice of individual hardware components are outlined below. A laboratory test used to verify the suitability of the selected equipment is also presented.

A.1 Second Narrows Bridge Data

All of the vibration measurement equipment available at the Earthquake Laboratory of the Department of Civil Engineering was used to measure the ambient vibrations of the Second Narrows Bridge. At the time of the test, three different types of sensors were available to measure vibrations:

- STATHAM strain gauge based accelerometer and amplifier,
- KISTLER piezo electric accelerometer with conditioner,
- RANGER seismometers and signal conditioner.

I will discuss the performance of these sensors in the following paragraphs.

The STATHAM accelerometer was used to record vertical accelerations of the approach span trusses and the main span. It was capable of recording signals up to $\pm 2.5g$. Fig. A.1 shows the locations where the accelerations were recorded. The arrows in the figure indicate the location and direction of the STATHAM measurements.

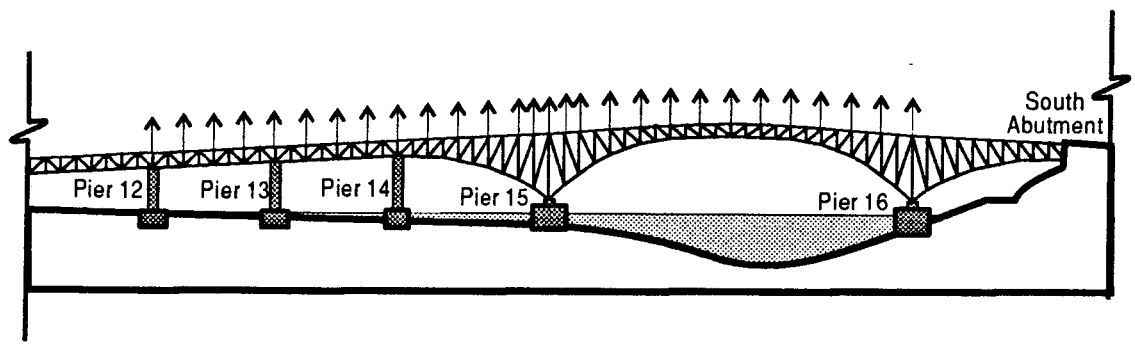

Fig. A.1: Locations of STATHAM Measurements on the Second Narrows Bridge

The plot in Fig. A.2 shows a portion of a typical signal recorded between piers 14 and 15 using the STATHAM accelerometer. The PSD of this record is shown in Fig. A.3. As you can see from Fig. A.2, the signal shows considerable drifts. This drifting was due to the amplifier used to condition the sensor's signal. In Fig. A.3 you can see that this drifting affects the signal predominantly in the range from 0 - 1 Hz. Because the fundamental modes of the structure were expected to measure below 1 Hz, the STATHAM accelerometer could not be used to confidently identify the Second Narrows Bridge's natural frequencies.

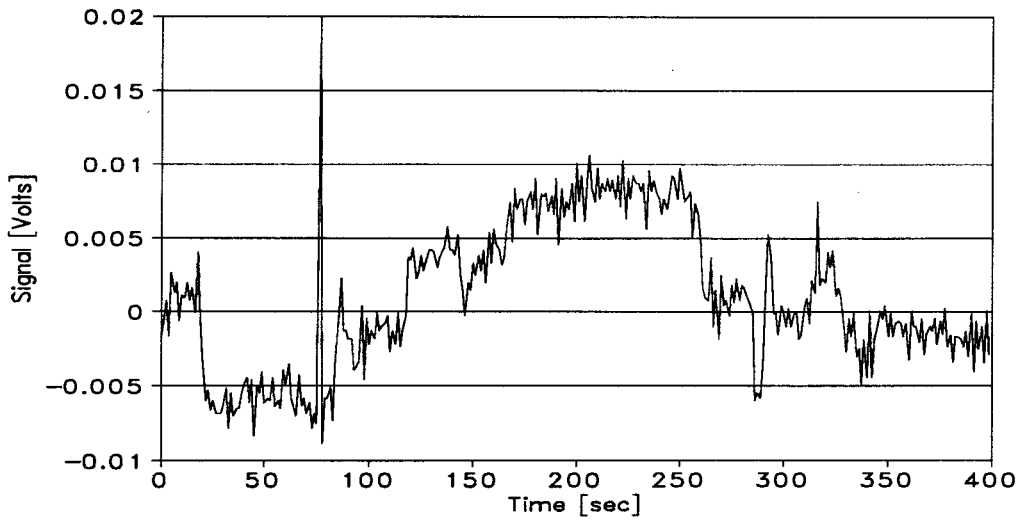

Fig. A.2: Typical Vibration Signal Recorded using the STATHAM Accelerometer

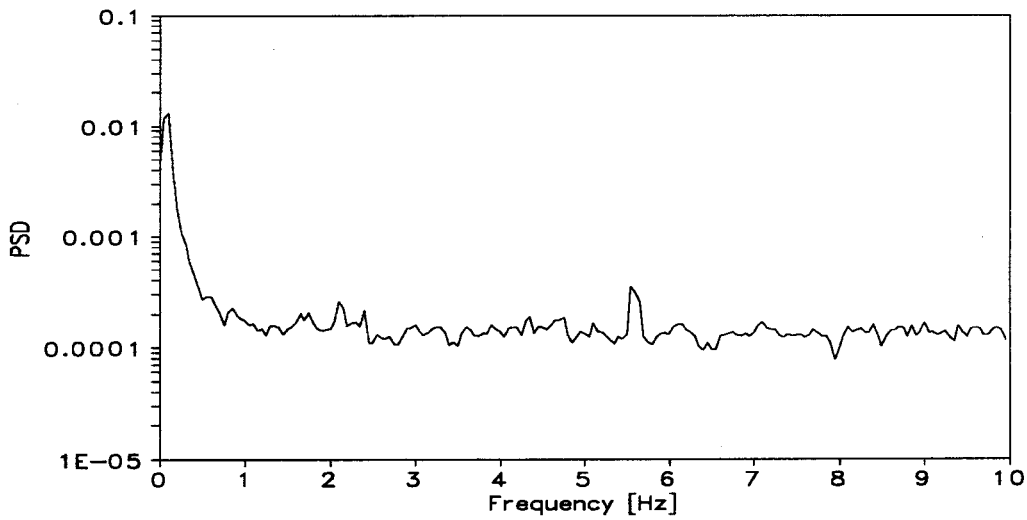

Fig. A.3: PSD of STATHAM Accelerometer Signal

A second series of measurements were conducted using both the KISTLER piezo electric accelerometer and the RANGER seismometer. The KISTLER accelerometer was used to measure the vertical vibrations and the RANGER was used to measure the vibrations transverse to the deck. The locations of the KISTLER and RANGER measurements are shown in Fig. A.4. The arrows in the figure indicate location and direction of the KISTLER measurements.

A portion of a typical acceleration record obtained using the KISTLER accelerometer is shown in Fig. A.5. The figure shows, similar to the STATHAM, the KISTLER accelerometer and conditioner exhibited large levels of drift. You can see how this drift affects the frequencies below 1 Hz in the corresponding PSD, shown in Fig. A.6. Because the signal obtained with the KISTLER accelerometer and conditioner exhibited even more drift than the STATHAM accelerometer, the records obtained with the KISTLER were even less suitable for ambient vibration analysis than those obtained with the STATHAM accelerometer and amplifier.

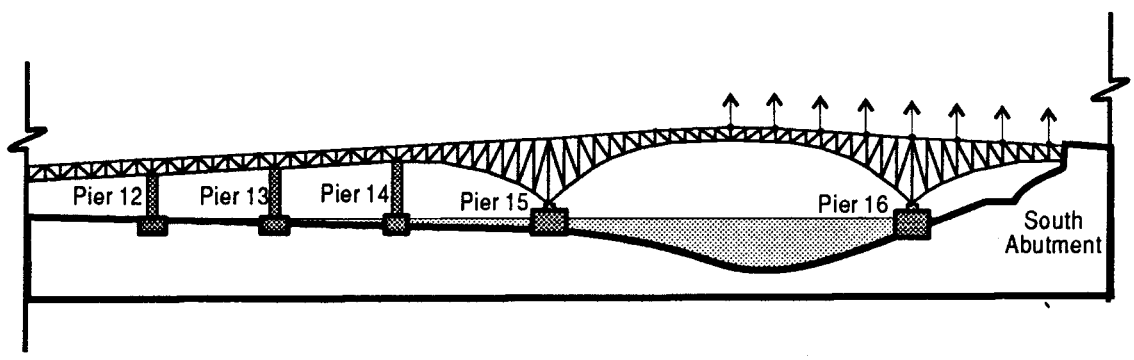

Fig. A.4: Locations of KISTLER and RANGER Measurements on the Second Narrows Bridge

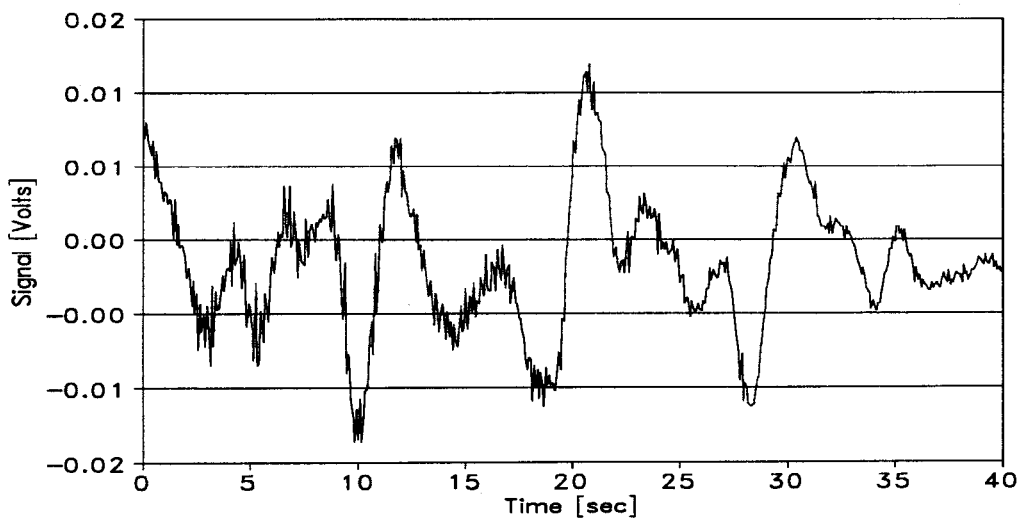

Fig. A.5: Typical Vibration Signal Recorded using the KISTLER Accelerometer

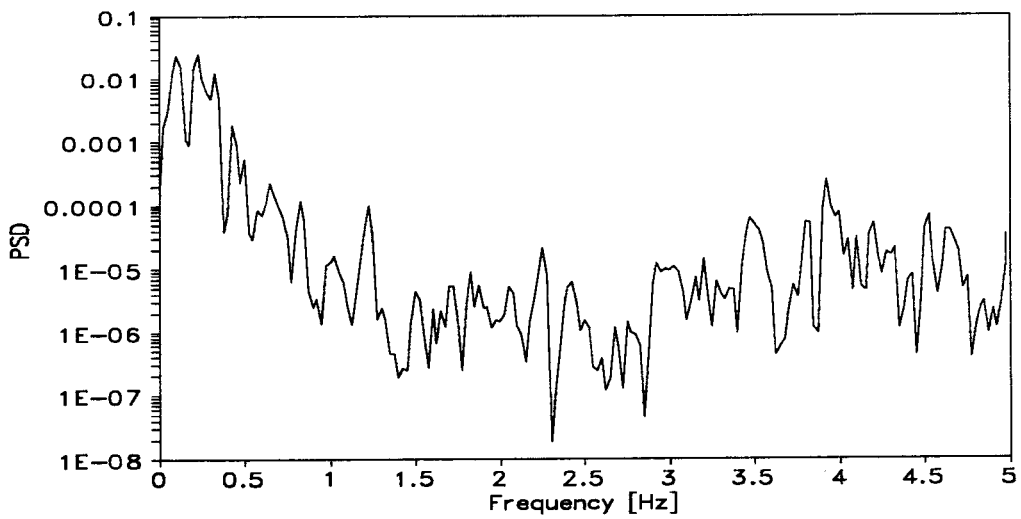

Fig. A.6: PSD of KISTLER Accelerometer Signal

As mentioned above, tests were also conducted using the Earthquake Engineering Laboratory's RANGER seismometers (Model: SD-214) and conditioner (Model: SC-201) (Ngok, 1981). A typical transverse vibration signal obtained with a RANGER seismometer near the center of the main span is shown in Fig. A.7. Unlike the STATHAM and the KISTLER, this transverse vibration signal did not exhibit drift. The recorded signals from a RANGER seismometer were suitable for identifying natural frequencies. Fig. A.8 shows the PSD used to identify the natural frequencies of the structure.

Although the RANGER seismometer signals were used to identify the natural frequencies, they could not be used to identify the mode shapes of the Second Narrows Bridge. Mode shapes can only be identified if a set of sensors produce accurate measurements of the vibration amplitudes. Initial laboratory tests of the RANGER seismometers showed, in the frequency range of interest (0 - 2 Hz), the sensors did not produce identical signals when all four sensors were subjected to the same excitation. In particular, the phase angle between instruments was inconsistent and the amplitude ratio was not constant between the four sensors. A detailed analysis of these instruments was subsequently made by (Yee, 1993) and confirmed the findings of the initial laboratory tests.

Another problem with the RANGER seismometers was that they could not measure the vertical vibrations of this bridge. The vertical accelerations of the bridge were so large, that the RANGER instrument saturated frequently.

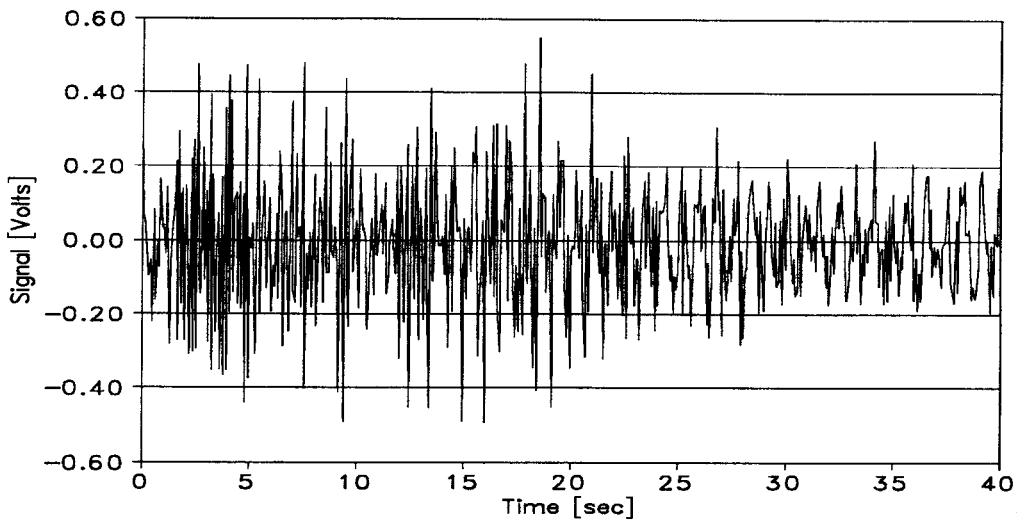

Fig. A.7: Typical Transverse Vibration Signal Recorded using the RANGER Seismometer

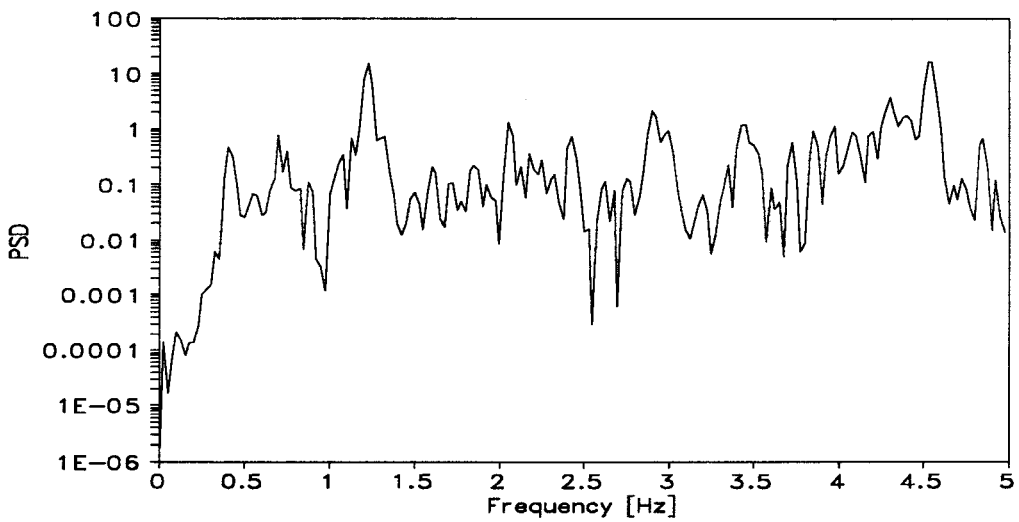

Fig. A.8: PSD of RANGER Seismometer Signal

A.2 Basic Electronics Terminology

During the investigation of the requirements for the measurement equipment, many electronics and data acquisition terms and concepts were explored. Since many of these terms and concepts are not generally encountered in structural engineering, they will be briefly explained in the following sections. Some of the fundamental terms are defined as follows:

Decade: A decade refers to a frequency ratio of 10:1. (e.g. 20Hz is one decade above 2Hz)

Decibels: Decibels are used extensively in the specifications of electronic equipment. They express the ratios between inputs and outputs. If the output of a device is larger than the input, the signal is amplified and the decibel value is positive. On the other hand, if the output is smaller than the input, the signal is attenuated and the decibel value is negative. The decibel values for voltage signals are calculated using:

$$\text{Voltage Gain in db} = 20\log\left(\frac{\text{voltage output}}{\text{voltage input}}\right) \tag{A-1}$$

Gain: Gain is the electronics term for amplification factor.

Octave: An octave refers to a frequency ratio of 2:1. (e.g. 6Hz is one octave above 3Hz)

A.3 Sensors

A.3.1 Sensor Specifications

A sensor or transducers is used to convert a physical phenomena into an electrical signal.

Accelerometers are transducers which produce an electrical signal proportional to acceleration. The characteristics of accelerometers can be described using the following parameters:

Frequency Range: The range of frequencies for which the sensor produces useful output. For ambient vibration measurements, transducers with a frequency range of 0 - 20 Hz are required.

Acceleration Range: This determines the range between the maximum positive and negative accelerations which the transducer can transform to electronic signals (e.g. ±2 g). For ambient vibration surveys, instruments with an acceleration range of ±0.5 g are sufficient.

Qutput/Sensitivity: The output refers to the ratio between the voltage produced and the amount of excitation. It is typically specified in Volts/g. High transducer output is desirable as it may eliminate the need for further signal amplification.

Noise: Noise is the signal level produced by a sensor when not subjected to vibration. The noise level determines the smallest accelerations which can be monitored. If the level of acceleration of interest is equal to the noise level of the instrument it is very difficult to interpret the results.

Dynamic Range: Dynamic range refers to the difference in signal levels which a transducer can detect. The ratio of the smallest detectable signal to the acceleration range of the transducer represents its dynamic range. For ambient vibration measurements, a large dynamic range is desired.

Saturation: When the physical excitation exceeds the acceleration range of the transducer, some transduces saturate. A saturated transducer produces a signal equal to

or above the level corresponding to the peak output level for a period of time which is much longer than the corresponding physical excitation. Saturation of the instrument is not desirable as it causes gross distortion of the signal and affects subsequent analysis.

To select the appropriate transducers, the anticipated vibrations had to be specified. The frequencies of interest for bridge vibrations generally lie in the 0.1 Hz - 20 Hz region. In addition, the maximum acceleration commonly encountered in the field lies above 0.25 g (J. C. Wilson, personal communication, spring 1991). Measurements undertaken by the author on Second Narrows Bridge in Vancouver, B.C. have shown peak acceleration levels of 0.35 g. On the other hand, the amplitudes of the vibrations associated with some the modes of interest can be as low as 0.1 mg - 0.01 mg. Thus, a transducer used for ambient vibration measurements should satisfy the following specifications:

- Frequency range 0-25 Hz
- Range ±0.5 g
- Sensitivity of at least 2 V/g
- Dynamic range of at least 100 db

A.3.2 Selected Sensors

The sensor selected for the measurement of bridge vibrations were the Kinemetrics[1] FBA-11 accelerometers which have the following nominal specifications:

---

1 Kinemetrics Systems, 222 Vista Avenue, Pasadena, California 91107.

- Natural Frequency: 50 Hz (damping: 70% critical)
- Full Scale Range: ±0.5 g
- Sensitivity: 5 Volts/g
- Dynamic Range: 130 db from 0-50 Hz (140 db from 0-10 Hz)

This type of sensor was recently used for ambient vibration measurements of the Golden Gate Suspension Bridge (Abdel-Gaffar & Scanlan 1985) and the Quincy Bayview Cable-Stayed Bridge (Wilson & Liu, 1990).

The frequency dependent gain of a sensor can be defined as the recorded acceleration divided by the actual acceleration level. Knowing the natural frequency and damping value of the sensor the gain of the sensor, can be computed. The gain functions for the first four FBA-11s transducers purchased for the HBES are plotted in Fig. A.8. As can be seen from this figure, the four instruments behave identically up to a frequency of 20 Hz. This is an important characteristic since the relative amplitude of individual sensors are used to compute the mode shapes of a structure. These sensors have slightly different natural frequencies and damping values so their response near resonance (50 Hz) varies slightly. This is of no consequence as the frequencies of interest generally lie below 20 Hz. Since the ambient vibration analysis is only concerned with the relative amplitudes of signals and all the sensors have similar characteristics, there is generally no need to correct the signals for the instrument response. Thus, ambient vibration data obtained from the FBA-11s can be used for analysis without requiring signal correction.

The Kinemetrics FBA-11 sensors implemented in the HBES hardware have met all the required specifications and have proven to be suitable for ambient vibration measurements.

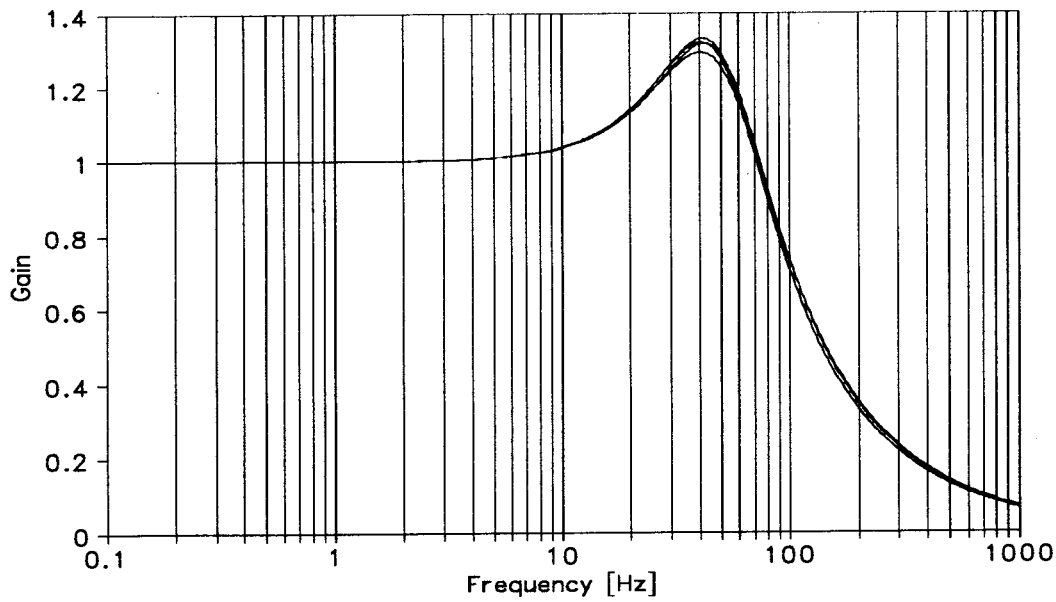

Fig. A.9: Gain of four FBA-11 Accelerometers used for the HBES.

A.4 Signal Conditioning Equipment

The electronic signal produced by the sensors are amplified and filtered before they are converted to a digital signal. This process is commonly referred to as signal conditioning. The key specifications for the amplifiers and filters required to obtain high quality ambient vibration data are given below.

A.4.1 Signal Conditioning Specifications

A.4.1.1 Amplifier Specifications

Either amplification or attenuation can be used to scale the amplitude of an electronic signal.

The level of the signal has to be matched to the conversion range of the A/D converter. Typical conversion ranges are ± 1 Volt and ± 10 Volts. The signals are best digitized if the signal levels approach the conversion range but do not exceed it. To achieve this, a large range of amplification levels have to be available such that signals of different levels can be matched effectively to the A/D conversion range.

This concept will be illustrated using a small example. A suitable gain has to be selected for a signal corresponding to an acceleration level of 0.04 mg and a A/D converter with a range of $\pm 1 Volts$. The signal voltage generated by the FBA-11 sensor with a sensitivity of 5 Volts/g will be 0.4 mV. The amplification will be selected such that a 0.5 mV signal will be amplified to 1 Volt to prevent the signal from exceeding the range of the converter. Therefore the amplification factor should be 1.0/0.0005=2000.

This example illustrates that in order to measure small accelerations effectively, large amplifications are required. In addition, many intermediate amplification levels should be available so that signals corresponding to larger accelerations can also be appropriately amplified. Therefore, the amplifiers selected for the HBES hardware should permit amplification factors of up to 2000 with many intermediate levels.

A.4.1.2 Filter Specifications

Bridge vibrations can contain large high frequency components due to impulsive traffic excitation arising from uneven expansion joints and pavement defects. The high frequency components of the vibration signal can be reduced using low pass filters. The desired response of an ideal low pass filter is to pass all signal components below a cutoff frequency without any change, and to totally remove any components above the cutoff frequency. Unfortunately such ideal filters can not be physically realized and real filters only approximate the properties

of ideal filters. Analog low-pass filters pass signal components below the cutoff frequency without much attenuation. Above the cutoff frequency, the attenuation increases with frequency. The signal components below the cutoff frequency also experience a time delay. This time delay results in a phase shift of the signal components which increases as the frequency of the signal approaches the cutoff frequency. The level and characteristics of the phase shift are a function of the filter design.

In addition to low pass filters, high-pass filters can be used to remove the low frequency components of a signal. For example, amplifier drift can cause a gradual movement of the signal baseline. To eliminate the effects of the drifting on the signal high-pass filters can be employed.

The properties of analog filters are described using the following parameters:

Pass Band: The band of frequencies which should pass the filter. For low-pass filters this is the range from zero to the cutoff frequency. For high-pass filters it is all frequencies above the cut-off frequency.

Cutoff Frequency: The frequency where the filter response drops down 3 db from the pass band response.

Insertion Loss: The nearly constant attenuation in the pass band of the filter.

Phase Shift: The shift in phase of the signal due to the filter.

Roll-off: Roll-off refers to the rate at which a filter's attenuation is increasing. Roll-off is generally specified in db/decade. For example, a low-pass filter with a 2 Hz cutoff frequency and a 6 db/decade roll-off reduces the amplitude signal components at 20 Hz by 50 % and at 200 Hz by 75 %.

Stop band: The stop band refers to the frequency range which should be attenuated by the filter. For low-pass filters the stop band are all frequencies above the cutoff frequency. For a high-pass filter the stop band is from DC to the cutoff frequency.

Low-pass filters for ambient vibration measurements must have a very high roll-off because the amplitudes of the high frequency components of the ambient vibration signal are much larger than those of the pass band frequencies. Figure A.10 shows a typical power spectrum for an ambient vibration record obtained from Second Narrows Bridge. If low pass filtering at 2 Hz is desired, the filter should have a roll-off which attenuates the signal by a factor of 100 per decade. This corresponds to a roll-off of 40 db/decade, which is equivalent to 12 db/octave. Low-pass filters should be selectable for several cutoff frequencies in the range from 2 to 20 Hz. In addition, some high pass filtering capability should exist to remove the low frequency components of the signal associated with drift.

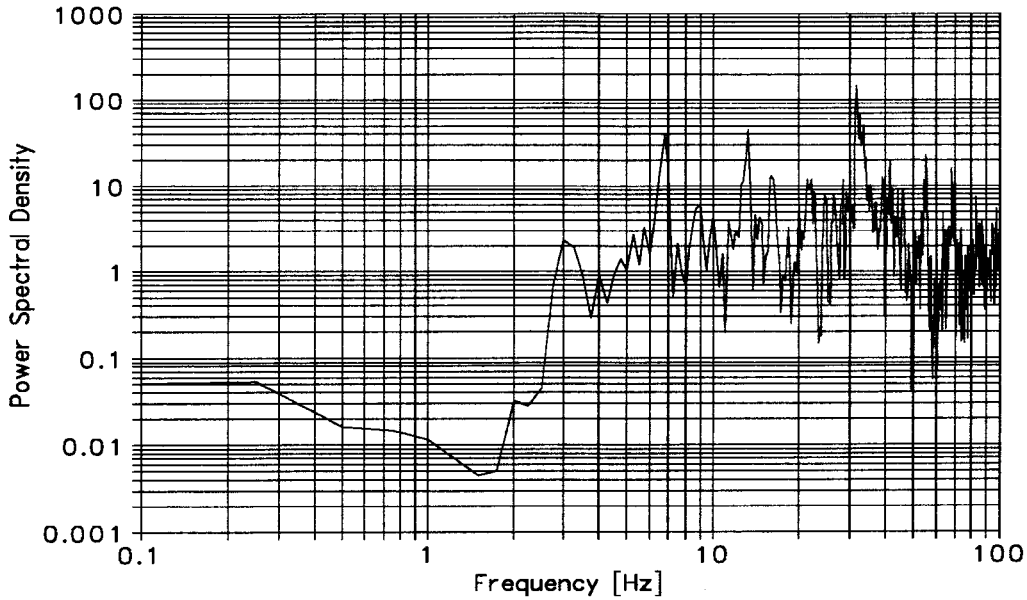

Fig. A.10: PSD of Vertical Signal of the Second Narrows Bridge between Piers 15 and 16

A.4.2 Selected Signal Conditioning Equipment

A portable Kinemetrics (Model # VSS-2) signal conditioner was selected for the HBES. This unit has eight signal conditioning cards (Model # AM-3I) mounted in a portable rack which contains the power supply and charging circuitry. The conditioner also has some circuitry which can be used to verify the proper operation of the FBA-11 sensors. The individual components of the signal conditioner are described below. The signal conditioning equipment meets required specifications and has proven to be very reliable in the field.

A.4.2.1 Amplifiers

The AM-3I card has built-in pre-amplifiers with a gain of 66 db. The amplified signal is then filtered and attenuated to obtain the desired level of amplification. With these cards the amplification level can be controlled using 11 selectable attenuation levels. The corresponding nominal amplification levels and effective sensitivities are specified in Table A.1. This table is very useful in the field because the attenuation settings can quickly be converted to acceleration levels. The large range of amplification levels has proven to be very useful to properly amplify all the signals encountered during the field work associated with this thesis.

Table A.1: Amplifications Levels of the Kinemetrics Signal Conditioner

Attenuation Setting db	Signal Amplification	Sensitivity V/g	Conversion Factor mg/V
66	1.00	5	200.000
60	2.00	10	100.237
54	3.98	20	50.237
48	7.94	40	25.178
42	15.85	79	12.619
36	31.62	158	6.325
30	63.10	315	3.170
24	125.89	629	1.589
18	251.19	1256	0.796
12	501.19	2506	0.399
6	1000.00	5000	0.200
0	1995.36	9976	0.100

A.4.2.2 Filters

The AM-3I signal conditioning cards are equipped with both high-pass and low-pass filters. The high-pass filters have a +12 db per octave roll-off and can be set for corner frequencies

of DC, 0.1 Hz, or 5.0 Hz. The low-pass filters have a roll-off of -12 db per octave and can be set for 2.5, 5.0, 12.5, 25.0, 50.0 Hz and OUT. The theoretical performance of all the available filters is illustrated in Fig. A.11. The gain in this figure is defined as the ration of the filtered signal over the unfiltered signal. This figure can be used to estimate the effect of the filters on particular frequency components. For example, if a sinusoidal 30 Hz signal with an amplitude of 1 Volt were filtered using the 2.5 Hz low-pass filter, then the filtered signal would only have an amplitude of 0.007 Volts. If the same signal were filtered using the 12.5 Hz low pass filter, the resulting signal would have an amplitude of 0.175 Volts.

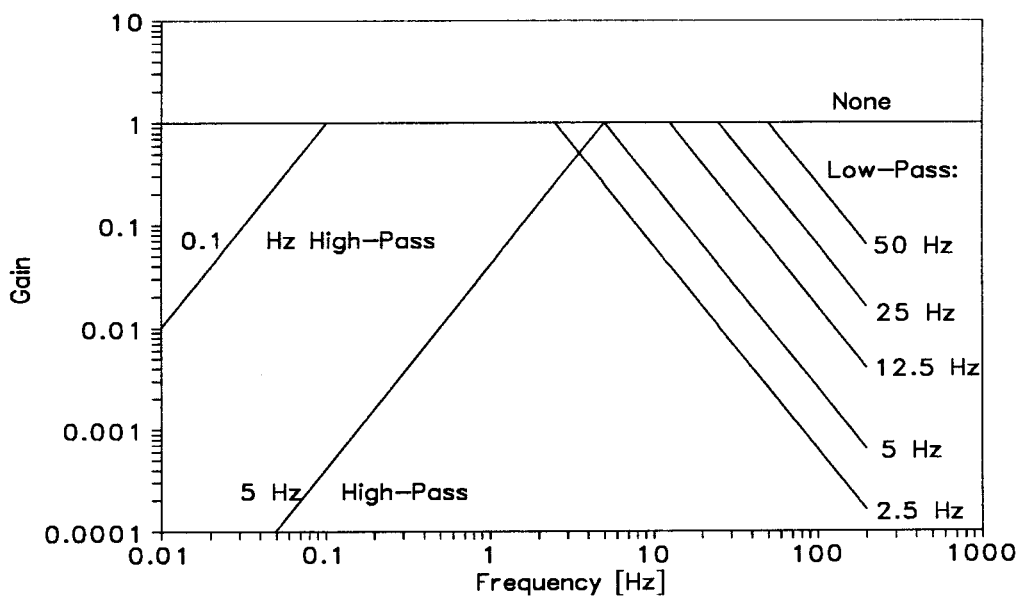

Fig. A.11: Theoretical Performance of the Filters of the AMI-3 Conditioning Cards

A.4.2.3 Power Supply

The signal conditioner was originally equipped with two 12 Volt batteries and charging circuitry. During testing, the accelerometers are powered by these batteries. If all eight accelerometers connected are used continuously the batteries last approximately 10 hours. A second set of batteries was installed to double the continuous operation time of the signal conditioner.

A.4.2.4 Sensor Verification Option

The signal conditioner also has circuitry which can be used to ascertain the proper operation of the connected FBA-11s. When this option is used, a 1 Volt heavy side function excitation signal is sent to the sensor and shortly thereafter the electronic damping of the sensor is removed. The sensors return signals which shows its response to the heavy side excitation and the release of electronic damping. This signal, known as the calibration signal, can then be used to determine the natural frequency and damping of the sensor. A typical calibration signal of an FBA-11 sensor is shown in Fig. A.12. The above procedure is describe in detail in the signal conditioner manual (Kinemetrics, 1992) and the analysis of the calibration signal is described in section C.2.1.5.

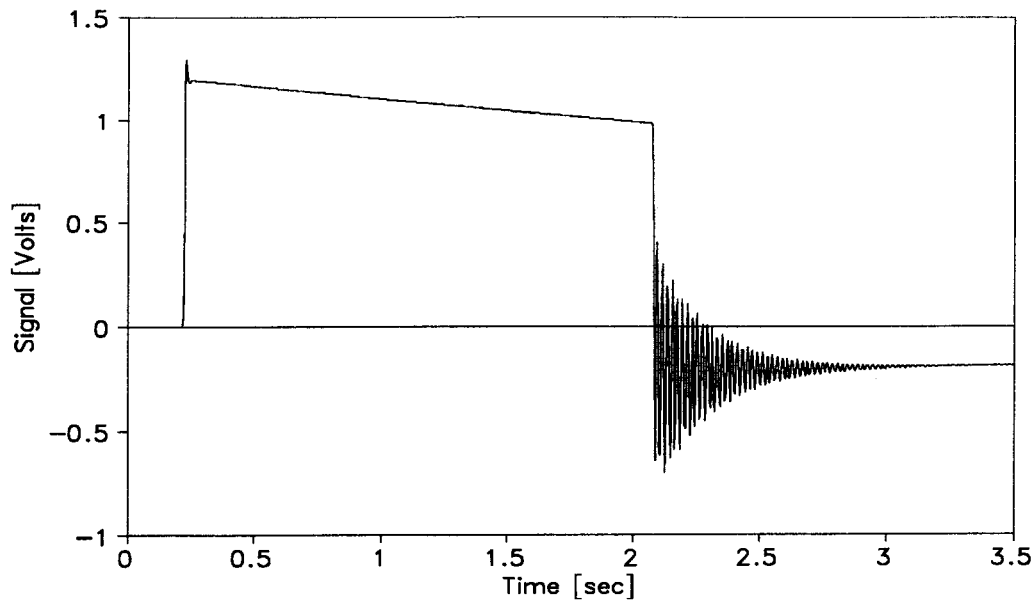

Fig. A.12: Typical Calibration Signal of a FBA-11 Accelerometer

A.5 Analog to Digital Conversion

Once the electrical analog signals have been suitably amplified and filtered, they must be recorded. Two choices for recording analog signals are analog systems and digital systems. While analog systems such as multi track tape recorders were quite popular in the past (Topf 1970), (Abdel-Ghaffar & Housner, 1977), recent advances in digital technology have made it possible to record and store large amounts of high resolution data. Therefore, digital data recording equipment was selected for the HBES. Some of the main concepts in the digitization of analog signals are briefly discussed before the selected system is described. For a thorough discussion of the concepts involved in digitization of analog signals, the reader is referred to Bendat & Piersol (1986) and/or Bracewell (1986).

A.5.1 Theoretical Background on Digitizing

Analog signals are continuous in time and amplitude. Converting an analog signal to digital data requires digitization of both the magnitude information and the time information. Fig. A.13 shows an analog signal and two sets of points which correspond to the digitized information. The analog signal shown in the figure is comprised of two sine waves of different period and amplitude. The long period sine wave has an amplitude ten times larger than the short period one. If a rough digitization is used then the digitized information can only assume values at the grid intersections. From these digitized values it would be impossible to reconstruct the original signal since the grid is too coarse both in time and amplitude. The signal is much better represented by the second set of symbols which uses a finer discretization for both time and amplitude. To digitize the analog signal with as little information loss as possible, the time and amplitude increments have to become very small. This would result in a good representation of the analog signal, except that the large amount of information would cause processing and storage problems. Thus, both the amplitude and time resolution have to be chosen appropriately. The amplitude discretization will be discussed below in the sections "Analog to Digital Conversion" and the choice of the time increment will be discussed under "Sampling".

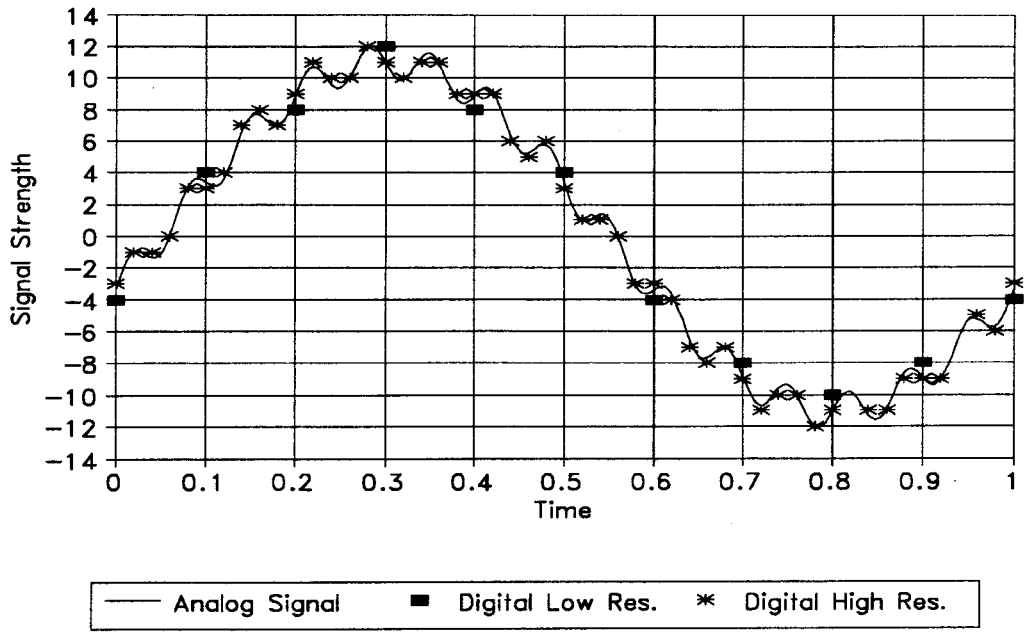

Fig. A.13: Analog Signal and Discretizations.

A.5.1.1 Analog to Digital Conversion

Analog signals, by definition, can assume any level within a certain range. Digital signals on the other hand, can only assume discrete levels. In the process of signal conversion, the analog signal is represented by discrete digital levels. The quality of this representation is most affected by the size of the increment between two digitization levels. The size of the increment between two levels is determined by the resolution and range of the analog to digital (A/D) converter. Converters with different resolutions and ranges are available. Common resolution in the vibration measurement field vary from 8 to 16 bits, while typical signal conversion ranges are ± 1 Volt and ± 10 Volts. Since the output is stored in binary form, a resolution of 8 bits corresponds to 256 levels and a 16 bit resolution corresponds to 65,536 levels.

Bendat and Piersol (1986, p. 340) demonstrated that the digitization of an analog signal has a quantization error with a standard deviation of 0.29 scale units. A scale unit is defined as the conversion range divided by the resolution. The quantization error can be used to determine the peak signal to noise ratio using

$$\text{Peak Signal to RMS Noise Ratio} = \frac{Resolution}{0.29} \tag{A-2}$$

This definition of signal to noise ratio is appropriate if the signal of interest is nearly as large as the conversion range. For ambient vibration measurements the peak signal level is often much larger than the signal component of interest. Therefore, the signal to RMS noise ratio should be defined as

$$\text{Signal to RMS Noise Ratio} = \frac{2*SignalLevel*Resolution}{Range*0.29} \tag{A-3}$$

This equation can be used to determine the signal to noise ratios corresponding to various signal levels and resolutions. Two sample calculations are shown below to illustrate the difference between 12 and 16 bit resolution in data conversion. The range is set to ±0.5g and the signal of interest has a 0.1mg level. The expected signal to noise ratios are

12 bit resolution:

$$\frac{2*0.0001*2^{12}}{(0.5-(-0.5))*0.29} = 2.8$$

16 bit resolution:

$$\frac{2*0.0001*2^{16}}{(0.5-(-0.5))*0.29} = 45$$

This example illustrates that for ambient vibration measurements a higher resolution is desirable as it increases the signal to digitization noise ratio. Since the use of lower resolution A/D

conversion results in the loss of information associated with low amplitude signals (Berry 1992), the A/D conversion for the ambient vibration data should have 16 bit resolution or better to capture the information with sufficient accuracy.

A.5.1.2 Sampling

The previous section dealt with the discretization of the signal amplitude. This section deals with the temporal discretization of the signal. To adequately represent an analog signal, it is sampled at fixed time intervals. The smaller these intervals are the better the analog signal will be approximated. However, the amount of memory required to store the digital signal increases with the number of samples. A sampling rate which results in a digital signal that represents the analog signal adequately and at the same time does not require excessive amounts of memory has to be selected. The main aspects of sampling are discussed in the following sections.

Nyquist Frequency

The sampling rate determines the largest frequency which can be resolved from a digitized signal. This frequency is known as the Nyquist frequency f_c and is calculated from the following equation:

$$f_c = \frac{1}{\Delta_t * 2} \tag{A-4}$$

where Δ_t sampling interval and f_c is the Nyquist frequency.

For example, if the frequencies below 20Hz are of interest a sample interval of 0.025 second would be sufficient. However, it is advisable to sample at a higher rate to avoid the aliasing (see below) of higher frequency signals.

Aliasing

Aliasing refers to the folding of higher frequencies about the Nyquist frequency. Aliasing introduces an error which is inherent in the analog to digital conversion process. Using the above equation with a 0.25 second sampling interval, the highest frequency which can be resolved will be 2 Hz. Frequency components of the analog signal which are higher than 2 Hz are folded into the frequency range of 0 - 2 Hz. Fig. A.14 shows a 1.5 and a 2.5 Hz sinusoid sampled at 0.25 second intervals. Since both sine waves coincide at these sample points, both signals will contribute to the spectrum at 1.5 Hz. The 2.5 Hz signal is said to have folded back into the spectrum at 1.5 Hz. For any frequency f in the interval $0 \le f \le f_c$, the higher frequencies which are aliased with f are $2nf_c \pm f$(for $n = 1,2,3..\infty$). To avoid aliasing, higher frequency components are removed from the analog signal using low-pass filters. Since low-pass filters do not have infinite roll-off, the cut-off frequency of the filters should be set lower than the Nyquist frequency to assure the higher frequencies are sufficiently attenuated.

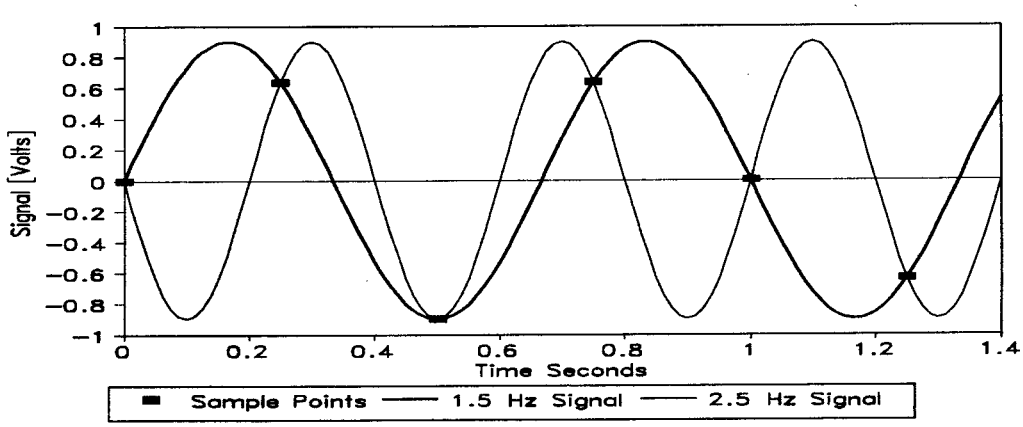

Fig. A.14: 1.5Hz and 2.5Hz Sinusoid Signals Sampled at 0.25 Second Intervals.

Frequency Resolution

The frequency resolution is a function of the sampling rate and the number of data points measured. The relation between record size and frequency resolution is given by

$$\Delta f = 2\frac{f_c}{N} \tag{A-5}$$

where Δf is the frequency resolution and N is the number of samples. The frequency resolution required for ambient vibration analysis will depend on the type of structure being investigated and the amount of information desired. To investigate structures which have closely spaced modes a frequency resolution sufficiently fine to clearly separate the frequencies has to be selected. Rearranging the above equation, the required amount of data points for a given Nyquist frequency and frequency resolution can be calculated.

Phase Shift

Theoretically all transducers should be sampled concurrently. In practice this requires either separate A/D converters for each channel or sample and hold amplifiers. More commonly, the individual channels are sampled in sequence and converted using the same A/D converter. This process introduces a phase shift between channels. Since the phase information forms an important aspect of the ambient vibration data analysis, it is important that the phase shift due to sampling is quantified. The phase shift depends on the frequency, the number of channels and the time delay between channels. It can be calculated using the following expression:

$$\phi = 360 f \Delta_c n \tag{A-6}$$

where, ϕ is the inter channel phase shift, f is the frequency of interest, Δ_c is the time delay between sampling of channels, and n is the number of channels.

A.5.1.3 Data Storage

Long continuous segments of data are taken, to obtain results with high frequency resolution. Generally several segments of data are acquired so that the results from individual segments can be averaged. All these readings have to be stored in digital form. The amount of memory required is a function of the number of samples, the number of channels and the resolution of the A/D conversion. A byte of memory consists of 8 bits. Hence, a 16 bit sample requires 2 bytes of memory for storage and a 8 bit sample requires 1 byte of memory. Assuming 2 bytes per sample, the memory requirements for data storage are calculated as follows:

$$\text{Memory Requirement} = 2*n*N \tag{A-7}$$

where, n is the total number of channels, and N is the number of points per channel. For example, a four channel data acquisition system for typical ambient vibration measurements would require 512 kb of memory to store 65536 samples per channel.

A.5.2 Data Acquisition Hardware

After a study of the specifications of several available data acquisition systems, the Keithley[2] Model 575 Measurement and Control was selected. This system was then implemented in to the HBES and specific software developed to acquire ambient vibration data. Some of the key specifications of Keithley acquisition system are listed below:

- Resolution: 16 bits
- Global Gain: 1, 2, 5, 10 programmable
- Range: ±10 Volts
- Conversion Time: 20μsec

---

2 Keithley Instruments ,Inc. 28775, Aurora Road, Cleaveland, Ohio 44139.

The implications which these specifications have on the acquisition of ambient vibration data are discussed in the following sections.

A.5.2.1 Analog to Digital Conversion

The 16 bit resolution combined with the global gain settings can be used to record very small signals. If the global gain is set to 10, then the theoretical discretization step size is $2/2^{16} = 30.5\mu Volts$. In practice however, the lowest two bits usually jump around due to electric noise. Thus, the practical discretization step size is $2/2^{14} = 122\mu Volts$. This corresponds to a dynamic range of 84 db.

A.5.2.2 Sampling

The Keithley is equipped with a AMM2 board which can be used to sample up to 16 Channels. During initial laboratory tests in the spring of 1992, some cross-talk between channels was observed. Cross-talk causes some of the signal in one channel to be read as part of the signal of the next channel. To eliminate the cross talk every alternate channel was grounded. Therefore, the system was configured to read only every second channel. It was recently discovered (February 1993) that the cross-talk had been due to a small fault of the AM-3I signal conditioning cards which was subsequently corrected. Since all the tests described in this thesis were conducted prior to this discovery, the characteristics of the data acquisition system will be discussed as they were during these tests.

Sampling Rate

The maximum sampling rate of the data acquisition system for one channel is 50kHz. For more channels, the maximum sampling rate can be calculated from

$$\text{Maximum Sampling Rate} = \frac{50000Hz}{\text{Number of Channels*2}} \tag{A-8}$$

Thus, for four channels the maximum sampling speed is 6250 Hz and for eight channels it is 3125 Hz.

Phase Shift

The phase shift between channels can be calculated using the technical specifications for the Keithley 575 Hardware. As shown in section A.5.1.2 the phase shift between the first and nth channel can be calculated as

$$\phi = 2f\Delta_c 360(n-1) \tag{A-9}$$

The expected phase shift between 2, 4, 6 and 8 channels is shown in Fig. A.15. This figure should be kept in mind when the phase information is used in the data reduction.

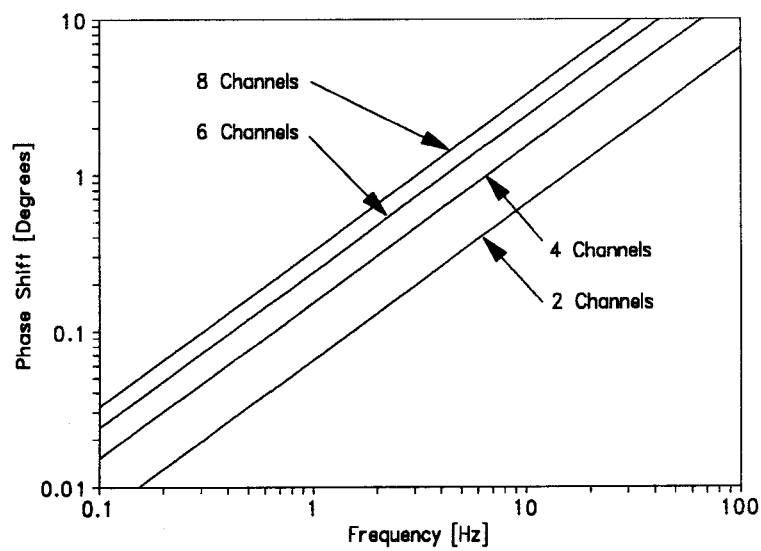

Fig. A.15: Phase shift for Keithley 575 Data Acquisition System.

Record Size Limits

If eight channels are sampled using the Keithley 575 data acquisition hardware, then a maximum of 6362 points per channel can be acquired. For computational efficiency, continuous ambient vibration data segments must have a total number of points N equal to 2^n (n is a positive integer). Since 6362 is not an even power of two, the maximum continuous data segment is selected to be 4096 points by the acquisition software. If longer records are desired, they can be formed as a series of 4096 point segments.

Frequency Resolution

As mentioned in section A.5.1.2, the frequency resolution is controlled by the Nyquist frequency and the number of points in a continuous data segment. As the maximum size of a data segment is set at 4096 the frequency resolution corresponding to a series of Nyquist frequencies can be computed. Fig. A.16 shows the relation between frequency resolution and Nyquist frequency for a segment length of 4096 samples. This figure can be used to obtain the frequency resolution associated with a given Nyquist frequency. For example, for the Nyquist frequencies of 5 Hz, 10 Hz and 20 Hz, the frequency resolutions would be 0.0024 Hz, 0.0049 Hz and 0.0098 Hz respectively.

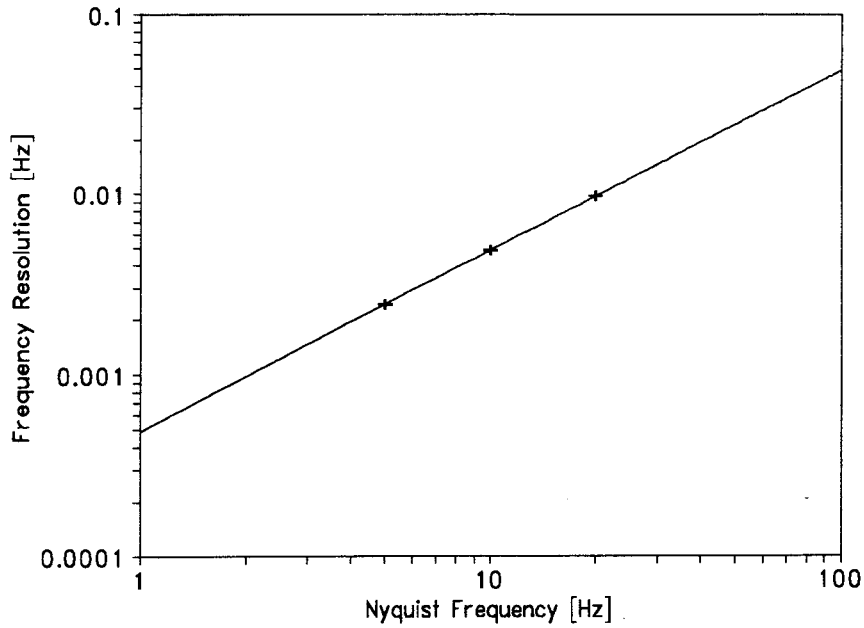

Fig. A.16: Frequency Resolutions Corresponding to a 4096 Sample Segment.

A.5.3 Data Acquisition Software

The Keithley 574 data acquisition hardware was purchased with a TurboC & C++ compatible driver Library. Using this library, a program for the acquisition of ambient vibration data was developed. The program was specifically designed for ambient vibration tests and thus ensures that all measurements are obtained in a consistent manner. The program permits the user to select the following options and parameters:

f_c	Nyquist frequency
N	Total number of points per channel

n	Number of channels
gain	Global gain
0/1	Calibration flag
filename	File for binary storage
site	Description of the site
setup	Description of the setup

For more information on the data acquisition program, refer to the manual in Appendix B

A.6 Hardware Test

A calibration test was performed to verify the suitability of the HBES hardware for ambient vibration testing. The objectives, setup and results for this calibration test are given below.

A.6.1 Hardware Test Objective

For ambient vibration studies, the measurement of relative signal strength forms the basis of the analysis. Therefore, the following test objectives were established:

- Determine the relative amplitude error between channels.
- Determine the relative phase shift between channels.

A.6.2 Hardware Test Description

All eight sensors were mounted on the shake table of the Earthquake Laboratory of the Department of Civil Engineering at UBC and subjected to broad band white noise excitation. The PSD of the white band noise is shown in Fig. A.17. The time histories for all eight sensors

were recorded using 40 samples per second and low-pass filters with a cut-off frequency of 12.5 Hz. These are typical sampling rates and filter settings for field testing. The serial numbers for the hardware components of each channel are listed in Table A.2 below so that these tests can be repeated in future, if desired.

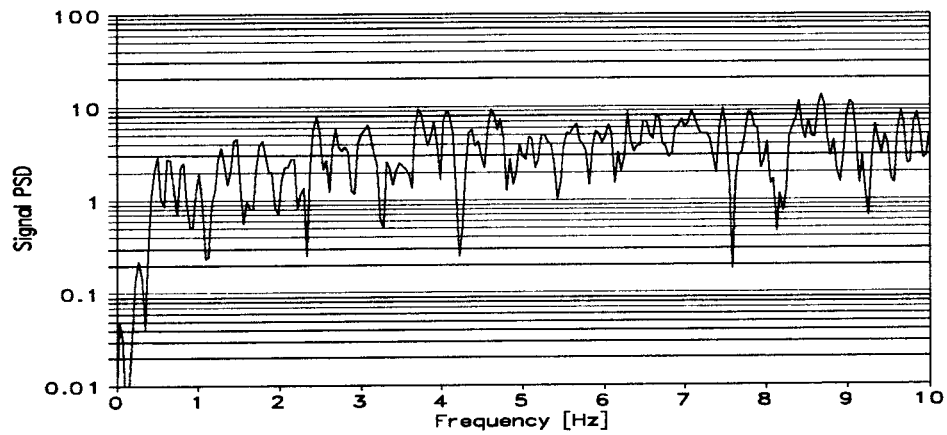

Fig. A.17: PSD of White Noise Excitation used for the Hardware Test

Table A.2: Configuration of Hardware Components for Hardware Test

Channel Number	FBA-11 Serial Number	AM-3I Serial Number	Cable Length
1	27468	0417	50m
2	27464	0418	50m
3	27465	0419	100m
4	27463	0420	100m
5	29467	0422	300m
6	29466	0423	300m
7	30201	0723	300m
8	30202	0724	300m

A.6.3 Hardware Test Data Analysis

The recorded time histories were used to compute the amplitude ratio and phase angle between each channel and channel number 1. For perfectly correlated sensors the amplitude ratio should be 1.00 and the phase angle should be 0.00. The error in relative amplitude and phase was computed for the frequency range 0.5 Hz to 10 Hz. The average of the absolute values of the relative amplitude ratio errors was computed as

$$e_{ABS_j} = \frac{1}{n} \sum_{k=1}^{k=n} | A_{1j}(f_k) - 1 | \tag{A-10}$$

where, e_{ABS_j} is the average absolute relative error of channel j, f_k is a discrete frequency, n is the number of discrete frequencies and A_{1j} is the amplitude ratio between channel 1 and j. In addition, absolute values of the mean relative amplitude errors were computed as

$$e_{MEAN_j} = \left| \left(\frac{1}{n} \sum_{k=1}^{k=n} A_{1j}(f_k) \right) - 1 \right| \tag{A-11}$$

where, e_{MEAN_j} is the mean relative error of channel j.

Both of these errors are shown in Fig. A.18 for sensors 2 to 8. The absolute relative errors for all sensors are less than 3.6 percent and the mean relative error is less than 2.8 percent. The largest errors are associated with channel number 4 and 7 and the least error is associated with channel number 3. The amplitude ratios for channels 3, 4 and 7 are shown in Fig. A.19. This figure indicates that the amplitude of channel 7 is approximately 3% smaller than channel 1 in the frequency range from 3 to 8 Hz. At frequencies larger than 8Hz this error increases. A similar trend applies to channel 4 at frequencies above 6Hz. Channel 3, on the other hand,

displays error values of less than 1 percent for the entire frequency range. The relative amplitude errors, which are less than 4 percent for all channels, were deemed acceptable for the purposes of the HBES.

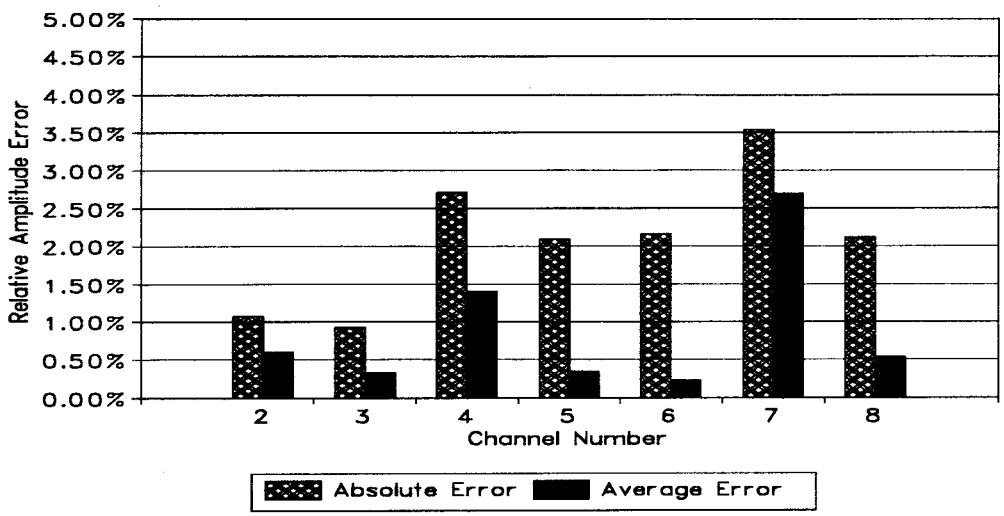

Fig. A.18: Absolute Amplitude Error and Mean Amplitude Error for All Channels of the HBES

The phase angles between each channel and channel 1 were computed from the test data. Then the frequency dependent phase shifts associated with the sampling hardware (as discussed in section A.5.2.2) was calculated. The average relative phase errors were then computed as

$$e_{\phi_j} = \frac{1}{n} \sum_{k=1}^{k=n} | \phi_{1j}(f_k) - \phi s_{1j}(f_k) | \tag{A-12}$$

where, e_{ϕ_j} is the relative phase error between channel 1 and j, $\phi_{1j}(f_k)$ is the computed phase angle between channel 1 and j and $\phi s_{1j}(f_k)$ is the phase shift between channel 1 and j due to sampling.

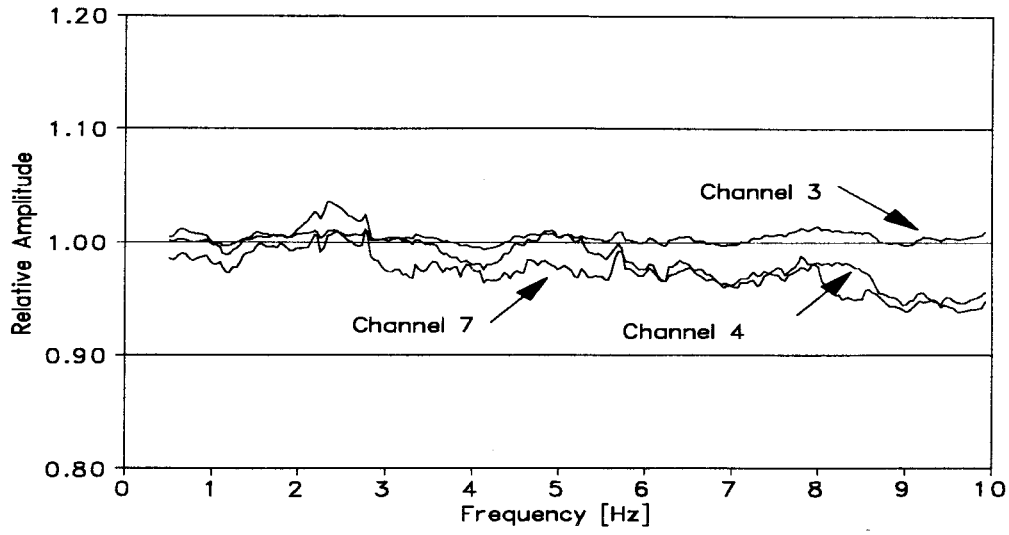

Fig. A.19: Relative Amplitude for Channels 3, 4 and 7 of the HBES

The relative phase errors, shown in Fig. A.20, for all channels except channel 4 is less than 1.3 degrees. Channel number 4 shows the largest error at 3.1 degrees. Relative phase angle errors below 5% were deemed acceptable for the HBES.

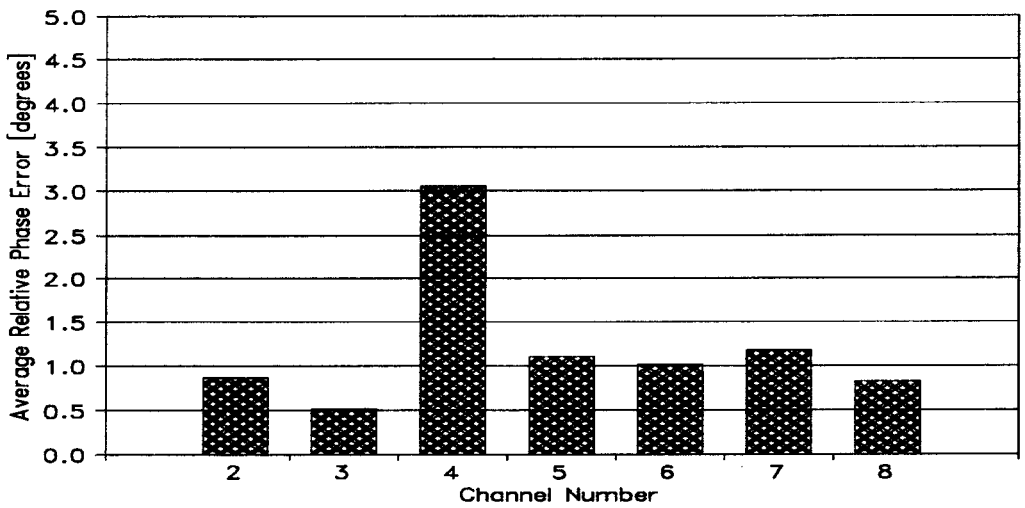

Fig. A.20: Average Relative Phase Errors for All Channels of the HBES

APPENDIX B: Program AVTEST User's Manual

B.1 Introduction to AVTEST

The purpose of the program AVTEST (Ambient Vibration TEST) is to provide an efficient tool to control the acquisition of ambient vibration data using the Keithley[2] 575 Measurement and Control System. The program was developed using Borland (1991) C++ and the Keithley driver library. The data acquired with AVTEST can be processed and analysed using the program ULTRA, which has been written as part of a series of computer programs used for collecting and processing ambient vibration data.

B.2 General

B.1 System Requirements for AVTEST

The TEST program will run on a variety of IBM compatible personal computers. The hardware requirements are:

Processors:	80286 & 80287
Memory:	640 kb
Monitors:	CGA
Hard Disk:	20 Mb
Keithley Products:	Interface Card and Software

2 Keithley Metrabyte / Asyst / DAC, Data Acquisition Division, 440 Myles Standish Blvd., Tauton, Ma 02780, July 1989.

B.2 AVTEST Program Installation

To install the program, the user only needs to copy the file AVTEST.EXE into the directory containing the Keithley hardware drivers. For more information on the installation of the Keithley drivers, refer to the Keithley 575 documentation.

B.3 AVTEST Program Execution

Prior to the execution of the data acquisition program AVTEST, the memory resident program K500.exe has to be loaded. This program is part of the Keithley 575 software and its function is to control the data acquisition hardware. For more information on executing K500.exe, refer to Keithley's KDAC500 Data Acquisition and Control Software Manual. The data acquisition program AVTEST is started from the Keithley directory by typing:

krun AVTEST <arg1> <arg2> ....

The input options are entered on the command line as <arg1> ... . The individual options are discussed in the following section.

B.3 Program Input Options

The various options for the data acquisition process are passed to the program AVTEST via the command line. The options have to be specified in the following sequence:

Nyquist frequency
Index to control the total number of points acquired per channel
Number of channels to be recorded
Global gain
Sensor calibration option

Filename
Site identifier
Setup description

The individual options are separated using spaces as delimiters. The first six options must be specified or the program will not start. The last two options default to the filename if they are not specified. Each of these options is described in more detail in the following sections.

B.3.1 Nyquist Frequency

The Nyquist, or folding frequency f_c, determines the maximum frequency which can be resolved from the data. Any frequency value between 0.1 and 100 Hz can be selected. The actual sampling frequency is set by the program at twice the Nyquist frequency. The corresponding sampling interval, Δt, is equal to $1/(2f_c)$.

B.3.2 Total Number of Points

This number is an index that controls the total number of samples N that will be collected per channel. The following selections are permitted:

Index	Number of points per channel
1	1024
2	2048
4	4096
8	8192
16	16384
32	32768
64	65536
128	131072

If the index is greater than 4, the data will be acquired in segments of 4096 points each. The amount of time required to obtain the data is $T = N/(2f_c)$. To estimate the duration of a test, approximately 10% of the measurement time has to be allowed for writing the data to disk. For example, the estimated time required to acquire 32768 points with a Nyquist frequency of 20 Hz is

$$\text{Duration of Test} = \frac{32768}{2*20} * 1.1 = 901.12 \text{ seconds} \cong 15 \text{ minutes}$$

B.3.3 Number of Channels

The number of channels which will be sampled has to specified. Since the current version of the program supports only 8 channels, this number has to be between 1 and 8.

B.3.4 Global Gain

The data acquisition hardware uses a 16 bit A/D converter with a range of ±10 Volts. The signals should be amplified to match the range of the A/D converter to reduce the signal to noise ratio due to the quantization error discussed in section A.4.1.1. The global gain is applied to all channels and can be set at 1, 2, 5, 10. These global gain settings correspond to the following effective conversion ranges for the A/D converter. The appropriate gain setting has to be determined by the user. For most ambient vibration tests, good results can be obtained with a global gain of 5, provided the signal conditioner gains are set to amplify the signals such that the peak signal levels do not exceed ±2 Volts.

Global Gain	Conversion Range [Volts]
1	±10
2	±5
5	±2
10	±1

B.3.5 Sensor Calibration Option

It is recommended that the performance of all the accelerometers are verified before and after a test by conducting sensor calibrations. To specify that calibrations should be performed enter "0" on the command line; otherwise enter "1" to skip the calibration.

The calibration routine will remind the operator to adjust the amplifier and filters for calibration (66db, filter OUT respectively). The calibration sequence consists of the following steps:

Step 1 Press any key to proceed with the calibration. The program will make a short "BEEP" sound.

Step 2 After the sound, the operator should turn the control key of the Kinemetrics signal conditioner from "Test" to "Calibrate".

Step 3 After roughly one second, the key should be turned to the "Natural Frequency" position and remain there until the calibration is completed. The the key is returned to the "Test" position.

Step 4 Once the data has been acquired, the individual calibration records (described in detail in section C.2.1.5) are displayed on screen.

Step 5 When all the records have been displayed, the operator is given the option to accept the calibration data or repeat the process.

B.3.6 Filename

A file name with a maximum length of six letters has to be entered on the command line to specify where the information will be stored. The data is stored in a binary format which is defined in section B.4. Two letters are added to the file name to identify the individual vibration and calibration records. This will be illustrated using the filename "Colqui" as an example. If '3' signals were recorded and a calibration was performed the program will create the following files:

Colqui01.bbb	1st signal vibration data
.	.
Colqui03.bbb	3rd signal vibration data
ColquiB1.bbb	1st signal before test calibration data
.	.
ColquiB3.bbb	3rd signal before test calibration data
ColquiA1.bbb	1st signal after test calibration data
.	.
ColquiA3.bbb	3rd signal after test calibration data

B.3.7 Site Identification

In addition to the filename, a more descriptive word can be entered to define the measurement site. However, this description has to be one continuous string of characters (e.g. "Colquitz_OverPass"). (Use Underscores or dashes instead of spaces.) If no site description is specified, the six letter filename will be used as a default.

B.3.8 Setup Description

For a more detailed description of the measurement setup, an additional word can be added. Again, this word has to be a continuous string of characters such as "Vertical_Setup_5". If no setup description is specified, the site description will be used as a default.

B.3.9 Insufficient Parameters Specified

If AVTEST is executed with insufficient parameters on the command line, the program will display a list of required parameters with the permissible values.

B.4 File Output Format

All the files are stored in binary format. The data is preceded by a header which identifies the file and transfers all the pertinent information. The units of the stored data are volts. The header contains the following information:

Identification string
Sampling interval
Number of sample points
Channel number
Global gain
Filename
Site
Setup
Year, day, month
Hour, minute, second

B.5 Typical Test Procedure

While each test is unique, the following steps may be followed to insure that good quality data will be obtained.

1 Install the sensors
2 Balance sensors
3 Connect cables between sensors and signal conditioner
4 Run the AVTEST program
5 Set gains and filters for calibration
6 Proceed with calibration
7 Set gains and filters for recording
8 Proceed with recording
9 Set gains and filter for calibration
10 Proceed with calibration
11 Inspect recorded time histories using ULTRA
12 Move sensors to new location.

For details on the balancing and calibration procedure, the reader should refer to the operating instructions for the sensors (Kinemetrics, 1991).

APPENDIX C: Program ULTRA User's Manual

C.1 Introduction to ULTRA

The program ULTRA (Universal Long Time Record Analysis) was developed to process and analyse one or two data records obtained from ambient vibrations tests. The program can be used to manipulate any type of time series. Conventions used in the program are chosen to facilitate the automatic and convenient processing of ambient vibration records.

C.1.1 Program Application

The program ULTRA forms a key component of the Hybrid Bridge Evaluation System. The program's main application is the reduction of ambient vibration data to determine structural mode shapes and frequencies of bridges. This information is then used by the program VISUAL to display and animate the mode shapes in three dimensions.

C.1.2 About This Manual

This manual is organized to resemble the structure of the program's menu. The author believes that when program reference manuals and user's manuals are provided separately, the most important information always seems to be lost somewhere between the two. Therefore, this manual will combine elements of a reference and a user's manual. The reader is encouraged to read this manual first in its entirety to become familiar with the program's scope and philosophy. Afterwards, this manual can be used as a reference.

C.1.3 System Requirements

ULTRA was developed to run on a variety of IBM compatible personal computers. The following hardware is supported:

Processors:	Intel 80286 & 80287, 80386 &80387, 80486
Monitors:	CGA, EGA, VGA
Printer:	HP Laserjet II or compatible;
Extended Memory:	2MB or more

C.1.4 Program Installation

The executable file ***ULTRA.EXE*** must be copied to a directory included on the path. (For information on the use of directories, the copy command and the path command the reader is referred to the DOS version 5 manual (Microsoft, 1991)).

C.1.5 Program Operation

The program can be operated either in interactive mode or in batch mode. The menu driven interactive mode is generally used for detailed analysis of one or two data records, while the batch mode can be used to sequentially reduce large amounts of data, two signals at a time.

C.1.5.1 ULTRA Menu Mode

The menu mode of the program allows the user to select a variety of data manipulation options via the graphic user interface and menu system. Menu selections are made either by selecting the first letter of the option or by highlighting the option with the cursor keys and then pressing Enter. The individual menu options are described in detail in the following sections. Fig. C.1 below shows the menu structure of the program. Pointing device (mouse) support is not provided.

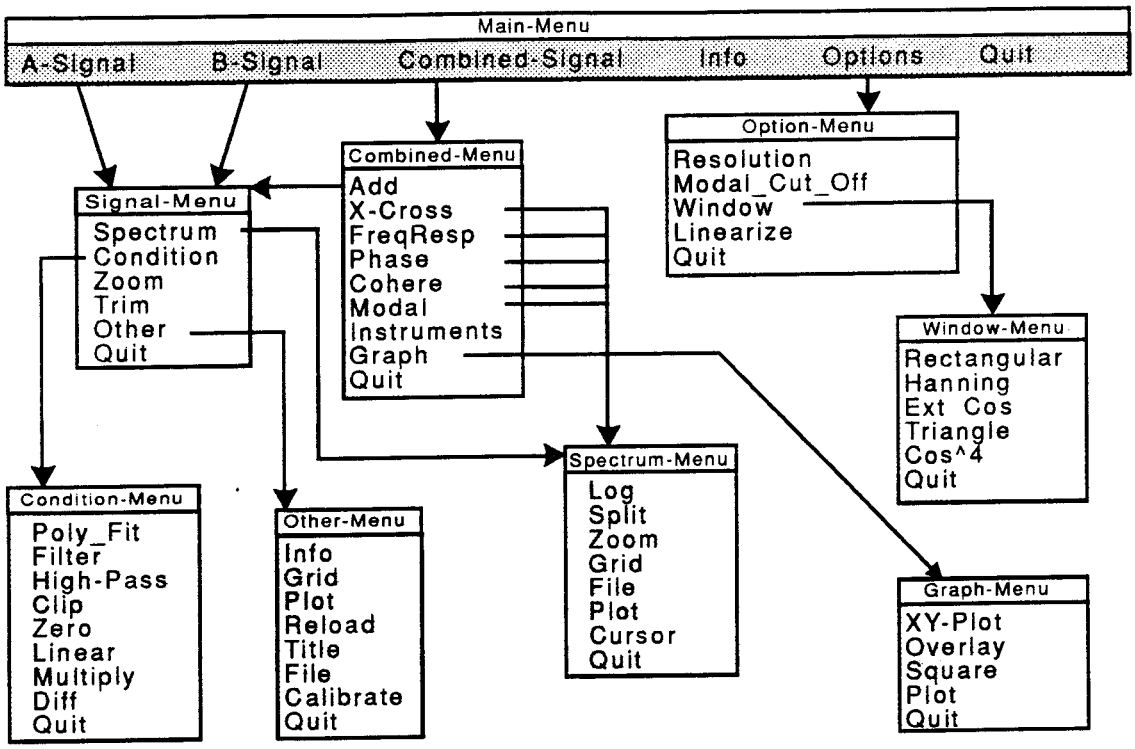

Fig. C.1: Menu Structure of Program ULTRA

C.1.5.2 ULTRA Batch Mode

ULTRA can also be run in batch mode. This mode is preferably used when large quantities of data need to be reduced. For the batch mode option, the commands and file names are entered on the command line as in the following example:

ultra *fileA fileB aczqspqqbczqspqqqt* (list of commands)

The program name is followed by the name of the file for the A_Signal and for the B_Signal. Then a string of letters corresponding to the first letter of the menu options selected for

processing the data is entered. The command string, shown in the above example, removes a constant trend from the A_Signal (commands aczq), computes its spectrum (command s) and then produces a hard copy (command pq) of the spectrum. The same operations are performed with the B_Signal and the program is then terminated. The character sequence corresponds to the following menu options:

Letter	**Command**	**Menu**
a	A-Signal	Main-Menu
c	Condition	Signal-Menu
z	Zero	Condition-Menu
q	Quit	Condition-Menu
s	Spectrum	Signal-Menu
p	Print	Spectrum-Menu
q	Quit	Spectrum-Menu
q	Quit	Signal-Menu
b	B-Signal	Main-Menu
c	Condition	Signal-Menu
z	Zero	Condition-Menu
q	Quit	Condition-Menu
s	Spectrum	Signal-Menu
p	Print	Spectrum-Menu
q	Quit	Spectrum-Menu
q	Quit	Signal-Menu
q	Quit	Main-Menu
t	Terminate	Quit-Menu

If only one single signal needs to be manipulated in batch mode the field for the second file name must contain a '0' (zero). For the above example, if only the spectrum for a single file is to be plotted the command line would read:

ultra *fileA 0 aczqspqqqt*

The batch mode can be used to perform most of the operations available in the interactive mode. Options which are not available in the batch mode will be identified in the following sections. Any command string not leading to the termination of the program will cause the program to switch to interactive mode.

C.2 ULTRA Menu Structure and Options

The main menu of the program provides the following options:

Menu Item	Action
A_Signal	Process the first signal
B_Signal	Process the second signal
Combined_Signals	Work with both signals
Info	Display information on program version and settings
Options	Change program options
Response	Compute response of a SDOF system to A-signal

The first two options prompt the user to enter a filename from which to load the signal, and then invoke the Signal-Menu. The Signal-Menu and the other options are explained in detail in the following sections.

C.2.1 Signal-Menu

Since ambient vibration records are generally very long (typically 32768 measured values), not all the data points are displayed on screen. Instead, three lines are displayed giving the local upper bound, local mean and local lower bound of the signal. Such plots are useful in the detection of signal drift, spikes and other anomalies. Higher resolution can be obtained using the ZOOM and TRIM options, which will be explained below.

The signals values which are read in and displayed by the program are assumed to be without units and are displayed as such. Therefore, all the frequency domain functions, except for the phase function, are also displayed without units.

C.2.1.1 Spectrum

The one-sided auto spectral density function $G_{xx}(f)$ for the entire record is calculated as an average of the auto spectra of segments of the data. The number of averages k used for the computation depends on the specified resolution (see section C.2.4.1). After the auto spectral density has been calculated it will be displayed and the Spectrum-Menu will be invoked. The calculation is based on the following formula, which makes use of the Fast Fourier Transform (FFT) algorithm (Cooley and Turkey, 1965):

$$G_{xx}(f) = \frac{2}{k*N\Delta t} \sum_{j=0}^{j=k-1} [X_j^*(f) X_j(f)] \tag{C-1}$$

where $X_j(f)$ is the discrete fourier transform of a segment of length N of the signal determined as

$$X_j(f) = FFT\{x_{(trimstart + j*N)} \ldots x_{(trimstart + (j+1)*N)}\} \tag{C-2}$$

$X_j^*(f)$ is its complex conjugate and *trimstart* defines the beginning of the portion and of the signal to be manipulated. Once this option is selected, the Spectrum-Menu is displayed to allow the user to manipulate the spectrum (see section C.2.1.6).

C.2.1.2 Condition-Menu

The options available under this menu are used to manipulate the signal in the time domain. For each of these options the manipulated signal replaces the original signal.

Poly-Fit

Occasionally it is desirable to remove a polynomial trend from the data. The Poly-Fit option computes a 4th order polynomial trend and then displays the estimated 4th order polynomial trend. Then the user is provided with the following 3 options:

Apply

Remove the 4th order polynomial trend from the signal and return to the Condition-Menu.

Info

Display the coefficients of the 4th order fit.

Quit

Return to the Condition-Menu without removing the trend.

Filter (Low-Pass)

Occasionally records that are processed contain significant signal strength outside the frequency range of interest. Examples of this may be amplifier and temperature drift or electrical signals from lighting transformers. These can show up as quite large peaks on the spectral plots. To improve the appearance of spectra, digital filtering can be employed to remove the unwanted frequency components. In addition, the appearance of time domain plots can also be improved by filtering. Low-pass filtering will make the signal appear smoother while high-pass filtering will remove most of the drifting. An example of low-pass filtering is shown in Fig. C.2 and Fig. C.3. For this analysis only, frequencies below 6Hz were of interest; thus both the time domain and frequency domain information were greatly enhanced by low pass filtering.

Both low-pass and high-pass filters can be applied to the signals. The filtering is achieved through convolution with a centered filter function. The length of the filter function is set at n=81. This length provides an acceptable roll-off and is computationally efficient. The filter response of both low-pass and high-pass digital filters is illustrated in Fig. C.4. This figure was generated from a 4096 point record with a low-pass cut-off frequency of 20 Hz and a high-pass cut-off frequency of 5 Hz.

The Filter option provides several choices for low-pass filter cut-off frequencies based on the Nyquist frequency of the data. These options are tabulated below:

Nyquist Frequency [Hz]	Option 1 [Hz]	Option 2 [Hz]	Option 3 [Hz]	Option 4 [Hz]	Option 5 [Hz]	Option 6 [Hz]
f_c	$0.8f_c$	$0.5f_c$	$0.3f_c$	$0.1f_c$	$0.05f_c$	$0.01f_c$

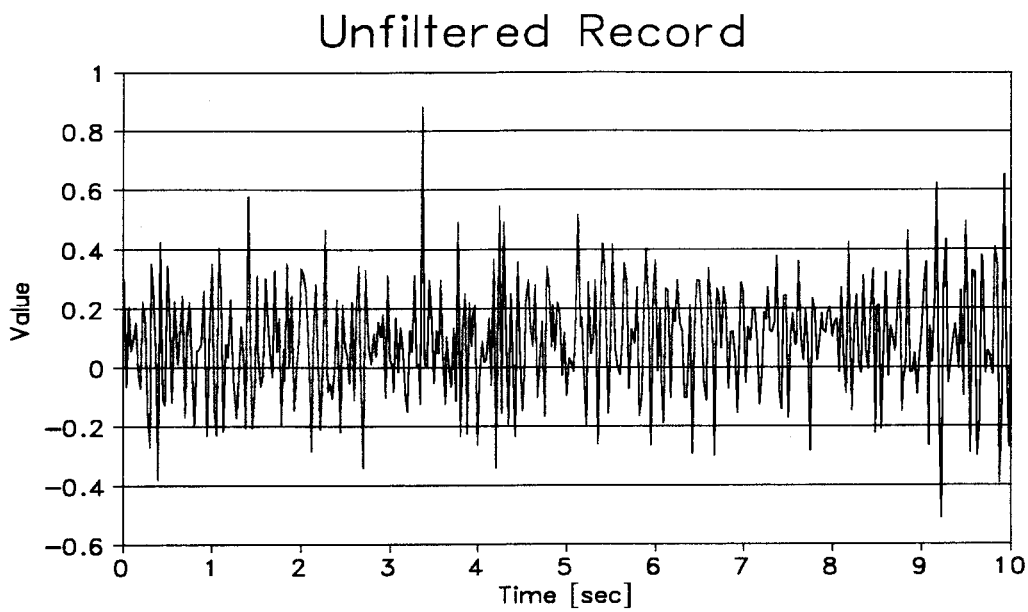

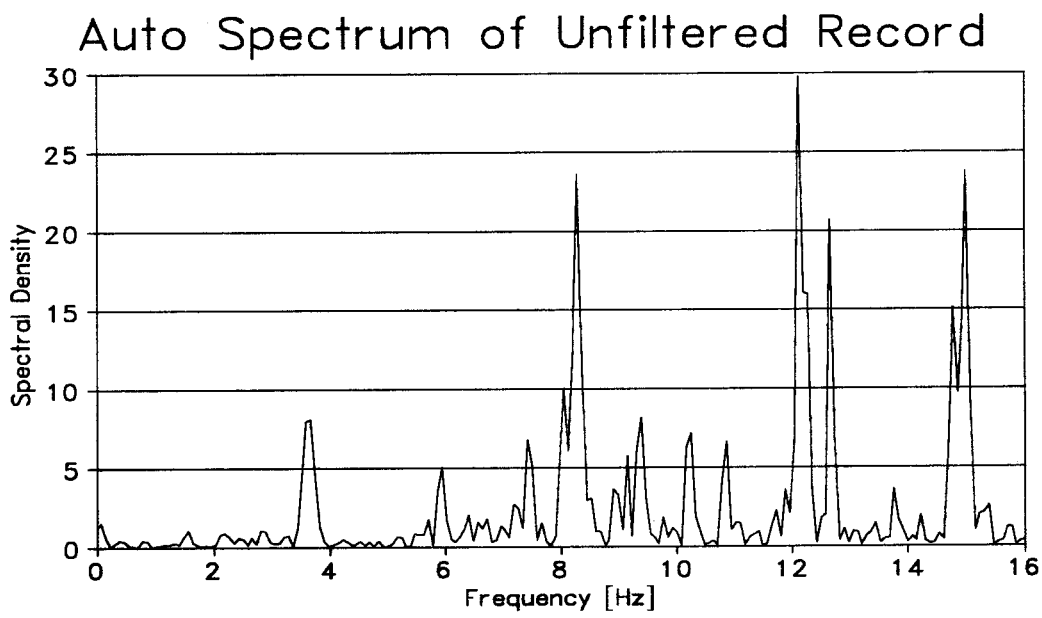

Fig. C.2: Low-Pass Filtering Example: Unfiltered Record and Spectrum

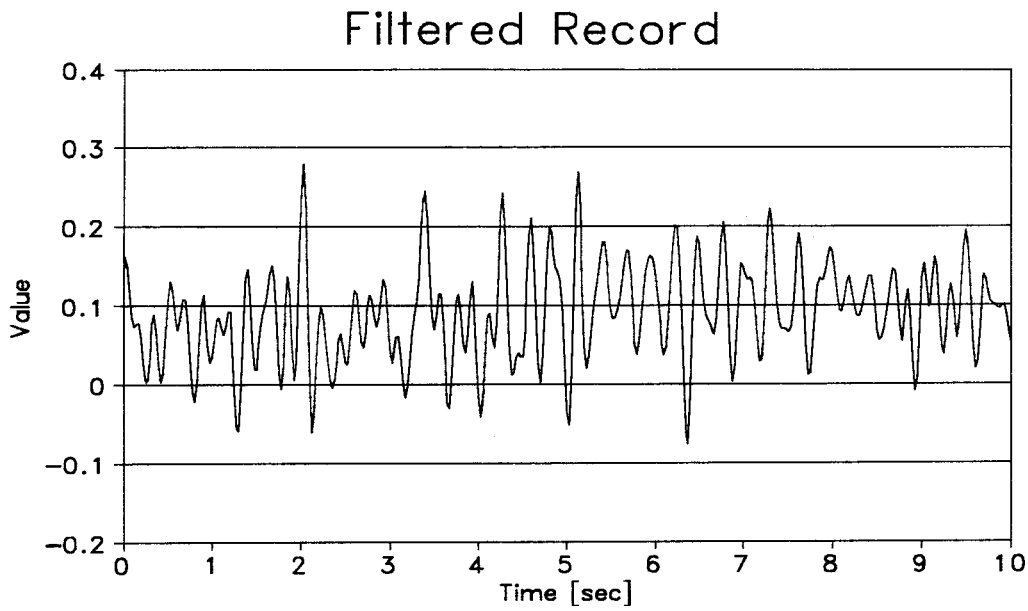

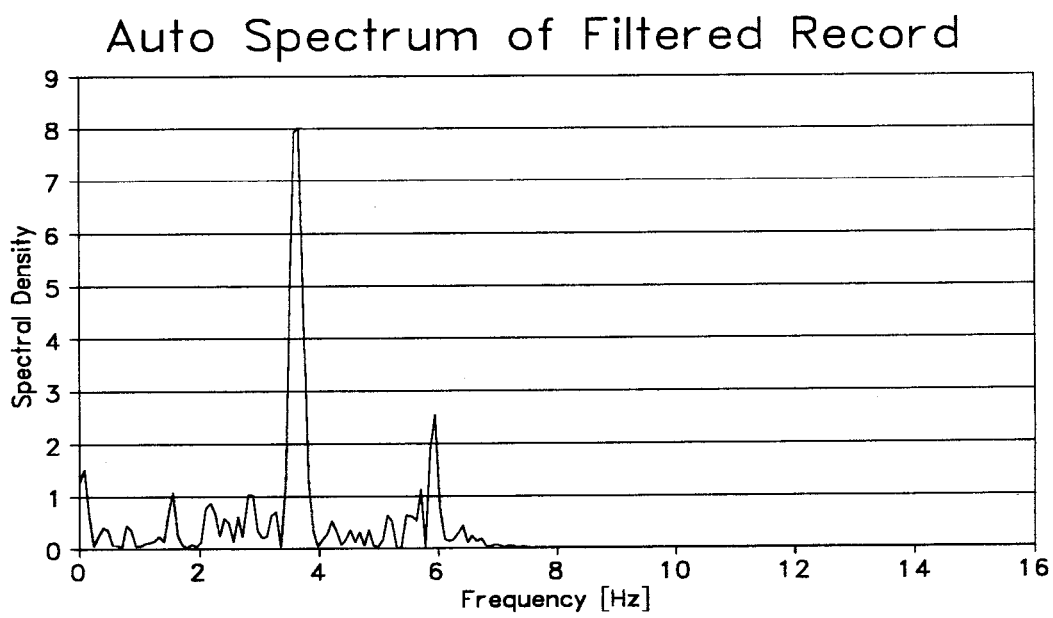

Fig. C.3: Low-Pass Filtering Example: Filtered Record and Spectrum

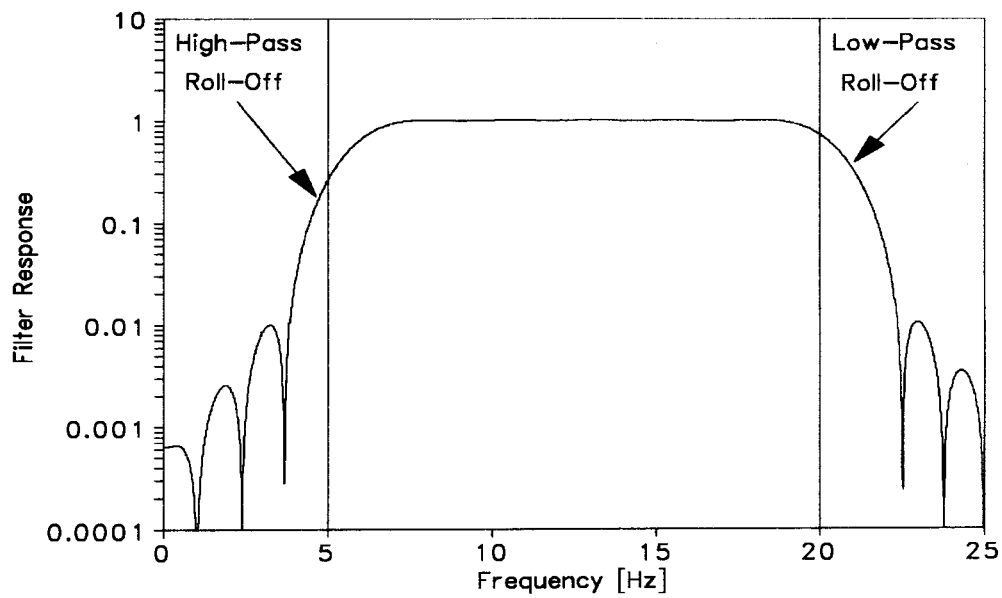

Fig. C.4: High-Pass and Low-Pass Response of ULTRA's Digital Filters

High-Pass (Filter)

The High-Pass option provides the high-pass cut-off frequencies at the same fractions of the Nyquist frequency as presented in the table above.

Zero

Instrument alignment and/or electronic balancing may not be perfect and hence a signal may be offset from zero. This option is used to remove any constant offset from the data record using the following formula:

$$y_j = x_j - \mu, \qquad \mu = \frac{1}{n}\sum_{i=1}^{n} x_i \tag{C-3}$$

An offset record before and after the Zero option has been used is shown in Fig. C.5.

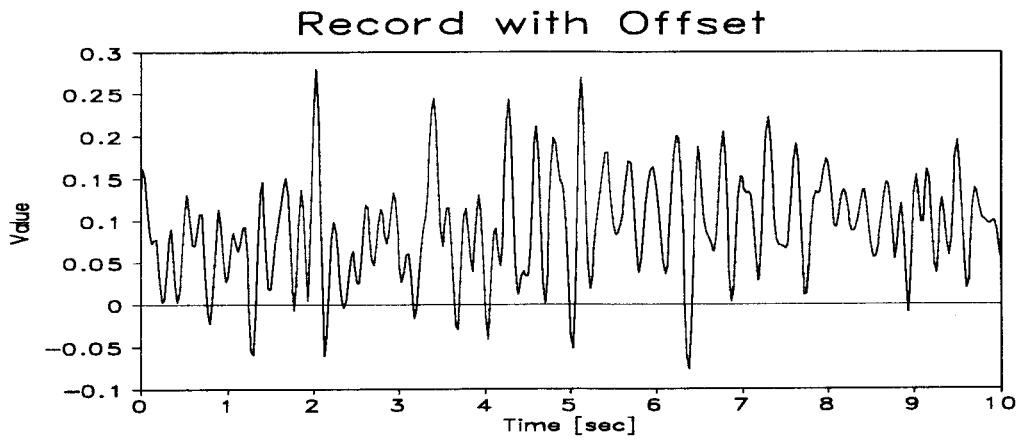

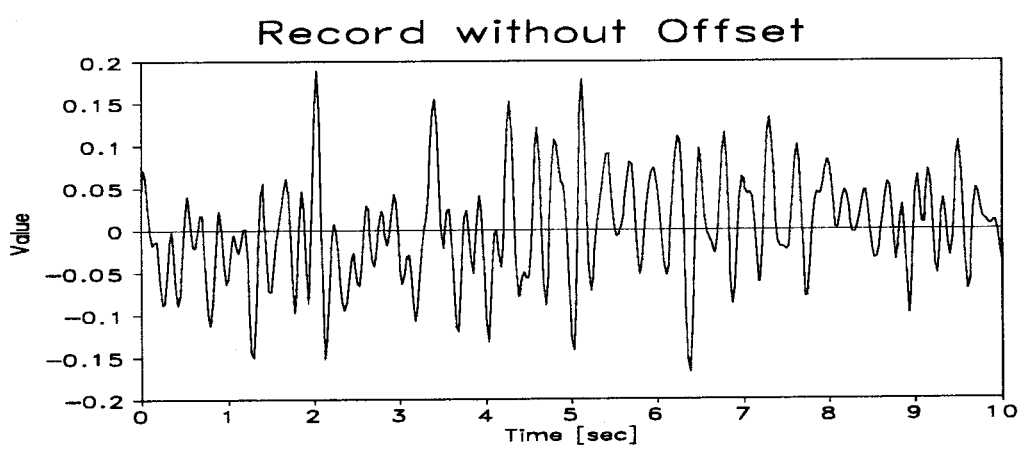

Fig. C.5: Example of Record with and without Offset

Linear

Temperature changes and amplifier drift can cause strong linear trends to be present in the signal. This options removes a linear trend from the data record using the following formula:

$$y_j = x_j - b_0 - b_1 * j, \quad b_1 = \frac{\sum t x_t - \bar{t} \sum x_t}{\sum t^2 - n(\bar{t})^2}, \quad b_0 = \mu - b_1 \bar{t}, \quad \mu = \frac{1}{n} \sum x \tag{C-4}$$

A record with a linear trend before and after the Linear option has been used is shown in Fig. C.6.

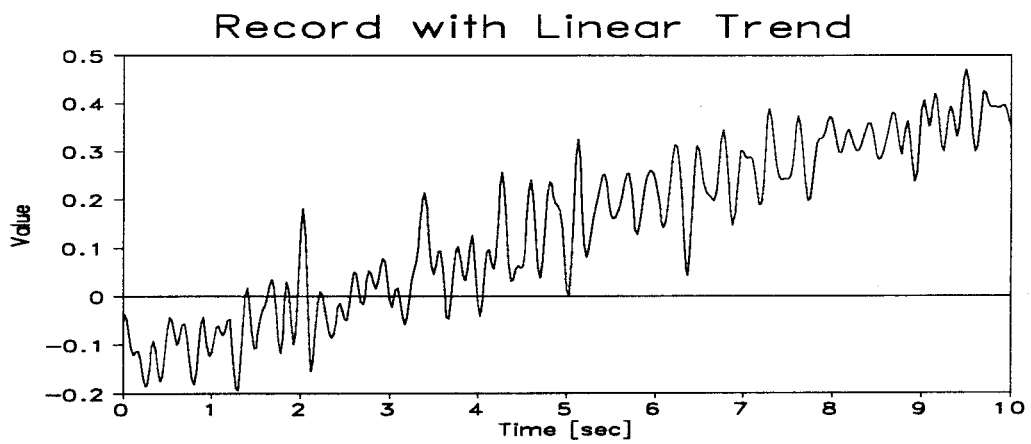

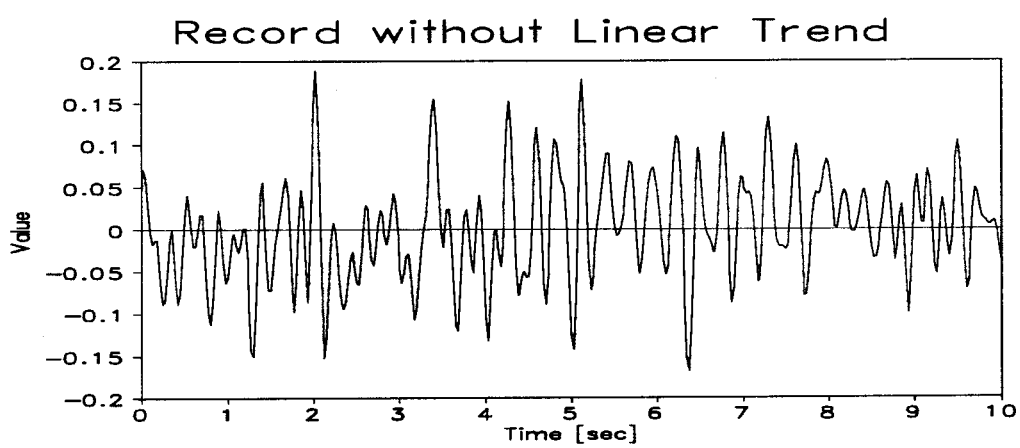

Fig. C.6: Example of Record with and without Linear Trend

Multiply

This option is used to multiply the signal by a constant.

$$y_j = x_j * \text{ constant} \tag{C-5}$$

If a multiplication was performed, it will be indicated on the hard copy output.

Clip

This feature is used to remove large spikes from a time signal. The user is prompted for a cut-off value and then the record is clipped using the following conventions:

$$y_t^* = \begin{cases} c & y_t > c \\ y_t & -c \le y_t \le c \\ -c & y_t < -c \end{cases} \tag{C-6}$$

$y_t =$ original data, $y_t^* =$ clipped data, $c =$ cut-off value (positive)

If clipping was performed, it will be indicated on the hard copy output.

Diff

This function numerically differentiates a signal using:

$$\hat{y}'_t = \frac{(y_{t+1} - y_{t-1})}{2\Delta t} \tag{C-7}$$

The beginning and end of the series are approximated using:

$$\hat{y}'_0 = \frac{(y_{t+1} - y_t)}{\Delta t} \qquad \hat{y}'_n = \frac{(y_n - y_{n-1})}{\Delta t} \tag{C-8}$$

If a differentiation was performed, it will be indicated on the hard copy output.

Int

This option is used to integrate the signal. The signal is integrated using a local cubic fit. Thus the area between y_t and y_{t+1} is approximated by:

$$Area = \frac{\Delta t}{24}(-y_{t-1} + 13y_t + 13y_{t+1} - y_{t+2}) \tag{C-9}$$

If a integration was performed, it will be noted on the hard copy output.

C.2.1.3 Zoom - Display

The Zoom option on the menu is used to zoom in or out on the displayed time series. Once the Zoom option has been selected additional key strokes will cause the following actions:

Key	Action
↓	Zoom in about the center of the display
↑	Zoom out about the center of the display
←	Move to the left by 1/4 of current display range
→	Move to the right by 1/4 of current display range
Enter	Select the current display range
ESC	Return to the previous display range

C.2.1.4 Trim - Manipulation

Occasionally it is desirable to process only a portion of a large data record. The TRIM option is used to graphically define a portion of the entire data record. Only the trimmed portion of the record will then be manipulated. First, the user selects an arbitrary starting point defining the beginning of the trimmed portion. Then the program allows the user to choose from a series of possible end points for the data portion. The possible end points are set by the program

such that the total number of points in the portion is equal to 2^n (i.e. 256, 512, 1024, ..etc). The restriction on data segment sizes is imposed in order to take advantage of computational savings in the Fast Fourier Transformation routine. (Bendat and Piersol (1986), Bracewell (1986)). Once the TRIM option has been selected, additional key strokes will cause the following actions:

Key	Action
↓	Reduce the step size for the first cursor
↑	Increase the step size for the cursor
←	Move the cursor to the left
→	Move the cursor to the right
Enter	Select the location of the first cursor Select the range between both cursors for future manipulations
ESC	Use the full record for future manipulations

The display range selected with ZOOM is automatically restricted to the trimmed portion of the signal.

C.2.1.5 Other-Menu

Info

This option is used to obtain information on the current signal. Once the option is selected, the

screen will display the following information:

Signal Loaded From File	*filename*	
Maximum Signal Value	*max*	
Minimum Signal Value	*min*	
Original Signal Multiplied By	*factor*	
Total Number of Samples	*n*	
Sample Interval	*dt*	*seconds*
Trim Start Time	*trimstart*	*seconds*
Trim End Time	*trimend*	*seconds*
Signal Fitted	*Yes/No*	
Signal Clipped	*Yes/No*	
Signal Differentiated	*0*	*times*
Free Memory	*memory*	*bytes*

Grid

This option is used to select grid lines for the display. The default is a display without grid lines. In order to add grid lines to the current display, select "Grid" repeatedly until the desired grid configuration is shown. The Grid command toggles through the following four options:

- No Grid (Default)
- Vertical Grid
- Horizontal Grid
- Both Grids

Plot

This option is provided to generate a hard copy of the current screen display. Selecting this option will send the screen image and the appropriate header to the printer, which should be connected to LPT1. The only printer supported is the HP Laserjet II or its equivalent.

Reload

This option allows the user to load another signal to replace the one currently selected. Select the option and specify the name of the file you want to retrieve. The information associated with the new file will then be loaded.

Title

This option is used to change the label used to describe the data on screen displays.

File

This option is used to store the current signal, which might have been trimmed, filtered, etc. on a file. The data is stored in a file using the "*.tim" format. For more information on this format see section C.3.1.

Calibrate

This option can be used to estimate the damping and natural frequency of Kinemetrics FBA-11 instruments using calibration records. The method used to obtain calibration records is described in section B.5. A typical calibration record is shown in Fig. C.7. Since the HBES system uses only FBA-11 accelerometers, calibrations for other instruments are not supported.

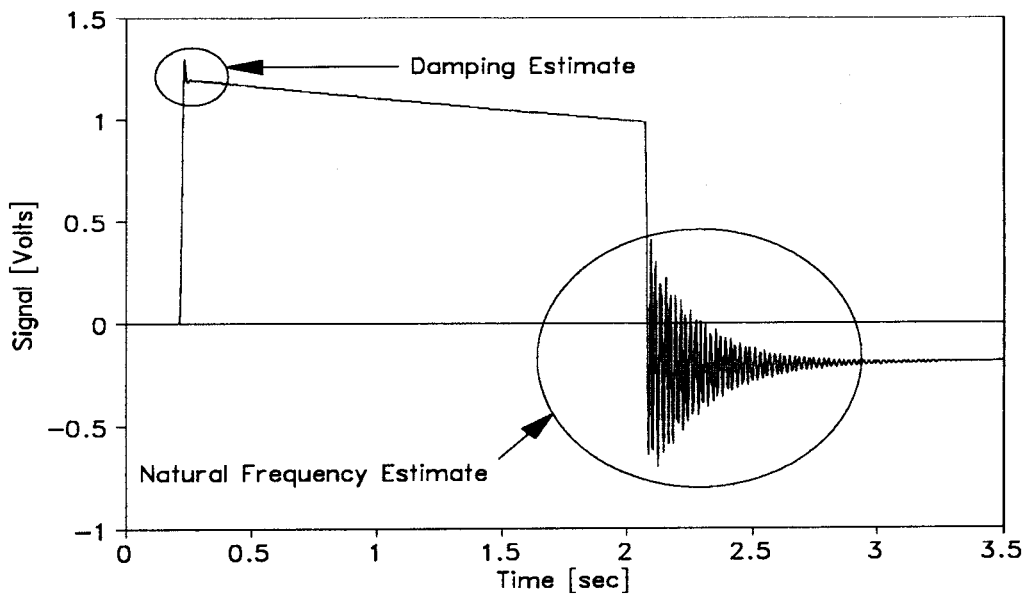

Fig. C.7: Typical FBA-11 Calibration Record Analysed by ULTRA

Sensor Damping Estimation

The damping value is estimated using the beginning of the calibration record which gives the response of the instrument to an excitation in the form of a Heaviside function. The acceleration response of a single degree of freedom system to a Heaviside base acceleration impulse of magnitude 'A' is given by

$$\ddot{x}(t) = A\left(1 - e^{-\xi\omega t}\left(\frac{\xi}{\sqrt{1-\xi^2}}\sin(\omega_D t) + \cos(\omega_D t)\right)\right) \tag{C-10}$$

Differentiating this expression once leads to:

$$\dddot{x}(t) = A\,e^{\xi\omega t}\left(\frac{\xi^2 w + 1}{\omega_D}\sin(\omega_D t)\right) \tag{C-11}$$

To find the maxima and minima of Eqn. C-10, Eqn. C-11 is set to zero:

$$\sin(\omega_D t) = 0 = \sin(n\pi) \qquad t = n\frac{\pi}{\omega_D} \tag{C-12}$$

Substituting this result into the first equation of this subsection yields:

$$\ddot{x}_{\left(n\frac{\pi}{\omega_D}\right)} = A - A*e^{\frac{-\xi\omega n\pi}{\omega_D}}\cos(n\pi) \tag{C-13}$$

This result can be used to derive the damping estimate based on the half cycle logarithmic decrement:

$$\begin{aligned}\frac{\ddot{x}(n\pi/\omega_D)}{\ddot{x}((n+1)\pi/\omega_D)} &= \frac{A(1-e^{-\xi\omega n\pi/\omega_D}\cos(n\pi))}{A(1-e^{-\xi\omega(n+1)\pi/\omega_D}\cos((n+1)\pi))} \\ &= \frac{-e^{-\xi\omega n\pi/\omega_D}}{e^{-\xi\omega n\pi/\omega_D}*e^{-\xi\omega\pi/\omega_D}} \\ &= -e^{\frac{\xi\pi}{\sqrt{1-\xi^2}}}\end{aligned} \tag{C-14}$$

By taking the natural logarithm of both sides, Eqn. C-14 can be solved for the damping value of the transducer.

$$\begin{aligned}&\ln\left|\frac{\ddot{x}_t}{\ddot{x}_{t+\pi/\omega_D}}\right| = \frac{\xi\pi}{\sqrt{1-\xi^2}} \quad \Rightarrow \quad \left(\frac{\ln\left|\frac{\ddot{x}_t}{\ddot{x}_{t+\pi/\omega_D}}\right|}{\pi}\right)^2 = \xi^2*\left(1+\left(\frac{\ln\left|\frac{\ddot{x}_t}{\ddot{x}_{t+\pi/\omega_D}}\right|}{\pi}\right)^2\right) \\ &\xi = \frac{\ln\left|\frac{\ddot{x}_t}{\ddot{x}_{t+\pi/\omega_D}}\right|}{\sqrt{\pi^2+\left(\ln\left|\frac{\ddot{x}_t}{\ddot{x}_{t+\pi/\omega_D}}\right|\right)^2}} \quad \text{or} \quad \xi = \sin\left(\tan^{-1}\left(\frac{\ln\left|\frac{\ddot{x}_t}{\ddot{x}_{t+\pi/\omega_D}}\right|}{\pi}\right)\right)\end{aligned} \tag{C-15}$$

The estimate of damping is based on the overshoot of the signal. The first maximum and the first minimum of the response to a rectangular impulse are used to estimate the damping. The first minimum 'min' occurs at the beginning of the response and the first maximum 'max' occurs after half a cycle (π/ω_D). The estimated damping $\hat{\xi}$ is based on

$$\hat{\xi} = \sin\left(\tan^{-1}\left(\frac{\ln\left|\frac{\ddot{x}_o}{\ddot{x}_{\pi/\omega_D}}\right|}{\pi}\right)\right) = \sin\left(\tan^{-1}\left(\frac{\ln\left|\frac{\min}{\max}\right|}{\pi}\right)\right) \tag{C-16}$$

While this method is conceptually quite simple, its implementation has some problems. Particularly, the values of 'min' and 'max' have to be estimated from the digitized record. However, the overshoot occurs in a very short time period. Thus to capture the maximum overshoot value, a large number of points has to be taken during this short time period. The hardware currently used for the calibration measurements is limited in acquisition speed, thus the values of 'min' and 'max' are approximated as follows:

1 Find the maximum digitized value, $\max_1$

2 Find the next maximum, $\max_2$

3 Estimate 'min'$=-\max_2$

4 Estimate 'max'$=\max_1-\max_2$

Typical estimates of $\max_1$ and $\max_2$ are shown in Fig. C.8.

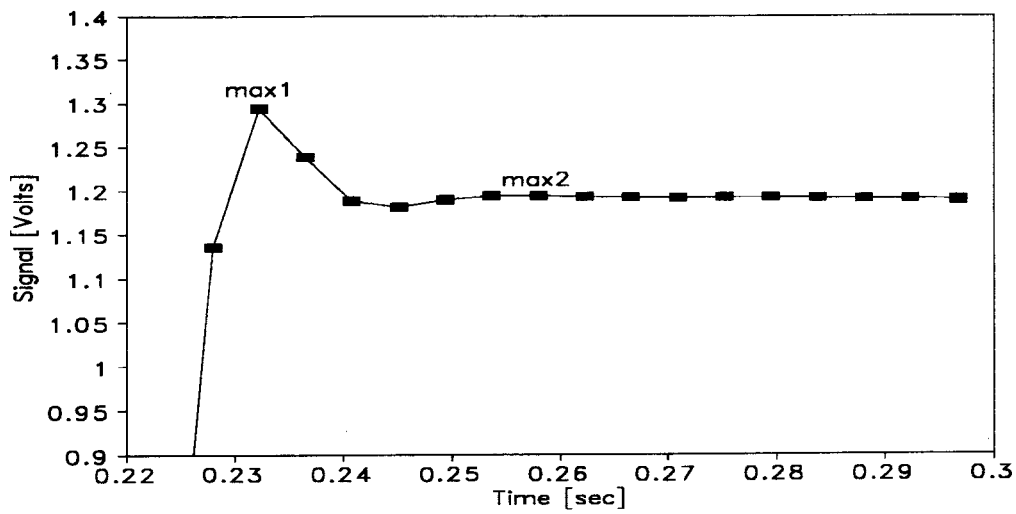

Fig. C.8: Typical Estimates used to Determine the Damping of a FBA-11

Sensor Natural Frequency Estimation

The natural frequency is estimated from the free vibration portion of the calibration record. This portion is shown in Fig. C.9 The program performs the following operations to estimate the natural frequency $\hat{\omega}_n$ of the FBA-11 instrument:

1. Isolate the free vibration segment.
2. Remove the linear trend from the segment.
3. Apply a high-pass filter to the segment.
4. Compute the spectrum of the segment.
5. Find the highest spectral value.
6. Record the associated frequency.

Regardless of the global option settings for Resolution and Window, the Auto Spectral Density is calculated using the maximum possible resolution and a Hanning window. (For the definition of Hanning Window, see section C.2.4.4)

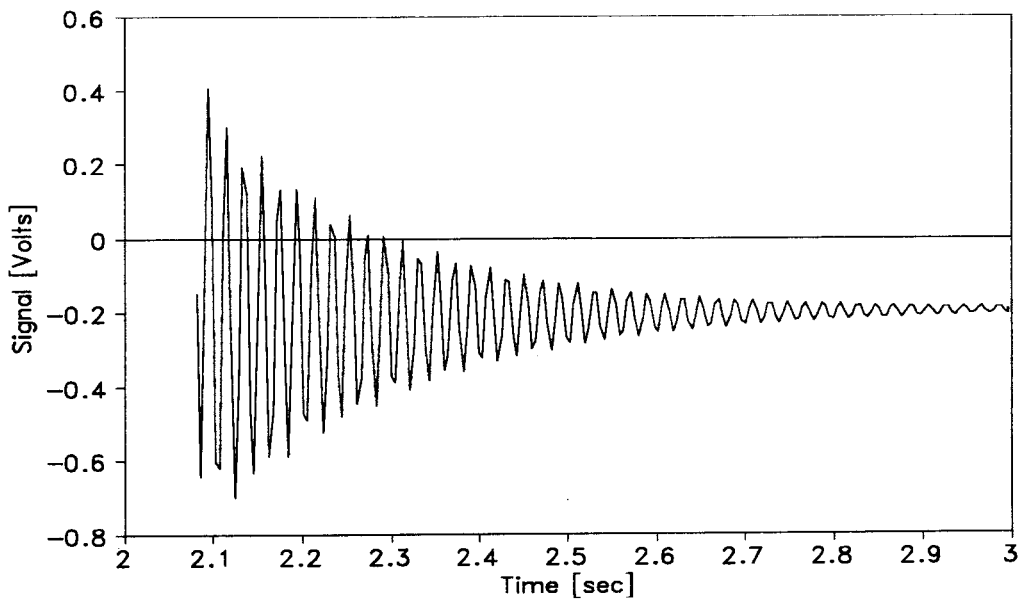

Fig. C.9: Segment of Typical Calibration Record Used to Determine the Natural Frequency of a FBA-11

C.2.1.6 Spectrum-Menu

The Spectrum-Menu is used to display, save and plot any computed spectra or frequency domain function.

Log

This option is used to select logarithmic scales for the display. The default is normal scales. To change the scales select "Log" repeatedly until the desired scaling is displayed. The Log command toggles through the following four options:

- o normal scaling of both magnitude and frequency
- o logarithmic scaling of magnitude, normal scaling of frequency
- o normal scaling of magnitude, logarithmic scaling of frequency
- o logarithmic scaling of both magnitude and frequency

Split

This option is used to quickly zoom in on the left hand side of the display. This option is particularly useful to improve the display of low frequency data quickly without using the Zoom option.

Zoom

This option is used in the same manner as the one described in section C.2.1.3.

Grid

This option is used in the same manner as the one described in section C.2.1.5.

File

This option is used to store spectral values on a file. For more information on the format used in the output file refer to section C.3.2.2.

Plot

This option performs the same function as the option in section C.2.1.5.

Cursor

The cursor option is used to identify individual points of a frequency domain function. To show a the cursor line, select the option and then use the cursor keys to direct the cursor as outlined below:

Key	Action
↓	Reduce the step size for the cursor
↑	Increase the step size for the cursor
←	Move the cursor to the left
→	Move the cursor to the right
ESC	Return to previous menu

The top two lines of the display show the magnitude and frequency of the current cursor position. In addition, the resolution of the discrete frequency function and the current step size of the cursor are displayed.

C.2.2 Combined-Menu

The Combined Menu item is used to obtain information based on both signals. This menu item can only be activated if the following three conditions are met:

Two signals have been loaded

Both signals have the same sampling rate

Both signals are trimmed to equal length.

All options available from this menu, which involve spectral calculations, are based on averages as outlined in section C.2.1.1.

C.2.2.1 Add

The "Add" option is used to create a new signal by adding the A_Signal and the B_Signal. The new signal $C(t)$ is defined by

$$C_{(t)} = A_{(trimstart\_A+t)} + B_{(trimstart\_B+t)} \tag{C-17}$$

This feature is particularly useful for the separation of torsional and translational modes. Once a new signal has been created, the Signal-Menu will automatically be displayed so that the new signal can be manipulated further. When the Signal-Menu is terminated, the C_Signal is no longer stored in memory. Thus, to preserve the C_Signal, it has to be saved to a file using the File option (see section C.2.1.5).

C.2.2.2 X_Cross - Cross Spectral Density

The average cross spectral density $G_{xy}(f)$ is obtained using

$$G_{xy}(f) = \frac{2}{k*N\Delta t} \sum_{j=0}^{j=k-1} [X_j^*(f)Y_j(f)] = C_{xy}(f) - iQ_{xy}(f) \tag{C-18}$$

where C_{xy} and Q_{xy} are the real and imaginary components of the one sided cross spectral density function, respectively. The fourier transforms of the signals $X_j(f), Y_j(f)$ are computed for k segments of the data.

$$X_j(f) = FFT\{A\_Signal_{(trimstart+j*N)} \ldots A\_Signal_{(trimstart+(j+1)*N)}\} \tag{C-19}$$
$$Y_j(f) = FFT\{B\_Signal_{(trimstart+j*N)} \ldots B\_Signal_{(trimstart+(j+1)*N)}\}$$

C.2.2.3 FreqResp - Frequency Response Function

The frequency response function $H_{xy}(f)$ is calculated assuming that Signal_A is the input and Signal_B is the output. The modulus of the frequency response function $|H_{xy}(f)|$ is calculated using

$$|H_{xy}(f)| = \frac{(C_{xy}^2(f) + Q_{xy}^2(f))^{1/2}}{G_{xx}(f)} \tag{C-20}$$

C.2.2.4 Phase - Phase Relationship

The phase of the frequency response function ,$\phi_{xy}(f)$, is obtained using

$$\phi_{xy}(f) = \tan^{-1}\left(\frac{Q_{xy}(f)}{C_{xy}(f)}\right) \tag{C-21}$$

The phase angle displayed in degrees is ranging between $0° \leq \phi_{xy} \leq 180°$.

C.2.2.5 Cohere - Coherence Function

The ordinary coherence function, $\gamma_{xy}^2(f)$, between the two signals is computed using:

$$\gamma_{xy}^2(f) = \frac{(C_{xy}^2(f) + Q_{xy}^2(f))}{G_{xx}(f) * G_{yy}(f)} \tag{C-22}$$

The coherence γ^2 is displayed in scalar values ranging from 0 to 1.

C.2.2.6 Modal - Modal Function

The modal function is obtained by filtering the frequency response function with two windows. These two filter windows are the phase-window and the coherence-window. The modal function (M(f)) is calculated using the following formula

$$M(f) = |H(f)| * PW(f) * CW(f) \tag{C-23}$$

where $PW(f)$ is the Phase-Window Function and $CW(f)$ is the Coherence-Window Function.

The value of the phase-window function is given by

$$PW(f) = \begin{Bmatrix} 1 & \text{for} & 0 \le \phi(f) \le \phi_c \\ 0 & \text{for} & \phi_c < \phi(f) < 180 - \phi_c \\ -1 & \text{for} & 180 - \phi_c \le \phi(f) \le 180 \end{Bmatrix} \tag{C-24}$$

where $\phi(f)$ is the Phase Function (degrees) and ϕ_c is the Modal-Cut-Off Angle (degrees). The value of the coherence-window function is given by

$$CW(f) = \begin{Bmatrix} 1 & \text{for} & \gamma_c^2 \le \gamma^2(f) \le 1 \\ 0 & \text{for} & 0 < \gamma^2(f) < \gamma_c^2 \end{Bmatrix} \tag{C-25}$$

where $\gamma^2(f)$ is the Coherence Function value and γ_c^2 is the Coherence-Cut-Off. Both the Modal-Cut-Off angle and the Coherence-Cut-Off are specified using the Option-Menu (see section C.2.3).

C.2.2.7 Instruments

This option is used to quickly analyse two calibration records, as described in section C.2.1.5. Once the option is selected, both signals will be analysed and then the damping and natural frequency for each channel will be displayed.

C.2.2.8 Graph

This option is used to select various displays for the two signals in the time domain.

XY-Plot

This selection will produce a XY-Plot of signal A on the X-axis and signal B on the Y-axis.

Overlay

This selection will display the time histories of both signals on the same plot.

Square

This selection will produce a XY-Plot of signal A on the X-axis and signal B on the Y-axis. In this plot, both axes are drawn to the same scale.

Plot

This option is used to produce a hard copy of the currently displayed plot.

C.2.3 Info

This option is used to display information about the program and the currently selected data processing options. Once this option has been selected the program displays:

```
Universal Long Time Record Analysis Program
Written by Andreas Felber
UBC Civil Engineering Version 0.20

Release Date:        April 16, 1992
Free Memory:         289345 bytes
Options:
Resolution:            High
Modal Cut Off:         5 degrees
Window Type:           Hanning
Coherence Cut Off:     95%
Linearization:         Automatic
```

C.2.4 Option-Menu

The Option-Menu is used to control various aspects of the calculations in the frequency domain. The program assumes default values until new values are specified. While the default values can not be changed permanently, the command line can be used to set the options at program start up.

C.2.4.1 Resolution

The spectral analysis of the signals can be performed using various levels of resolution. The level of resolution depends on the number of averages k used to perform operations in the frequency domain. Four different resolution options are available as described below. As more averages are taken on a record with n data points, the number of points per segment $N = n/k$ decreases. At the same time, the frequency increment $\Delta f = 1/N\Delta t$ increases for all the frequency domain functions and thereby their resolution is lowered.

High - Resolution

If the total number of points in the record, n, is less than 4096, then no averaging is performed. Otherwise, $k = n/4096$ averages are used.

Medium - Resolution

If n is less than 4096, two averages are used. Otherwise, $k = n/2048$ averages are used.

Low - Resolution

If n is less than 4096, four averages are used. Otherwise, $k = n/1024$ averages are used.

Very Low - Very Low Resolution

If n is less than 4096, eight averages are used. Otherwise, $k = n/512$ averages are used.

Batch Codes

To select the resolution in batch mode, the corresponding code letters listed in the table below have to be used.

Resolution	Batch Code Letter
High	h
Medium	m
Low	l
Very_Low	v

C.2.4.2 Modal-Cut-Off

The Modal-Cut-Off value is used for the calculation of the Modal function (see section C.2.2.6). The Modal-Cut-Off value can be set to any of the values listed in the table below. To select one of these values in batch mode use the corresponding code letter.

Modal-Cut-Off [degrees]	Batch Code Letter
3	3
5	5
10	1
20	2
40	4
60	6
90	9

C.2.4.3 Coherence-Cut-Off

The Coherence-Cut-Off value is used for the calculation of the Modal function (see section C.2.2.6). The Coherence-Cut-Off value can be set to any of the values listed in the table below. To select one of these values in batch mode use the corresponding code letter.

Coherence [%]	Batch Code Letter
99.0	1
97.5	2
95.0	3
90.0	9
80.0	8
70.0	7
0.00	0

C.2.4.4 Window

Windows are used in signal processing to control side-lobe leakage. For a detailed discussion on side-lobe leakage the reader is referred to Ramirez (1985). Side-lobe leakage can be controlled by pre-multiplying a data segment of length T by a window before the FFT is computed. The original time domain signal stored by the program is not affected by the window. There are a variety of window types used in practice and each has its specific advantages and disadvantages. The program ULTRA currently incorporates five common window types shown in Fig. C.10 below. The mathematical forms of the windows are given below.

Rectangular - Window:

The Rectangular window has a constant amplitude (A=1) for the entire segment length.

Hanning - Window

$$A = 0.5\left(1 - \cos\frac{2\pi t}{T}\right) \tag{C-26}$$

Extended Cosine - Window

$$A = \begin{Bmatrix} 1 & 0.1T < t < 0.9T \\ 0.5\left(1 - \cos\frac{2\pi 5t}{T}\right) & \text{otherwise} \end{Bmatrix} \tag{C-27}$$

Triangle - Window

$$A = \begin{Bmatrix} 2t/T & 0 < t < 0.5T \\ 2 - 2t/T & \text{otherwise} \end{Bmatrix} \tag{C-28}$$

Cos^4 - Window

$$A = 0.5\left(1 - \cos\frac{2\pi t}{T}\right)^2 \tag{C-29}$$

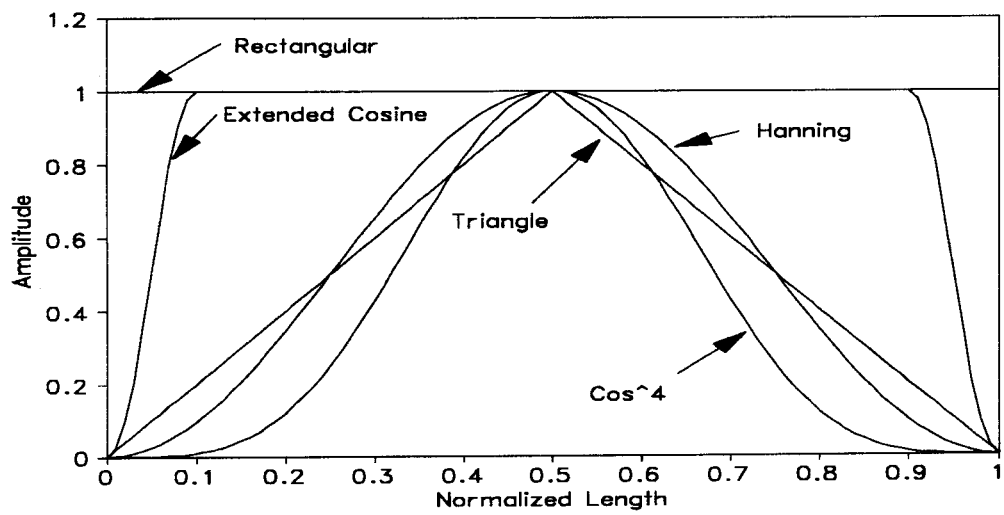

Fig C.10: Window Types

Batch Codes

In order to select a window type in batch mode, the corresponding code letter listed in the table below has to be used.

Window Type	Batch Code Letter
Rectangular	r
Hanning	h
Extended_Cosine	e
Triangle	t
Cos^4	c

C.2.4.5 Linearize

Linear trands contained in the data cause large spectral values near the low frequency end of the computed spectrum. To remove these generally unwanted large values, the linear trend in each segment is removed automatically before the spectral parameters are computed. For the purpose of ambient vibration measurement analysis this does not lead to any misinterpretation of the information. However, if the linear trend forms an important part of the data analysis, its automatic removal can cause problems. By default, the program automatically removes the linear trend from the individual signal segments prior to processing.

Automatic

Select this option to invoke the automatic segment linear trend removal.

Manual

Select this option to override the automatic segment linear trend removal.

C.2.4.6 Defaults

For the current version of ULTRA, the options default to

Parameter	**Value**
Resolution:	*High*
Modal Cut Off:	*5* degrees
Window Type:	*Hanning*
Coherence Cut Off:	*95%*
Linearization:	*Automatic*

C.3 ULTRA Input and Output File Formats

ULTRA was designed to handle a variety of input data formats. The conventions and assumptions associated with each format are outlined below.

C.3.1 Data Input Files

Data files are specified using the name of the file without an extension. The program then scans the current directory for a matching file with an admissible extension. Once such a file has been identified, the program will read the data. The file extensions and the corresponding file formats are listed below in the order in which the program scans for them.

C.3.1.1 ZONIC Spectral Analyzer Files (Extension *.tim)

This file format is used to import files which were generated using the ADCNV conversion program, which translates data from the Spectral Analyzer proprietary format to ASCII. Aside from the actual data values, *.*tim* files also contain pertinent information on the settings of the spectral analyzer during the recording. For convenient record keeping, ULTRA keeps track of all this information and includes it when printouts of the data are made.

C.3.1.2 Short Form ASCII Files (Extension *.aaa)

This format is used to import ASCII data generated by other programs or with an ASCII editor. Apart from the data, a label, the number of data point and the time increment between data points is required. The format of the data is unformated. A *.aaa file with the label "Test", 7 data points and time increments equal to 0.02 can be specified in any of the following ways:

Test 7 0.02	Test	Test,	Test
-0.45 0.22 0.87	7	7,	7
-0.67 0.1 1.7e-8	0.02	0.02,	0.02
	-0.45	-0.45,	-0.45 0.22
	0.22	0.22,	
	0.87	0.87,	0.87 -0.67 0.1 1.7e-8
	-0.67	-0.67,	
	0.1	0.1,	
	1.7e-8	1.7e-8,	

Since the entire program is based on the manipulation of records with 2^k (k is an integer) data points, odd length records need to be padded. If records have exactly $2^k \geq 256$ data points, no padding will occur. Otherwise, for a record with N data points padding will be performed to increase the number of points to the one after the next 2^k. The table below gives examples of original number of data points N and number total data points after padding used by ULTRA.

Number of Points, Original Record Length N	Number of Points, Padded Record Length n
57	512
128	256
256	256
511	1024
512	512
1023	2048

C.3.1.3 Binary Files (Extension *.bbb)

The program also accepts binary files as input. The format of the binary files has to be as specified in the documentation of the program AVTEST which is described in appendic B.

C.3.2 Output Files

C.3.2.1 Time Series

Manipulated signals can be stored in a file with the *.*tim* format used for input files. This format corresponds to the ASCII format used with the ZONIC AND 3524 Dual Channel FFT Signal Analyzer and has an extensive file header such as the one shown below:

```
            100,AD3525
 17/21
 91,  7,29
  8,18,44
                0,TIME
                1,A
                0,INST
                0,NORM
                4,        2.00000000e+001
           4096,               4
                1,HANN
                1,ON
                7,        4.47213595e+000
                0,V
                0,off
                1,DC
                7,        4.47213595e+000
                0,V
                0,off
                1,DC
                1,Vrms
                0,NORM
                0,off
                0,        1.00000000e+000,
            16384,                  0,          0.00000000e+000,
1.95312500e-002
         8.62545753e-002
         9.55351309e-002
         7.45351309e-002
```

For a detailed description of this header, the reader is referred to the manual of the conversion program ADCNV[1].

1 AD-1459 File Conversion Program V4.00, A&D Company Limited
Distributed by: ZONIC+AND 25 Whitney Drive, Milford, Ohio, 45150

C.3.2.2 Frequency Functions

All the computed frequency domain function can be stored on file. The files are all written in ASCII format and are differentiated by their extension. The following sections show examples of the different file headers.

Auto Spectrum *.PSD

```
Auto Spectrum For
Filename
Title
Number of Points      4096
Frequency Interval    0.01
  0.00
-1.23
  4.56
...
```

Cross Spectrum *.XSD

```
Cross Spectral Density For
A_Signal Filename
B_Signal Filename
Number of Points      4096
Frequency Interval    0.01
  0.00
-1.23
  4.56
....
```

Frequency Response Function *.FRQ

```
Frequency Response Function For
A_Signal Filename
B_Signal Filename
Number of Points      4096
Frequency Interval    0.01
  0.00
-1.23
  4.56
  ...
```

Phase Function *.PHS

```
Phase Function For
A_Signal Filename
B_Signal Filename
Number of Points     4096
Frequency Interval   0.01
  0.00
  5.23
  4.56
  ...
```

Coherence Function *.COH

```
Coherence Function For
A_Signal Filename
B_Signal Filename
Number of Points     4096
Frequency Interval   0.01
  0.00
  1.00
  0.56
  ...
```

Modal Function *.MOD

```
Modal Function For
A_Signal Filename
B_Signal Filename
Number of Points     4096
Frequency Interval   0.01
Modal Cut Off degrees: 20
Coherence Cut Off      : 0.7000
Cross-Spectral Cut Off: Ignore
  0.00
  0.70
  4.56
  ...
```

APPENDIX D: Program VISUAL User's Manual

D.1 Introduction to VISUAL

The program VISUAL was developed to illustrate and animate, mode shapes obtained from ambient vibration data reduced with ULTRA. To accomplish this, the program uses three types of files: a Structure file, a Measurement file, and a series of Modal files which contain the modal ratios. The Modal files are described in the ULTRA user's manual and the Structure and Measurement files are described below.

D.1.1 About this Manual

This program should be used in conjunction with the program ULTRA and as such the user is assumed to be familiar with ULTRA. As in the ULTRA user's manual, this manual is organized to reflect the menu structure of the program and it is intended to be both a user's and a reference manual. The potential user is encouraged to read the entire manual before using the program.

D.1.2 System Requirements

The program was compiled to run on a IBM compatible PC computer. The following hardware is supported.

Processor:	Intel 80386 & 80387 or 80486
Extended Memory:	4MB or more
Monitor:	VGA
Printer:	HP Laserjet II or compatible

D.1.3 Installing VISUAL

The executable file VISUAL.exe must be copied to a directory included on the path. (For information on the use of directories, the copy command and the path command, the reader is referred to the DOS version 5 manual (Microsoft, 1991)).

D.1.4 How to run VISUAL

The program can be start from any directory, that contains the necessary structure file (*.str), measurement file (*.mes) and associated modal ratio files (*.mod). To start the program, in a directory that contains a structure file called ***bridge*** and a series of PMR files with names specified in the measurement file called ***vert***, enter the following on the command line.

Visual *bridge vert*

File extensions should not be provided.

D.2 VISUAL Menu Structure and Options

The program is operated via a menu. Menu selections are made either by selecting the first letter of the option or by highlighting the desired option using the cursor keys and then pressing "Enter". The program's menu structure is illustrated in Fig. D.1. The individual options of the menu are described below.

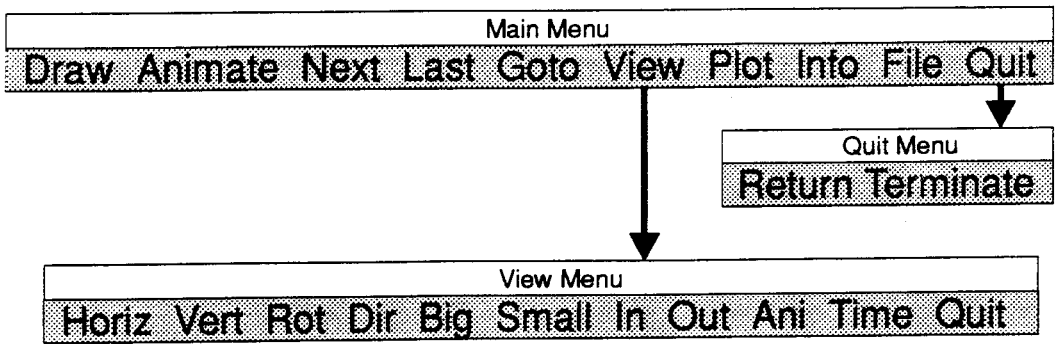

Fig. D.1: Menu Structure of the Program VISUAL

D.2.1 Draw

Draws the structure geometry including node numbers.

D.2.2 Animate

This option animates the measured vibration shapes of the structure at the selected frequency. The speed and amplitude of the animation can be respectively controlled with the "Ani" and "Time" option of the View Menu. While the animation is displayed, the top of the screen shows the corresponding frequency, period and frequency increment Δf of the modal files.

D.2.3 Next

This option increments the current frequency by Δf and animates the corresponding deflected shape.

D.2.4 Last

This option decrements the current frequency by Δf and animates the corresponding deflected shape.

D.2.5 Goto

This option allows the user to select a particular frequency for which the shape is to be animated.

D.2.6 View Menu

This menu is used to control how the structure's geometry is displayed as well as the speed and amplitude of the animation. The original image of the structure can be rotated about three axes. These axes are orthogonal to each other and remain fixed with respect to the screen's principal axes. The individual options for the manipulation of the view and the animation are described below.

Horiz Rotate the structure about the horizontal screen axis.

Vert Rotate the structure about the vertical screen axis.

Rot Rotate the structure about the outward normal of the screen.

Dir Controls the direction of the rotations. Every time this option is selected, the direction of rotation is reversed.

Big Increases the size of an individual rotation by 50%.

Small Reduces the size of an individual rotation by 33%.

In Increases the size of the structure by 25%.

Out Decreases the size of the structure by 20%.

Ani Changes the scale factor for the animated shape.

Time Sets the time delay used in the animation.

Quit Returns to the main menu.

D.2.7 Plot

This option produces a hard copy of the last displayed image on a HP Laserjet II compatible laser printer. After this option has been selected, an additional key has to be pressed to initiate printing. The escape key "Esc" can be pressed to return to the main menu without printing.

D.2.8 Info

This option displays the version and release date of the program and the criteria used to arrived at the modal ratios. A typical info display is shown below.

```
VISUAL 3_Dimensional Mode Animation Program
Written By Andreas Felber
UBC Civil Engineering    Version 0.20
Release Date: September 18 1992
Free Memory: 376640 bytes

Modal CutOff degrees: 10.00
Coherence CutOff      : 0.9500
Cross Spectral CutOff: Ignore
```

D.2.9 File

This option creates a file which contains all the joint coordinates and numerical values of the modes shape vector. The format of this file is described in section D.3.2.

D.2.10 Quit Menu

This option requires further confirmation before the program is terminated.

Return Returns to the main menu.

Terminate Terminates the program.

D.3 VISUAL File Formats

D.3.1 Input File Formats

D.3.1.1 Structure Files (Extension *.str)

The structure file, which has the extension **.str*, is used to define the geometry of a three dimensional stick-model of the structure. The model consists of nodes connected by line elements. In addition, initial scaling of the structure geometry is controlled in this file. The structure input file information is arranged as shown in the example below which corresponds to the portal frame shown in Fig. D.2.

Description	Example
Structure Description Xup Xlow Yup Ylow N i x y z . . . . E k j	Colquitz Fixed Bent #2 40 -5 30 -5 6 0 0 0 0 1 0 24 0 2 32 24 0 3 32 16.7 0 4 32 10.6 0 5 32 0 0 5 0 1 1 2 2 3 3 4 4 5

The first line of the **.str* file is used to identify the structure. The second line contains the information for the initial size of the display of the structure. "Xup" and "Xlow" are used to define the upper and lower limits of the X-axis, respectively. Similarly, "Yup" and "Ylow" are used to defined the limits of the Y-axis. In the third line, the number of nodes N=6 of the model is specified and then the individual node numbers and their coordinates x, y, and z are listed. Node numbers have to start with zero and are to be numbered consecutively in ascending order. The line after the last node information contains the number of line elements of the structure; in this case E=5. The line elements follow, but are not numbered and only identified by the two end nodes k and j.

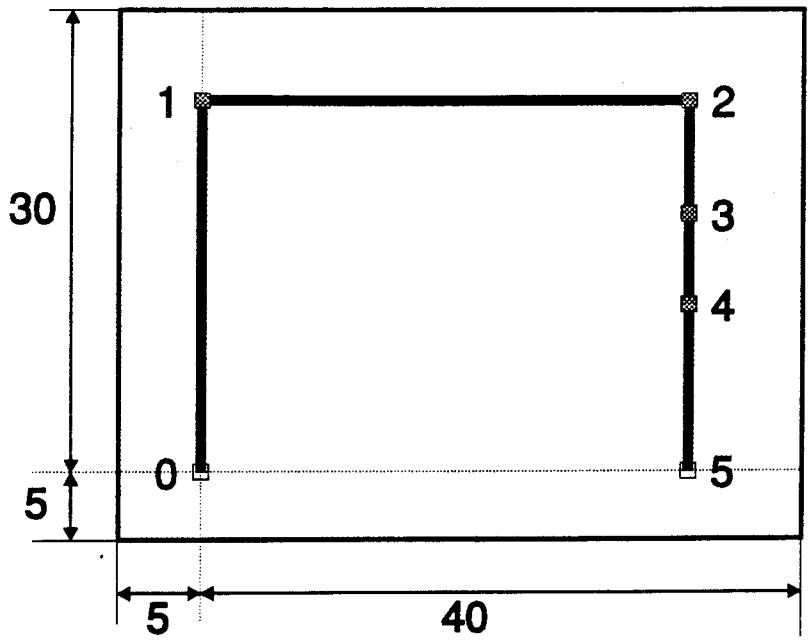

Fig. D.2: Portal Frame Corresponding to the Sample VISUAL Input File.

D.3.1.2 Measurement Files (Extension *.mes)

The measurement file, which has the extension *.*mes*, is used to provide information about the modal ratio files and the location and orientation corresponding to the direction of the modal ratios. A typical measurement file which describes out of plane mode shapes information for the portal frame example is shown below.

Description	Example
Measurement Description M file1 n i j k	Fixed Pier Longitudinal Measurements 4 4lo2l 4 0 0 1 3lo2l 3 0 0 1 2lo2l 2 0 0 1 1lo2l 1 0 0 1

The first line of the *.*mes* file is used to describe the measurements. The next line is used to specify the number of modal ratio files, M. Each of the following M lines gives the name of the *.*mod* file, the node number of the structure to which the *.*mod* file corresponds and the direction cosines of the modal ratio.

11.3.1.3 Modal Ratio Files (Extension *.mod)

Modal ratio files are produced by the program ULTRA and their format is documented in section C.3.

D.3.2 Output File Format

The program can produce an output file which contains all the information required to plot individual mode shapes. These mode shape files have the extension *.shp. A typical file for the portal frame example is shown below. Note that the x, y and z coordinates are given for each instrumented node along with the relative modal displacements dx, dy and dz. This file can be readily imported into any spreadsheet or graphic program for plotting.

```
VISUAL UBC Civil Engineering Version (0.20)
Modal Ratio Data File
Date & Time of Printing: Wed Sep 30 16:31:19 1992

Structure     :Portal Frame
Measurements:Fixed Pier Longitudinal Measurements
Modal CutOff degrees: 10.00
Coherence CutOff      : 0.0000
Cross-SpectralCutOff: Ignore
Frequency:     1.6406Hz (+-0.0195Hz) Period     0.6095 sec.
Node            x              y              z              dx             dy
dz
    1   0.000e+00    2.400e+01   0.000e+00   0.000e+00   0.000e+00   9.864e-01
    2   3.200e+01    2.400e+01   0.000e+00   0.000e+00   0.000e+00   1.000e+00
    3   3.200e+01    1.670e+01   0.000e+00   0.000e+00   0.000e+00   5.922e-01
    4   3.200e+01    1.060e+01   0.000e+00   0.000e+00   0.000e+00   3.175e-01
```

APPENDIX E: Program SUBSAP User's Manual

SUBSAP is a small program written in C to perform search and replace operations on selected alphanumeric strings in a text file. These strings are called "tokens." The tokens are replaced with numerical constants to facilitate parametric studies with structural analysis programs such as SAP90. Since typical input files for these programs can contains several thousands of lines, the replacement of parameters by hand can be very tedious and is error prone. To improve the speed and reliability of parametric studies, using SAP90 for example, the following procedure can be employed:

Step 1 Create a regular SAP90 input file and replace the parameters to be varied with tokens. Then save the file with the extension **.inp*.

Step 2 Create a file containing the numerical values which replace the tokens and store it with the extension **.var*.

Step 3 Run the program SUBSAP program to produce a SAP90 input file. The typical command for running the program is

SUBSAP file1 file2

The output file will have the name "file1."

Step 4 Run SAP90 to perform the analysis of "file1."

Step 5 Repeat Steps 2, 3 and 4 as many times as desired to perform the parametric study.

The following sections outline the system requirements, program installation and the format of the tokens and the variable files.

E.1 General

E.1.1 System Requirements

Since this program operates in text mode it will function on any IBM compatible personal computer with at least 256kb of memory.

E.1.2 Installing SUBSAP

The executable file ***SUBSAP.EXE*** must be copied to a directory included on the path. (For information on the use of directories, the copy command and the path command, the reader is referred to the DOS version 5 manual (Microsoft, 1991)).

E.2 Token and File Formats

E.2.1 Token Format

The tokens can be used to replace real and integer valued parameters in a SAP90 file. The original file, which must have the extension **.inp* can contain up to 99 different integer and real tokens. These tokens are identified as '$REAL1, $REAL2, ..,$REAL99' for real valued parameters and '$INT1, $INT2, .., $INT99' for integer valued parameters. A portion of the **.inp* file used for the Colquitz River Bridge Stick-Model is shown below to illustrate the use of tokens. This file contains one integer token and four different real tokens. After running SUBSAP, these tokens will be replaced by the values given in the example file shown in the

next section.

```
Colquitz River Bridge Stick Model (ft-kips)
SYSTEM
V=$INT1
.
.

MASSES
34     40  6  M=$REAL1,$REAL1,$REAL1,0,0,0
128  146  6  M=$REAL1,$REAL1,$REAL1,0,0,0
228  246  6  M=$REAL1,$REAL1,$REAL1,0,0,0
328  346  6  M=$REAL1,$REAL1,$REAL1,0,0,0
428  440  6  M=$REAL1,$REAL1,$REAL1,0,0,0
.
.

FRAME
NM=3
1  A=7.5  J=7.95      I=4.4,4.4         AS=6.5,6.5   E=580e3   G=194e3  M=0.035
2  A=12    J=25          I=16,9                AS=10,10       E=580e3    G=194e3
M=0.056
3  A=$REAL4  J=10  I=$REAL2,$REAL3  AS=$REAL4,$REAL4  E=4176e3  G=1392e3  M=0.00
29     28     34    M=3,3  LP=3,0:  EAST  Abutment
35     34     40    M=3,3
.
.
```

E.2.2 Variable File Format

Tokens are replaced with the constants contained in a variable file with the extension **.var*. The format of the variable file is illustrated using the **.var* file for the Colquitz River Bridge Stick-Model below.

Description	Example Variable *.*var* File
Identifier Number of Integer Variables Integer variables Identifier Number of Real Variables Real Variables	***INTEGERS*** 1 10 ***REALS*** 4 2.71 added mass 6.74 vertical stiffness 723 transverse stiffness 5.51 area

The format of the variable file is free and commas are optional. All character strings in the *.*var* file are ignored and can be used for notes. The identifiers INTEGERS and REALS are used to improve readability.

APPENDIX F: Details of Individual Test Setups

F.1 Colquitz River Bridge Test Setups

The individual test setups used for the ambient vibration and pullback tests conducted on the Colquitz River Bridge are described in detail in this section. All the sensors locations are referenced using the numbering scheme outlined in section 4.3.4.1.

F.1.1 Ambient Vibration Tests

For ambient vibration measurements (AVM) the sensors were mounted at the locations described in the following sections. The accelerations were recorded at 40 samples per second in 8 segments of 4196 points. All signals were conditioned with 12.5 Hz low-pass filters. The sampling rate and filter setting were chosen to adequately capture the behaviour of the structure in the range of 0 Hz to 10 Hz.

F.1.1.1 Vertical AVM Setup

The sensor locations used to determine the vertical modes of the deck are summarized in Table F.1. All sensors were mounted pointing up.

Table F.1: Sensor Locations for Vertical Ambient Vibration Survey at the Colquitz River Bridge

Filename	Description	Sensors	Locations	Signal Conditioner Attenuation [db]
COAV00	Preliminary on Deck	1,2,3,4	13,11,17,19	42
COAV0X	Preliminary on Deck	1,2,3,4	13,9,21,25	48
COAV01	East Abutment	1,2,3,4	13,14,1,2	48
COAV02	1st Span 1/3	1,2,5,6	13,14,3,4	48
COAV03	1st Span 2/3	1,2,3,4	13,14,5,6	48
COAV04	2nd Span 1/4	1,2,5,6	13,14,9,10	48
COAV05	2nd Span 1/2	1,2,3,4	13,14,11,12	48
COAV06	3rd Span 1/4	1,2,5,6	13,14,17,18	48
COAV07	3rd Span 1/2	1,2,3,4	13,14,19,20	48
COAV08	3rd Span 3/4	1,2,5,6	13,14,21,22	48
COAV09	4th Span 1/4	1,2,3,4	13,14,25,26	48
COAV10	4th Span 1/2	1,2,5,6	13,14,27,28	48
COAV11	4th Span 3/4	1,2,3,4	13,14,29,30	48
COAV12	5th Span 1/3	1,2,5,6	13,14,33,34	48
XOAV12	5th Span 1/3	1,2,5,6	13,14,33,34	48
YOAV12	5th Span 1/3	1,2,5,6	13,14,33,34	54
COAV13	5th Span 2/3	1,2,3,4	13,14,35,36	54
XOAV13	5th Span 2/3	1,2,3,4	13,14,35,36	48 to 54
YOAV13	5th Span 2/3	1,2,3,4	13,14,35,36	54
COAV14	West Abutment	1,2,5,6	13,14,37,38	54
COAV15	Collocation	1,2,3,4	13,13,13,13	48
COAV16	Collocation	1,2,5,6	13,13,13,13	48

F.1.1.2 Transverse AVM Setup

The sensor locations used to determine the transverse modes of the deck are summarized in Table F.2. Sensor number 1 was mounted pointing up and the remaining sensors were mounted pointing north.

Table F.2: Sensor Locations for Transverse Ambient Vibration Survey at the Colquitz River Bridge

Filename	Description	Sensors	Locations	Signal Conditioner Attenuation [db]
COAT01	Transverse Collocation 1	1,2,3,4	13up,13,13,13	48
XOAT01	Transverse Collocation 1	1,2,3,4	13up,13,13,13	48,30,30,30
COAT02	Transverse Collocation 2	1,2,5,6	13up,13,13,13	48,30,30,30
COAT03	1st Transverse Setup	1,2,3,4	13up,13,1,1 on abutment	48,30,30,30
COAT04	2nd Transverse Setup	1,2,5,6	13up,13,3,5	48,30,30,30
COAT05	3rd Transverse Setup	1,2,3,4	13up,13,7,9	48,30,30,30
COAT06	4th Transverse Setup	1,2,5,6	13up,13,11,15	48,30,30,30
COAT07	5th Transverse Setup	1,2,3,4	13up,13,17 on deck, 19 on deck	48,36,36,36
COAT08	6th Transverse Setup	1,2,5,6	13up,13,21 on deck, 23 on deck	48,36,36,36
COAT09	7th Transverse Setup	1,2,3,4	13up,13,25 on deck, 27 on deck	48,36,36,36
COAT10	8th Transverse Setup	1,2,5,6	13up,13,29 on deck, 31 on deck	48,36,36,36
COAT11	9th Transverse Setup	1,2,3,4	13up,13,33,35	48,30,30,30
COAT12	10th Transverse Setup	1,2,3,4	13up,13,37,37 on abutment	48,30,30,30

F.1.1.3 Longitudinal AVM Setup

The sensor locations used to determine the longitudinal modes of the deck are summarized in Table F.3. All sensors were mounted pointing west.

Table F.3: Sensor Locations for Longitudinal Ambient Vibration Survey at the Colquitz River Bridge

Filename	Description	Sensors	Locations	Signal Conditioner Attenuation [db]
COAL00	Expansion Bent	5,6,3,4	45,46,31 on pier, 32 on pier	42
COAL01	Fixed Bent	5,6,3,4	41,42,15,16	42
COAL02	Fixed Bent & Pier	5,6,3,4	41,41+,15 on pier, 16 on pier	36
COAL03	Coupling	1,2,3,4	13up,13,15,16	48,36,36,36

F.1.2 Pullback Tests

For the pullback tests the accelerations were recorded at 200 samples per second to capture the release and the transient free vibration of the structure in detail. The individual records consisted of 4096 samples and were conditioned using a 50 Hz low pass filter. The sampling rate and filter setting were chosen to adequately capture the behaviour of the structure in the range of 0 Hz to 20 Hz. The locations of the sensors for all the pullback tests are given in the following sections.

F.1.2.1 Transverse Pullback Test Setup

The sensor locations for the transverse pullback tests are summarized in Table F.4. All sensors were mounted pointing north.

Table F.4: Sensor Locations for Transverse Pullback Tests at the Colquitz River Bridge				
Filename	**Description**	**Sensors**	**Locations**	**Signal Conditioner Attenuation [db]**
COTP01	1st Transverse Pull Test, Computer Failure One Channel Backup Data	3	23	66
COTP02	2nd Transverse Pull Test	1,2,3,4, Load Cell	13,43,23,23 on pier	54
COTP03	3rd Transverse Pull Test	1,2,3,4, Load Cell	13,43,23,23 on pier	54

F.1.2.2 Longitudinal Pullback Test Setup

The sensor locations for the longitudinal pullback tests are summarized in Table F.5. All sensors were mounted pointing west.

Table F.5: Sensor Locations for Longitudinal Pullback Tests at the Colquitz River Bridge				
Filename	**Description**	**Sensors**	**Locations**	**Signal Conditioner Attenuation [db]**
COLP01	1st Longitudinal Pull Test	5,6,3,4, Load Cell	45,46,31,32	66
COLP02	2nd Test Aborted due to sticky release device			54
COLP03	2nd Test Aborted due to sticky release device			54
COLP04	2nd Longitudinal Pull Test	5,6,3,4, Load Cell	41,42,15,16	54
COLP05	3rd Longitudinal Pull Test	5,6,3,4, Load Cell	41,41+,15 on pier, 16 on pier	48

F.1.3 Sensor Mounting Details

Sensors were attached to the structure using three different mounting details. These details required minimal hardware to provide a good attachment of the sensor to structure for the

duration of the measurement. The main advantages of using these mounting details (as shown in Fig. F.1) are that the sensors are easy to install and that no permanent marks are left on the structure after the sensors are removed.

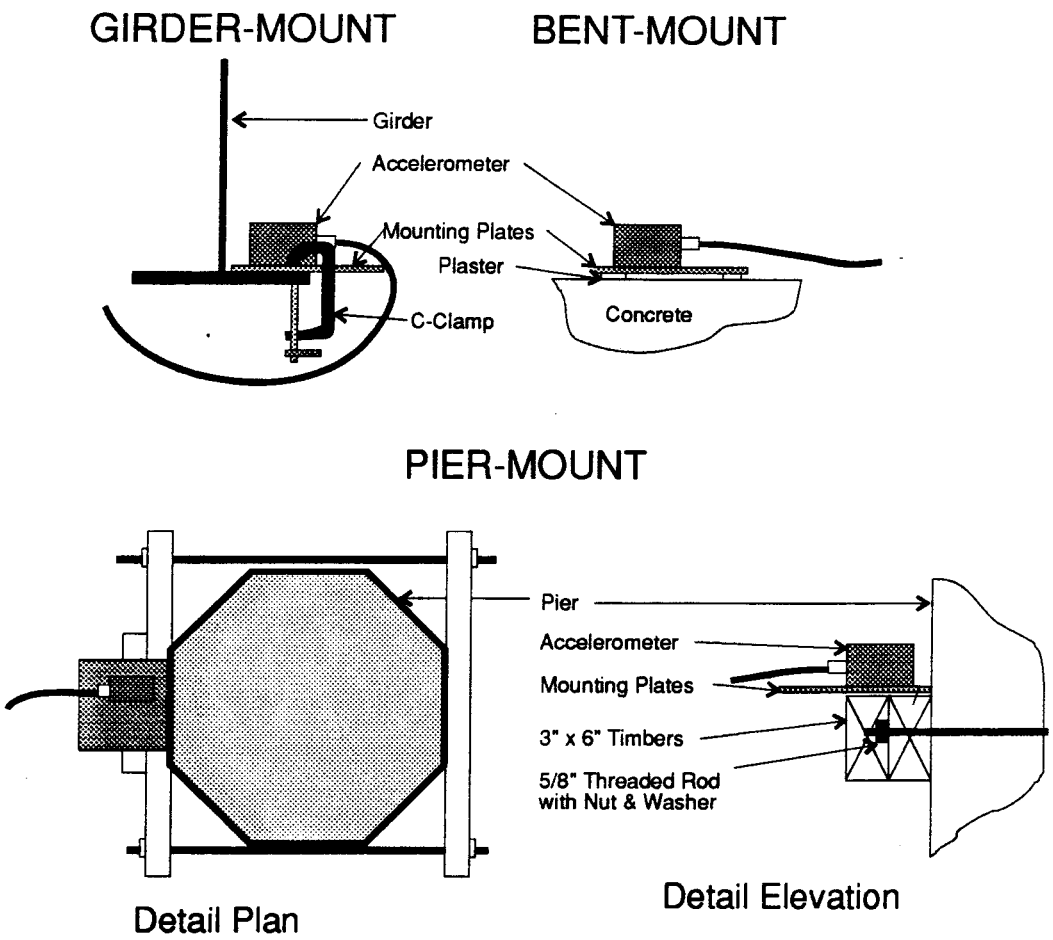

Fig. F.1: Typical Sensor Mounting Details Used at the Colquitz River Bridge

F.2 Squamish Wharf Test Setup

All signals of the Squamish wharf ambient vibration setups, listed in Table F.6, were low pass filtered at 12.5 Hz and recorded at 40 samples per second. For each setup, 8 segments consisting of 4096 points for a total of 32768 points were obtained.

Table F.6: Sensor Locations for Squamish Wharf

Setup	File Name	Ch. #1	Ch. #2	Ch. #3	Ch. #4	Signal Conditioner Attenuation [db]
1	SQA01	3T	3L	11L	12T	0
2	SQA02	3T	3L	10T	11T	0
3	SQA03	3T	3L	8T	9T	0
4	SQA04	3T	3L	6T	7T	0
5	SQA05	3T	3L	4T	5T	0
6	SQA06	3T	3L	1L	2L	0
7	SQA07	3T	3L	13T	13L	0
8	SQA08	13T	13L	7T	7L	0

Note: T = pointing west; L= pointing south

APPENDIX G: Index of Terms and Abbreviations

This section presents an index which can be used to quickly locate the definitions of terms used throughout this document. The terms and abbreviations are listed in alphabetical order below.

Output	A.2
Pass Band	A.3.2.1
Phase Shift	A.4.1.2
Roll-off	A.3.1.2
Sampling	A.4.1.2
SAP90	3.3.4
Saturation	A.2
Sensitivity	A.2
Stop band	A.3.1.2
SUBSAP	E
ULTRA	C
VISUAL	D